UNIVERSITY OF LONDON

IMPERIAL COLLEGE OF SCIENCE AND TECHNOLOGY

DEPARTMENT OF ELECTRICAL ENGINEERING

STARTING PERFORMANCE OF SYNCHRONOUS MOTORS

---

by

Glanville Francis Thomas WIDGER, B.Sc.(Hons)

Thesis submitted for the degree of
Doctor of Philosophy in the
Faculty of Engineering

April 1967

ABSTRACT

The thesis describes an investigation of the conditions which determine the starting characteristics of a synchronous motor. The asynchronous performance, at a given slip, may be estimated from the two axis operational admittances, $Y_d(js\omega_o)$, $Y_q(js\omega_o)$, expressed as complex functions of the slip. The functions are commonly depicted as frequency response loci. Four methods, two new, are described and compared, for the experimental determination of the operational admittance loci of a synchronous motor of any size and type.

The methods used for calculating the parameters from which the operational admittance loci of laminated pole synchronous motors may be derived are well known. The loci of several laminated pole synchronous motors are calculated in this manner.

New two-axis equivalent circuits for the solid pole synchronous motor are derived. With the aid of a fast computer the operational admittance loci of many solid pole machines are calculated from the new equivalent circuits. The effects of flux distribution in the solid iron, saturation of the solid iron (with particular consideration of the pole tips), and the connection of adjacent solid poles by end-rings, are all considered in the calculations.

Comparisons are shown between the calculated and measured operational admittance loci, obtained for both types of synchronous motors. The theoretical mean and oscillating torques and currents, derived from the loci,

are then compared with the torques and currents measured.

The agreement between the measured and calculated results is very good for nearly all of the machines tested, but where variations exist explanation is suggested for the discrepancy.

ACKNOWLEDGEMENTS

The work described in this thesis was carried out under the supervision of Dr. B. Adkins, D.Sc., M.A., M.I.E.E., Reader in Electrical Engineering, Imperial College of Science and Technology. The author wishes to express his gratitude to Dr. Adkins for his helpful guidance, constant encouragement, and keen interest.

The author also wishes to express his gratitude to Mr. K.F. Raby and Mr. D.D. Stephen, both of A.E.I. Ltd., for their guidance, encouragement and interest, particularly in the initial stages, and to Dr. E.M. Freeman, of King's College, London, for the same, in the latter stages.

Further acknowledgement is due to members of the staff of A.E.I. Ltd.; Mr. J.D. Edwards, who designed and built the "axis resolution" equipment, and made it suitable for application to this work; and to Mr. E.H. Harrison and Mr. A. Twardzicki for allowing the author to test machines in their charge.

Finally, the author wishes to express his gratitude to A.E.I. Ltd., for the award of a research fellowship to enable this work to be carried out, and for the use of their excellent reproduction and photographic facilities in the production of this thesis.

LIST OF CONTENTS

LIST OF SYMBOLS

$A = A(js\omega_o)$	:	Imaginary part of $jY_d(js\omega_o)$
$B = B(js\omega_o)$	:	Real part of $jY_d(js\omega_o)$
B	:	Flux density - webers/m^2
B_{mo}	:	Maximum surface value of B
B_s	:	Saturated level of flux density (1.75wb/m^2)
$C = C(js\omega_o)$	:	Imaginary part of $jY_q(js\omega_o)$
C_1, C_2	:	Damping coefficients
$D = D(js\omega_o)$	:	Real part of $jY_q(js\omega_o)$
E	:	Electric field intensity
f_o	:	Supply frequency - c/s
H	:	Magnetic field intensity - AT/m
H_{mo}	:	Maximum surface value of H
I, i	:	Electric current - p.u.
i_d	:	Instantaneous direct axis current
i_q	:	Instantaneous quadrature axis current
i_o	:	Instantaneous zero sequence current
i_a, i_b, i_c	:	Instantaneous phase currents
i_f	:	Instantaneous field current

i_{kd}	:	Instantaneous direct axis damper current
i_{kq}	:	Instantaneous quadrature axis damper current
I_{dm}	:	Maximum value of direct axis current
$\bar{I}_d$	:	R.M.S. phasor value of i_d
$\bar{I}_q$	:	R.M.S. phasor value of i_q
I_d	:	R.M.S. value of direct axis current, i_d
I'_d	:	R.M.S. value of d.a. transient current
I''_d	:	R.M.S. value of d.a. sub-transient current
j	:	Complex operator
J	:	Electric current density - amps/m^2
J	:	Moment of Inertia
K	:	Mechanical stiffness
K	:	Constant given by eqn. 2.18
K'	:	Constant given by eqn. 10.27
k_{w1}, k_{w2}	:	Combinations of winding and flux factors
L	:	Inductances
L_a	:	Stator leakage inductance
L_{md}	:	Direct axis magnetising inductance
L_{mq}	:	Quadrature axis magnetising inductance

L_{kd}	:	Direct axis damper leakage inductance
L_{kq}	:	Quadrature axis damper leakage inductance
L_f	:	Field leakage inductance
L	:	Lengths
L_S	:	Length of pole arc from tip to tip
L_B	:	Length of pole body surface path
P	:	Number of poles
p	:	Differential operator, $^d/_{dt}$
R, r	:	Resistance - p.u.
r_a	:	Armature resistance
r_e	:	Resistance of iron to eddy currents
r_f	:	Field winding resistance (Armature refer)
r_{kd}, r_{kq}	:	Damper winding resistances (Armature refer)
S	:	Reluctance
s	:	slip - p.u.
T_e	:	Electromagnetic torque
T	:	Turns
T	:	Time constants
T_{1-7}	:	As defined in reference 3
T'_d	:	D.A. transient short circuit time constant
T'_{do}	:	D.A. Transient open circuit time constant

T''_d	:	D.A. sub-transient short circuit time constant
T''_{do}	:	D.A. sub-transient open circuit time constant
T''_q	:	Q.A. sub-transient short circuit time constant
T''_{qo}	:	Q.A. sub-transient open circuit time constant
V	:	Voltage - p.u.
V_a, V_b, V_c, v_a, v_b ..	:	Phase voltages, R.M.S. and instantaneous values
V_m	:	Maximum value of the phase voltages
V_d, V_q, v_d, v_q	:	Two axis voltages, R.M.S. and instantaneous
V_t	:	Tachometer voltage
V_S	:	Pole shoe voltage (Prop. to p. shoe flux)
V_B	:	Pole body voltage
V_{B1}, V_{B2}	:	Component of V_B
V_{FL}	:	Field leakage voltage (across X_f)
W; w	:	Input power, total, instantantaneous
W	:	Gross axial core length
X	:	Reactances
$X_a, X_{md}, X_{mq}, X_f, X_{kd}, X_{kq}$	:	Reactances defined at f_o corresponding to L_a, L_{md}, ...
X_e	:	Eddy current leakage reactance

X_d	:	Direct axis synchronous reactance
X'_d	:	Direct axis transient reactance
X''_d	:	Direct axis sub-transient reactance
X_q	:	Quadrature axis synchronous reactance
X''_q	:	Quadrature axis sub-transient reactance
$X_d(p)$	:	Direct axis operational impedance
$X_q(p)$	:	Quadrature axis operational impedance
$X_d(js\omega_o)$, $X_q(js\omega_o)$	:	Frequency functions corresponding to $X_d(p)$, $X_q(p)$
$Y_d(js\omega_o)$, $Y_q(js\omega_o)$	:	Two axis operational admittance frequency functions
Z	:	Impedances
Z_{NL}	:	General non-linear solid iron impedance
Z_B	:	Pole body iron impedance
Z_S	:	Simple pole shoe impedance (Distribution neglected)
Z'_S	:	Equivalent pole shoe impedance (including distribution)

α, β, γ	:	Arbitrary angles
δ	:	Load angle
δ	:	Depth of penetration (Maximum)
Δ	:	Given by eqn. 2.46
ξ	:	Instantaneous depth of penetration
θ	:	Angle of the direct axis with phase A
φ	:	General phase angle
λ	:	Constant given by eqn. 10.32
ρ	:	Iron resistivity - ohm-metres
μ_o	:	$4\pi \times 10^{-7}$ Permeability of air
μ_r	:	Relative permeability
τ	:	Time constant
ψ_d, ψ_q	:	Direct and quadrature axis flux linkages
Φ	:	Flux - webers
$\Phi_{f\ell}$	:	Field leakage flux (tip to tip leakage)
Φ_b	:	Pole body fluxes
Φ_s	:	Pole shoe flux
Φ_g	:	Main air gap flux
Φ_t	:	Total flux/pole
Φ_a	:	Stator leakage flux
ω	:	Angular rotor speed - rads/sec
ω_o	:	Angular synchronous speed - rads/sec

CHAPTER 1

INTRODUCTION

There are in existence several types of synchronous motors, but all types may be placed into one of two classes. In one class may be placed all synchronous motors having rotors of laminated iron, and in the other, those having rotors of unlaminated 'solid' iron. Almost without exception synchronous motors have rotors with salient poles, around which is wound the main field winding.

All the motors with laminated rotors have a separate starting winding. This winding is usually a complete 'squirrel cage' winding located in slots in the pole face. However, laminated pole machines are sometimes built with a so called 'grid' winding, in which the end connections are only made between adjacent bars on a single pole, and do not connect the bars of one pole to the bars of another. This latter configuration is not common and is not dealt with in this thesis. Motors having solid iron poles do not require a separate starting winding, since the solid iron of the poles acts itself as a starting winding.

During starting the main field is unexcited and starting torque is produced by slip frequency currents in either the starting winding in the case of laminated pole machines, or the solid iron in the case of unlaminated machines. However, it is normal practice to close the main field winding through a resistance

several times larger than the winding resistance in order to provide additional starting torque and to limit the induced voltage in the winding at standstill. The concentration of the main field winding on the direct axis, the saliency of the poles, and the arrangement of the electrical circuits in the squirrel cage or the solid iron, cause appreciable dissymetry between the two axes. Consequently the torque produced at a given slip is not a steady value, but has a component oscillating at twice slip frequency. Occasionally synchronous motors of either kind are built with brushless excitation schemes, where the rectifiers are present in the field winding during starting. The alternate conducting and non-conducting state of the rectifiers give rise to additional pulsation at slip frequency. The present thesis does not deal with this special case.

The two-axis theory of the synchronous machine, due to Park[1,2], can be used to calculate the current and torque of the synchronous machine, during asynchronous operation, if the machine parameters are known. The parameters of the laminated pole motor are mainly resistances and inductances which can be determined by design calculations, and confirmed by tests. The parameters of the solid pole motor can also be expressed as impedances, but the values vary with both the slip frequency and the flux in a complicated manner.

An assumption is made that the squirrel-cage winding may be considered to be equivalent to two discrete circuits, one on each axis; and that the solid iron may also be represented by two equivalent systems, one on each axis. The theory introduces two operational

functions, the direct axis operational impedance, $X_d(p)$, and the quadrature axis operational impedance $X_q(p)$. For calculations relating to asynchronous running at constant slip, s, these operational impedances transform to $X_d(js\omega_o)$, and $X_q(js\omega_o)$. It is more convenient, however, to use the inverse functions, the operational admittances, $Y_d(js\omega_o)$, and $Y_q(js\omega_o)$, in calculations relating to asynchronous running. The real and imaginary parts of the inverse functions may be determined at any slip frequency and plotted in the complex plane. Points in the complex plane relating to $Y_d(js\omega_o)$, at slip frequencies from zero to infinity, describe the direct axis operational admittance frequency locus and points relating to $Y_q(js\omega_o)$, the quadrature axis operational admittance frequency locus.

The asynchronous performance, at a given slip, may be determined directly from the real and imaginary components of the two axis operational admittance functions at that slip frequency.

The thesis is divided into three parts. Part I records a theoretical study of the method of calculating the asynchronous torques, currents and power factor of a synchronous motor from the operational admittance frequency functions; the methods used to obtain the operational admittance frequency loci, by measurement; and the methods used to measure the asynchronous torques, currents and power of the motor.

Although the general method of calculating the asynchronous performance from the operational admittances is well known[3], a study of the principle is given here in much greater detail. A graphical method of estimating the asynchronous torques, currents and power factor, from the two axis operational admittance loci, neglecting the effect of armature resistance, is given. The asynchronous performance, including the effect of armature resistance, is calculated using the computer. The effect of the presence of armature resistance in a salient pole machine is to introduce a dip in the torque, current and power factor characteristics in the half speed region, and a theoretical study of the effect of different values of armature resistance on the characteristics of the machine is given. Finally a very simple empirical rule is derived to determine the extent of the half speed dip in the mean torque characteristic from the half speed values of the operational admittances.

Of the methods used to measure the operational admittance loci of the machine two are new. The new methods used are the "axis resolution method[4]", and the dynamic impedance test. The axis resolution method is a method where the phase quantities of an asynchronously running machine are dynamically resolved into their axis counterparts. The axis admittances can then be deduced from measurements of axis current, voltage and power. The dynamic impedance test determines impedances from oscillograms of phase current and voltage, using values at the instants when the phase current is equal to the appropriate axis current. The other two methods are based on the variable frequency static impe-

dance test and the sudden short circuit test.

The phase current of a synchronous motor, running asynchronously is relatively easy to measure. However, the torque characteristics are considerably more difficult to obtain, and several methods have been tried and compared. The methods used to measure torque are the output power measurement method - only applicable to mean torque, the use of a strain gauge torque-meter, and the acceleration method. A new method of determining the instantaneous torque with oscillating component unattenuated, using electronic multiplication and addition to measure the instantaneous input power, has been applied. Although the latter method is not accurate to a high degree, a direct record of torque/time for the motor can be obtained from a single start.

Part II is entirely devoted to the laminated pole synchronous machine. The first section deals with the method of calculating the operational admittances of the machine, which is well known[3]. The latter section shows the comparison between the measured and calculated machine characteristics and discusses reasons for discrepancies.

Part III, which is almost entirely new, is devoted to the solid pole synchronous motor. There have been many applications of the linear eddy current theory to solid pole machinery, in the past[5,6,7,8,9], but calculation of the flux density at the surface of the iron

shows the fallacy of such an application. A non-linear approach such as that adequately explained by Argawal[10] gives more sensible results over normal operating regions. Bharali and Adkins[11] and Chalmers[19] applied the non-linear theory successfully to round rotor turbo-alternators running asynchronously at very low slips. McConnell and Sverdrup[14] and Angst[15] have applied the non-linear theory to solid round rotor induction motors. However, to the author's knowledge, no-one has attempted to apply such a non-linear theory to a salient solid pole synchronous machine over the whole operating range of slip, as has been done here.

The new method, given here, is divided into three parts. First of all, the two axis equivalent circuits of the solid pole motor are derived from very careful consideration of the flux paths in the solid rotor. The effects of the distribution of flux entering the solid pole shoe, the possibility of complete saturation in the pole tips, the separate effect of eddy currents in the pole body, the presence or absence of end rings connecting adjacent solid poles, and the full account of the effect of the main field winding, are all allowed for in the equivalent circuits. Secondly, the non-linear impedances are inserted into the equivalent circuit - the pole body impedance is linearised when the flux linking the pole body is very low, and the operational admittance functions are calculated. Both the non-linearity and the flux distribution make the problem extremely complicated and a fast computer is required to calculate the operational admittance functions. Thirdly, the asynchronous characteristics are

calculated from the two axis functions.

Comparison is shown between the measured and calculated operational admittances, torques and currents etc., obtained for machines of widely different sizes and speeds.

PART I

THEORY AND MEASUREMENT TECHNIQUES APPLICABLE TO ALL SYNCHRONOUS MOTORS

CHAPTER 2

THEORY OF ASYNCHRONOUS OPERATION

Although the results derived in this chapter are applicable to both the laminated and solid pole type of synchronous machine, the intermediate steps to the results are, in some parts, somewhat different. To avoid confusion the derivations are made as for the laminated pole machine. At the end of each section, however, the differences in the procedure are indicated, and the necessary references made to the third part of the thesis, which deals with the solid pole machine in detail.

2.1. BASIC EQUATIONS

In the two axis theory, first developed by Park,[1,2] the phase quantities are transformed to axis quantities. The transformation of phase voltages and currents to axis voltages and currents, having the same effects as the phase values is:-

$$\begin{bmatrix} v_d, & i_d \\ v_q, & i_q \\ v_o, & i_o \end{bmatrix} = 2/3 \begin{bmatrix} \cos\theta & \cos(\theta-2\pi/3) & \cos(\theta-4\pi/3) \\ \sin\theta & \sin(\theta-2\pi/3) & \sin(\theta-4\pi/3) \\ 1/2 & 1/2 & 1/2 \end{bmatrix} \cdot \begin{bmatrix} v_a, & i_a \\ v_b, & i_b \\ v_c, & i_c \end{bmatrix} \quad .. (2.1)$$

where θ is the angle between the axis of phase A winding and the direct axis and, in general, is some function of time depending on the mode of machine operation.

For balanced operation $v_o, i_o = 0$

The transformed laminated pole machine is now as shown in Fig.1. The starting winding has been replaced by two equivalent windings one on each axis; for convenience the diagram is drawn with the field stationary and the armature rotating.

Park's equations governing the operation, using the convention of Adkins[3], are:-

$$\left.\begin{aligned} v_d &= p\psi_d + \omega\psi_q + r_a i_d \\ v_q &= p\psi_q - \omega\psi_d + r_a i_q \end{aligned}\right\} \qquad (2.2)$$

and the electromagnetic torque, T_e, is given by:-

$$T_e = \omega_o/2\ (\psi_q i_d - \psi_d i_q) \qquad (2.3)$$

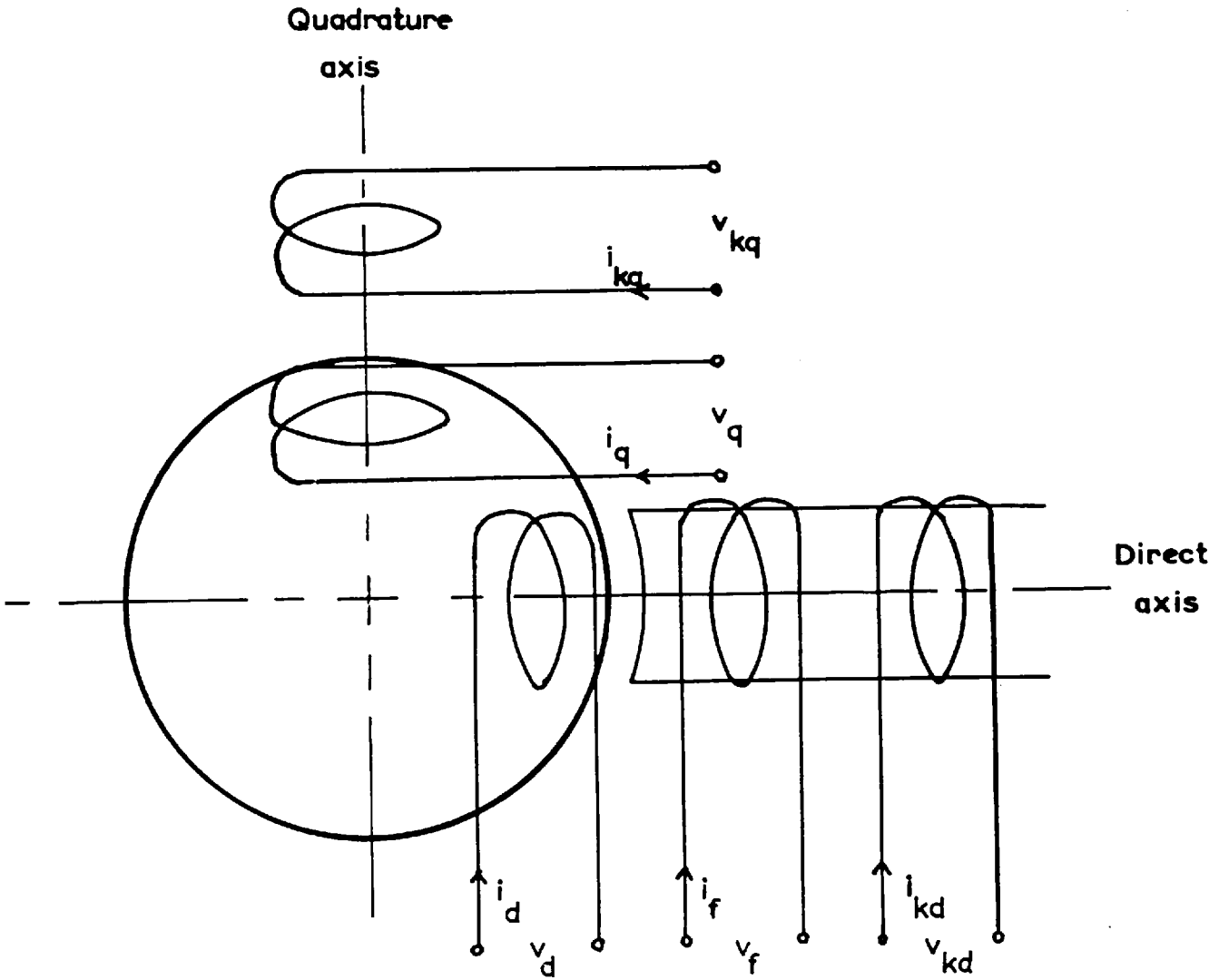

Fig.1. Two axis representation of a Synchronous machine, with laminated poles

2.2. OPERATIONAL IMPEDANCE

The direct axis flux linkage in the conventional machine shown in Fig.1 is given by:-

$$\psi_d = L_{md}i_f + L_{md}i_{kd} + (L_{md} + L_a)i_d \qquad (2.4)$$

For the field winding circuit, where r_f includes both winding and external resistance, and there is no excitation:-

$$0 = [r_f + (L_{md} + L_f)p]i_f + L_{md}pi_{kd} + L_{md}pi_d \qquad (2.5)$$

Similarly for the squirrel cage starting winding, the damper circuit:-

$$0 = L_{md}pi_f + [r_{kd} + (L_{md} + L_{kd})p]i_{kd} + L_{md}pi_d \qquad (2.6)$$

If equation (2.4) is multiplied throughout by the operator p, these three equations (2.4), (2.5). (2.6) may be represented by the direct axis equivalent circuit shown in Fig.2(a).

Similarly equations may be written for the quadrature axis circuits:-

$$\left.\begin{aligned} \psi_q &= L_{mq} i_{kq} + (L_{mq} + L_a) i_q \\ 0 &= [r_{kq} + (L_{mq} + L_{kq})p] i_{kq} + L_{mq} p i_q \end{aligned}\right\} \qquad (2.7)$$

and may be represented in the same way by the quadrature axis equivalent circuit in Fig.2(b).

By eliminating the secondary currents, i_f, i_{kd} in equation (2.4), (2.5), (2.6) and i_{kq} in equation (2.7):-

$$\psi_d = \frac{T_4 T_6 p^2 + (T_4 + T_5)p + 1}{T_1 T_3 p^2 + (T_1 + T_2)p + 1} \cdot L_d i_d$$

$$\psi_q = \frac{T_7 p + 1}{T_8 p + 1} \cdot L_q i_q$$

where T_1 .... T_8 are time constants.

Replacing all inductances by reactances referred to datum frequency ω_o, the quantity $\frac{\omega_o \psi_d}{i_d}$, which has dimensions of impedance, may be written as $X_d(p)$, the direct axis operational impedance.

$$X_d(p) = \omega_o \psi_d / i_d \qquad (2.8)$$

then:-

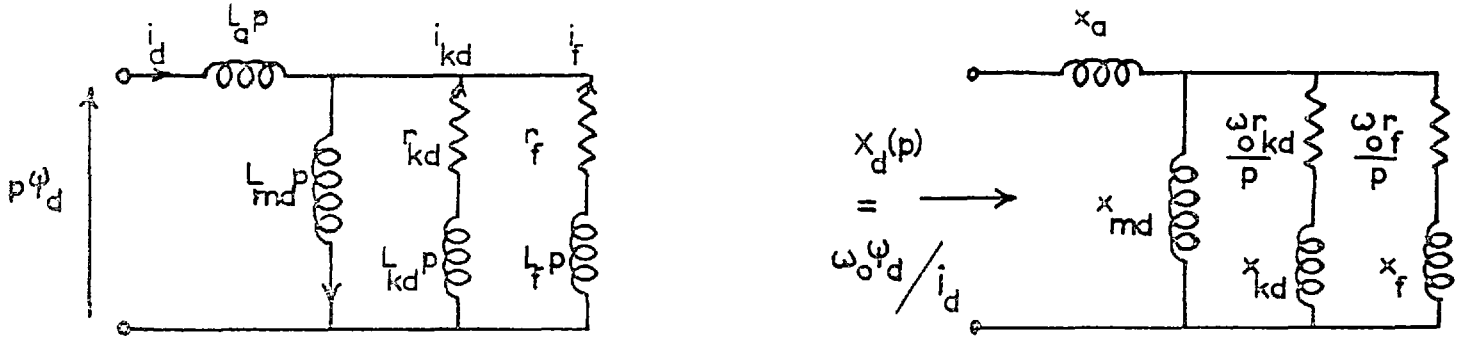

(a) Direct axis

(b) Quadrature axis

Fig. 2 Laminated pole synchronous machine equrvalent circuits, with the field winding closed and unexcited.

$$X_d(p) = \frac{T_4T_6p^2 + (T_4 + T_5)p + 1}{T_1T_3p^2 + (T_1 + T_2)p + 1} \cdot X_d \qquad (2.9)$$

also,

$$X_q(p) = \omega_o\psi_q/i_q \qquad (2.10)$$

then

$$X_q(p) = \frac{T_7p + 1}{T_8p + 1} \cdot X_q \qquad (2.11)$$

the quadrature axis operational impedance.

Equation (2.9) may be written:-

$$X_d(p) = \frac{(1+T'_dp)(1+T''_dp)+(T_5-T''_d)p}{(1+T'_{do}p)(1+T''_{do}p)+(T_2-T''_{do})p} \cdot X_d \qquad (2.12)$$

since it may be shown[3]:-

$$T_6 = T''_d$$

$$T_4 = T'_d$$

$$T_3 = T''_{do}$$

$$T_1 = T'_{do}$$

Also,

$$X_q(p) = \frac{(1 + T''_qp)}{(1 + T''_{qo}p)} \cdot X_q \qquad (2.13)$$

where $T_7 = T''_q$

$$T_8 = T''_{qo}$$

In the case of the solid pole machine similar impedances $X_d(p)$, $X_q(p)$ exist. However because of the many current paths present in the solid iron the impedances cannot be expressed in terms of a few time constants and reactances.

2.3. THE DUALITY OF THE EQUIVALENT MAGNETIC CIRCUIT AND ELECTRIC CIRCUIT

2.3.1. The Development of the Equivalent Electric Circuit from the Equivalent Magnetic Circuit

Fig. 3a shows the direct axis magnetic circuit of a laminated pole machine, over one pole pitch. It may be replaced by the equivalent circuit of Fig. 3b. The laminated iron may be considered to have zero reluctance. The reluctances of the stator leakage path, air gap, squirrel cage leakage path, and field leakage path may be represented by equivalent air-gaps of reluctances S_a, S_g, S_{kd}, $S_{f\ell}$, respectively.

The equivalent iron circuits, Fig. 3b, may be redrawn as an analogous electric circuit, Fig.4a, the currents in the circuit being the fluxes, and the voltages the M.M.F's.

Since, in a synchronous motor, the stator voltage and frequency applied are usually fixed, the total flux linking the primary winding is fixed. Consequently, the M.M.F.'s required to maintain the fluxes adjust themselves accordingly. Thus, the equivalent

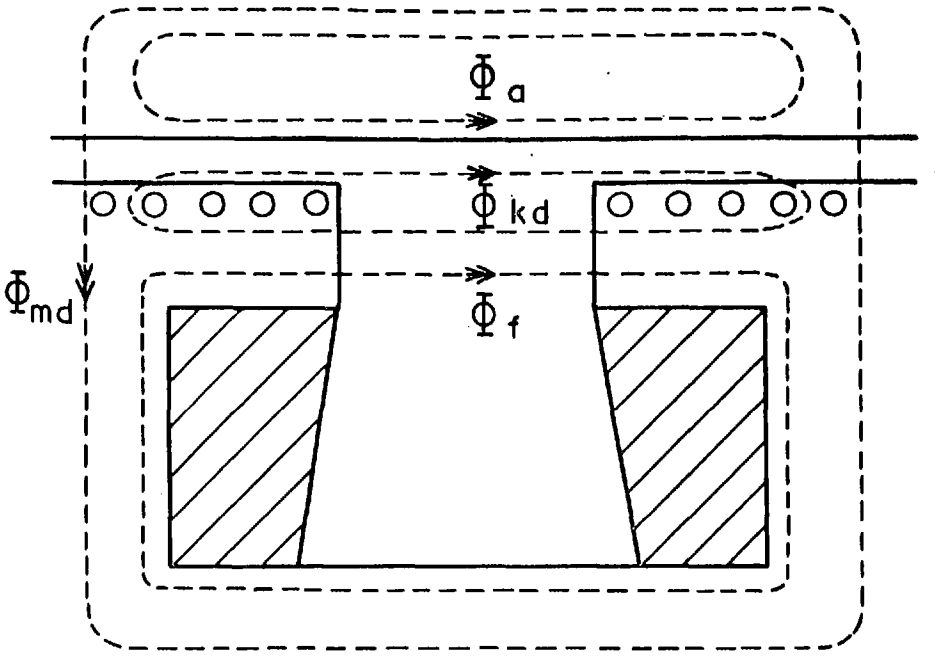

(a) Direct axis flux paths of a laminated pole motor

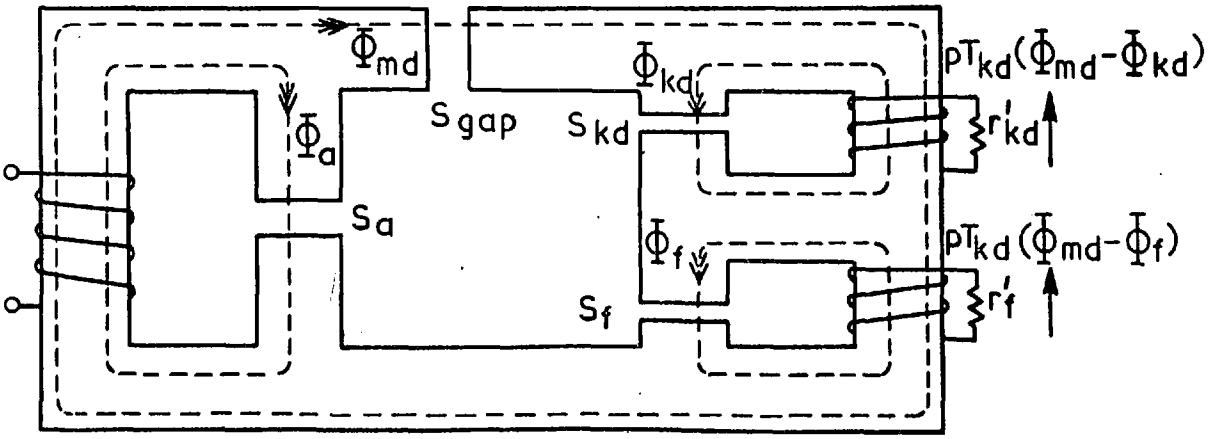

(b) Direct axis equivalent iron circuit of a laminated pole motor

Fig. 3.

circuit of Fig.4a is inconvenient to manipulate since the 'current' injected is to be fixed and the 'voltage' applied, which corresponds to the M.M.F., is unknown.

If the equivalent circuit of Fig.4a is inverted, so that all reluctances are replaced by 'reciprocal reluctances', then, retaining the same relationships between flux, M.M.F.,and reluctance, all series branches become parallel and vice versa. The new equivalent circuit is that of Fig.4b.

Fig. 4b is seen to be very similar to that derived previously from the equations, - (Fig.2a). If the reciprocal reluctances of Fig.4b are multiplied by the primary turns squared and by the winding factors etc, and also operated on by the operator 'p', the equivalent circuits of Fig.2a and Fig.4b become identical.

It is apparent, therefore, that the voltage across an impedance, in an equivalent circuit, is directly proportional to the rate of change of flux linking the component of the magnetic circuit, corresponding to that impedance. Under sinusoidally changing conditions the voltage across the impedance is directly proportional to the flux, and the current through the same impedance is directly proportional to the M.M.F. driving the flux through that component of the magnetic circuit.

The equivalent circuits of the solid pole machine are derived in a similar manner, in Part III.

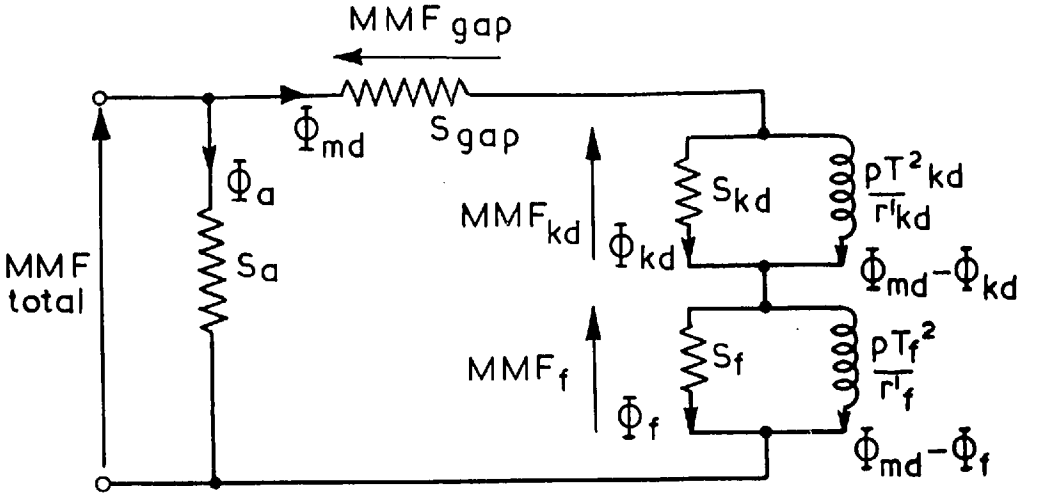

(a) Direct axis equivalent iron circuit as an electric circuit

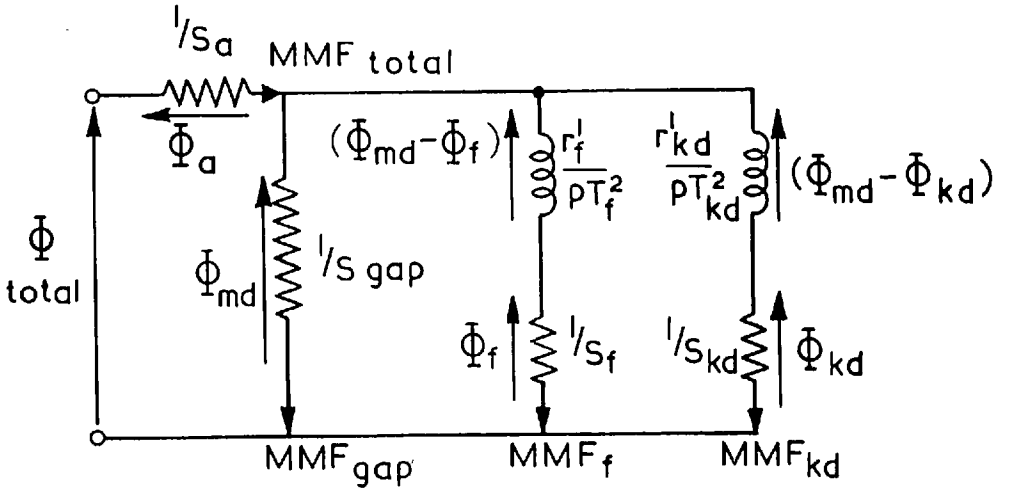

(b) Circuit of (a) inverted

Fig. 4.

2.3.2. The Relationship Between Equivalent Circuit Impedance and Magnetic Circuit Reluctance

Consider a section of material in a P-pole machine. Under sinusoidal conditions the flux, Φ', through it is given by:-

$$\Phi' = \frac{V'}{j\ 4.44\ k_{w2}\ f_o T}\ e^{js\omega_o t} \qquad (2.14)$$

where V' is the component of the primary voltage inducing it.

The component of primary M.M.F. required to maintain the the flux, Φ', is given by:-

$$\text{M.M.F.}' = \frac{2.12\ k_{w1}\ I'\ T}{P}\ e^{js\omega_o t} \qquad (2.15)$$

where I' is the appropriate proportion of the primary current.

The reluctance of the section of material is given by:-

$$S' = \frac{\text{Ampere-turns applied to the section}}{\text{Flux through it}}$$

$$= \frac{\text{M.M.F.}'}{\Phi'}$$

$$= \frac{j\ 9.42\ k_{w1}\ k_{w2}\ f_o\ T^2}{P} \cdot \frac{I'}{V'} \qquad (2.16)$$

Now, since V' and I' are both primary voltages and

currents, $\frac{V'}{I'}$ (= Z') is a primary referred impedance,

$$Z' = \frac{9.42\ k_{w1}\ k_{w2}\ f_o\ T^2}{P} \cdot j\ \frac{1}{S'} \qquad (2.17)$$

Z' is therefore inversely proportional to the iron reluctance, S'. In particular, Z', is the equivalent circuit impedance representing the reluctance S'.

$$Z' = j\ K\ \frac{1}{S'}$$

where

$$K = \frac{9.42\ k_{w1}\ k_{w2}\ f_c\ T^2}{P} \qquad (2.18)$$

k_{w1}, k_{w2} are combinations of winding factors, flux factors, etc.

2.4. ASYNCHRONOUS OPERATION AT CONSTANT SLIP

2.4.1. Transformed Basic Equations for Steady Asynchronous Running

Fig. 5 shows the position of the armature winding at time t. The axis of phase A is at angle θ to the direct axis and the instantaneous speed and acceleration of the windings are $\dot{\theta}$, and $\ddot{\theta}$, respectively.

Consider a reference axis rotating at constant velocity ω_o, in the anti-clockwise direction, and located so that it lies along the direct axis at time zero. The instantaneous angle between this reference and the axis of phase A is the load angle δ, by which the axis of phase A lags behind the reference. In accordance with this definition the angle δ is zero when the motor is unloaded.

Then

$$\theta = \omega_o t - \delta \qquad (2.19)$$

Using equation (2.19), the phase voltage v_a is given by

$$\begin{aligned} v_a &= V_m \cos \omega_o t \\ &= V_m \cos (\theta + \delta) \\ &= V_m \cos \theta \cos \delta - V_m \sin \theta \sin \delta \end{aligned} \qquad (2.20)$$

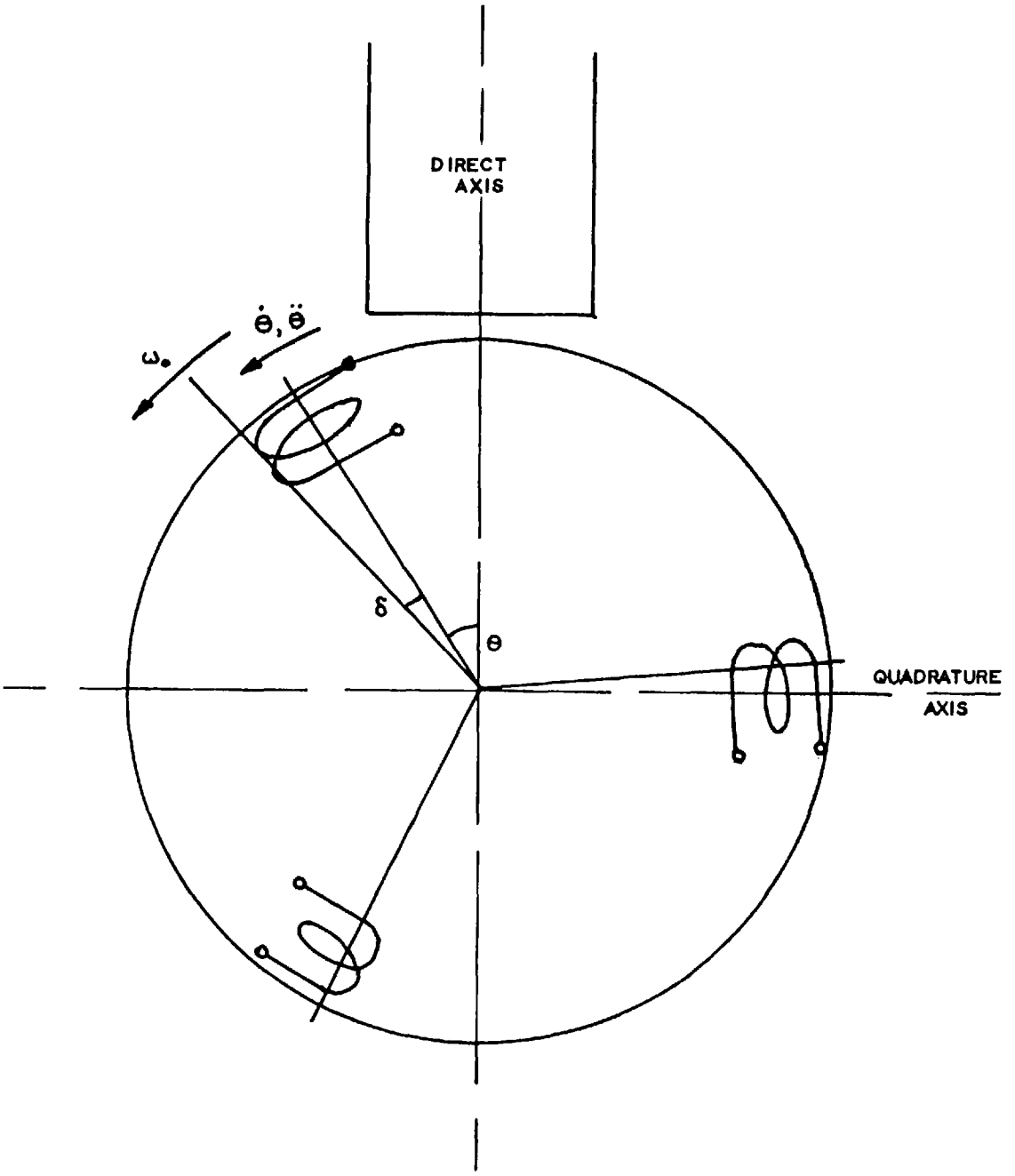

Fig. 5. The relationship between θ, δ and $\omega_o t$.

The inverse transformation relating the phase to axis quantities is:-

$$v_a = v_d \cos\theta + v_q \sin\theta \qquad (2.21)$$

Comparing equations (2.20) and (2.21)

$$\left.\begin{aligned} v_d &= V_m \cos\delta \\ v_q &= -V_m \sin\delta \end{aligned}\right\} \qquad (2.22)$$

During asynchronous running at constant slip s, θ becomes $(1-s)\omega_o t$, $\dot{\theta}$ becomes $(1-s)\omega_o$, and $\ddot{\theta}$ becomes zero.

Substituting in (2.19) gives:-

$$\delta = s\omega_o t$$

and hence equation (2.22) becomes:-

$$\left.\begin{aligned} v_d &= V_m \cos s\omega_o t \\ v_q &= -V_m \sin s\omega_o t \end{aligned}\right\} \qquad (2.23)$$

To convert the basic equations (2.2) into phasor form, p is replaced by $js\omega_o$. Thus the equations in phasor form become:-

$$\left.\begin{aligned} V &= js\omega_o \underline{\Psi}_d + (1-s)\omega_o \underline{\Psi}_q + r_a \underline{I}_d \\ jV &= -(1-s)\omega_o \underline{\Psi}_d + js\omega_o \underline{\Psi}_q + r_a \underline{I}_q \end{aligned}\right\} \qquad (2.24)$$

and

$$\left.\begin{aligned} X_d(js\omega_o) &= \omega_o \underline{\Psi}_d / \underline{I}_d \\ X_q(js\omega_o) &= \omega_o \underline{\Psi}_q / \underline{I}_q \end{aligned}\right\} \qquad (2.25)$$

where $\underline{\Psi}_d$, $\underline{\Psi}_q$, $\underline{I}_d$, $\underline{I}_q$ are phasors and V a scalor with magnitudes equal to the r.m.s. magnitudes.

It is more convenient when dealing with current and torque to use the operational impedance functions in their admittance form:-

$$\left.\begin{aligned} Y_d(js\omega_o) &= 1/X_d(js\omega_o) = A(js\omega_o)+jB(js\omega_o) \\ Y_q(js\omega_o) &= 1/X_q(js\omega_o) = C(js\omega_o)+jD(js\omega_o) \end{aligned}\right\} \qquad (2.26)$$

where $A(js\omega_o)$, $B(js\omega_o)$, $C(js\omega_o)$, $D(js\omega_o)$ are the respective real and imaginary components of the admittances at slip frequency $s\omega_o$. In further use these components will be written in the more concise form A, B, C, D.

Replacing p by $js\omega_o$ in equations (2.12), (2.13), $Y_d(js\omega_o)$, $Y_q(js\omega_o)$ for the laminated pole machine are:-

$$Y_d(js\omega_o) = \frac{(1+js\omega_o T'_{do})(1+js\omega_o T''_{do})+js\omega_o(T_2-T''_{do})}{(1+js\omega_o T'_d)(1+js\omega_o T''_d)+js\omega_o(T_5-T''_d)} \cdot {}^1/X_d \qquad (2.27)$$

$$Y_q(js\omega_o) = \frac{(1 + js\omega_o T''_{qo})}{(1 + js\omega_o T''_q)} \cdot {}^1/X_q \qquad (2.28)$$

The limiting values of these expressions are obtained when s = 0, and s = ∞.

When s = 0

$$Y_d(0) = 1/X_d$$

$$Y_q(0) = 1/X_q$$

when s = ∞

$$Y_d(\infty) = \frac{T'_{do} \cdot T''_{do}}{T'_d \cdot T''_d} \cdot {}^1/X_d = {}^1/X''_d \qquad (2.29)$$

the direct axis subtransient reactance

$$Y_q(\infty) = \frac{T''_{qo}}{T''_q} \cdot {}^1/X_q = {}^1/X''_q \qquad (2.30)$$

the quadrature axis subtransient reactance

In general, as s changes from zero to infinity, these functions describe a locus in the complex plane from $1/X_d$ to $1/X''_d$ in the case of the direct axis; and

from $1/X_q$ to $1/X''_q$ in the case of the quadrature axis. The operational admittances of a laminated pole machine, in fact, trace the locus of a semi-circle or combination of semi-circles as shown in Fig. (6). The loci of the laminated pole machine are discussed in more detail in chapter 6.

The operational admittance loci of the solid pole machine are somewhat different in both derivation and appearance. Chapter 10 deals, in detail, with the derivation of the equivalent circuits and the consequent admittance loci obtained over the complete frequency range.

If the two axis operational admittance frequency functions are known, over the complete frequency range, zero to infinity, it is theoretically possible to calculate the performance of the machine under all conditions. The theory of asynchronous operation, derived next, is one mode of operation that may be estimated using the functions.

2.4.2. Theory of asynchronous operation neglecting the effect of armature resistance

2.4.2.1. Phase A current

If $\omega_o \underline{\psi}_d$, $\omega_o \underline{\psi}_q$ are determined by solving equations (2.2) with the small armature resistance volt drop neglected, the following simple result is obtained:-

$$\left.\begin{aligned} \omega_o \underline{\psi}_d &= -jV \\ \omega_o \underline{\psi}_q &= V \end{aligned}\right\} \qquad (2.31)$$

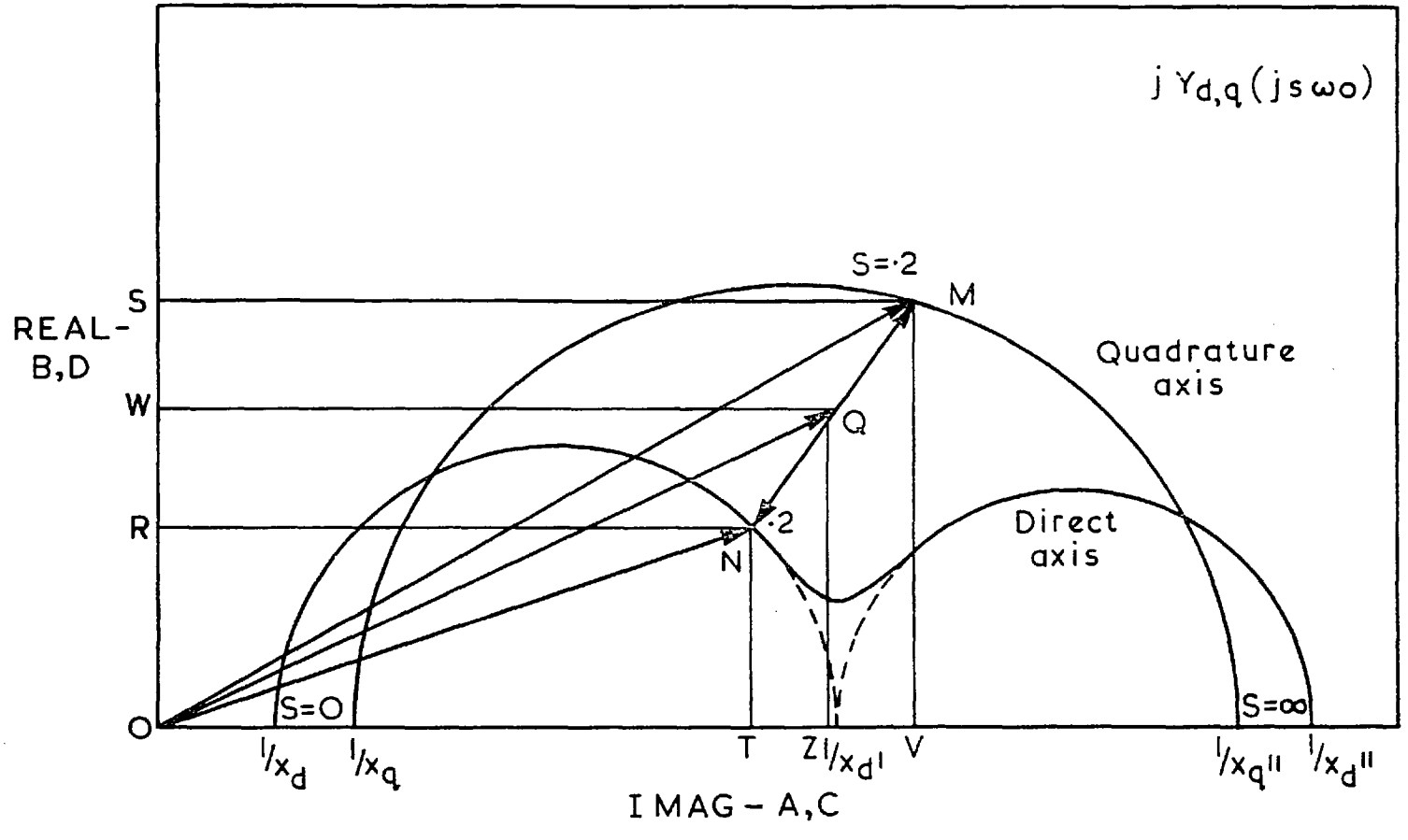

Fig. 6. The loci of a typical laminated pole motor

Using this simple derivation,

$$\left.\begin{aligned} \underline{I}_d &= -jV(A + jB) \\ \underline{I}_q &= V(C + jD) \end{aligned}\right\} \qquad (2.32)$$

from equations (2.25),(2.26),(2.31)

Thus

$$i_d = \sqrt{2}\ \mathrm{Re}\{-jV(A+jB)e^{js\omega_o t}\}$$

i.e.. $$i_d = V_m\ (A \sin s\omega_o t + B \cos s\omega_o t)$$

Similarly

$$i_q = V_m\ (C \cos s\omega_o t - D \sin s\omega_o t) \qquad (2.33)$$

Using the inverse transformation

$$i_a = i_d \cos\theta + i_q \sin\theta$$

i.e.

$$i_a = i_d \cos(1-s)\omega_o t + i_q \sin(1-s)\omega_o t \qquad (2.34)$$

and substituting i_d, i_q from equation (2.33) into (2.34) the instantaneous current in phase A becomes:-

$$i_a = V_m \left[\frac{B+D}{2} \sin \omega_o t - \frac{A+C}{2} \cos \omega_o t + \frac{D-B}{2} \sin(1-2s)\omega_o t + \frac{C-A}{2} \cos(1-2s)\omega_o t \right] \qquad (2.35)$$

2.4.2.2. Phase and total input power

The instantaneous power entering phase A is given by the product of the instantaneous phase current and phase voltage.

$$w_a = V_m^2 \sin \omega_o t \left[\frac{B+D}{2} \sin \omega_o t - \frac{A+C}{2} \cos \omega_o t + \frac{D-B}{2} \sin(1-2s)\omega_o t + \frac{C-A}{2} \cos(1-2s)\omega_o t\right]$$

$$= \frac{V_m^2}{4} \left[(B+D)+(B+D) \cos 2\omega_o t - (A+C) \sin 2\omega_o t -(D-B) \cos 2s\omega_o t - (C-A) \sin 2s\omega_o t +(D-B) \cos 2(1-s)\omega_o t +(C-A) \sin 2(1-s)\omega_o t\right] \quad .. (2.36)$$

However when the total power W, is obtained by adding the three phase powers, the terms of twice supply frequency and twice speed frequency vanish:-

$$W = \frac{V_m^2}{4} \left[(B+D)+(A-C) \sin 2s\omega_o t +(B-D) \cos 2s\omega_o t\right] \quad .. (2.37)$$

2.4.2.3. Output torque

The basic instantaneous torque equation is given by:-

$$T_e = \frac{\omega_o}{2} (\psi_q i_d - \psi_d i_q) \quad (2.3)$$

Neglecting armature resistance, r_a , i_d and i_q

are given by equations (2.28), and:-

$$\left.\begin{aligned} \omega_o\psi_d &= \sqrt{2}\ \mathrm{Re}\left\{-jV\ e^{js\omega_o t}\right\} = V_m \sin s\omega_o t \\ \omega_o\psi_q &= \sqrt{2}\ \mathrm{Re}\left\{\ V\ e^{js\omega_o t}\right\} = V_m \cos s\omega_o t \end{aligned}\right\}$$

from eqn. (2.31)

Hence substituting in (3)

$$T_e = 1/2\left[V_m \cos s\omega_o t . V_m(A\sin s\omega_o t + B\cos s\omega_o t)\right.$$

$$\left. - V_m \sin s\omega_o t .\ V_m(C\cos s\omega_o t - D\sin s\omega_o t)\right]$$

$$T_e = \frac{V_m^2}{4}\left[(B+D)+(A-C)\sin 2s\omega_o t + (B-D)\cos 2s\omega_o t\right].$$

.. (2.38)

Since the armature resistance is neglected and the theory ignores stator iron loss, the p.u. output torque equals the p.u. input power, the expression for which is derived in the previous section 2.4.2.2. given by equation (2.37).

2.4.2.4. Graphical determination of the torques, currents, and power factors from the operational admittance loci

A typical pair of admittance loci for a laminated pole machine is shown in Fig. 6. The torque, at a given slip, during asynchronous running, can be determined by the following graphical method. The points marked on the loci are for a slip of .2 p.u. The direct axis

current and voltage vary sinusoidally at a slip frequency corresponding to this slip, and the direct axis operational admittance, for this condition, is the vector ON. The ordinate NT is 'B', and the abscissa NR is 'A'. Similarly OM is the quadrature axis operational admittance vector. The ordinate MV is 'D' and the abscissa MS is 'C'.

$$\text{Thus } SR = (B - D)$$
$$VT = (A - C)$$
$$\text{so } MN = \sqrt{\left[(B - D)^2 + (A - C)^2\right]}$$

Q bisects MN:-

$$WQ = (A + C)/2$$
$$ZQ = (B + D)/2$$
$$\text{so } OQ = \sqrt{\left[\frac{(A + C)^2}{2} + \frac{(B + D)^2}{2}\right]}$$

Comparing these results with equations (2.35), (2.38) the following per unit values are obtained if the applied voltage is 1 p.u. ($V_m = \sqrt{2}$).

ZQ	=	Mean torque.
MN	=	Peak to Peak oscillating torque.
OQ	=	R.M.S. supply frequency component of phase current.
MN/2	=	R.M.S. component of current at frequency $(1-2s)\omega_o$.

Furthermore, the direct axis power factor is given by:-

NT/ON

The quadrature axis power factor is given by:-

MV/OM

and the phase power factor is given by:-

QZ/OQ

2.4.3. Theory of Asynchronous Operation Including the Effect of Armature Resistance.

2.4.3.1. Phase current.

Equations (2.24) may be written:-

$$\left.\begin{aligned} V &= \omega_{o}\underline{\psi}_{d}(js+r_a Y_d) + \omega_{o}\underline{\psi}_{q}(1-s) \\ jV &= -\omega_{o}\underline{\psi}_{d}(1-s) + \omega_{o}\underline{\psi}_{q}(js+r_a Y_q) \end{aligned}\right\} \quad (2.39)$$

from eqns. (2.25), (2.26)

Solving for $\omega_{o}\underline{\psi}_{d}$, $\omega_{o}\underline{\psi}_{q}$ gives:-

$$\omega_{o}\underline{\psi}_{d} = -jV\left[\frac{(1-2s) + jr_a Y_q}{(1-2s) + jsr_a(Y_q+Y_d)+r_a^2 Y_q Y_d}\right] \quad .. \quad (2.40)$$

$$\omega_{o}\underline{\psi}_{q} = V\left[\frac{(1-2s) + jr_a Y_d}{(1-2s) + jsr_a(Y_q+Y_d)+r_a^2 Y_q Y_d}\right] \quad .. \quad (2.41)$$

Substituting the complex components of Y_d, Y_q from equation (2.26), the real and imaginary parts of $\omega_{o}\underline{\psi}_{d}$, $\omega_{o}\underline{\psi}_{q}$ may be obtained:-

$$\mathrm{Re}(\omega_{o\perp d}) = \frac{V}{|\Delta|^2}\left[\frac{r_a}{(1-2s)}C - \frac{sr_a}{(1-2s)}(A+C) - \frac{r_a^2}{(1-2s)}(BC+AD) - \frac{sr_a^2}{(1-2s)^2}(BC-AD) + \frac{r_a^3}{(1-2s)^2}A(C^2+D^2)\right] \quad .. (2.42)$$

$$\mathrm{Im}(\omega_{o\perp d}) = \frac{V}{|\Delta|^2}\left[-1 + \frac{r_a}{(1-2s)}D + \frac{sr_a}{(1-2s)}(B+D) - \frac{r_a^2}{(1-2s)}(AC-BD) - \frac{sr_a^2}{(1-2s)^2}(C^2+D^2+AC+BD) - \frac{r_a^3}{(1-2s)^2}B(C^2+D^2)\right] \quad .. (2.43)$$

$$\mathrm{Re}(\omega_{o\perp q}) = \frac{V}{|\Delta|^2}\left[1 - \frac{r_a}{(1-2s)}B - \frac{sr_a}{(1-2s)}(B+D) + \frac{r_a^2}{(1-2s)}(AC-BD) + \frac{sr_a^2}{(1-2s)^2}(A^2+B^2+AC+BD) - \frac{r_a^3}{(1-2s)^2}D(A^2+B^2)\right] \quad .. (2.44)$$

$$\mathrm{Im}(\omega_{o\perp q}) = \frac{V}{|\Delta|^2}\left[\frac{r_a}{(1-2s)}A - \frac{sr_a}{(1-2s)}(A+C) - \frac{r_a^2}{(1-2s)}(BC+AD) + \frac{sr_a^2}{(1-2s)^2}(BC-AD) + \frac{r_a^3}{(1-2s)^2}C(A^2+B^2)\right] \quad .. (2.45)$$

where

$$|\Delta|^2 = \left[1 - \frac{sr_a}{(1-2s)}(B+D) + \frac{r_a^2}{(1-2s)}(AC-BD)\right]^2 + \left[\frac{sr_a}{(1-2s)}(A+C) + \frac{r_a^2}{(1-2s)}(AD+BC)\right]^2 \quad (2.46)$$

Using equations (2.25), (2.26)

$$\left.\begin{aligned} \underline{I}_d &= \omega_o \underline{\Psi}_d \quad (A + jB) \\ \underline{I}_q &= \omega_o \underline{\Psi}_q \quad (C + jD) \end{aligned}\right\} \quad (2.47)$$

i.e.

$$\left.\begin{aligned} \underline{I}_d &= [\mathrm{Re}(\omega_o \underline{\Psi}_d).A - \mathrm{Im}(\omega_o \underline{\Psi}_d).B] \\ &+ j[\mathrm{Im}(\omega_o \underline{\Psi}_d).A + \mathrm{Re}(\omega_o \underline{\Psi}_d).B] \\ \underline{I}_q &= [\mathrm{Re}(\omega_o \underline{\Psi}_q).C - \mathrm{Im}(\omega_o \underline{\Psi}_q).D] \\ &+ j[\mathrm{Im}(\omega_o \underline{\Psi}_q).C + \mathrm{Re}(\omega_o \underline{\Psi}_q).D] \end{aligned}\right\} \quad (2.48)$$

The instantaneous values of axis currents are then obtained in a similar manner to that in section 2.4.2.1. They are:-

$$
\left.
\begin{aligned}
i_d &= V_m \left[-B. \frac{\mathrm{Re}(\omega_o \underline{\psi}_d)}{V} - A. \frac{\mathrm{Im}(\omega_o \underline{\psi}_d)}{V} \right] \sin s\omega_o t \\
&+ V_m \left[A. \frac{\mathrm{Re}(\omega_o \underline{\psi}_d)}{V} - B. \frac{\mathrm{Im}(\omega_o \underline{\psi}_d)}{V} \right] \cos s\omega_o t \\
i_q &= V_m \left[C. \frac{\mathrm{Re}(\omega_o \underline{\psi}_q)}{V} - D. \frac{\mathrm{Im}(\omega_o \underline{\psi}_q)}{V} \right] \cos s\omega_o t \\
&- V_m \left[C. \frac{\mathrm{Im}(\omega_o \underline{\psi}_q)}{V} + D. \frac{\mathrm{Re}(\omega_o \underline{\psi}_q)}{V} \right] \sin s\omega_o t
\end{aligned}
\right\}
$$

.. (2.49)

Comparing i_d, i_q of equations (2.49) with those of (2.35) it is observed that:-

$$
\left.
\begin{aligned}
&\text{A is replaced by} \quad -A. \frac{\mathrm{Im}(\omega_o \underline{\psi}_d)}{V} \; -B. \frac{\mathrm{Re}(\omega_o \underline{\psi}_d)}{V} \\
&\text{B is replaced by} \quad -B. \frac{\mathrm{Im}(\omega_o \underline{\psi}_d)}{V} \; +A. \frac{\mathrm{Re}(\omega_o \underline{\psi}_d)}{V} \\
&\text{C is replaced by} \quad C. \frac{\mathrm{Re}(\omega_o \underline{\psi}_q)}{V} \; -D. \frac{\mathrm{Im}(\omega_o \underline{\psi}_q)}{V} \\
&\text{D is replaced by} \quad D. \frac{\mathrm{Re}(\omega_o \underline{\psi}_q)}{V} \; +C. \frac{\mathrm{Im}(\omega_o \underline{\psi}_q)}{V}
\end{aligned}
\right\}
$$

.. (2.50)

Thus the solution for the phase current, including the effect of armature resistance, is that of equation (2.35), with the substitution of (2.50).

N.B. If r_a is zero it is seen from equations (2.42 ... 2.45) that

$$\left.\begin{aligned} \mathrm{Re}(\omega_o \underline{\psi}_d) &= 0 \\ \mathrm{Im}(\omega_o \underline{\psi}_d) &= -V \end{aligned}\right\} \quad \text{and} \quad \left.\begin{aligned} \mathrm{Re}(\omega_o \underline{\psi}_q) &= V \\ \mathrm{Im}(\omega_o \underline{\psi}_q) &= 0 \end{aligned}\right\}$$

and the substitution (2.45) reverts to A, B, C, and D as expected.

2.4.3.2. Phase and total input power

The instantaneous input power is obtained by the product of the instantaneous current and voltage. The instantaneous input power to phase A is:-

$$w_a = i_a . v_a$$

$$= i_a . V_m \sin \omega_o t$$

The solution for the phase and total instantaneous input power is identical to that given in equations (2.36), (2.37) with again the substitution of (2.50).

2.4.3.3. Output torque

The basic electromagnetic torque of the machine, T_e, is given by equation (2.3). The instantaneous torque may be most conveniently found by first obtaining the torque in complex form, by the phasor multiplication given by:-

$$T_e = \frac{\omega_o}{2} (\underline{\psi}_q^* . \underline{I}_d - \underline{\psi}_d^* . \underline{I}_q)$$

Now if $\omega_o \underline{\psi}_q^* . \underline{I}_d = U + jV$

$$\text{then} \quad U = \frac{V^2}{|\Delta|^2}\left[B - \frac{r_a}{(1-2s)}(A^2+B^2-AC+BD) + \right.$$

$$\left. + \frac{r_a^2}{(1-2s)^2} D(A^2+B^2)\right] \quad .. \quad (2.51)$$

$$V = \frac{V^2}{|\Delta|^2}\left[-A + \frac{r_a}{(1-2s)}(BC+AD) - \right.$$

$$\left. - \frac{r_a^2}{(1-2s)^2} C(A^2+B^2)\right] \quad .. \quad (2.52)$$

from equations (2.40),(2.41),(2.25), and (2.26)

Furthermore if

$$\omega_o \underline{\psi}_q = \hat{\omega_o \underline{\psi}}_q \cos(s\omega_o t + \delta_1)$$

$$\text{where} \quad \delta_1 = \tan^{-1} \frac{Re(\omega_o \underline{\psi}_q)}{Im(\omega_o \underline{\psi}_d)}$$

and $\quad i_d = I_{dm} \cos(s\omega_o t + \delta_1 + \varphi)$

the instantaneous value of $\omega_o \psi_q . i_d$ can be shown to be given by:-

$$\omega_p \psi_q . i_d = U + U\cos 2(s\omega_o t + \delta_1) - V\sin 2(s\omega_o t + \delta_1) \quad .. \quad (2.53)$$

Similarly

$$\omega_o \psi_q . i_d = R + R\cos 2(s\omega_o t + \delta_2) - S\sin 2(s\omega_o t + \delta_2)$$

where $R = -\frac{V^2}{|\Delta|^2}\left[D - \frac{r_a}{(1-2s)}(A^2+B^2-AC+BD) + \frac{r_a^2}{(1-2s)^2}D(A^2+B^2)\right]$

$S = \frac{V^2}{|\Delta|^2}\left[C - \frac{r_a}{(1-2s)}(BC+AD) + \frac{r_a^2}{(1-2s)^2}A(C^2+D^2)\right]$

and $\delta_2 = \tan^{-1}\frac{Im(\omega_o \underline{\psi}_d)}{Re(\omega_o \underline{\psi}_d)}$

The instantaneous torque T_e is then given by

$$T_e = \tfrac{1}{2}\left[(U-R)+U\cos 2(s\omega_o t + \delta_1) - V \sin 2(s\omega_o t+\delta_1) - R\cos 2(s\omega_o t + \delta_2) + S \sin 2(s\omega_o t+\delta_2)\right]$$

This simplifies to:-

$$T_e = \tfrac{1}{2}\left[(U-R)+(U\cos 2\delta_1 - V\sin 2\delta_1 - R\cos 2\delta_2 + S\sin 2\delta_2)\cos 2s\omega_o t - (U\sin 2\delta_1 + V\cos 2\delta_1 - R\sin 2\delta_2 - S\cos 2\delta_2)\sin 2s\omega_o t)\right] \quad .. (2.54)$$

The expression for instantaneous torque differs from that of the instantaneous power, if the armature resistance is included in the

derivation.

The instantaneous output torque is calculated from:-

$$T_e = \tfrac{1}{2}(\omega_o \psi_q . i_d - \omega_o \psi_d . i_q)$$

whereas the instantaneous input power is calculated from:-

$$W = \tfrac{1}{2}(v_d . i_d + v_q . i_q)$$

If armature resistance is neglected then:-

$$\omega_o \psi_q = v_d$$

$$\omega_o \psi_d = -v_q$$

and the expressions for instantaneous input power and output torque are identical.

2.4.3.4. The effects of armature resistance on the torques and currents over the half speed region.

The equations derived in the previous three sections determine input current, input power and output torque of a synchronous machine, if the operational admittances of the machine are known. The equations are so complicated, when the effect of armature resistance is allowed for, that observation of them gives the reader no indication as to how the torques, currents and power of the machine vary with changing slip. It is noticed, however, that terms of the type $r_a/(1-2s)$ do

appear frequently, and hence it is easily seen that as s approaches .5, these terms attain infinite magnitude.

In order to determine the torques and currents with varying slip the equations were programmed on a computer.

Fig. 7 shows curves of mean torque against slip for a synchronous machine, with the field short circuited, for different values of armature resistance. The range of values is from approximately 1/7 winding resistance to about 7 times the winding resistance. The curve with zero armature resistance is also shown for comparison.

It is observed that the effect of armature resistance is to increase the mean torque before half speed and to reduce it after half speed. Although the maximum value of torque before, and the minimum value of torque after, half speed appear to be unaltered by the value of resistance in the calculation, it is clearly seen that the slip, over which the increase and decrease are effective, changes very considerably with variation of armature resistance. As the value of armature resistance is decreased the 'dip' becomes steeper, until, at zero value of resistance, the dip disappears.

Fig. 8 shows that, with the field an open circuit, the extent of the half speed dip is much less. This is because, at half speed, the sal-

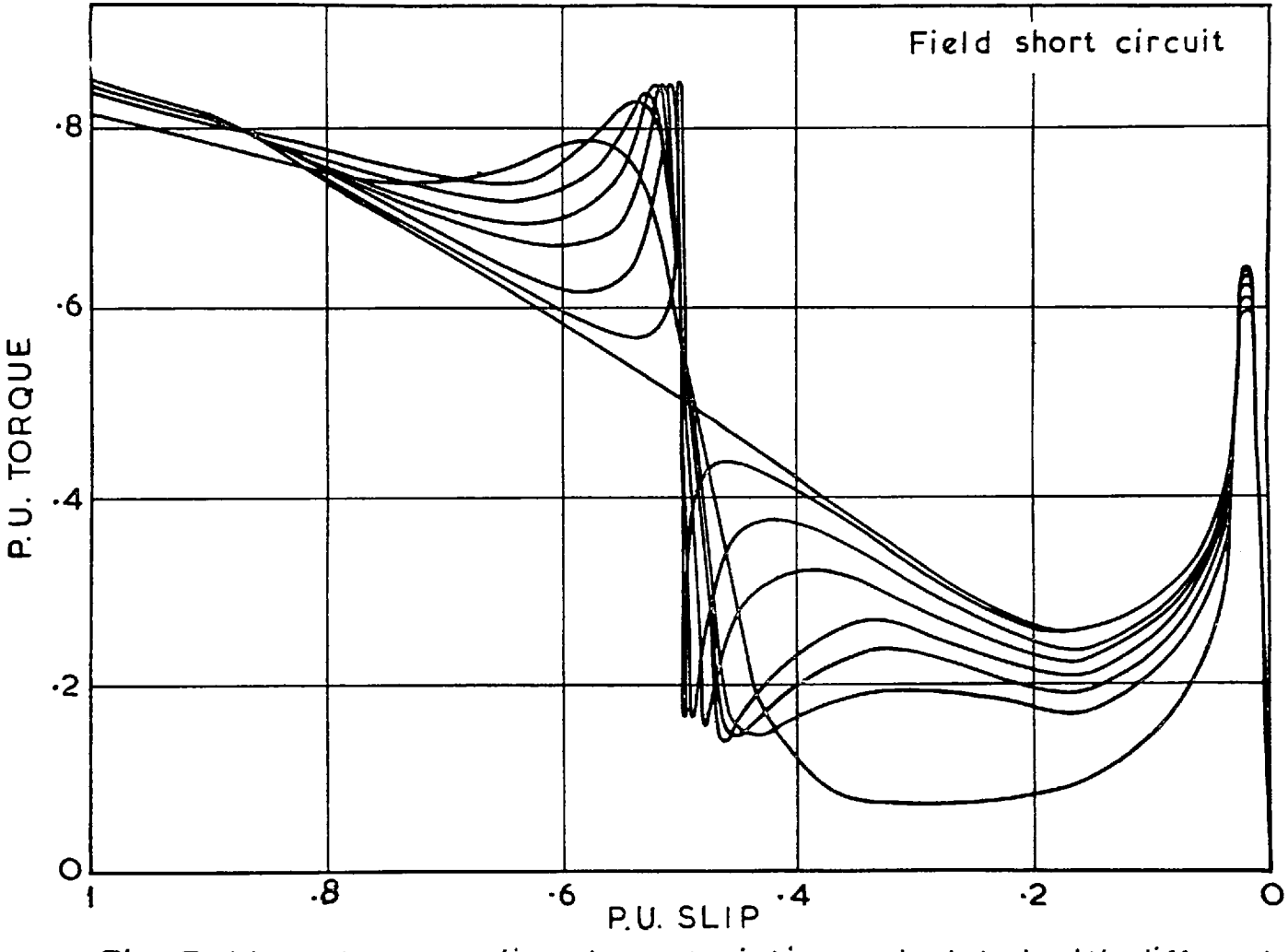

Fig. 7 Mean torque-slip characteristics calculated with different values of armature resistance

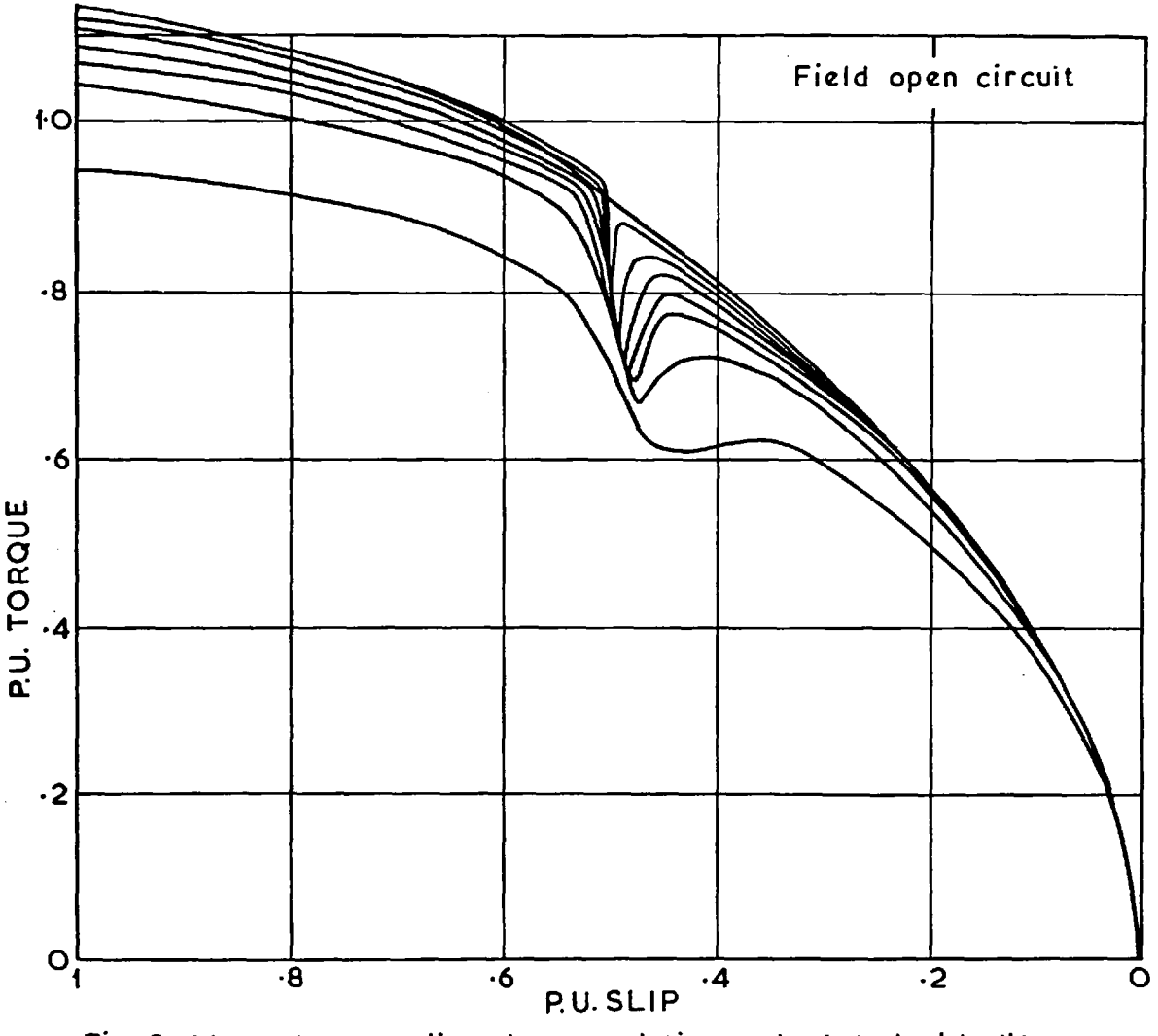

Fig. 8 Mean torque-slip characteristics calculated with different values of armature resistance

iency of this particular machine is the least with its field on open circuit, i.e. with this connection of the main field there is the least vector difference between the direct and quadrature axis operational admittance vectors.

The conclusions are that the saliency of the machine, as just defined, determines the magnitude of the dip, whereas the value of armature resistance determines the extent of the slip over which the dip is present.

A further, more obvious effect of increase of armature resistance, is to reduce the mean output torque, for a given applied voltage, due to the reduction of the main flux.

Similar, but less serious, half speed dips, due to armature resistance, also occur in the characteristics of oscillating component of torque, and of current.

It was shown, empirically, using the computer, that if saliency is defined as $|\overline{Y}_d - \overline{Y}_q|/|\overline{Y}_d + \overline{Y}_q|$ and the dip expressed as, maximum to minimum magnitude of the dip in the mean torque, divided by $|\overline{Y}_d + \overline{Y}_q|$, all in p.u. then:-

$$\text{Dip} \approx (\text{Saliency})^2$$

i.e. a simple rule is obtained to determine, at the design stages, the severity of the dip there is liable to be in the mean torque - speed characteristic of a machine.

CHAPTER 3

METHODS OF OBTAINING THE OPERATIONAL ADMITTANCE FREQUENCY LOCI BY MEASUREMENT

Several methods have been proposed and applied to obtain the operational admittance frequency loci of a synchronous machine by measurement.

The most well known and certainly the most reliable method is the variable frequency static impedance test. More recently a method of obtaining the axis currents and voltages has been derived using the technique of brightening the electron beam of an oscilloscope, displaying the phase current and voltage, at the instants when the axis currents and voltages are equal to the phase values. In this way the axis currents and voltages are distinguished. This method, however, can only satisfactorily be used at low slips, and consequently only a very small part of the loci can be obtained.

Two new methods are discussed here; the axis resolution method which is a new method of obtaining the axis quantities by dynamically resolving the phase quantities; and the dynamic admittance test which follows the same principle as the spot brightening method but is applicable over the whole frequency range.

The parameters obtained from the sudden short circuit tests can be used to derive the admittance loci of the laminated pole type of machine. However, this is an indirect method and does not give very accurate results.

3.1. THE VARIABLE FREQUENCY STATIC IMPEDANCE TEST

The variable frequency static impedance test is a measure of the complex impedance when a variable frequency single phase supply is applied to two phases connected in series, and the rotor is locked at standstill. If the rotor is locked in such a position that the induced voltage in the field winding is a maximum, the direct axis operational admittance may be calculated[20] from:-

$$\frac{V}{2I} = r_a + js/Y_d(js\omega_o) \qquad (3.1)$$

where V is the voltage applied, and I the current through, the two phases in series. $s\omega_o$ is the frequency of application.

Similarly, if the rotor is locked electrically at right angles to this position zero voltage is induced in the field winding, and the quadrature axis impedance may be calculated according to a similar equation to (3.1).

The supply is usually obtained from an alternator of similar or larger capacity to the machine under test, driven by a D.C. machine. The control of speed, and hence frequency, of the set may be by Ward-Leonard control, the set being electrically coupled to another motor-generator set. In this manner a steady frequency supply may be obtained from approximately normal supply frequency to 5 c/s.

3.2. THE AXIS RESOLUTION METHOD

3.2.1. Principle of the Method

The axis resolution method is a new method of obtaining the operational admittance frequency loci. The phase currents and voltages are dynamically resolved into their equivalent axis counterparts. The axis quantities are recorded and the admittances are calculated, at the required frequency, from the recordings.

Unlike the static impedance method, the axis resolution method is a method of obtaining the operational admittance loci during asynchronous running, and hence it is likely to produce more reliable results in the prediction of the same performance. A brief outline of the method, which is due to Edwards,[4] is given here.

The resolution is carried out by two small high precision machines, one resolving the current and the other the voltage. Each 2-pole machine has a distributed three-phase winding on the stator, a uniform air-gap, and a round rotor on which is wound a distributed two-phase winding. The terminations of the two phase rotor windings are brought out of the machine via silver brushes and stainless steel sliprings.

Plate 1 shows a view of the resolvers and gear train in their housing, with cover removed. The gear train, whose ratio may be easily changed, is to ensure that both the test machine and the resolver machines rotate at equal pole speeds.

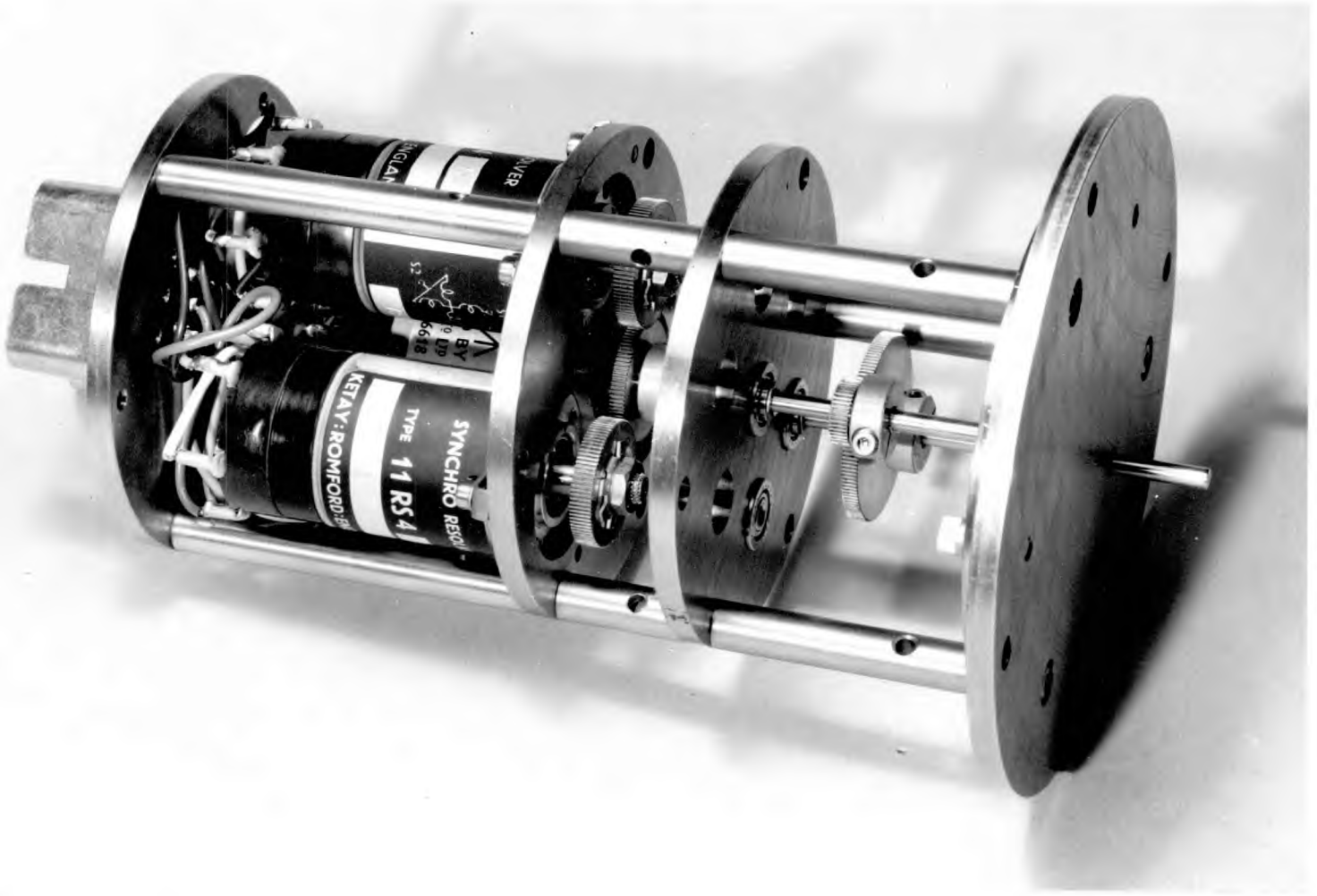

Plate 1 The resolver unit showing the resolver machines and gear train

Consider the current resolving machine. Suppose that the stator three-phase windings are fed with currents:-

$$\left.\begin{aligned} i_a &= \hat{I} \cos(\omega_o t) \\ i_b &= \hat{I} \cos(\omega_o t - 2\pi/3) \\ i_c &= \hat{I} \cos(\omega_o t - 4\pi/3) \end{aligned}\right\} \qquad (3.2)$$

and the rotor is rotated at speed $(1-s)\omega_o t$. If the magnetising current may be neglected the outputs of the rotor windings M, N are:-

$$\left.\begin{aligned} i_m &= \hat{I} \cos(s\omega_o t + \theta_o) \\ i_n &= \hat{I} \cos(s\omega_o t + \pi/2 + \theta_o) \end{aligned}\right\} \qquad (3.3)$$

- in order that the stator and rotor M.M.F.'s balance at any instant. θ_o is the angle between rotor winding M and the stator winding of phase A at time zero.

If θ_o is made zero then:-

$$\left.\begin{aligned} i_m &= \hat{I} \cos s\omega_o t \\ i_n &= \hat{I} \sin s\omega_o t \end{aligned}\right\} \qquad (3.4)$$

In particular if the input currents are of the form described by equation 2.35, with corresponding i_b, i_c - the phase currents of a salient pole synchronous machine running asynchronously at slip s, then:-

$$\left.\begin{aligned} i_m &= V_m (A \sin s\omega_o t + B \cos s\omega_o t) = i_d \\ i_n &= V_m (C \cos s\omega_o t - D \sin s\omega_o t) = i_q \end{aligned}\right\} \quad (3.5)$$

- the axis currents of the machine.

It can be seen, therefore, that subject to the approximation mentioned above, the resolving machine is able to perform the transformation of phase currents to axis currents, as defined in equation (2.1). If the three currents, that are fed into the resolving machine, are proportions of the phase currents of the machine to be tested; if the rotor of the resolving machine is mechanically coupled to the rotor of the test machine, so that the rotors travel at the same pole speed; and, if θ_o is adjusted to zero; then, during asynchronous running, the output of the resolver two-phase windings are signals proportional to the two axis currents of the test machine. Similarly, if proportions of the phase voltages of the test machine, are current-fed into the three-phase windings of the second resolver machine, and the same conditions apply, as above, the output of the second resolver two-phase windings are signals proportional to the axis voltages of the test machine.

The axis output signals from the resolvers may be either recorded, or after suitable amplification, measured using ammeters and voltmeters. After prior calibration, discussed later, the magnitude of the operational admittances may be calculated as the ratio of the appropriate axis current and voltage. The angle of the admittances may be obtained using either elec-

tronic multipliers, or after amplification, wattmeters.

The method of resolution, as previously mentioned, is subject to the approximation of neglecting the magnetising current in the resolvers. Clearly, at low slips, the magnetising current becomes increasingly important. It can be easily shown[4] that the ratio of secondary current, i_2, to primary current, i_1, in the resolver is given by:-

$$\frac{i_2}{i_1} = \frac{jX_m}{j(X_2+X_m)+r_2/s} \qquad (3.6)$$

where X_m is the magnetising reactance,
X_2 is the rotor winding leakage reactance
and r_2 is the rotor winding resistance
- of the resolver machines

As 's' approaches zero the "response" of the resolver falls to zero. However, the slip at which the response starts to seriously fall can be reduced by artificially increasing X_2. This was done by introducing external inductance in series with each of the two-phase secondary windings. The response of the resolvers was then constant to a slip of .01.

3.2.2. Application of the Test

Because the resolution takes place dynamically the transformation of phase to axis quantities can take place during a single motor start from either standstill or from minus full speed. The axis signals,

which are recorded using an ultra-violet recorder, are the direct and quadrature axis voltage and current, and the direct and quadrature axis powers obtained by the product of the respective voltage and current, using Hall effect multipliers. Fig. 9 shows the schematic arrangement for the test. A photograph, plate 2, shows the resolver gear coupled to a large machine using a toothed belt. An accelerometer is coupled directly to the shaft of the large machine.

The first part of the test procedure, which is the alignment of the resolver rotors with that of the test machine, is done using the principle of the single phase static impedance test. It can be shown[20] that if the rotor of the test machine is set up in the quadrature axis position, the current and voltage of one of the supplied phases are equal to $\sqrt{3}/2$ of the quadrature axis current and voltage respectively. In this situation both the direct axis current and voltage are zero. The stators of the two resolving machines are, thus, each rotated so that the output from one rotor winding is zero and the other consequently a maximum. The secondary windings of the two resolving machines having zero output represent the direct axis, and the other pair the quadrature axis. The resolver stators are locked in this position.

The calibration, which is the second part of the test procedure, is carried out immediately after the alignment, while the test machine is still set up for the static impedance test. Since it is known that the axis current and voltage are $2/\sqrt{3}$ times the phase values in this test, the calibration is easily performed by re-

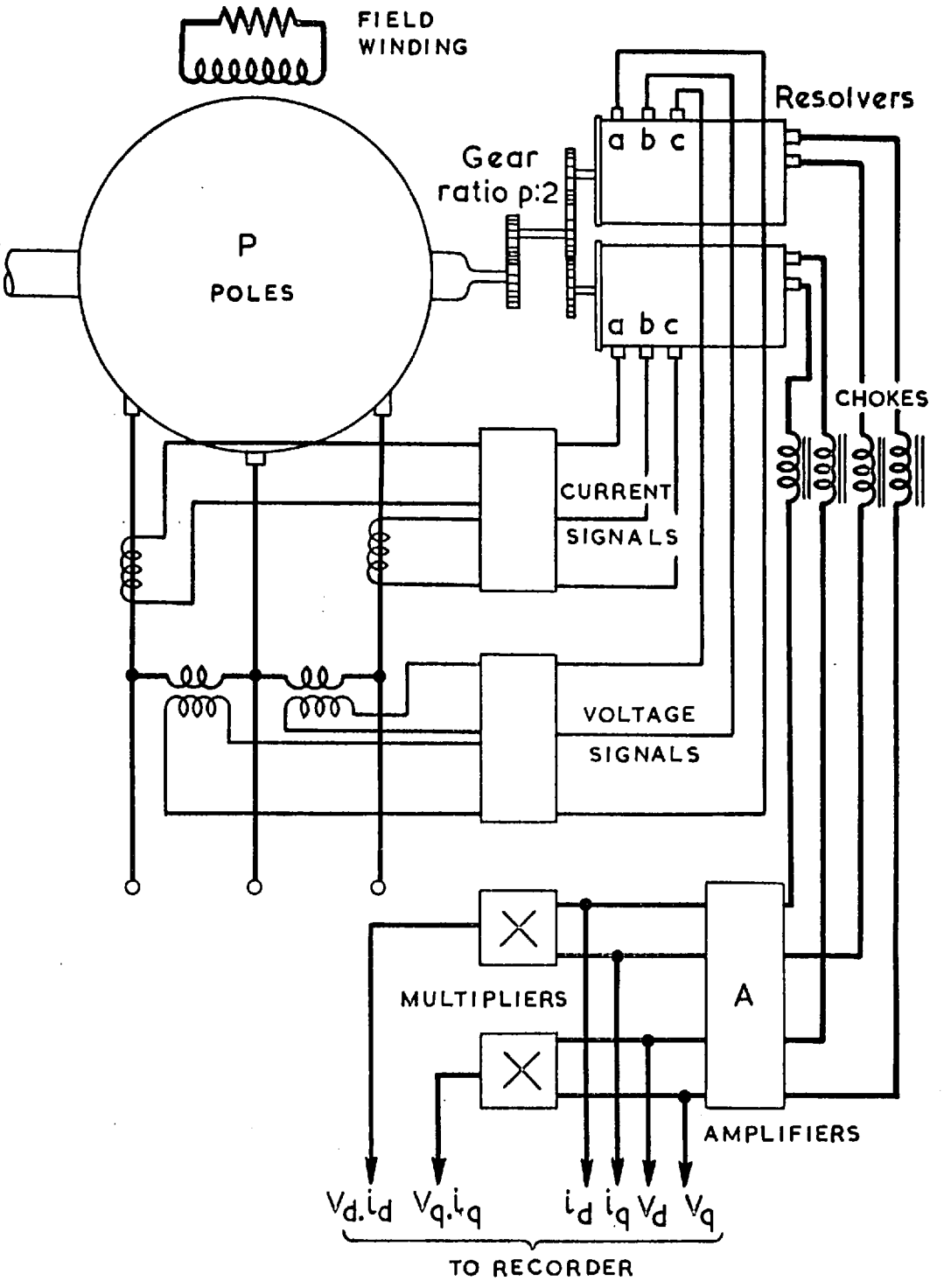

Fig. 9. Schematic arrangement for the axis resolution test

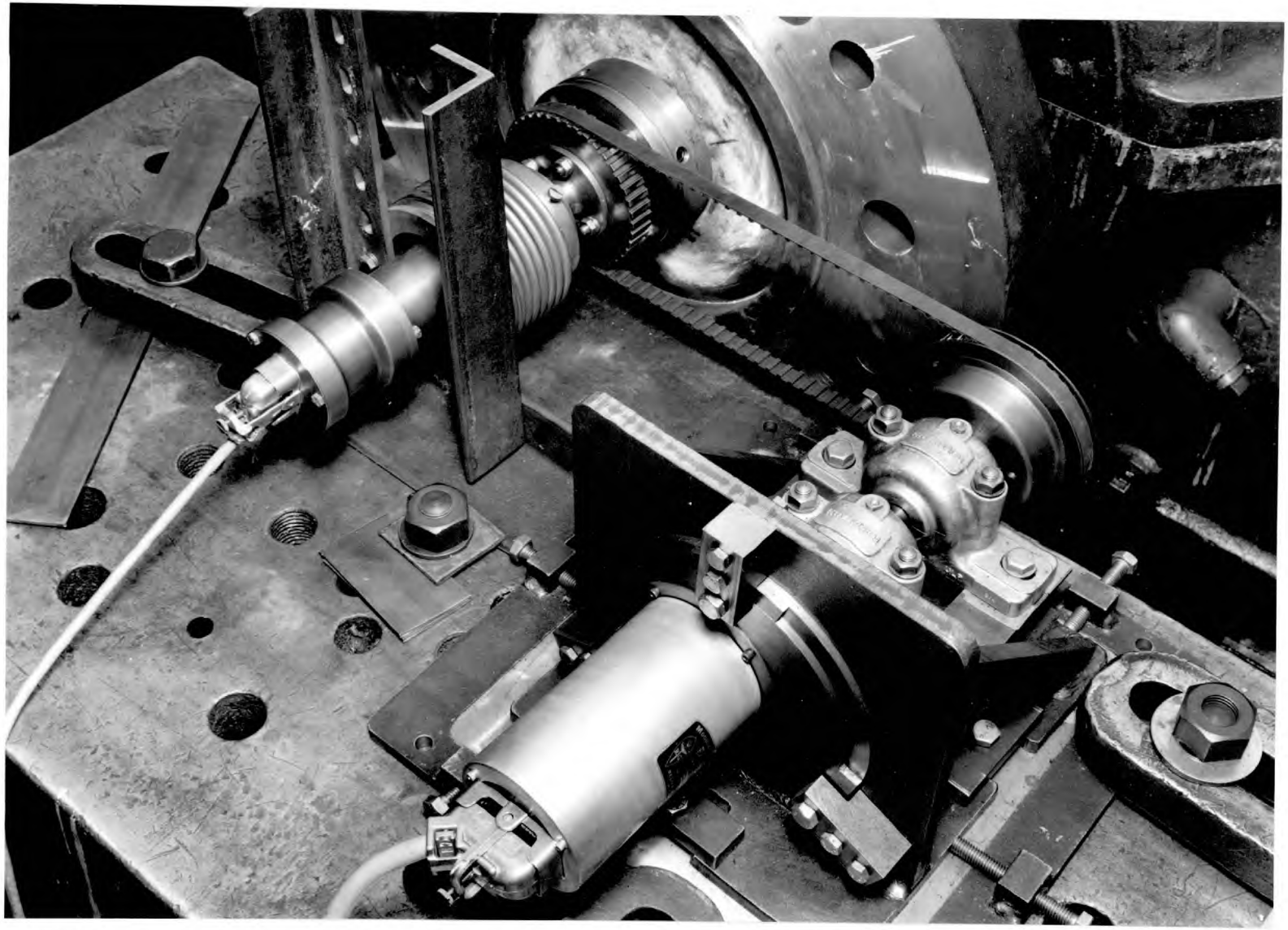

Plate 2 The resolver unit and accelerometer coupled to a large machine

cording the resolver outputs while the voltage and current of the single phase supply are measured with meters. The calibration must be carried out for both axis positions of the test machine. The axis powers require no calibration since they are only required to determine angles of the operational admittances, and it is shown in Appendix I that $\cos \varphi_{d,q} = {}^{a-b}/_{a+b}$, where a, b are the respective amplitudes of the instantaneous power shown in Fig. 87.

The alignment and calibration completed, the supply cable to the third phase of the test machine is restored. The machine is started by the direct on line application of the three phase supply. As the machine accelerates to synchronism the signals representing axis currents, voltages and powers are recorded. The instantaneous sum of the axis powers is also recorded since this is the total instantaneous power entering the machine, and as shown in Chapter 2 is approximately equal to the instantaneous output electromagnetic torque. A typical recording is shown in Fig. 10 for a 100 H.P. machine.

The magnitude of the axis operational admittances is obtained by the ratio of appropriate axis current and voltages at different speeds, i.e. at different axis frequencies, using the calibration previously obtained. The admittance angles are calculated from the axis powers at the appropriate speeds according to Appendix I.

The real part of the operational admittances must be corrected for armature resistance in a similar way

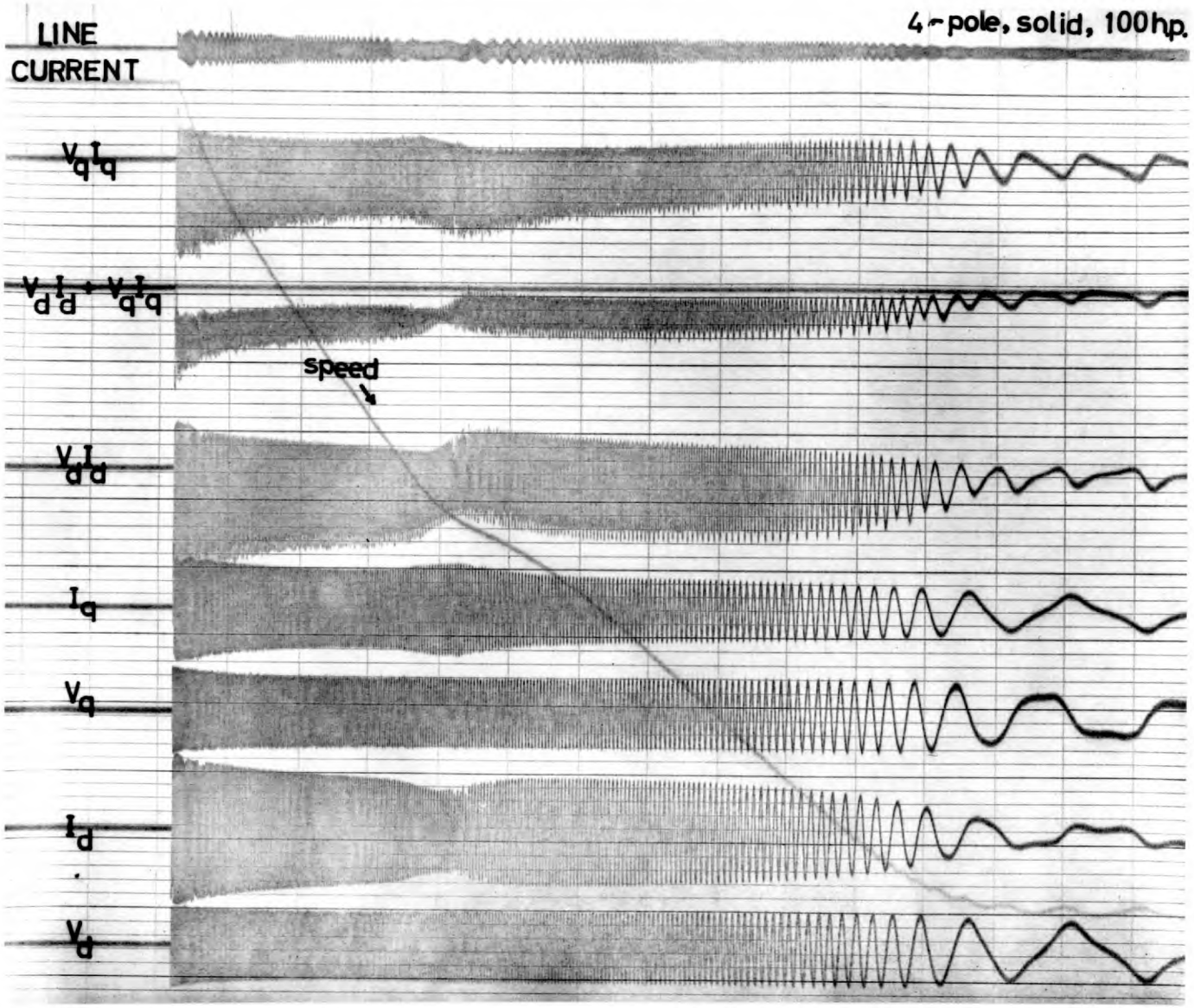

Fig.10 Recording of axis quantities obtained by the resolution method

to the calculation from static impedance tests. In this respect the resolver method is advantageous over the static impedance test in that the value of armature resistance remains small compared with the real part of the operational impedances over the whole frequency range.

3.3. THE DYNAMIC ADMITTANCE TEST

3.3.1. Principle of the Method

The dynamic admittance test is a method of determining the two axis complex operational admittances from oscillograms of phase voltage and current taken when the machine is running asynchronously at steady slip. As in the case of the axis resolution method, the axis operational admittances are measured in the presence of both axes fluxes.

Consider the expression for the instantaneous phase current, neglecting armature resistance, derived in Chapter 2 (Eqn. 2.30). It is:-

$$i_a = \frac{V_m}{2}[(B+D)\sin\omega_o t - (A+C)\cos\omega_o t + (D-B)\sin(1-2s)\omega_o t + (C-A)\cos(1-2s)\omega_o t] \quad .. (3.7)$$

Consider an instant of time such that the supply frequency sine term is equal to zero;-

$$(B+D)\sin\omega_o t = 0$$

$$\text{then} \qquad \omega_o t = n\pi \quad \text{where } n=0,1,2,3, \ldots \qquad (3.8)$$

If it is coincidental that at this same instant of time θ, the instantaneous angle between the direct axis and phase A winding (Refer to Chapter 2), equals zero or an integral number of π radians, then:-

$$\theta = (1-s)\omega_o t = m\pi \quad \text{where } m=0,1,2,3, \ldots \qquad (3.9)$$

From eqns. (3.8) and (3.9):-

$$(1-2s)\omega_o t = (2m-n)\pi \tag{3.10}$$

and in particular

$$\left.\begin{aligned} \sin\,(1-2s)\omega_o t &= 0 \\ \cos\,(1-2s)\omega_o t &= 1 \end{aligned}\right\} \tag{3.11}$$

Substituting eqn. (3.11) into eqn. (3.7) and using (3.8) gives:-

$$i_a = \frac{V_m}{2}(-2A)$$

$$\text{or} \quad A = -i_a/V_m \tag{3.12}$$

Similarly when:-

$$\omega_o t = (2n+1)\pi/2, \quad \theta = (2m+1)\pi/2$$
$$D = i_a/V_m \tag{3.13}$$

when:-

$$\omega_o t = (2n+1)\pi/2, \quad \theta = m\pi$$
$$B = i_a/V_m \tag{3.14}$$

when:-

$$\omega_o t = n\pi, \quad \theta = (2m+1)\pi/2$$
$$C = i_a/V_m \tag{3.15}$$

Clearly, therefore, the use of the method relies on the possibility of finding coincidence in time, when the prominent values of the sine component of the supply frequency terms of phase A current, i.e. prominent values of phase A voltage, and θ occur simultaneously. Furthermore it is then necessary to be able to measure the instantaneous value of phase A current at that time.

3.3.2. Application of the Test

The machine is driven at constant slip using a D.C. machine coupled back to back with another machine driven by an induction motor. This enables stable constant slip operation at all speeds. With the synchronous machine supplied as a motor, its field in one of its alternative connections, an oscillogram is taken.

It is necessary to record three signals on the oscillogram:-

1. Phase A current.
2. Phase A voltage.
   The latter signal is used to find the instants of time when $\omega_o t = n\pi$, and $\omega_o t = (2n-1)\pi/2$. At these instants, the phase voltage signal passes through zero and maximum values respectively.
3. A tachometer signal, v_t. A single phase A.C. tachometer is coupled to the synchronous machine and its stator so aligned that its output, which is of speed frequency, is

$$v_t = V_{tm} \sin \theta = V_{tm} \sin (1-s)\omega_o t$$

When the tachometer voltage passes through zero, $(1-s)\omega_o t = m\pi$, and when the tachometer voltage reaches a peak $(1-s)\omega_o t = (2m-1)\pi/2$.

Thus coincidences between certain values of the phase voltage, v_a, and the tachometer voltage, v_t, give instants of time when the phase current, i_a, is simply equal to the product of the maximum value of phase voltage V_m, and the appropriate component of operational admittance, which is to be found.

A typicallength of oscillogram is shown in Fig.11. The tachometer voltage signal is superimposed upon the phase voltage signal in order that the required coincidences between values of each could more easily be found.

Phase A power is recorded on the oscillogram shown, although it is of no use in the method, as it contained too many frequency components (eqn. 2.36), but it is shown for additional interest.

Due to non-sinusoidal distribution of flux on the quadrature axis a severe third speed frequency harmonic is injected, via the leakage reactance of the supply, on to the phase voltage. This causes some difficulty in determining the coincidences over part of the slip range. It is assumed, however, because of the distribution of the three phase windings, that they did not respond to the third harmonic voltage and certainly there is no evidence of it in the phase current oscillograms.

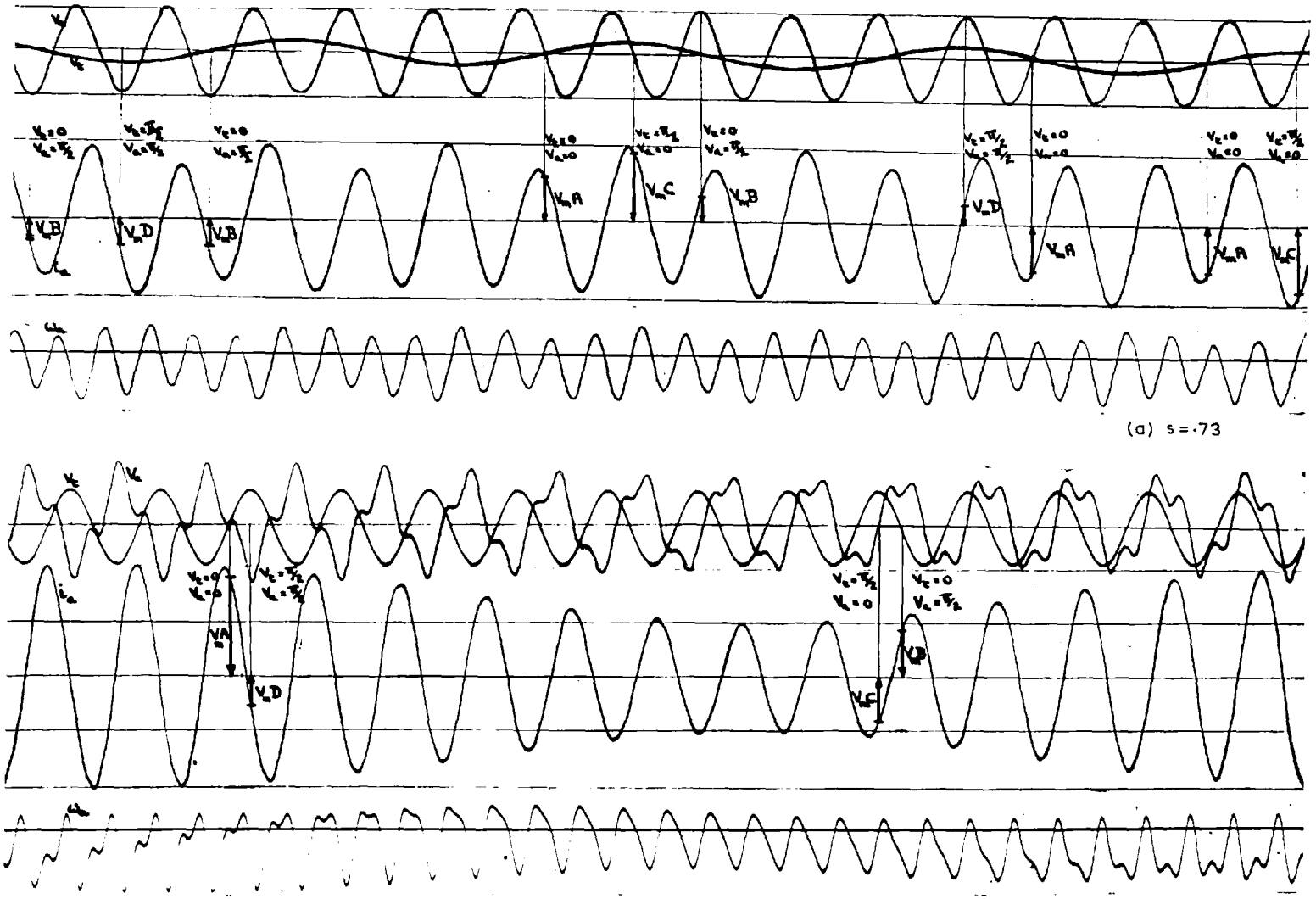

Fig. 11. Determination of the operational admittances by the Dynamic admittance test (for details see text)

3.4. THE SUDDEN SHORT CIRCUIT METHOD

The sudden short circuit method is an indirect method of obtaining the operational admittance loci, and moreover, is only strictly applicable to the laminated pole synchronous motor.

The object of the sudden short circuits is to obtain the subtransient and transient reactances and time constants, and the steady state reactance of the machine. Using these parameters the two axis operational admittance loci of a laminated pole machine may be calculated by a method given in Part II.

The short circuit tests applied to the machine are the direct axis sudden short circuit, with the field winding supplied through a source of low internal impedance, and the quadrature axis sudden short circuit test. The method of application of these tests are explained by Wright.[13]

3.5. COMPARISONS OF THE DIFFERENT METHODS OF OBTAINING THE ADMITTANCE LOCI BY MEASUREMENT

Of the four methods discussed, the variable frequency single phase static impedance test is undoubted the most reliable because of its simplicity. The only instrumentation required in the test is a moving iron voltmeter and ammeter, and an electrodynamic multi-range wattmeter. All these meters respond satisfactorily to frequencies of 50 c/s and less. However, in order to obtain meaningful results, the following precautions must be taken. Firstly, care must be taken to ensure that the total flux produced in the machine is of the same order, at the different frequencies, i.e. the voltage applied to the test machine must be of magnitude proportional to the frequency of application. Because of the effects of iron saturation, particularly in the solid iron case, it is clear that results obtained at flux levels widely different from those at which asynchronous performance is to be predicted, will not predict the performance with satisfactory accuracy. Secondly, care must be taken in the alignment of the test machine rotor to the appropriate position, and in the case of the quadrature axis test, to ensure that the main field is on open circuit, lest with a slight error in alignment, the current induced in it leads to error in measurement of the impedance.

Despite the advantage of simplicity, there are several disadvantages in the use of the method.

1. The operational admittance loci may only be obtained at frequencies from approximately normal supply frequency to frequencies of the order of 5 c/s.

If attempts are made to obtain results at lower frequency, at any reasonable flux level, the supply alternator, which may be carrying full load current, is turning so slowly that it becomes overheated.

2. There is difficulty in the calculation of the impedances from the results of the test at low frequency. Referring to equation (3.1) it is seen that in order to obtain the axis admittance the value of armature resistance must be subtracted from the total real part of the impedance obtained. At the frequencies below 10 c/s the armature resistance may become a substantial part of the total real part of the impedance. The armature resistance varies with temperature, and with frequency due to skin effect in the conductors, and so the value of resistance is not known accurately. Consequently at low frequencies there may be appreciable error in estimating the real part of the impedance.

3. The method is one in which one axis impedance is obtained in the absence of the other axis flux, whereas, during asynchronous running, for which the performance is to be predicted from results of the test, both axis fluxes are present together. This disadvantage could be overcome by either applying a two phase static impedance test, in a manner shown in Fig. 12, or alternatively by a three phase static test and Scott connecting the meters so that one set would read the direct axis quantities and the other set simultaneously the quadrature axis quantities. However, the comparisons of the results of tests, shown later, do not suggest the need for this.

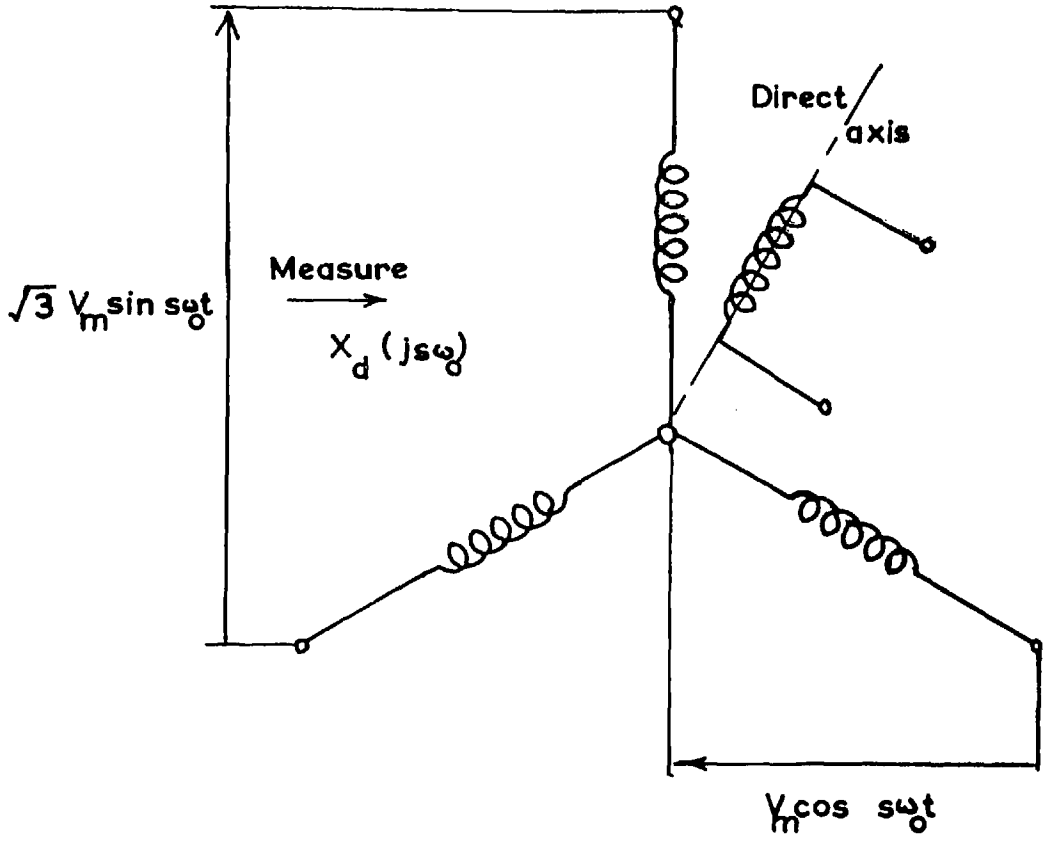

Fig. 12. Circuit for static impedance measurement with both axes excited.

Although there may be some harmonics, tooth ripple for example, in the voltage supply from the single alternator, these may be considered negligible and the current waveform obtained is purely fundamental owing to the smoothing effect of the large inherent inductances in the circuit.

The variable frequency static impedance test can be equally well applied to both large and small machines. However, the application of the test to both axes of a large machine at several frequencies and with maybe more than one field connection, takes considerable time, and hence is costly.

The axis resolution method would appear, at first glance, to be the best method. It has the following obvious advantages:-

1. The frequency range over which it is useful can be from twice supply frequency (machine plugging) to a frequency of the order of .5 c/s.

2. It is a method of measuring the operational impedance in the presence of both axes fluxes, i.e. during asynchronous running.

3. A record containing the information for the calculation of both axes loci can be obtained in a single start. It is therefore an ideal test for newly constructed large machines, since it causes little delay to their factory progress.

Despite these advantages there are two serious disadvantages.

1. The most serious disadvantage is the half speed effects on almost all the recorded signals. Despite avoiding measurements in the half speed region, at slips between .35 and .65, it appears from the results obtained that the half speed effects are even more widespread, and a distinct discontinuity is found between impedance calculated before and after half speed. Although the armature resistance is subtracted from the real parts of the impedances calculated, any attempt to make proper allowance for armature resistance over the half speed region, would make analysis of the results of the test considerably more tedious than it already is.

2. During a start of a large machine the supply voltage may vary quite considerably and that consequently the results obtained are not at constant voltage, and hence constant flux, as is ideally desired.

The dynamic admittance test is another test in which the operational impedances may be obtained in the presence of both fluxes. The method has several disadvantages.

1. The method is only suitable for laboratory machines, although it is possible to apply it to large machines during a start.

2. There is considerable difficulty in obtaining the measurements at low slip, when the non-sinusoidal voltage makes detection of the coincidences

very difficult, and around the half speed region, when there is serious error found in the measurements, due to half speed armature resistance effects.

3. Because of the necessary high recording speed the test can be very expensive in recording paper.

The fourth and least accurate method of obtaining the operational admittance loci, is the sudden short circuit method. It is an indirect method since it relies on the determination of the sub-transient, and transient time constants and reactances, from which the loci are calculated. Error can, thus, occur in both parts of the estimation of the loci. It can occur in the determination of the sudden short circuit parameters, and it is well known that the transient and sub-transient parameters cannot be obtained from the sudden short circuit results with a high degree of accuracy. There may be also error in the assumption that the sudden short circuit equations (6.6), (6.8) transform exactly, during asynchronous running to the equations (6.1), (6.4) describing the loci.

Moreover, this method of obtaining the loci is only applicable to any degree of accuracy at all, to the laminated pole synchronous motor, and extremely erroneous results are obtained should it be attempted to be applied to the solid pole type of machine.

For comparative purposes, all the methods except the axis resolution method, which was not available at the time, have been applied to the laminated pole micro-machine (Fig.13). The method applied to the large solid pole machines was the axis resolution method, with a confirmatory supply frequency single phase static impedance test. The static impedance test has been applied at three frequencies to one large machine in order to compare with the axis resolution method over a greater frequency range. (Fig.14).

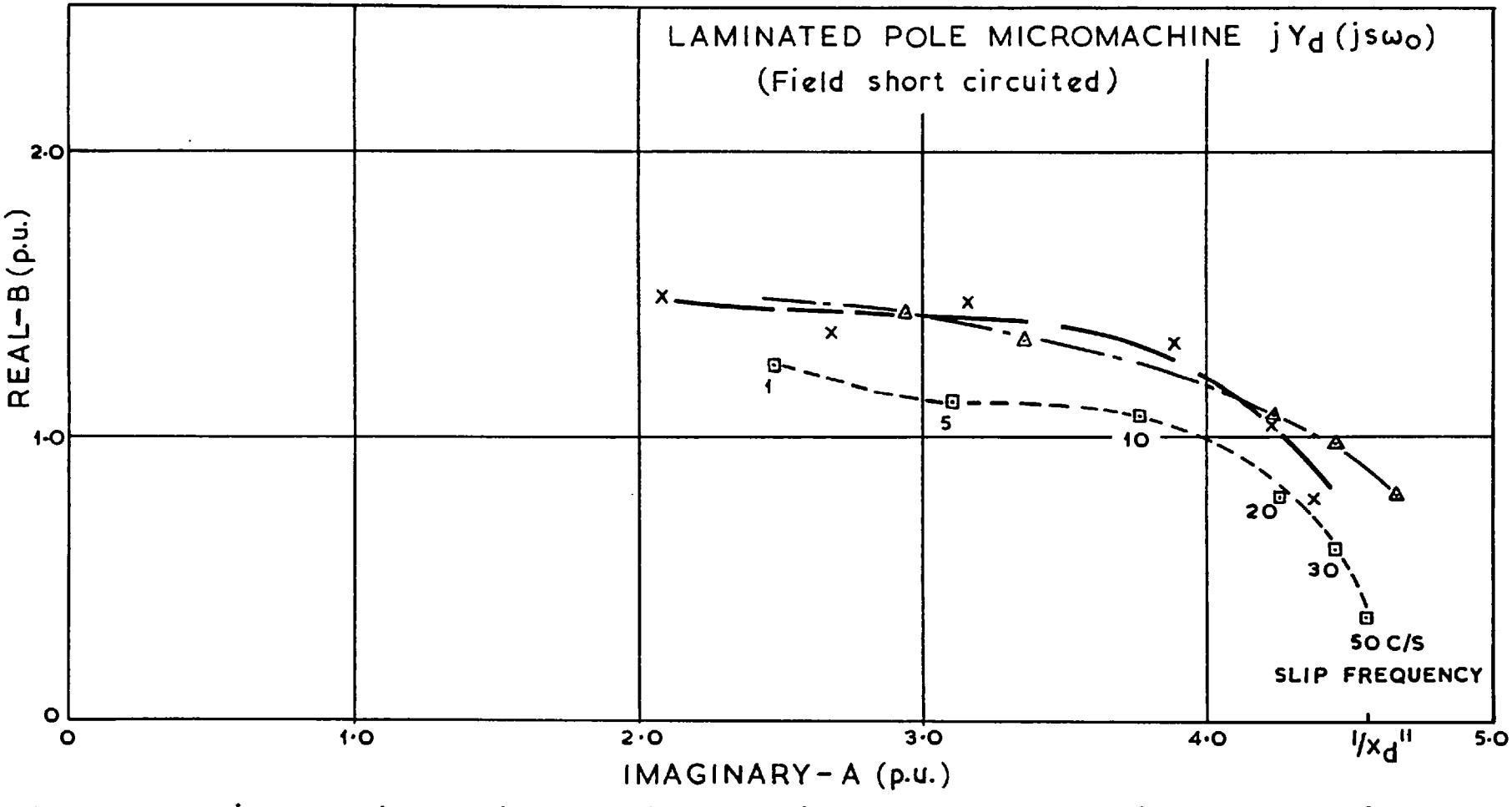

Fig. 13 Comparison of direct axis operational admittance frequency loci obtained by different methods

——x—— Dynamic impedance tests

—·—△—·— Static impedance tests

- - - -□- - - - From results of sudden short circuit test

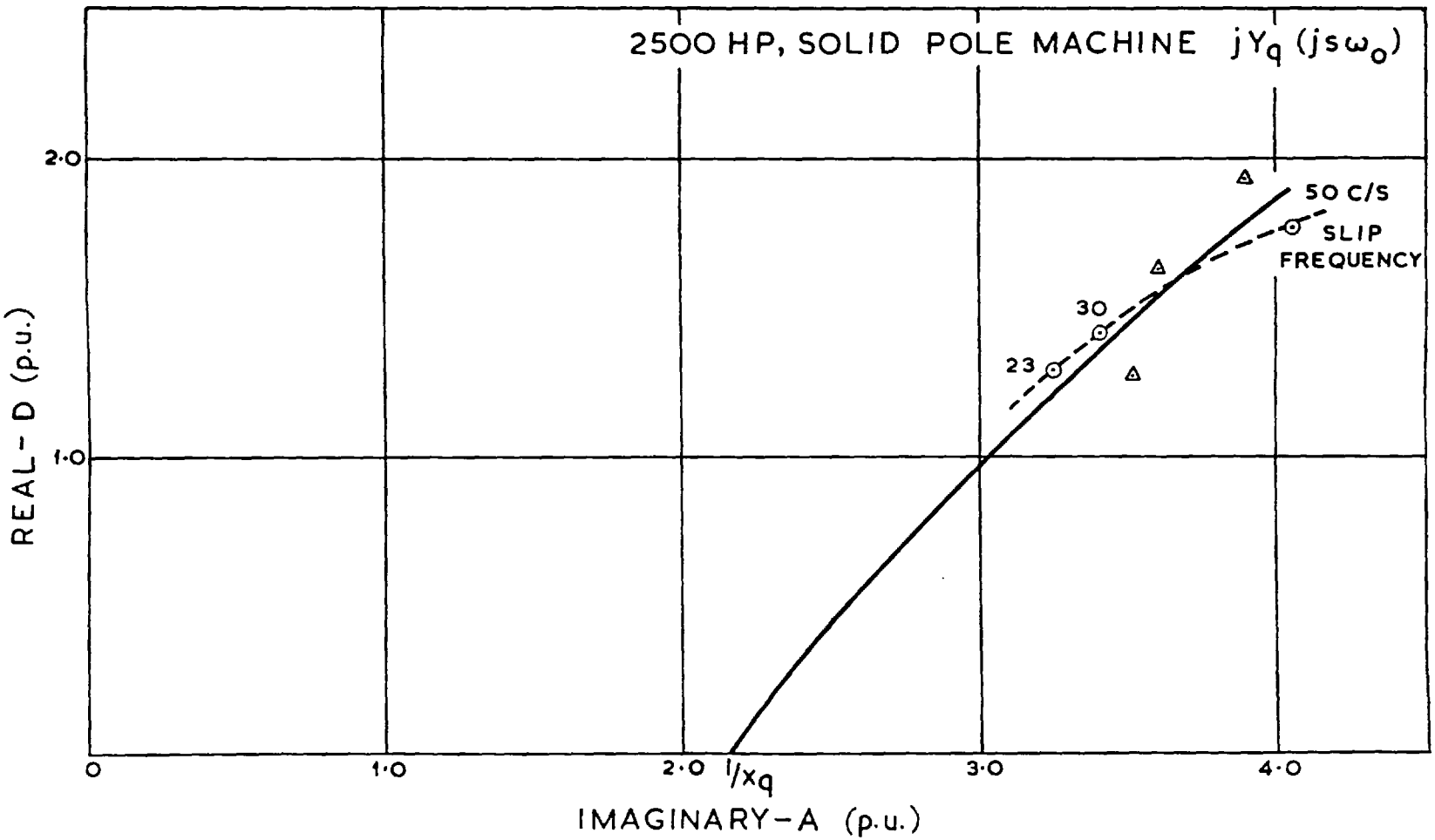

Fig. 14 Comparison of quadrature axis operational admittance frequency loci

—△— Axis resolution method

- - -⊙- - - Static impedance tests

CHAPTER 4

TORQUE, CURRENT, AND POWER MEASUREMENT

Although the input power and current of an induction machine are relatively easy to measure, the methods available to measure torque, particularly under transient conditions, are not as satisfactory. It is seen in chapter 2 that when a salient pole synchronous machine runs asynchronously its torque is not a steady value but has a component oscillating at twice slip frequency. The oscillating torque, in machines of particularly severe saliency, can be of zero-peak amplitude well in excess of the mean torque. It is important, therefore,to be aware of the proportions of the torques, at the design stage, in order that the machine and coupled load can be adequately designed to withstand them.

All of the present available methods, of measuring the oscillating component of the electromagnetic torque, produce a signal which is attenuated by different amounts at different slip frequencies. Several methods of measuring torques are discussed here, including a new method which, although not accurate to a high degree, does produce the mean and oscillating torque-speed characteristic unattenuated.

4.1. MEASUREMENT OF MEAN TORQUE, BY MEAN OUTPUT POWER MEASUREMENT

The measurement of mean output torque by mean output power measurement is the most satisfactory method available. The machine, to be tested, is mechanically coupled to a D.C. machine. In order that the latter set is able to run stably at all speeds, the D.C. machine is coupled, Ward-Leonard fashion, to another D.C. machine driven by an induction motor.

The test is performed in two parts. The unsupplied synchronous motor is driven by the coupled D.C. machine at the desired speed, and the power entering the D.C. machine, required to maintain this speed, is measured. The three phase supply is then applied to the synchronous motor, with its main field connected in one of its alternative connections (e.g. field closed through a discharge resistance) and the output power from the coupled D.C. machine measured. The speed of the set and the excitation of the coupled D.C. machine are maintained at the same value for both parts of the test. The sum of the 'no-load' and the 'on-load' powers, divided by the speed is the mean torque of the synchronous motor at that speed.

If the armature reaction flux weakening effect in the D.C. machine is ignored, and its field is maintained on constant voltage, the electromagnetic torque of the D.C. machine is proportional to its armature current. Consequently careful observation of this current gives a very good indication of any sharp changes of torque with speed. Current measurement could be used to es-

timate the electromagnetic torque of the synchronous motor, but in fact power measurements were used and the currents were only used to detect any irregularity of the torque characteristic.

4.2. MEASUREMENT OF MEAN AND OSCILLATING TORQUE USING A STRAIN GAUGE TORQUE-METER

4.2.1. Description of the Torque-meter

The torque-meter consists of three main parts:-

Firstly a tube S on whose outer surface are attached four strain gauges, A, B, C, D, located in 45^{o} formation as shown in Fig.15. The strain gauges are connected in a bridge circuit. The advantages of such a system are:-

(a) The use of a thin 'torque tube' enables fairly large strains to be produced.

(b) The combination of the 45^{o} formation of location of the gauges and the connection as a bridge results in the cancellation of any signal obtained in the gauges through bending moment.

(c) The output signal from the bridge is twice as great as the strain signal obtainable from any one of the gauges.

The second main part of the torque-meter is a transistor D.C. amplifier. The purpose of this is to amplify the signal obtained from the bridge so that the brush noise, which is superimposed on the signal

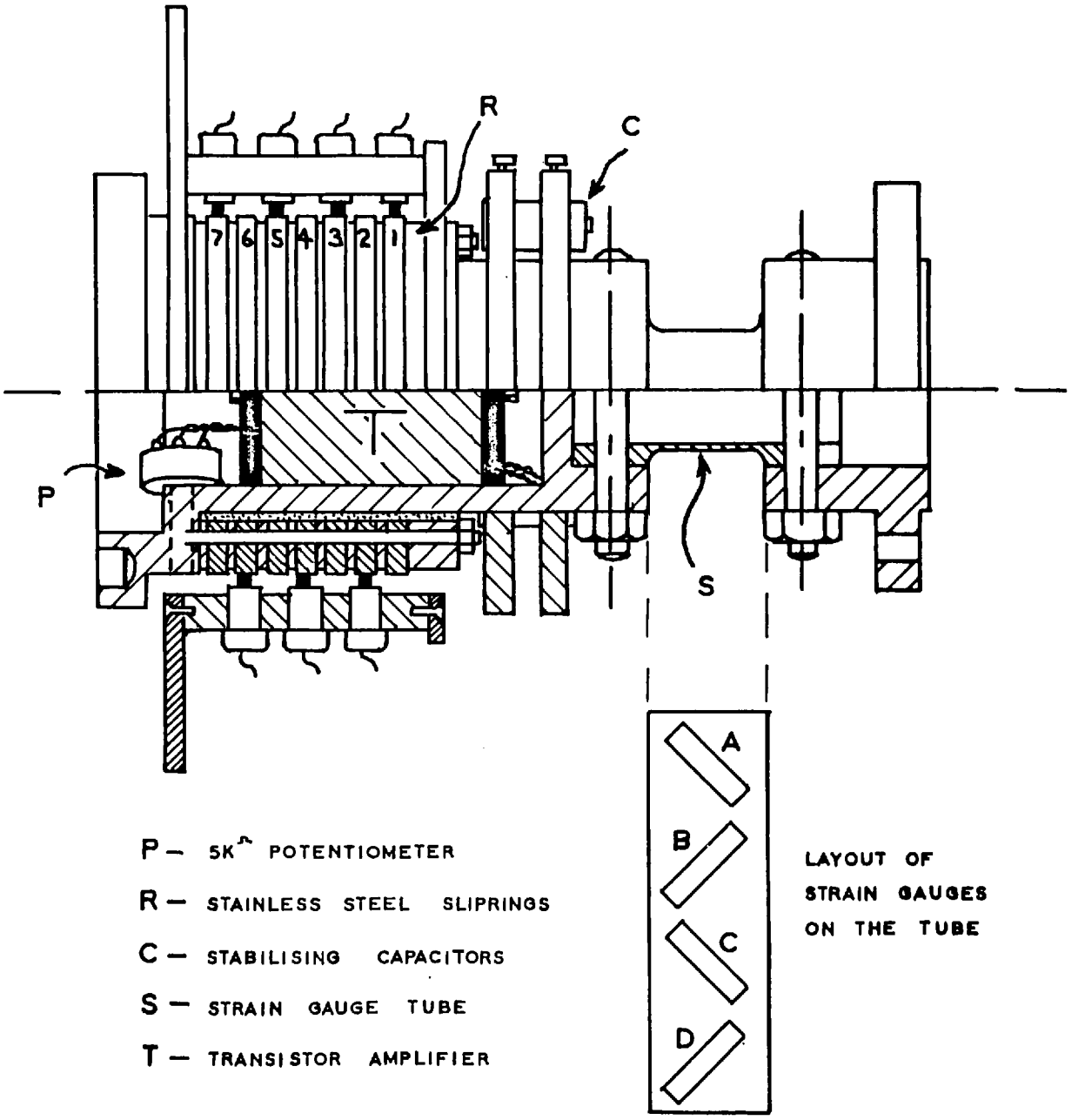

Fig. 15. Half-sectional diagram of the strain gauge torquemeter.

as it leaves the moving contacts, is negligibly small compared with the signal.

The third main part of the torque-meter is the set of stainless steel sliprings, R, by which the supplies are connected to the rotating parts and from which the output is obtained. The brushes are of silver graphite (85% silver) and are pressed onto the rings with particularly high spring pressure to keep contact resistance to a minimum. Although seven sliprings are shown in Fig.15 only four are used; those for carrying the 10^{V}, 20^{V} supplies, the 0^{V}, and the output signal.

Although the rating of the strain gauges is such that the supply to the bridge must not exceed 20^{V} while it is also necessary that the balance point of the bridge is very near zero voltage for satisfactory operation of the amplifier, it was possible to use the transistor amplifier supplies to supply also the strain gauge bridge. This was done by connecting the bridge in series with a 500 ohm high stability resistance, across the full 30^{V} as shown in Fig. 16.

At either end of the torque-meter is a flange for coupling purposes.

4.2.2. The Torque-meter Transistor Amplifier

Fig. 16 shows the circuit details of the amplifier. It is of the two stage long-tailed pair type. The germanium transistors of each stage were chosen to have matched characteristics. This choice

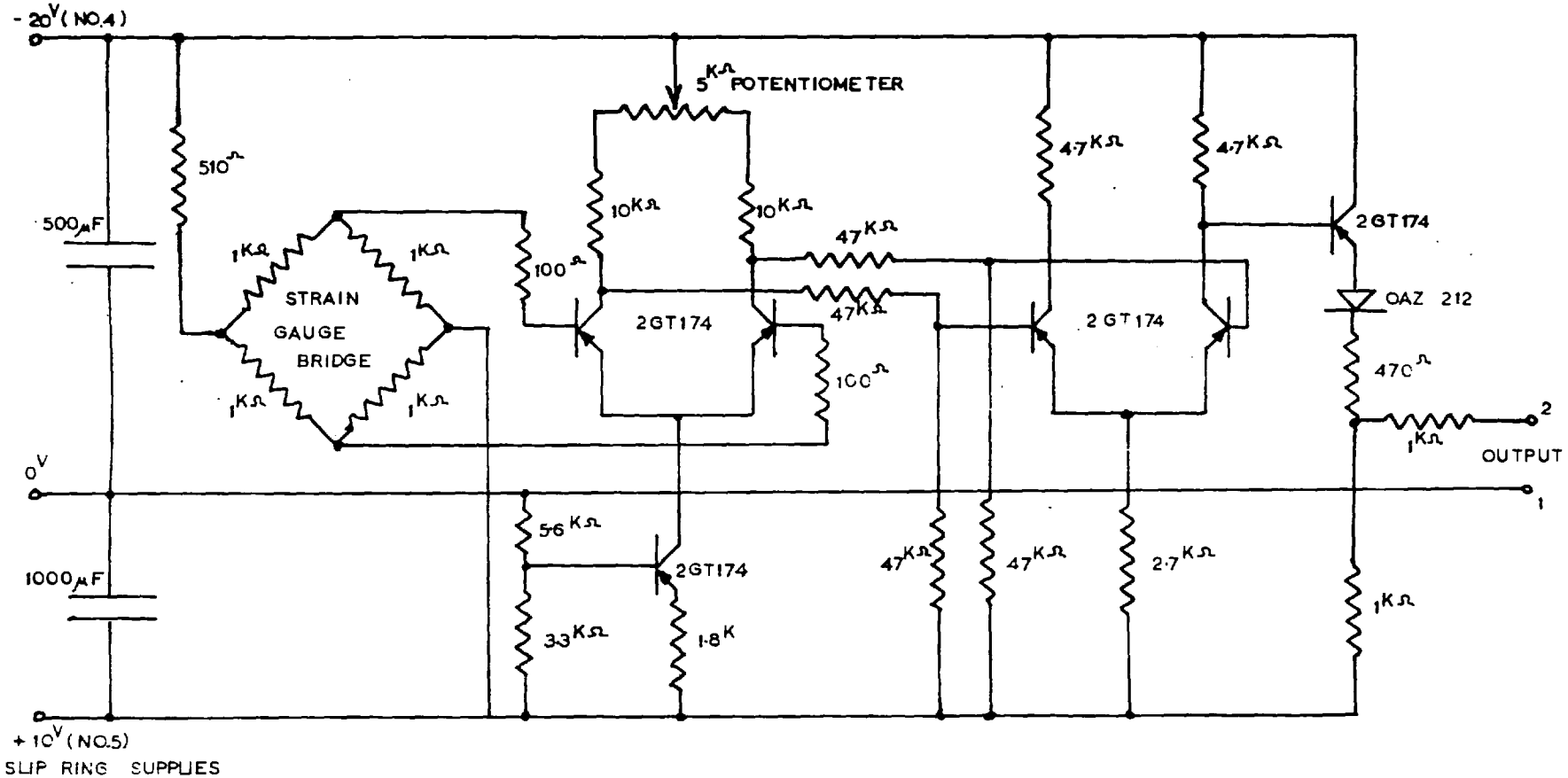

Fig. 16. Circuit diagram of strain gauge bridge and transistor amplifier.

results in the minium of drift due to temperature change in transistors of a pair. An emitter follower is used as the last stage to reduce the output impedance of the amplifier. However, a one kilohm resistor was inserted in series with the output to ensure that, if by accident, the output were shorted to the 0^{V}, 10^{V}, 20^{V}, supply points, no damage should result, and thus no need for dissembly of the torque-meter.

The circuitry was mounted on vero-board, between two ebonite discs, and then filled with molten wax. When set, the amplifier took the form of a cylinder $2\frac{1}{4}$" diameter by 3" long and was an interference fit inside the body of the torque-meter.

The amplifier was found to have a constant voltage gain of 1260 from D.C. to 15 k/cs with negligible phase shift. Maximum D.C. input to the amplifier was $\pm$ 4 mv. with distortionless output; a shaft torque corresponding to approximately $\pm$ 50 lb.ft..

Two additional precautions were taken to prevent brush noise, interfering with the performance of the amplifier. Firstly, two brushes were paralleled on diametrically opposite sides of each slipring. This ensured that, if due to eccentricity of rotation, the contact pressure of one brush increased slightly the other would decrease approximately by the same amount. The total brush contact per ring, therefore, would remain almost constant. Secondly, large capacitors were connected in parallel with the supplies on the torquemeter, to filter out any brush noise that still remained.

4.2.3. Estimation of mean electromagnetic torque

Although the strain gauges were carefully positioned at 45^{o} helices on the torque tube, it was found that the alignment of the gauges was imperfect; and despite the fact that the torque-meter was connected between the synchronous machine and the coupled D.C. machine after very careful alignment of height and horizontal positioning of the two machines, there was still sufficient eccentricity in rotation and misalignment to produce a large bending moment in the torque tube. The result was that even when the shaft torque was zero a speed frequency output signal of approximately 300mv. peak to peak was obtained. An output signal of this order, due to an oscillating torque alone, would correspond to a peak to peak torque of approximately 2 lb.ft. As the peak mean torque of the synchronous machine tested, the laminated pole micromachine at Imperial College, was only of the order of 2 to 3 lb.ft., when supplied at .35 p.u. voltage, the torque tests were performed at a higher voltage .64 p.u. This voltage was as high as was practical to use because:-

(a) The current drawn at this voltage reached the limit of the supply protection.

(b) As the machinery accelerated through the mechanical resonant frequency of the set, the amplitude of the shaft oscillating torque almost reached both the saturation level of the torque-meter amplifier and the yield point of the torque tube.

It was found that the values of the torques obtained during a steady slip test were identical to those obtained, at the same value of slip, during a twenty second start. As a result, it was more convenient to take one recording, during a start, from which measurements at any slip could be deduced. The mean shaft torque characteristic obtained had to be increased by the ratio J_1+J_2/J_2 to obtain the mean electromagnetic torque of the synchronous machine. This is seen by putting $\omega=0$ in equation (13.10) of Appendix II.

The torque-meter was recalibrated before and after each test, by the application of stationary kilogramme weights at the radius of the flywheel. The torquemeter was found to have a linear response up to a torque of approximately 30 lb.ft..

4.2.4. Estimation of the oscillating component of electromagnetic torque

Equation (13.10) of Appendix II shows that the amplitude of oscillating torque in the shaft is quite different from that produced electromagnetically by the synchronous machine. In order that the amplitude of electromagnetic oscillating torque could be calculated from that measured by the torquemeter, it was necessary to know the inertia ratio J_2/J_1+J_2, ω_n the natural frequency of torsional resonance, and τ the damping time constant.

The natural frequency and the mechanical damping time constant τ, were found by taking a recording of the damped oscillation when an impulse, a torsional

jerk,was applied to the shaft. The behaviour of the torque following an impulse is given by equation (13.7) in Appendix II. The natural frequency, ω_n, was easily measured from the recording and the time constant from a semi-logarithmic plot.

Using the values of ω_n, ζ and the inertias, the frequency response - the amplitude of oscillating shaft torque to the amplitude of oscillating electromagnetic torque could be calculated over the relevant frequency range, (s = 0 to 1.). This response was then used to estimate the electromagnetic torque from the shaft torque measured by the torquemeter.

4.3. MEASUREMENT OF MEAN AND OSCILLATING TORQUE USING AN ACCELEROMETER

The method of obtaining the torque characteristics, by measuring the acceleration of the machine, during a start, is a well known one and has been applied most usefully to large machines where other methods are impracticable. The mean torque can be accurately obtained by the product of the inertia and acceleration, if the value of the inertia is accurately known. The acceleration may be measured by a drag cup type of machine, or by the combination of a precision D.C. tachometer and a differentiating circuit. Some filtering out of speed frequency noise is necessary in both cases.

The amplitude of the oscillating component of electromagnetic torque is very difficult to obtain accurately since it is attenuated by different amounts at different speeds. The attenuation is caused by both the mechanical characteristics of the inertia-shaft arrangement and by the characteristics of the filter circuit. Thus, determination of the amplitude depends on the calibation curves of the differentiating circuit, and more uncertainly on the frequency response of the inertia-shaft system.

No work was done on the design or construction of an accelerometer, although an A.C. tachometer and differentiating circuit were used to find the mean torque characteristic of a large machine.

4.4. ESTIMATION OF MEAN AND OSCILLATING TORQUE BY THE MEASUREMENT OF TOTAL INSTANTANEOUS INPUT POWER

It is seen that, under steady slip conditions, the expression for the total instantaneous input power (Eqn. 2.37) is identical to that for the instantaneous output torque (Eqn. 2.38) when armature resistance and stator iron loss is ignored. Consequently a recording of instantaneous input power is suggested as a new way in which the torque speed curve, complete with oscillating component unattenuated, can be obtained from a single start.

The total instantaneous input power may be obtained either by summing the instantaneous input power of the three phases (Fig.17), by a method using a principle of the two wattmeter method, or, if signals representing axis currents and voltages are available, by summing the instantaneous axis powers.

Recordings are shown in Fig.18 of the total instantaneous input power, with three different field connections, as the laminated pole micromachine at Imperial College, ran up to synchronism. The initial part of the record had to be excluded because the original recording was too long for complete reproduction.

It is apparent that there is a severe amount of mush present on the characteristics obtained. Equations 2.36 show that there are four components in the instantaneous power of Phase A; the D.C. component (B+D); a component oscillating at twice supply frequency. e.g. 100 c/s for all values of slip; and two components oscillating at frequencies that are functions

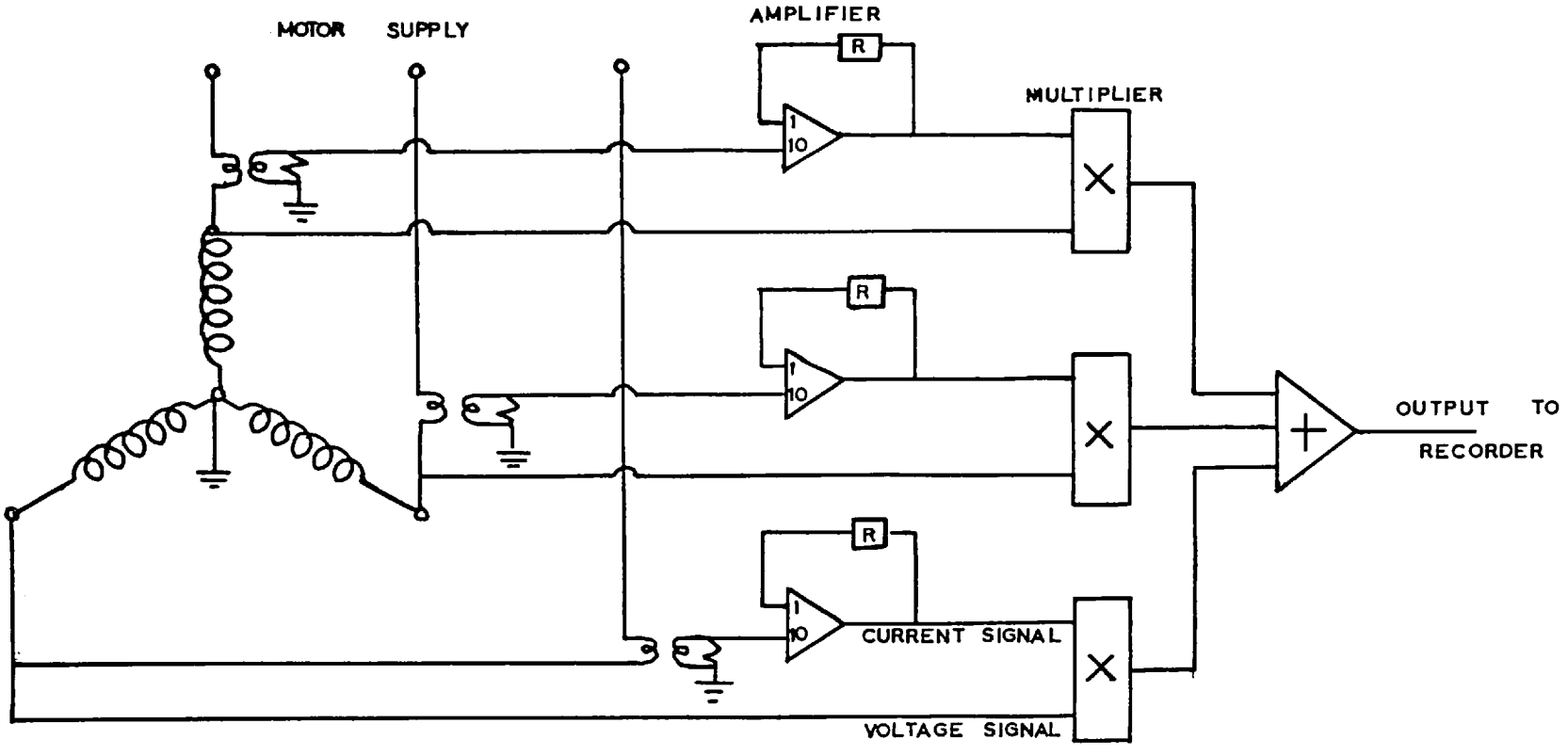

Fig. 17. Circuit for measurement of the instantaneous total input power.

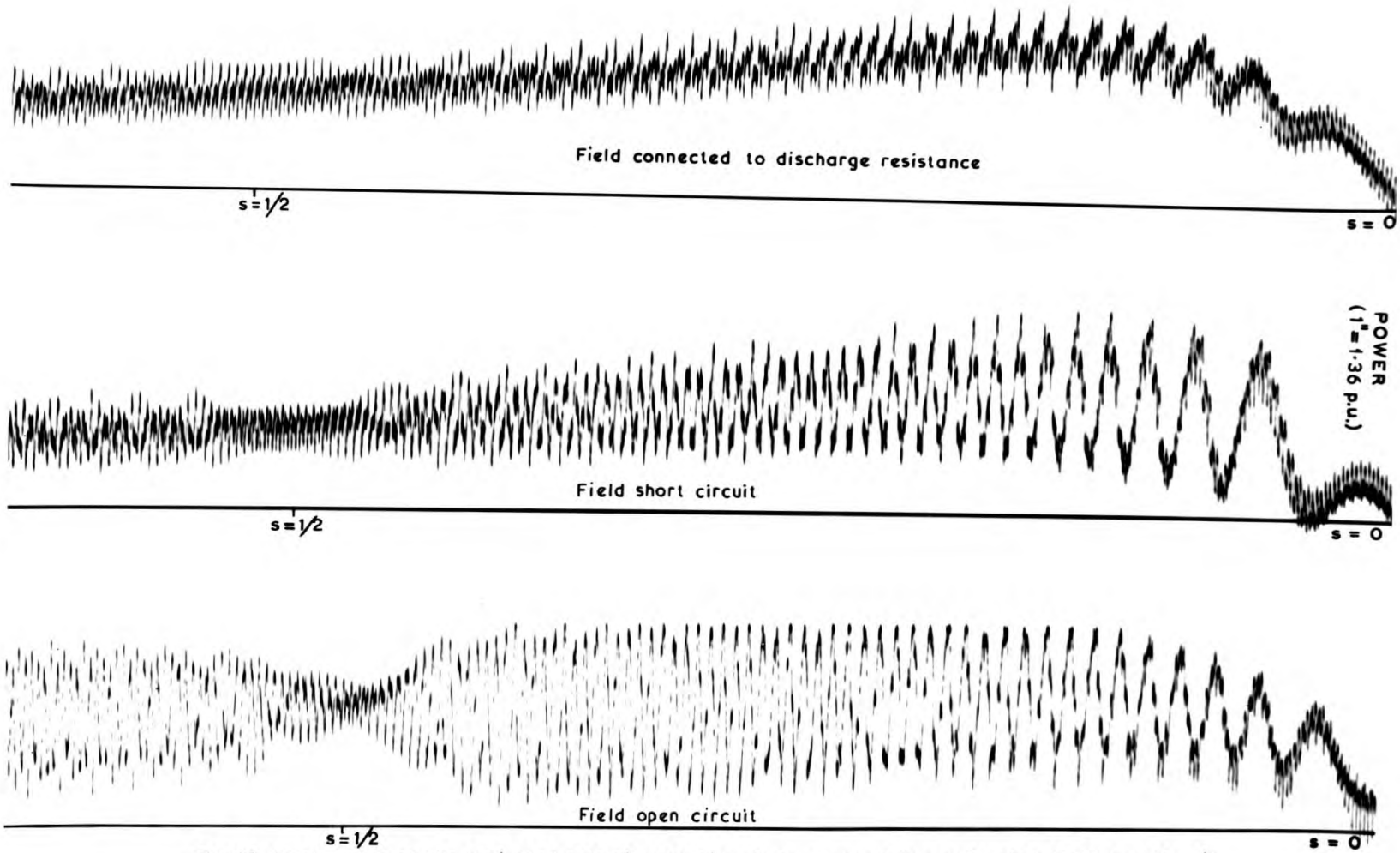

Fig. 18. Input power of the laminated pole micromachine during a run up to synchronism (0·35 p.u. voltage)

of slip - the twice slip frequency (0-100 c/s), and the twice speed frequency (100-0 c/s) components. If all the three phases were perfectly balanced, i.e. firstly were supplied with a constant identical sinusoidal voltage, whose phases were exactly 120^{o} apart, and secondly the three phases of the machine were completely balanced, then the twice speed frequency and the twice supply frequency components would have vanished in the summation of the three phase powers. The mush, therefore, is not erratic spurious pick up signal, but merely components that did not completely vanish at the summation. The mush, however, is not so large as to make the measurements too difficult, although it is clear that accurate measurement of the oscillating component, with the field connected onto the discharge resistance, is not possible.

Despite the limitations of the method this is the only way that a display of the complete torque-speed curve (neglecting stator losses) is possible without attenuation of the oscillating component.

4.5. MEAN INPUT CURRENT MEASUREMENT

The mean input current of an asynchronously running synchronous motor is the best simple way of checking the prediction of the magnitude of the operational admittances. Neglecting armature resistance, it is seen that, from equation (2.35), the magnitude of the supply frequency component of the phase current is given by the vector mean of the two axis operational admittances, at 1 p.u. voltage.

The current may be measured using ammeters, whilst the machine is operating at steady slip, or by a recording during a start.

Fig. 19 shows a recording of phase current, phase voltage, and phase power during a start.

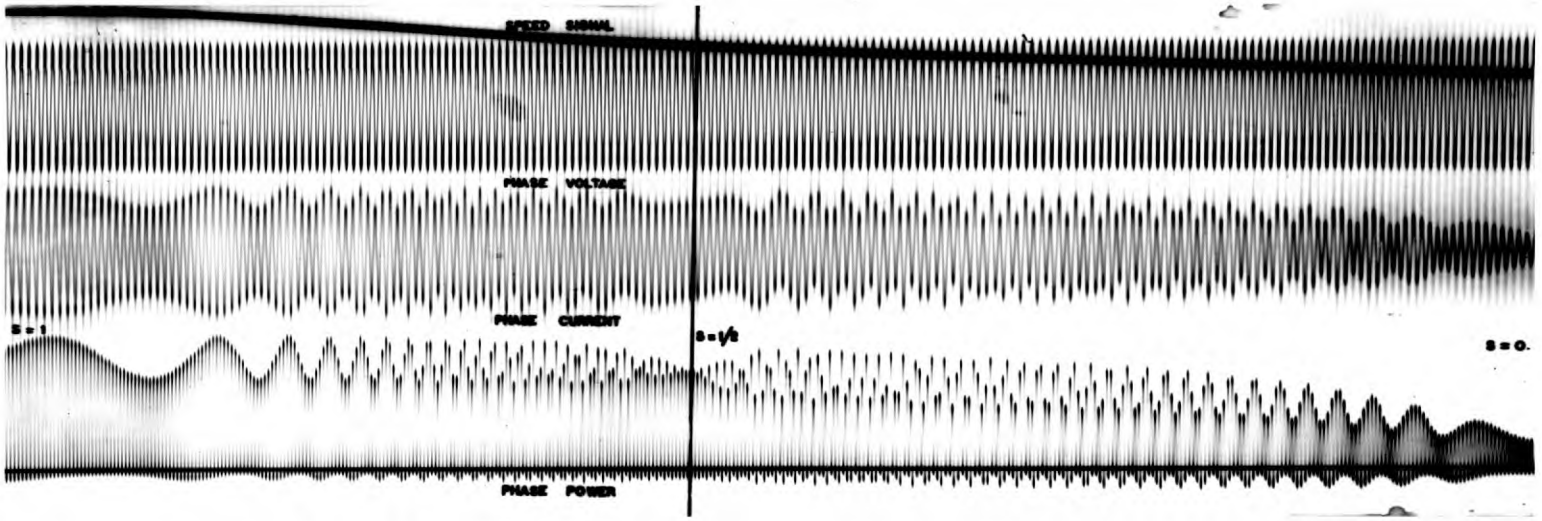

Fig. 19. Phase voltage, current and power of the laminated pole micromachine during starting.

4.6. COMPARISON OF THE METHODS OF MEASURING TORQUE

The most accurate method of obtaining the mean torque characteristic, by measurement, is the mean output power method. Accuracy better than 1% can be achieved if the method is applied in the two parts described. The method, however, is only suitable for laboratory machinery since it necessitates steady running, at the constant slip at which the measurement is required. The oscillating component of electromagnetic torque cannot be measured using the output power method.

The torquemeter method of obtaining the torques of a laboratory machine is a good method if its inherent disadvantages can be overcome. The main disadvantage is the presence of the uncancelled bending moment torque due to misalignment of both the torquemeter coupling and of the strain gauges on the torque tube. Some speed frequency brush noise is also found on the output. Calibration of the gauge, although here was performed by the application of stationary weights to an arm, would best be performed using the output power method of measuring the mean torque. The oscillating component of electromagnetic torque is attenuated in the shaft, by different amounts at different speeds, due to the mechanical characteristics of the system. In order to obtain the oscillating component of electromagnetic torque the attenuation characteristic is required to be known. It is determined from the inertias, stiffness, and damping in a manner shown in Appendix II. Since the values of stiffness and damping are difficult to determine accurately so, too, is the oscillating component of electromagnetic torque.

The accelerometer method of obtaining torque is the most suitable for large machines and gives satisfactory results for the mean torque if the accelerated inertia is accurately known. If the test machine is coupled to an additional inertia the oscillating component of electromagnetic torque, measured by the accelerometer method, suffers similar attenuation to that observed in the shaft, using the torquemeter. There is, in fact, further attenuation, in the case of the accelerometer method, due to the frequency characteristics of any differentiating circuit that may be employed.

The estimation of mean and oscillating torque by measurement of total instantaneous input power, although not accurate to a high degree, is a very satisfactory method of obtaining both components of electromagnetic torque. The oscillating component is not subject to any attenuation and hence it may well be considered that the oscillating component of electromagnetic torque may be most accurately obtained by this method.

Fig.20 shows the comparison between the mean torque characteristics of the laminated pole micromachine, with field connected onto a discharge resistance, obtained by the output power method, that obtained by the torquemeter calibrated by stationary weights on an arm, and that obtained by the input power method. The accelerometer method was not applied to the micromachine.

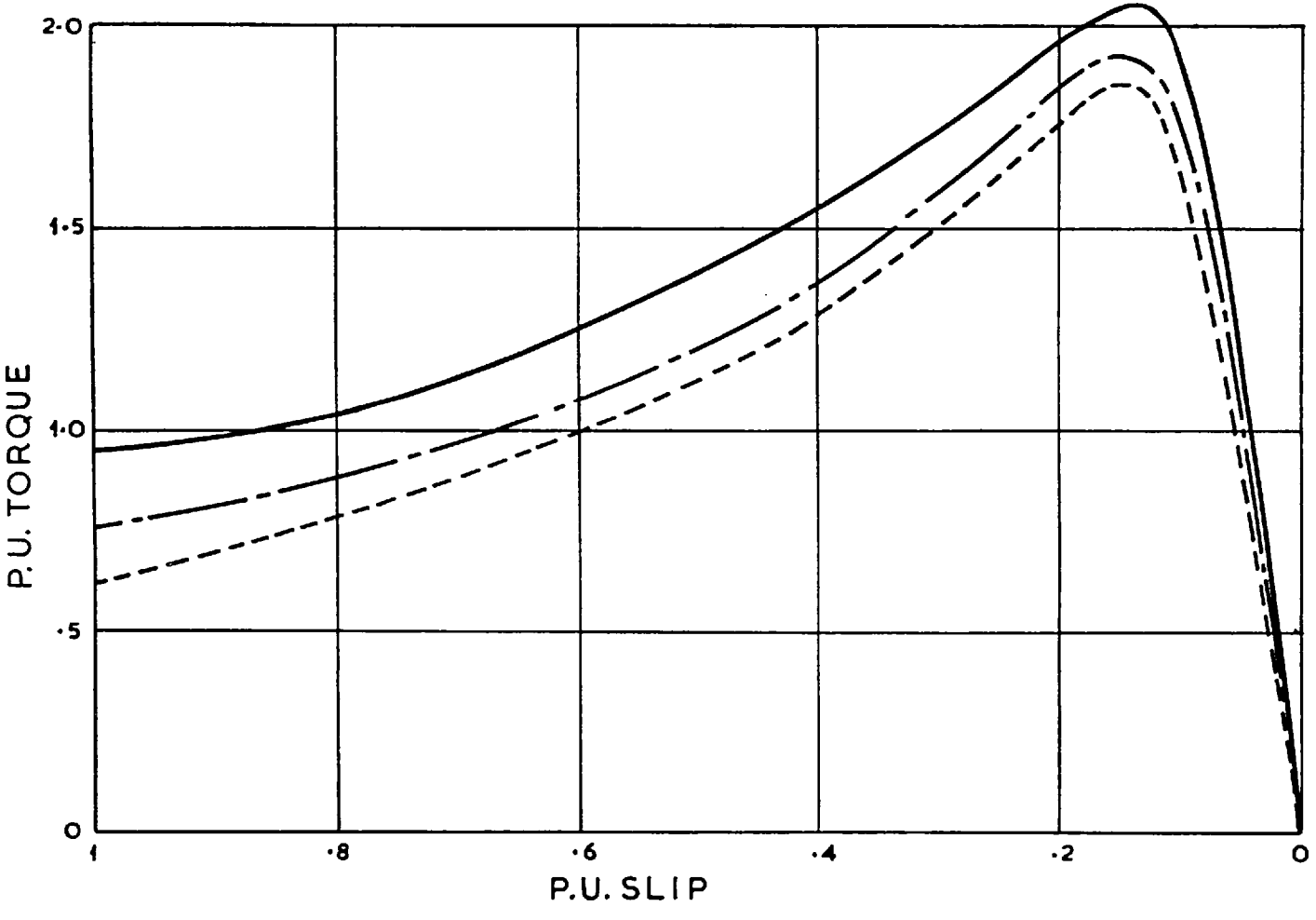

Fig. 20 Comparison of measured mean torque-slip characteristics of the laminated pole micromachine

——— Measured by input power method
— - — Measured by output power method
- - - - - Measured using torque-meter

PART II

THE LAMINATED POLE SYNCHRONOUS MOTOR

CHAPTER 5

INTRODUCTION

The rotor of the most common type of laminated salient pole synchronous motor is constructed of laminations dovetailed into a solid forged 'spider'. The laminations have slots in which are placed the bars of the squirrel cage winding. The main field winding is wound around the salient poles and the ends brought out either to slip rings or, in the case of a brushless machine, to a rectifier bridge. Because of the large centrifugal forces on the laminations at high speed, no large salient pole machines, having less than eight poles, are normally constructed.

During starting the torque is produced by both the squirrel cage and the main field winding. The main field is unexcited, but is closed through a discharge resistance. The discharge resistance serves two purposes; to limit the voltage induced in the field winding during starting, and to enable the field winding to contribute to the driving torque.

The main reason for the choice of a laminated pole machine instead of the cheaper solid pole version is the necessity to obtain starting characteristics to suit a particular application. The slip, at which the peak torque of a machine with a squirrel cage winding is produced, is determined by the correct choice of the resistance of the winding. Little change in the starting characteristics of a solid pole machine can be obtained unless the whole iron material of the rotor

is replaced. It is clear, therefore, that should a synchronous motor be required having, for example, a low starting current, or perhaps a high torque at low slip to damp oscillations about synchronous speed, the laminated pole machine would be the choice.

The laminated pole machine has discrete windings. Hence it is relatively easy to calculate the resistances and reactances of the windings of this type of machine, since both the paths of the current in them and the paths of the flux linking them can be readily determined.

With the assumption that the squirrel cage winding can be replaced by two equivalent windings, one on each axis, the two axis equivalent circuits of the laminated pole synchronous machine can be obtained. The derivation is given in Chapter 2. Fig. 2 shows that the quadrature axis equivalent circuit is like that of a conventional induction motor and the direct axis equivalent circuit like that of an induction motor with a double cage winding. It is apparent, therefore, that the methods of calculating the asynchronous torques, currents, etc., directly from the equivalent circuits or from the induction motor circle diagram, may be applied.

The method of calculation used here, however, is the two axis method using the operational admittance frequency loci, but the analogy to the induction motor circle diagram is given.

It was found that accurate determination of the asynchronous performance of all laminated pole synchronous machines could not be obtained by a direct axis equivalent circuit with two secondary branches and a

quadrature axis equivalent circuit with a single secondary branch. It is shown that, with an additional secondary branch on each axis, more accurate determination of the asynchronous performance can be obtained. This additional branch adequately accounts, also, for the sub-sub-transient effect found in short circuit oscillograms.

CHAPTER 6

THE THEORY OF THE LAMINATED POLE SYNCHRONOUS MOTOR

Much of the theory of the laminated pole synchronous motor and its equivalent circuits is given in the general theory of Chapter 2. The present chapter deals with a more detailed extension of the results found in Chapter 2.

6.1. THE EQUIVALENT CIRCUIT IMPEDANCE

An equivalent circuit reactance is derived from the reluctance of the path through which the appropriate flux passes. Since flux is a distributed phenomenon reluctances of the paths of all sections of that flux must be calculated and the mean effective value for the total flux evaluated. After the mean representative reluctance is obtained, the equivalent circuit reactance must be calculated using the constant given by equation (2.18). The method of calculating the equivalent circuit values of resistance is indicated in Chapter 2.3.1.

Before considering further the equivalent circuit of the laminated pole synchronous machine the significance of the equivalent circuit resistances and reactances is restated (See Fig.2).

X_a, the stator leakage reactance, is representative of the reluctance to the flux leaking across individual or groups of stator slots.

X_f, the field leakage reactance, is representative of the reluctance to flux leaking from pole to pole.

X_{md}, the direct axis magnetising reactance, is representative of the reluctance to the main flux crossing the main air gap on the pole axis.

X_{mq}, the quadrature axis magnetising reactance, is representative of reluctance to the main flux crossing the main air gap on the interpole axis.

X_{kd}, X_{kq}, the direct and quadrature axis squirrel cage leakage reactances, are representative of the reluctances to flux leaking across individual slots, or groups of slots of the direct and quadrature axis squirrel cage windings respectively.

r_f, the main field resistance, is the primary referred value of main field winding resistance.

r_{kd}, r_{kq}, the direct and quadrature axis squirrel cage winding resistances, are the primary referred values of appropriate resistance.

It is seen in Chapter 2 that, at any slip, the magnitude and phase of the voltage across the above reactances is a measure of the magnitude and phase of the flux linking that path corresponding to the appropriate react-

ance; and that the magnitude and phase of the voltage across the above resistances is a measure of the magnitude and phase of the flux linking the appropriate winding. Similarly the current through the impedances is a measure of the M.M.F. required to maintain the flux linking the appropriate path or winding.

6.2. THE CIRCLE DIAGRAMS

If the admittances of the equivalent circuits, i.e. the axis currents at 1 p.u. voltage, are calculated at frequencies from zero to infinity, and the real and imaginary parts plotted against one another, the locus obtained for the quadrature axis is a semi-circle and that for the direct axis a combination of two semi-circles.

The locus of the quadrature axis equivalent circuit 'operational' admittance can be compared with the traditional induction motor circle diagram (Fig. 21).

6.2.1. The Induction Motor Circle Diagram

The induction motor circle diagram is a very well known graphical method of obtaining the characteristics of the induction motor. It is obtained as follows:-

The induction motor is first run up to the no load value of slip, at which the phase current and input power is measured. The armature resistance copper loss is subtracted from the input power and the resulting power factor calculated. Hence the vector OA, in Fig. 21, can be drawn. The induction motor is then locked at standstill and the p.u. current and power factor, excluding armature resistance, obtained at rated voltage. If it is not possible to do this second test at rated voltage, because of heating considerations, the test may be performed at reduced voltage and the value of current obtained scaled up to the rated voltage value. The second test gives the vector OB.

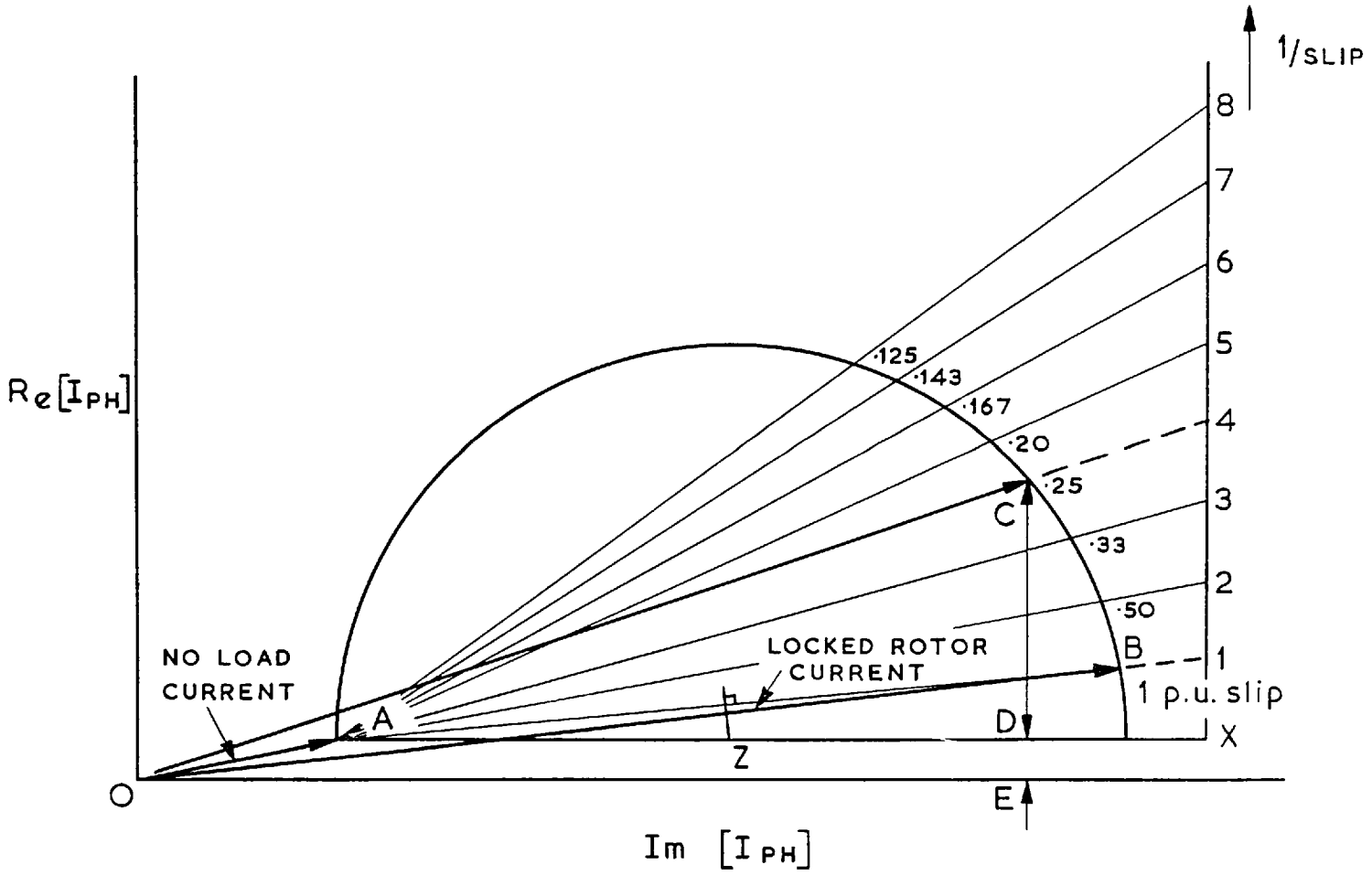

Fig. 21. The Induction Motor Circle Diagram

AB is known to be the chord of the semi-circle whose diameter lies on AX. The point where the perpendicular bisector of AB cuts AX gives Z the centre of the circle, and hence the semi-circle may be drawn. The vector AB is extended to a scaling line XY. The intersection of AB with XY gives the point marked 1. With X as zero XY is a linear scale representing the inverse of slip.

The operating point on the semi-circle for a slip of .25 p.u. for example, is found by drawing the line from A to 1/.25 = 4 on the inverse slip scale. The point of intersection of the line from A to the scale, with the semi-circle gives the operating point s = .25.

The following information is obtained from the diagram for operation at this slip:-

1. OC is the p.u. phase current.
2. EC/OC is the power factor.
3. EC is the p.u. input power.
4. DE is the no load loss.
5. CD is the p.u. output torque.

6.2.2. The Quadrature Axis Operational Admittance Frequency Locus

The admittance of the quadrature axis equivalent circuit of a synchronous machine at frequency $s\omega_o$ is given, in the reactance, time constant form, by equation 2.28.

Replacing T''_{qo} in eqn. 2.28 by $\frac{X_q}{X''_q} T''_q$ from eqn. 2.30 and rearranging, the quadrature axis admittance may be written:-

$$Y_q(js\omega_o) = 1/X_q + \left(\frac{1}{X''_q} - \frac{1}{X_q}\right) \frac{js\omega_o T''_q}{1 + js\omega_o T''_q} \qquad (6.1)$$

Now a function of the form $\frac{js\omega_o T''_q}{1 + js\omega_o T''_q}$ describes a semi-circle in the complex plane as the frequency changes from 0 to ω, and it has zero value at $s\omega_o = 0$ and unit value at $s\omega_o = \infty$.

The expression, therefore, describes a semi-circle in the complex plane from $1/X_q$ to $1/X''_q$ as the slip changes from zero to infinity. The locus is shown in Fig. 22. In fact the $Re\{jY_q(js\omega_o)\} = D$, is drawn against $Im\{jY_q(js\omega_o)\} = C$, (c.f. eqn. 2.26), in order that the susceptances $1/X_q$, $1/X''_q$, lie on the imaginary axis.

If there is no saliency in the synchronous machine, whose quadrature axis locus is as Fig.22, then, providing its field winding is on open circuit, its direct axis locus would be the same, i.e. the real and imaginary components of the two axis operational admittances are equal for all slips.

$$\begin{aligned} A &= C \\ B &= D \end{aligned} \qquad (6.2)$$

Substituting (6.2) into equations (2.35) and (2.38) it is seen that:-

The mean torque is equal to D.

The phase current is equal to $C^2 + D^2$

The power factor is equal to $D/\ C^2 + D^2$

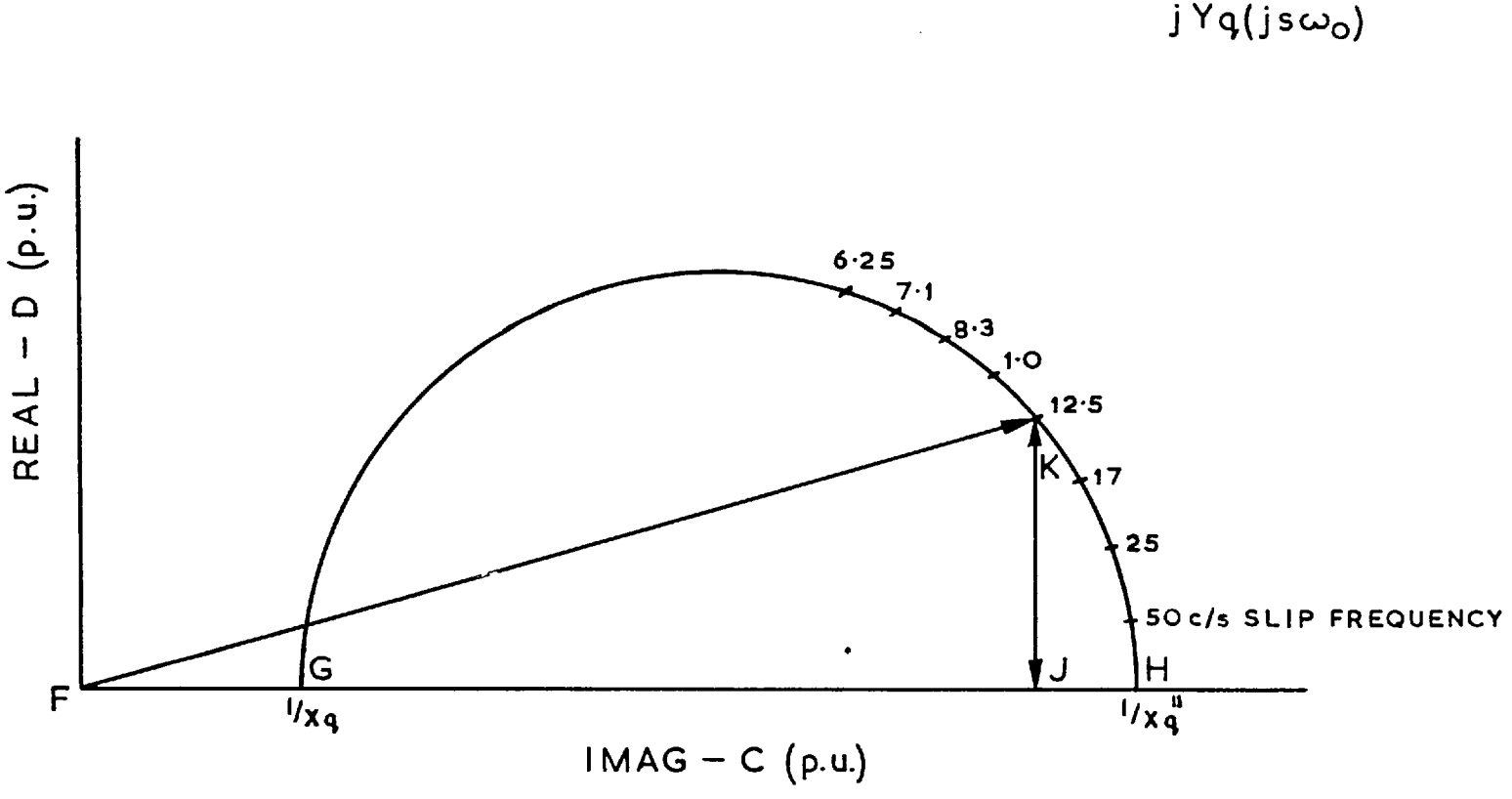

Fig. 22. The quadrature axis operational admittance frequency locus of a laminated pole synchronous motor

Furthermore, if the squirrel cage resistance and reactance, the leakage reactance, and the magnetising reactance of the synchronous machine are the same as that of the induction motor, whose circle diagram is given in Fig. 21 and the no load loss of both machines is neglected, the synchronous motor and the induction motor have identical asynchronous characteristics. In particular the frequency loci of the synchronous machine (Fig.22) and the traditional induction motor circle diagram (Fig.21) are identical.

Comparing the two diagrams at a slip of .25 p.u.

The mean torque = KJ from the frequency loci.
= CD from the circle diagram.
The phase current = FK from the frequency loci.
= OC from the circle diagram.
The power factor = JK/FK from the frequency loci.
= EC/OC from the circle diagram.

Thus it is clear that the operational admittance frequency loci of the synchronous machine is no more than a more sophisticated representation of the traditional induction motor circle diagram.

6.2.3. The Direct Axis Operational Admittance Frequency Locus

The expression for the direct axis operational admittance, in reactance, time constant form, is given in equation 2.27.

In a normal machine, when there is no large external resistance in the field, $r_f \ll r_{kd}$ and then $T'_{do} \gg T''_{do}$ and $T'_d \gg T''_d$.

$Y_d(js\omega_o)$ may be simplified to:-

$$Y_d(js\omega_o) = \frac{(1+js\omega_o T'_{do})(1+js\omega_o T''_{do})}{(1+js\omega_o T'_d)(1+js\omega_o T''_d)} \cdot \frac{1}{X_d} \qquad (6.3)$$

Rewriting in partial fraction form, using the above approximation and equation 2.29.

$$\text{and that} \quad X'_d = \frac{T'_d}{T'_{do}} \cdot X_d \qquad (6.4)$$

$$Y_d(js\omega_o) = \frac{1}{X_d} + \left(\frac{1}{X'_d} - \frac{1}{X_d}\right) \frac{js\omega_o T'_d}{1+js\omega_o T'_d} + \left(\frac{1}{X''_d} - \frac{1}{X'_d}\right) \frac{js\omega_o T''_d}{1+js\omega_o T''_d} \qquad (6.5)$$

In the complex plane the term $\left(\frac{1}{X''_d} - \frac{1}{X'_d}\right)\frac{js\omega_o T''_d}{1+js\omega_o T''_d}$ describes a semi-circle of base diameter $\left(\frac{1}{X''_d} - \frac{1}{X'_d}\right)$, the term $\left(\frac{1}{X'_d} - \frac{1}{X_d}\right)\frac{js\omega_o T'_d}{1+js\omega_o T'_d}$ describes a semi-circle of base diameter $\left(\frac{1}{X'_d} - \frac{1}{X_d}\right)$, and the term $\frac{1}{X_d}$ is constant, as the slip frequency changes from zero to infinity.

The direct axis operational admittance, at any frequency, is the vector sum of the three terms at that frequency. With typical values of time constants and reactances, the complete locus is as shown in Fig. 23(a).

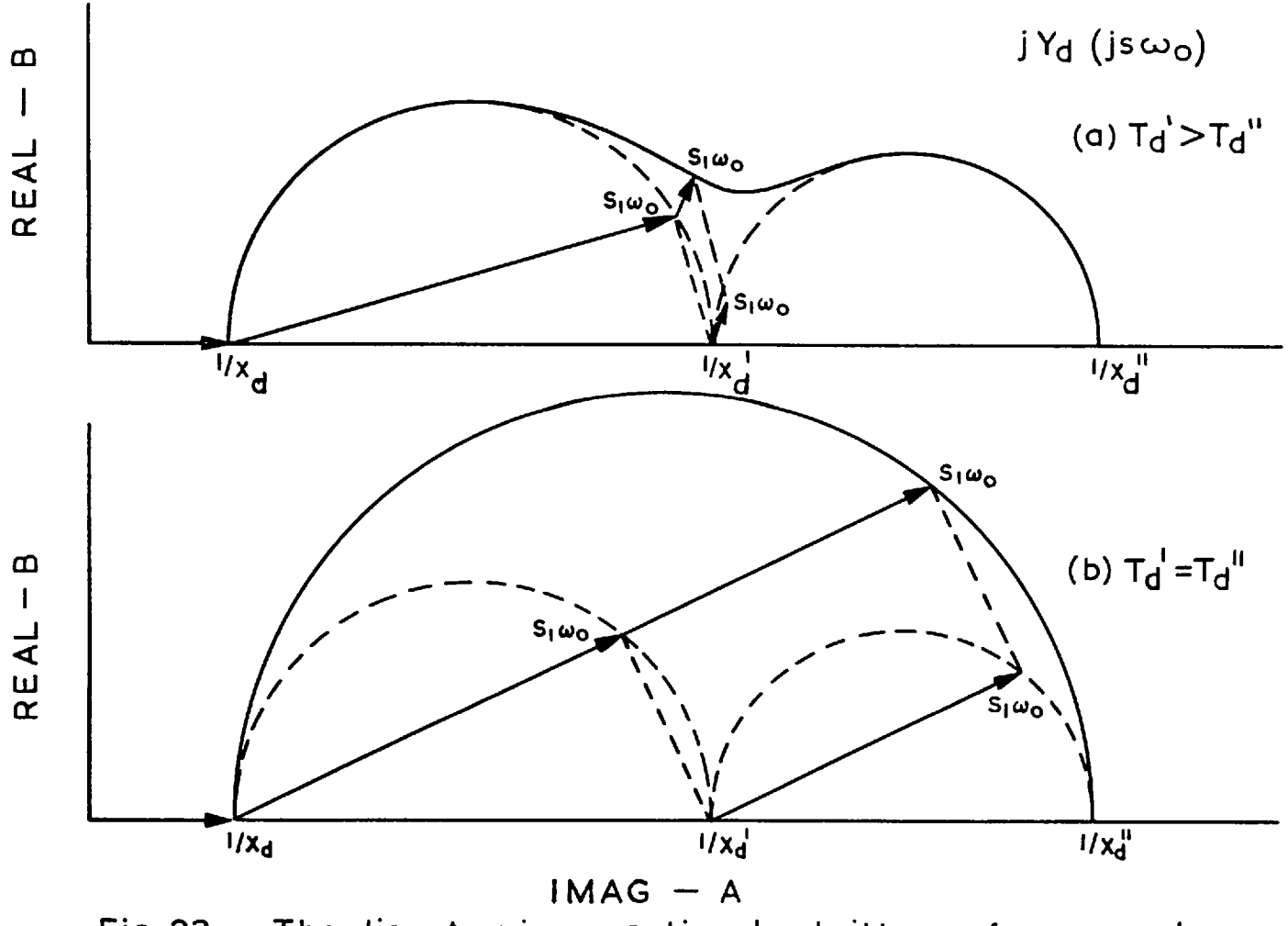

Fig. 23. The direct axis operational admittance frequency locus of a laminated pole synchronous motor

It can be observed that there is a dip in the locus between the two semi-circles, which is due to the large difference between the transient and sub-transient time constants. If sufficient external resistance is inserted into the field circuit, such that the transient and sub-transient time constants become the same, then the vectors of each semi-circle have the same angle at all frequencies. Consequently the vector addition of the two produces a single semi-circle with base diameter from $\frac{1}{X_d}$ to $\frac{1}{X''_d}$ (Fig. 23b).

The direct axis operational admittance frequency locus is equivalent to the circle diagram of an induction motor with double cage winding.

6.2.4. Determination of the Loci from the Results of Sudden Short Circuit Tests

The purpose of the sudden short circuit tests described by Wright[13] is to determine the sub-transient and transient time constants and reactances, and the synchronous reactances of the machine. Inserting the values obtained into equations (6.1) and (6.4) the two axis operational admittance frequency loci may be calculated.

6.2.4.1. The direct axis sudden short circuit

The synchronous machine is driven at full speed, with the three phase windings on open circuit, and excited by a supply having negligible internal impedance. The three phases of the machine are suddenly shorted together and

a recording taken of the decay of phase current following the sudden short circuit.

The equation governing the decay is given by the inverse Laplace transformation of the 'p' form of equation 6.4. It is:-

$$y_d(t) = \frac{1}{X_d} + \left(\frac{1}{X'_d} - \frac{1}{X_d}\right) e^{-t/T'_d} + \left(\frac{1}{X''_d} - \frac{1}{X'_d}\right) e^{-t/T''_d} \qquad (6.6)$$

If equation (6.6) is multiplied throughout by the R.M.S. phase voltage, the direct axis current, following the sudden short circuit, is given by:-

$$i_d(t) = I_d + (I'_d - I_d) e^{-t/T'_d} + (I''_d - I'_d) e^{-t/T''_d} \qquad (6.7)$$

The reactances X'_d, X''_d, and time constants T'_d, T''_d may be conveniently obtained by measuring the amplitudes of the sub-transient and transient currents and plotting them on semi-logarithmic paper against time. Extrapolation of the plots to time zero gives the initial value of current from which the appropriate reactance can be calculated, and from the slope of the plots the time constants may be determined. The synchronous reactance, X_d, may be calculated from the final steady value of current.

6.2.4.2. The quadrature axis sudden short circuit

The three phase stator windings of the machine are connected to the three phase supply, with the field winding on open circuit. The motor is driven by an auxiliary D.C. machine, so that there is the minimum slip speed between the rotating M.M.F. wave, yet without the rotor locking into synchronism on account of the reluctance torque. When the M.M.F. wave passes into the quadrature axis position the three phase supply is suddenly disconnected, and simultaneously the three phase terminals of the machine shorted together. An oscillogram is taken of the decay of the three phase currents of the machine.

The equation governing the decay of current is:-

$$y_q(t) = \frac{1}{X''_q} e^{-t/T''_q} \qquad (6.8)$$

The reactance, X''_q, and the time constant T''_q, are again obtained from the semi-logarithmic plot of the decaying current.

The asynchronous torques, currents, powers, and power factor of the laminated pole machine are calculated from the equations in Chapter 2, once the two axis operational admittance functions are known. The exact expressions for the torques, currents, etc., (eqns. 2.49 and 2.54) are not so simple as those for the round rotor induction motor, since in a salient pole synchronous motor the combination of the saliency and the armature

resistance seriously effects the performance of the machine in the half speed region. However, an approximate estimation of the asynchronous performance can be obtained graphically - corresponding to the induction motor circle diagram method - from the two axis operational admittances loci, as given in section 4.2.4. of Chapter 2.

CHAPTER 7

COMPARISON OF THE MEASURED AND CALCULATED RESULTS OF LAMINATED POLE MACHINES

7.1. THE LAMINATED POLE MICROMACHINE

The micromachine, which is located in the electrical engineering laboratories at Imperial College, is a model of a large synchronous machine.

It is so constructed that the rotor is easily removed and, since several rotors of different types are available, the micromachine is able to simulate almost all types of synchronous machine.

Although the four pole machine (stator no. 334819) has a nominal rating of 2 KVA, it is designed to have a low copper loss, and hence is able to withstand a continuous overload of over twice this rating. The machine is three phase, star connected, having 126 turns in series per phase located in 18 slots.

The rotor used for the present work is a laminated salient pole rotor, (no.334818) with a complete squirrel cage winding having 6 bars per pole and one bar per interpole space. Both the bars and the end-rings are of copper. The field winding has 660 turns per pole and an overall resistance of 19.7 ohms.

The following p.u. base values were chosen:-

1 p.u. voltage = 220^{V} line = 127^{V}/phase

1 p.u. current = 6^{A}/phase

then:-

1 p.u. power = 2.28^{KW}

1 p.u. torque = 14.5 Nm.

The following p.u. parameters were then calculated for this stator/rotor combination using well known methods:-

Equivalent circuit parameters		Corresponding transient parameters	
X_a	= .130	X_d	= 1.53
X_{md}	= 1.40	X'_d	= .280
X_f	= .17	X''_d	= .206
X_{kd}	= .15	X_q	= .82
X_{mq}	= .74	X''_q	= .214
X_{kq}	= .095	T'_d	= .16 secs
r_f	= .0058	T''_d	= .0165 secs
r_{kd}	= .0425	T''_q	= .026 secs
r_{kq}	= .027		

The above parameters were also determined from the results of tests applied to the machine. The tests applied were the direct and quadrature axis sudden short circuit tests and slip tests. Because of the difficulty in measuring the value of stator leakage reactance, X_a, particularly for the high current conditions, the calculated value was assumed in the determination of the equivalent circuit reactances from the short circuit parameters.

The test values obtained were:-

Equivalent circuit parameters		Corresponding transient parameters	
X_{md}	= 1.51	X_d	= 1.64
X_f	= .23	X'_d	= .332
X_{kd}	= .17	X''_d	= .215
X_{mq}	= .80	X_q	= .93
X_{kq}	= .09	X''_q	= .21
r_f	= .0061	T'_d	= .18 secs
r_{kd}	= .046	T''_d	= .017 secs
r_{kq}	= .032	T''_q	= .021 secs

7.1.1. Comparison of the Measured and Calculated Operational Admittance Frequency Loci

Fig. 24 shows the comparison between the calculated direct axis operational admittance frequency loci with three different connections of the main field, - field short circuited, field open circuited, and field connected onto a discharge resistance of .036 p.u. The loci were determined from the calculated values of parameters given above. The value of discharge resistance inserted into the field was such that the transient and sub-transient short circuit time constants were the same, and as shown in Chapter 6 the direct axis locus, in this case, is a single semi-circle from $1/X_d$ to $1/X''_d$. The locus for the field open circuited is a semi-circle from $1/X_d$ to a value of $1/X''_d$, modified by the omission of field leakage reactance.

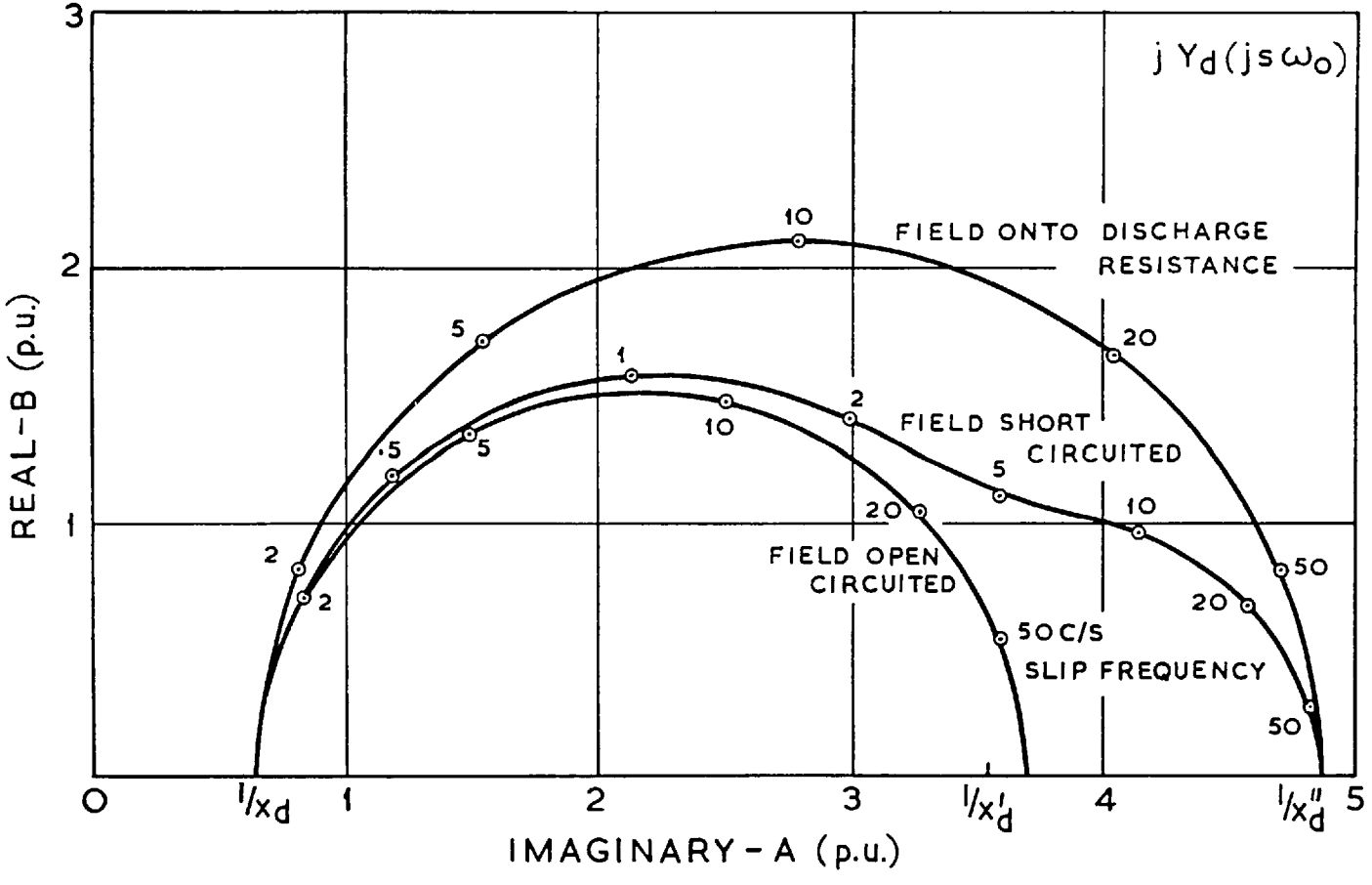

Fig. 24. Direct axis operational admittance frequency loci calculated for the laminated pole micromachine

Fig.25 shows the comparison between the direct axis operational admittance frequency loci with field short circuited determined from calculated equivalent circuit parameters, that calculated from the equivalent circuit parameters determined from sudden short circuit tests, and that measured by the most reliable direct method - the variable frequency single phase static impedance test. Figs. 26, 27 show the same comparison for the other two connections of the main field winding. Fig.28 shows a similar comparison for the quadrature axis.

Although the agreement between the loci completely calculated and the loci calculated from measured short circuit parameters is fairly good, neither of these compare so well with the actual machine loci directly measured using the static impedance test. The error is particularly evident at high slip frequencies when the real part of the operational admittances measured is somewhat larger than estimated. Reason for the discrepancies is given in Chapter 8.

7.1.2. Comparison of the Measured and Calculated Starting Performance

Fig. 29 shows the comparison between the torque-slip characteristics measured by the output power method with the different main field connections. It is observed that it is only with the field on open circuit that there is sufficient saliency in the machine to produce a half speed dip in the mean torque-slip characteristic.

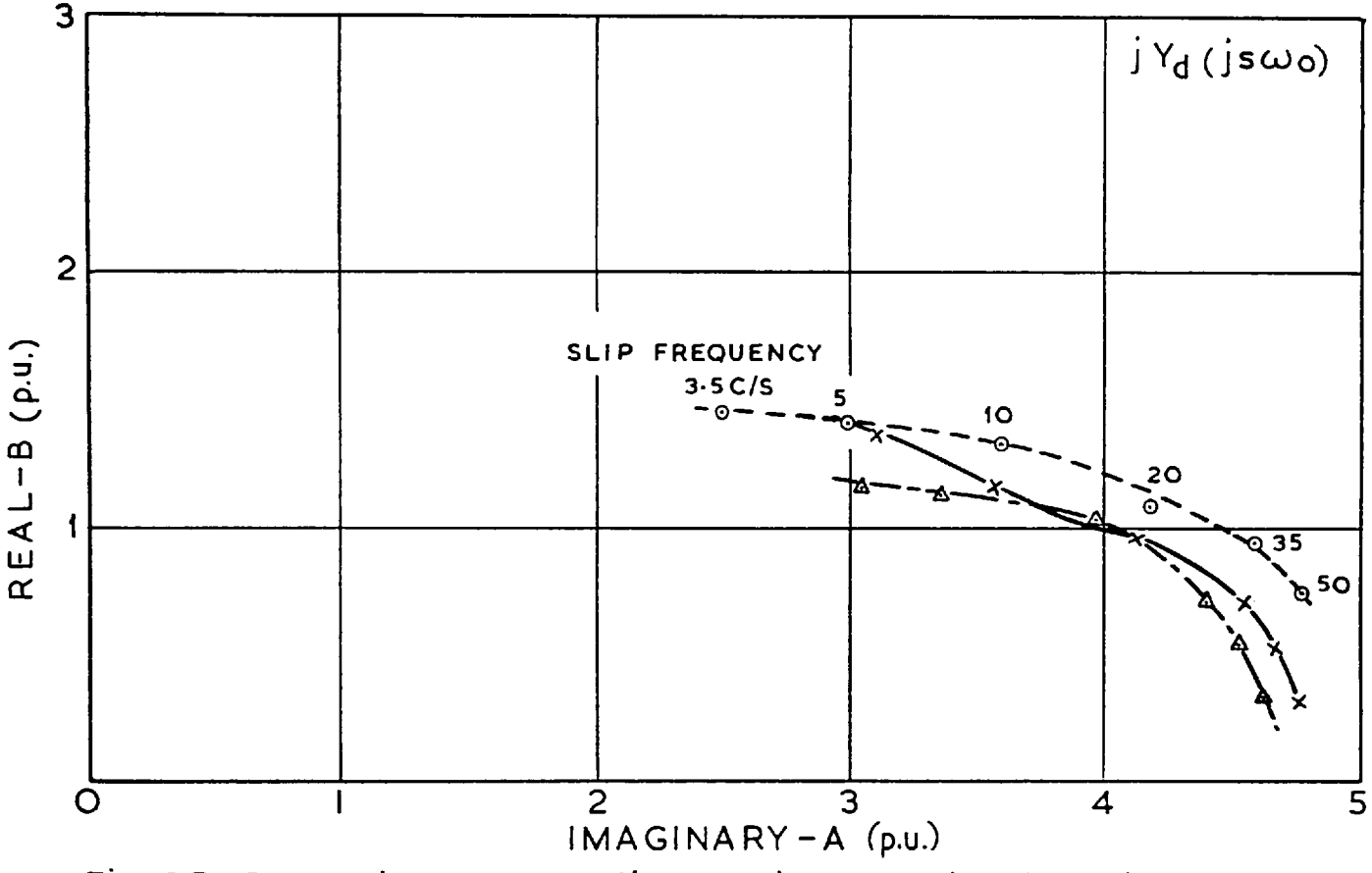

Fig. 25. Comparison of the direct axis operational admittance frequency loci of the laminated pole micromachine, with field short circuited

---⊙--- Measured by the static impedance test

—-△—— Calculated from measured short circuit parameters

——×—— Directly calculated

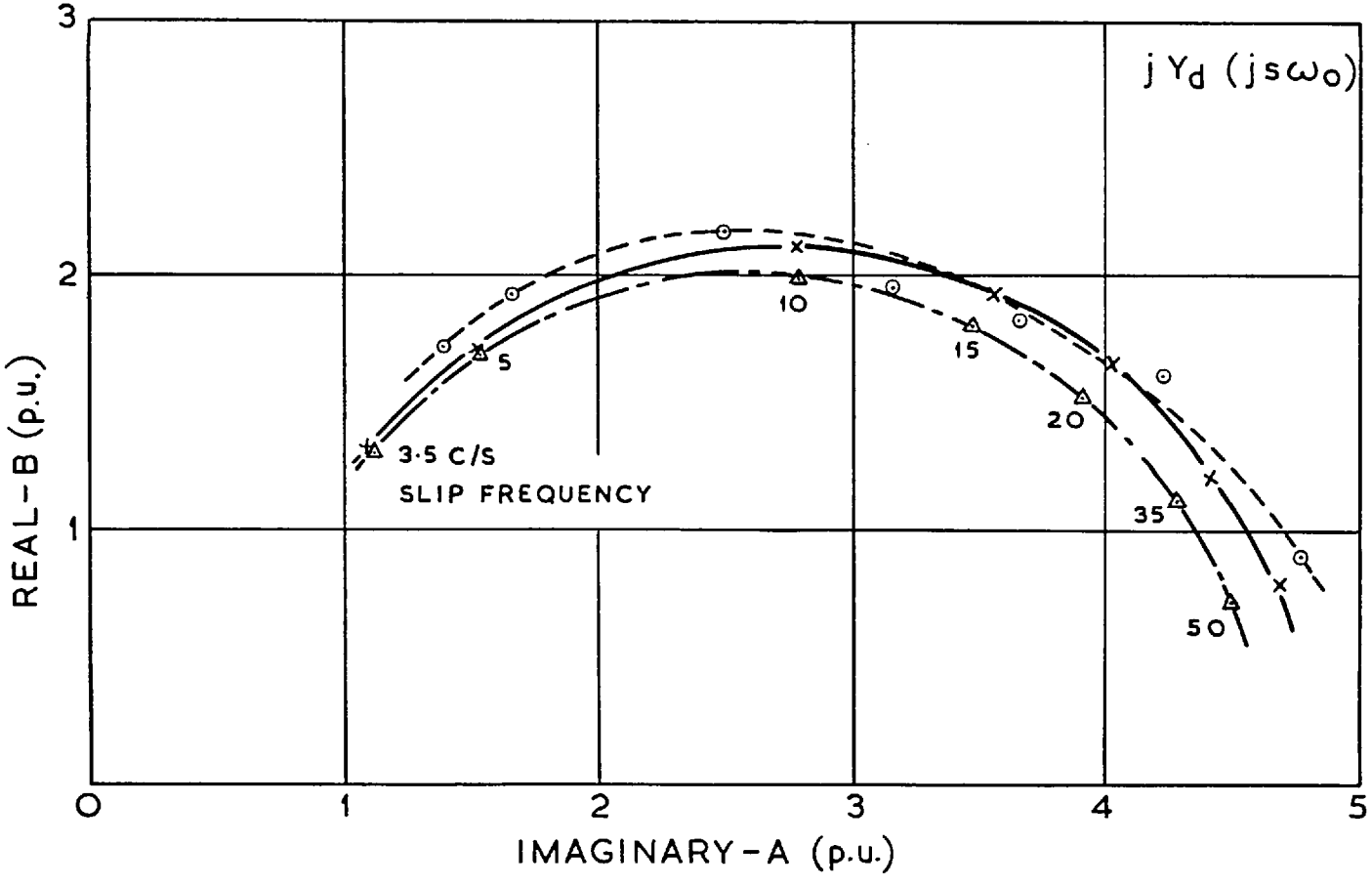

Fig. 26. The direct axis operational admittance frequency loci of the laminated pole micromachine, with field connected to discharge resistance

---⊙--- Measured by the static impedance test

—-△— Calculated from measured short circuit parameters

——×—— Directly calculated

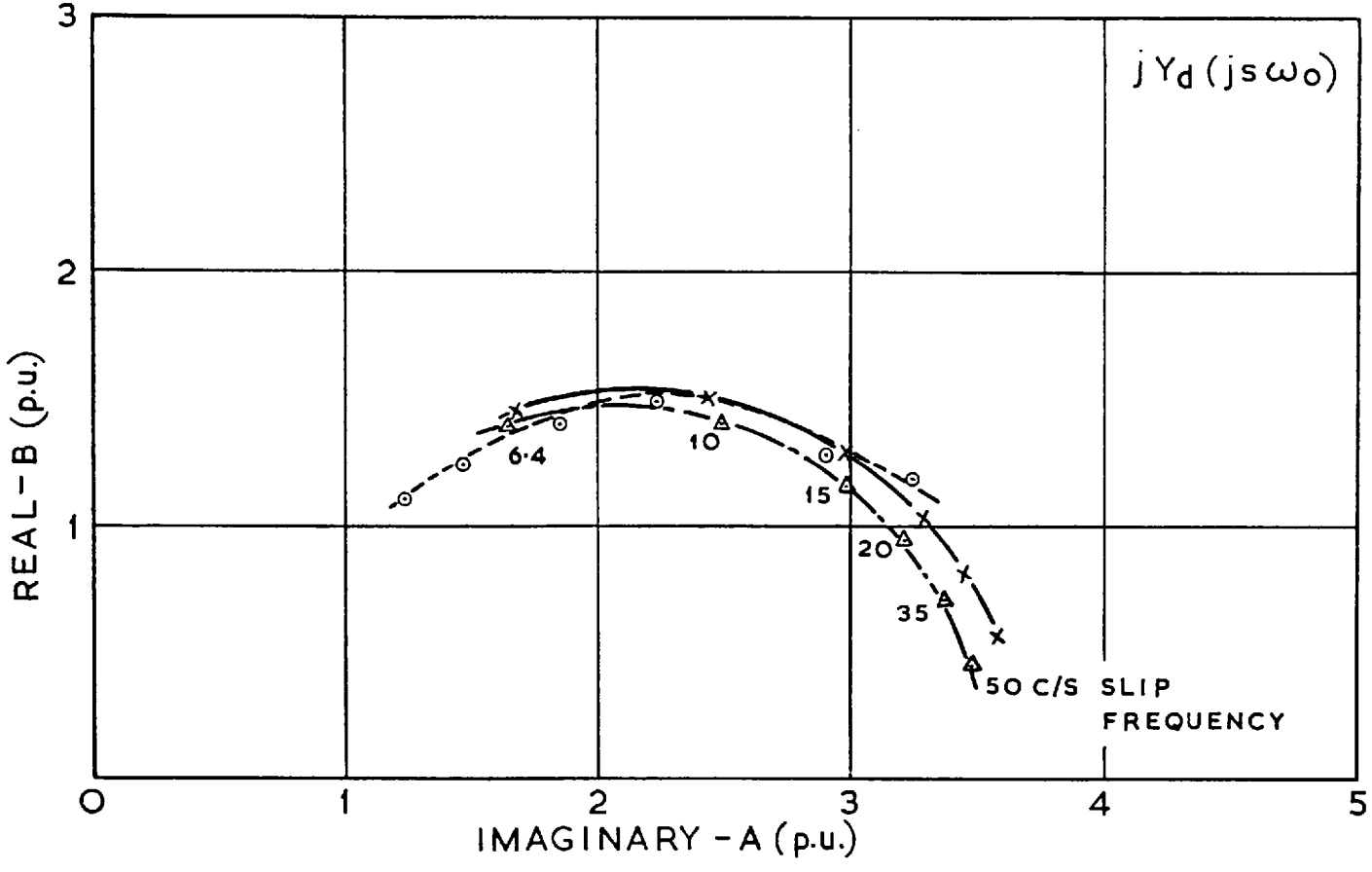

Fig. 27. The direct axis operational admittance frequency loci of the laminated pole micromachine, with field on open circuit

---⊙--- Measured by the static impedance test

—·—△— Calculated from measured short circuit parameters

——×—— Directly calculated

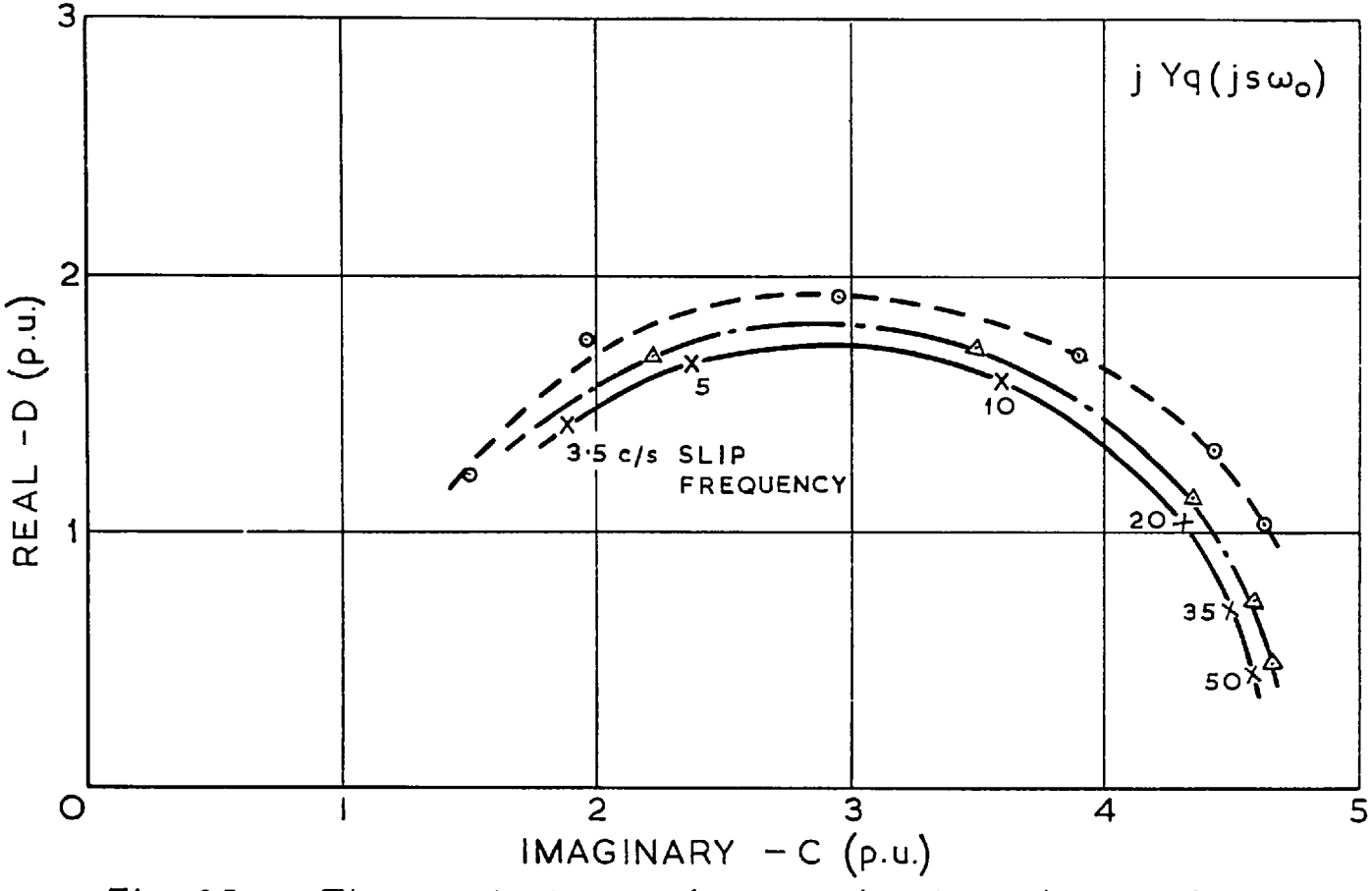

Fig. 28. The quadrature axis operational admittance frequency loci of the laminated pole micromachine

— — —o— — Measured by the static impedance test

——·—Δ—— Calculated from measured short circuit parameter

——x—— Directly calculated

Figs. 30, 31, 32 show, for each of the field connections, the comparison between the measured mean torque-slip characteristic, that calculated from the loci obtained from static impedance results, and that estimated from the calculated machine parameters. It is observed that the estimation of torque from the measured admittance loci agrees well with the measured torque characteristics. However, the torques estimated from the calculated parameters are pessimistic at high slips.

Fig. 33 shows part of the recording of shaft torque measured by the torque-meter, taken as the micromachine ran up to synchronous speed. Using the response characteristic given in Appendix IV the inducing electromagnetic oscillating torque of the micromachine was estimated, and is shown in Fig. 34. Both the oscillating torque characteristic, determined from the admittance loci derived from static impedance results and the characteristic determined from calculated parameters agree quite well with that obtained by measurement.

Fig. 35 shows similar comparisons for the mean phase current - slip characteristics, and that the agreement between them all is good.

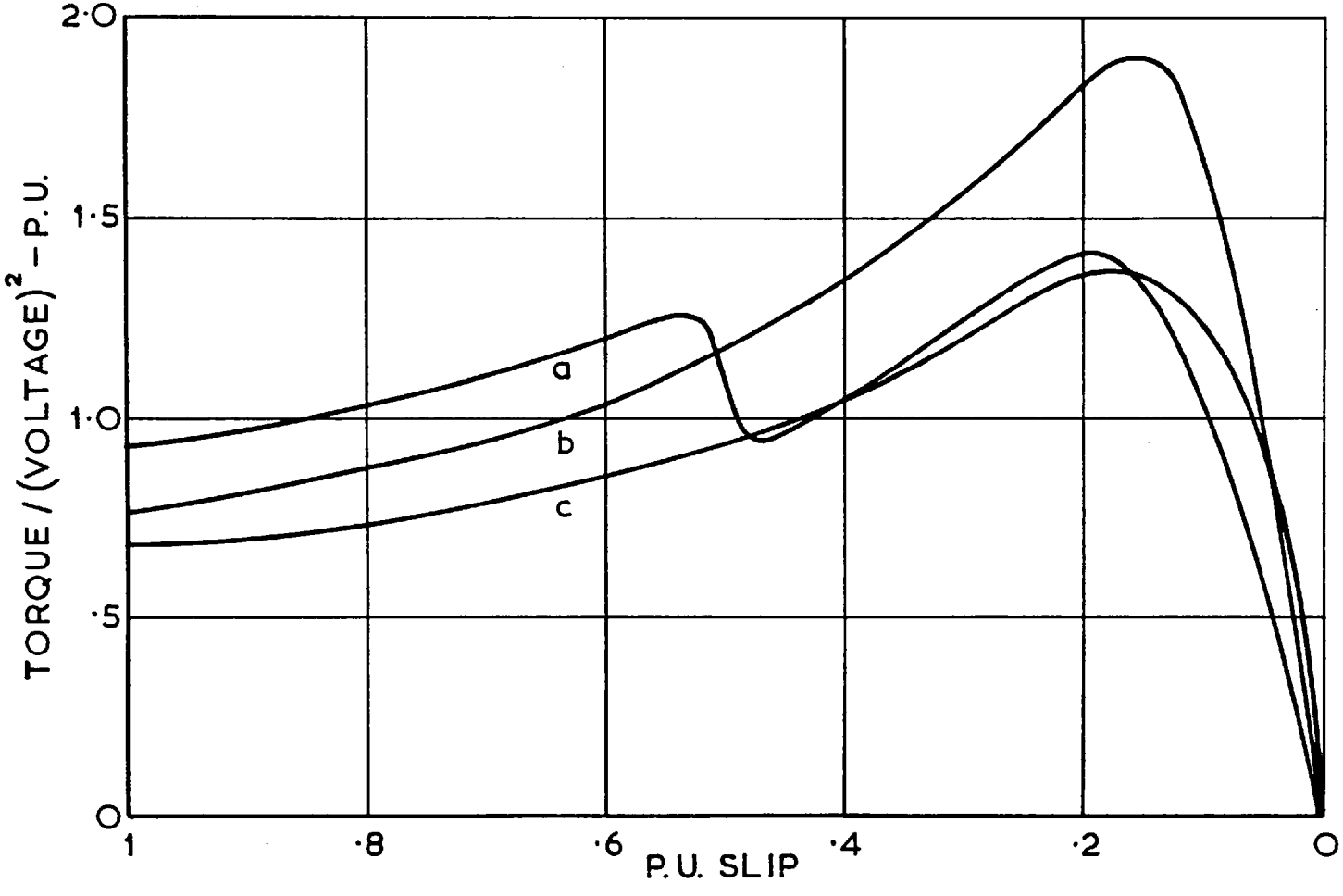

Fig. 29 Mean torque slip characteristics of the laminated pole micromachine measured with different field connections

a. Field open circuited
b. Field connected to discharge resistance
c. Field short circuited

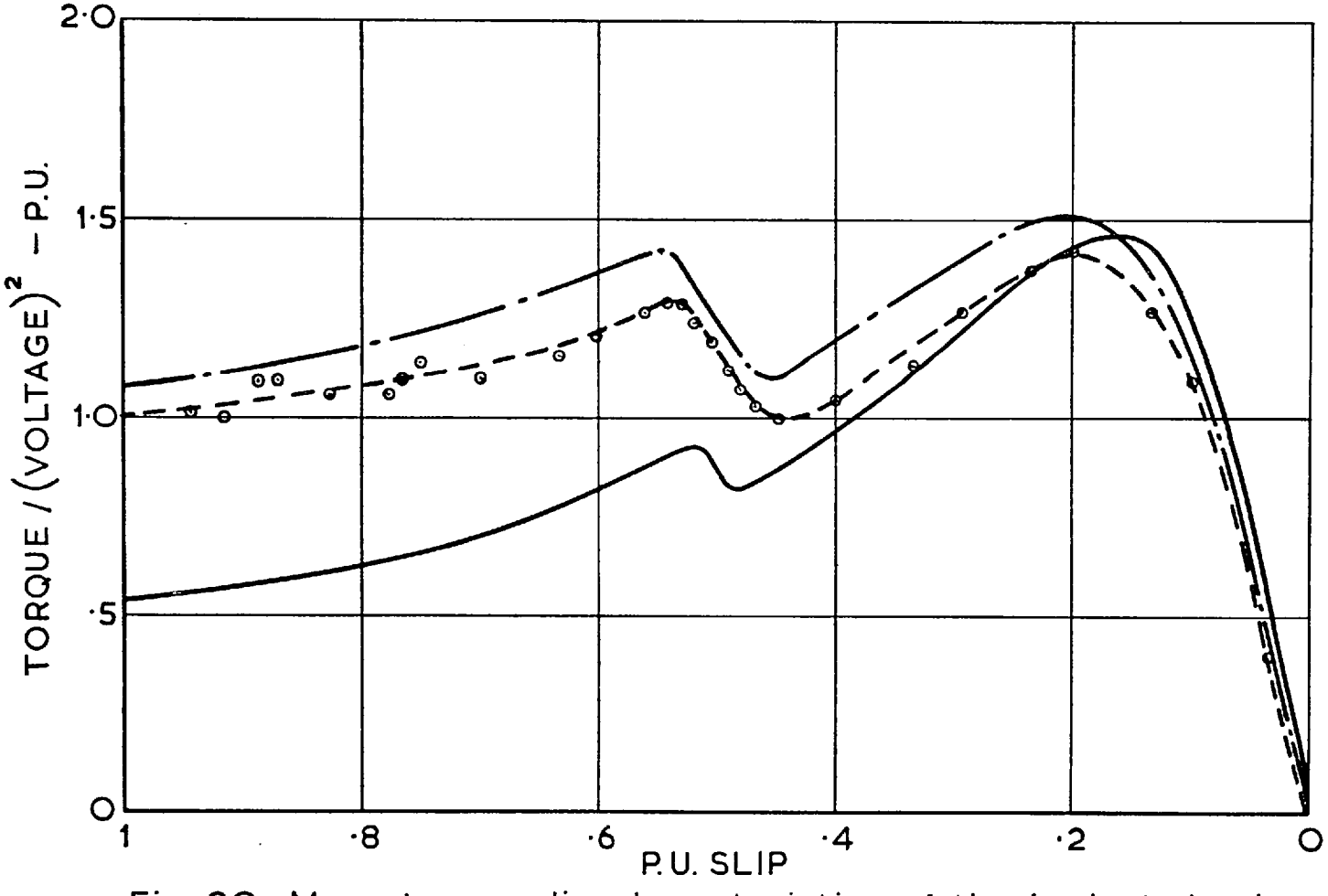

Fig. 30 Mean torque slip characteristics of the laminated pole micromachine with field connected on open circuit

– – ⊖ – – Measured by output power method
— - —— Calculated from static impedance test results
—————— Calculated

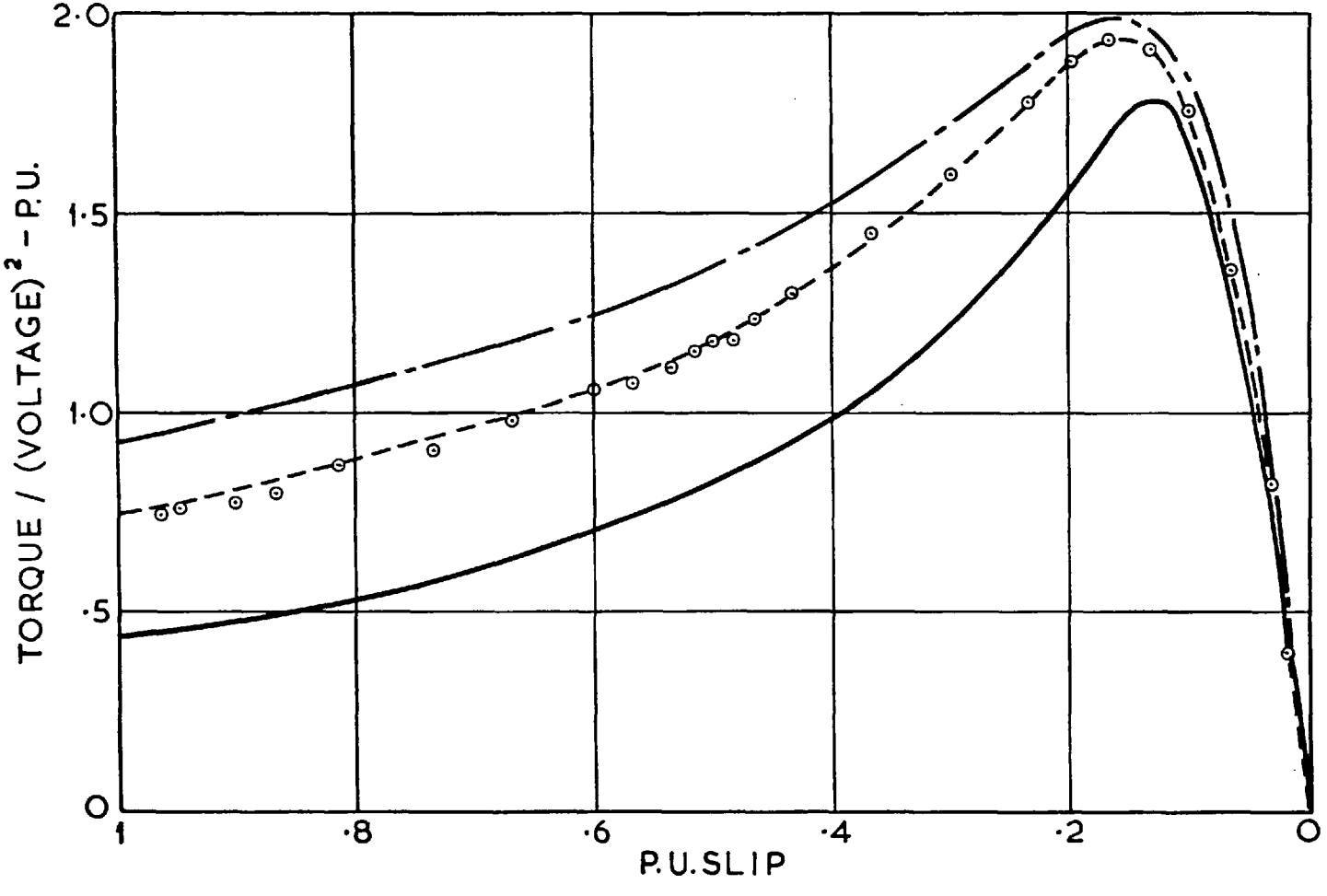

Fig. 31. Mean torque-slip characteristics of the laminated pole micromachine with field connected to discharge resistance

---⊙--- Measured by output power method
—— - —— Calculated from static impedance test results
———— Calculated

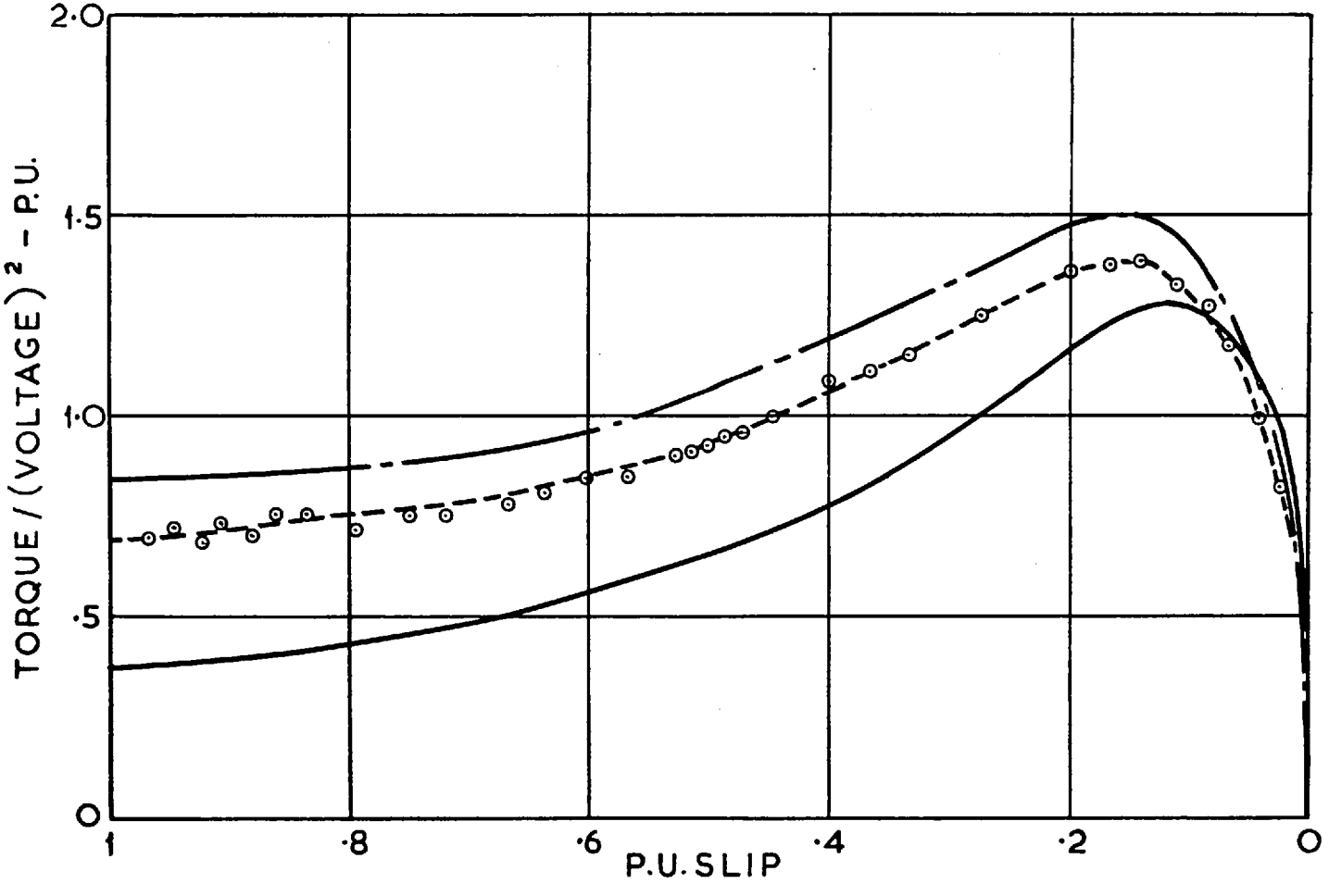

Fig. 32 Mean torque-slip characteristics of the laminated pole micromachine with field short circuited

---⊙--- Measured by output power method

——·—— Calculated from static impedance test results

——————— Calculated

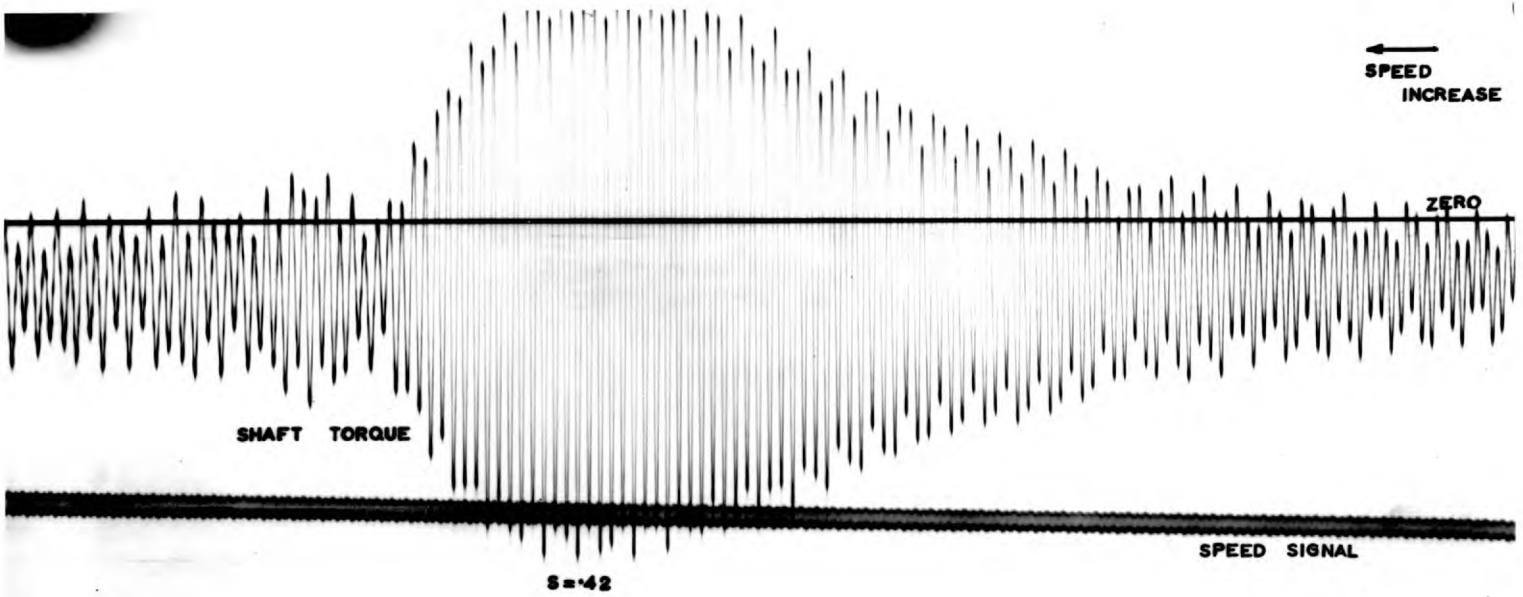

Fig. 33. Run up shaft torque passing through the mechanical torsional resonant frequency.

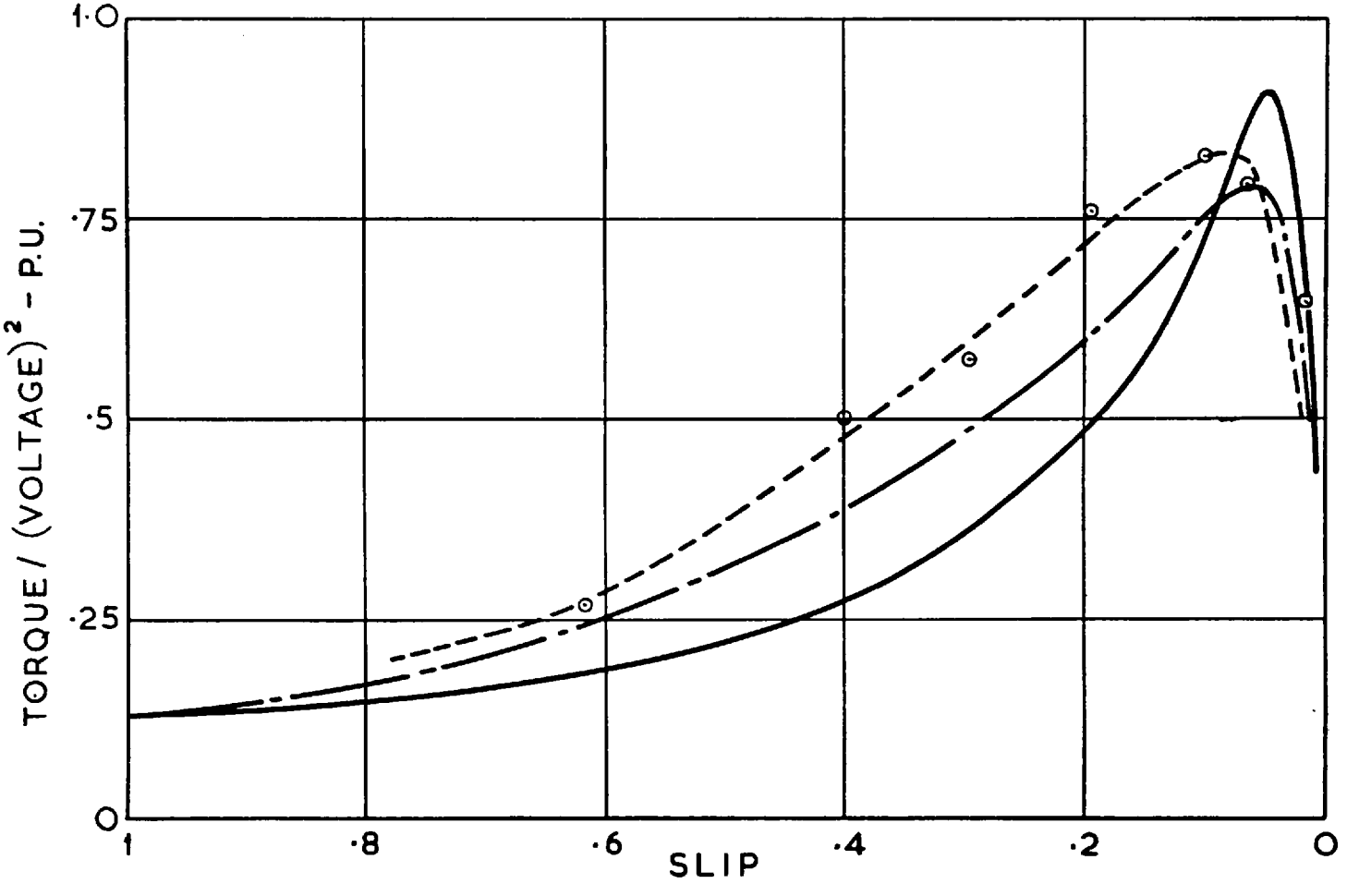

Fig. 34 Zero peak amplitude of oscillating torque measured for the laminated micromachine with field short circuited

---⊙--- Measured using torque-meter
—— - —— Calculated from static impedance test results
——————— Calculated

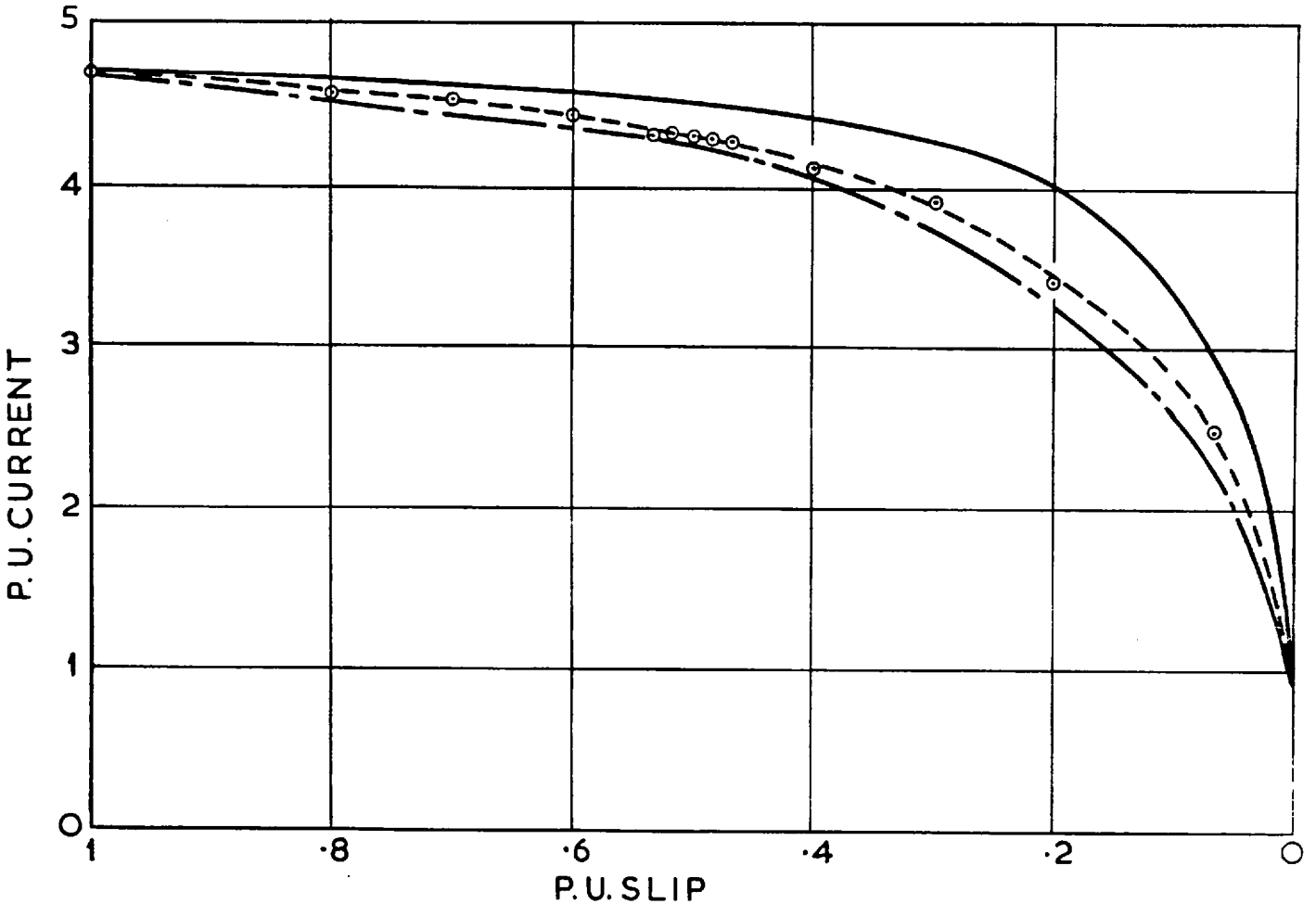

Fig. 35. Mean phase current-slip characteristics of the laminated pole micromachine with field short circuited

---⊙--- Measured by ammeter
——— Calculated from static impedance test results
——— Calculated

7.2. THE LARGE LAMINATED POLE MACHINES

Such detailed comparisons, as shown for the micro-machine, are not available for the large machines.

7.2.1. The 600 H.P., 14 Pole Machine

Although torque measurements could not be obtained for this machine it was possible to apply the axis resolution method, and Fig.36 shows the comparison between the direct axis admittance loci obtained with the field short circuited, and that directly calculated from the design parameters.

Despite the scatter of points obtained from the results of the test, some resemblance between points of the calculated loci, and those measured is evident. As the single phase static impedance test was applied to the machine at supply frequency, the appropriate value of admittance is also included in the figure for further comparison.

7.2.2. The 3000 H.P., 18 Pole Machine

The axis resolution method was not available at the time that this machine was tested. However, a torque-slip characteristic was obtained by the accelerometer method. The very good agreement between the measured and calculated characteristics is shown in Fig. 37.

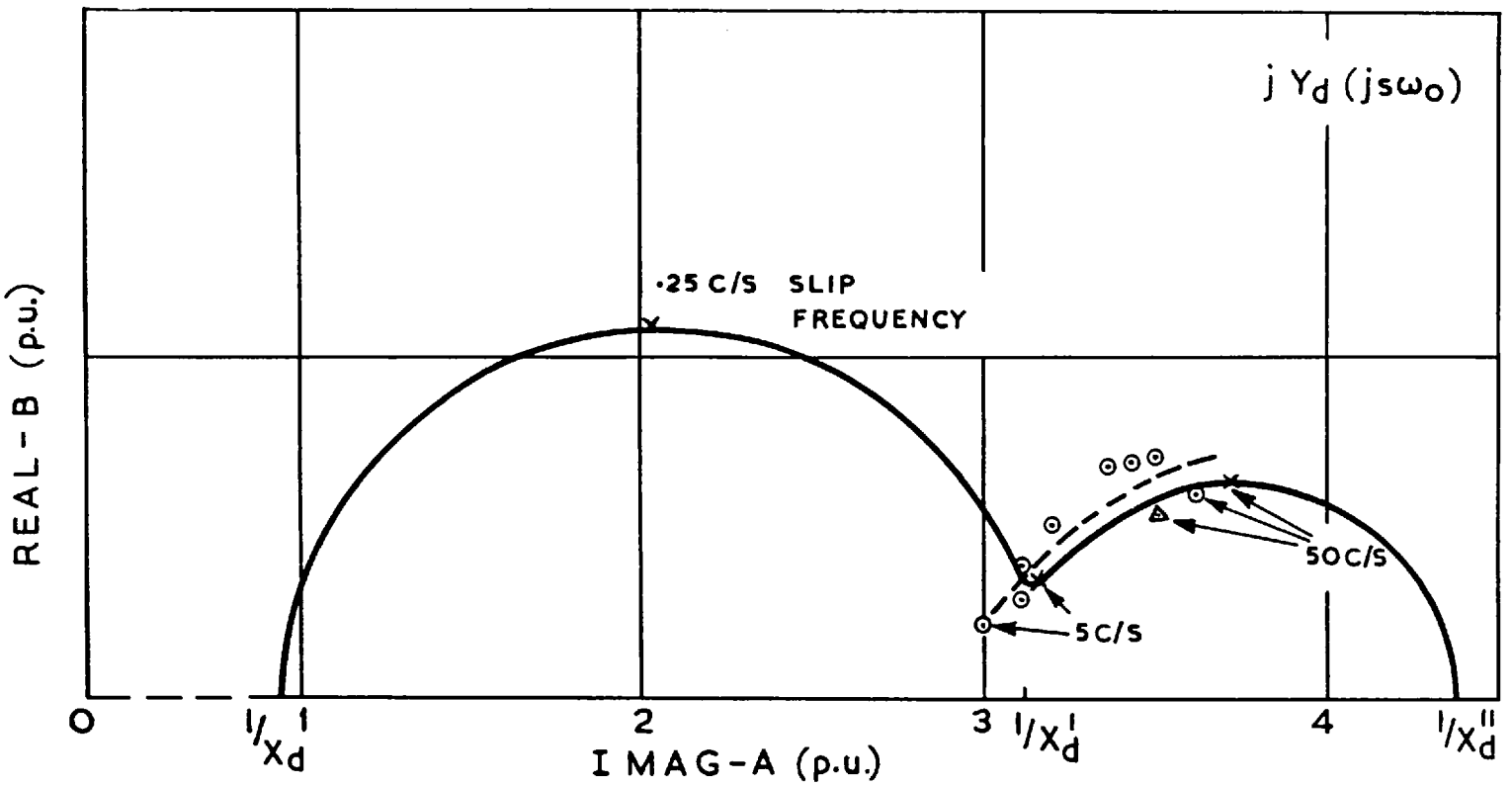

Fig. 36 The direct axis admittance loci of the 600 H.P., 14 pole machine with field short circuited.

Calculated locus

Measured by the axis resolution method

Static impedance test value

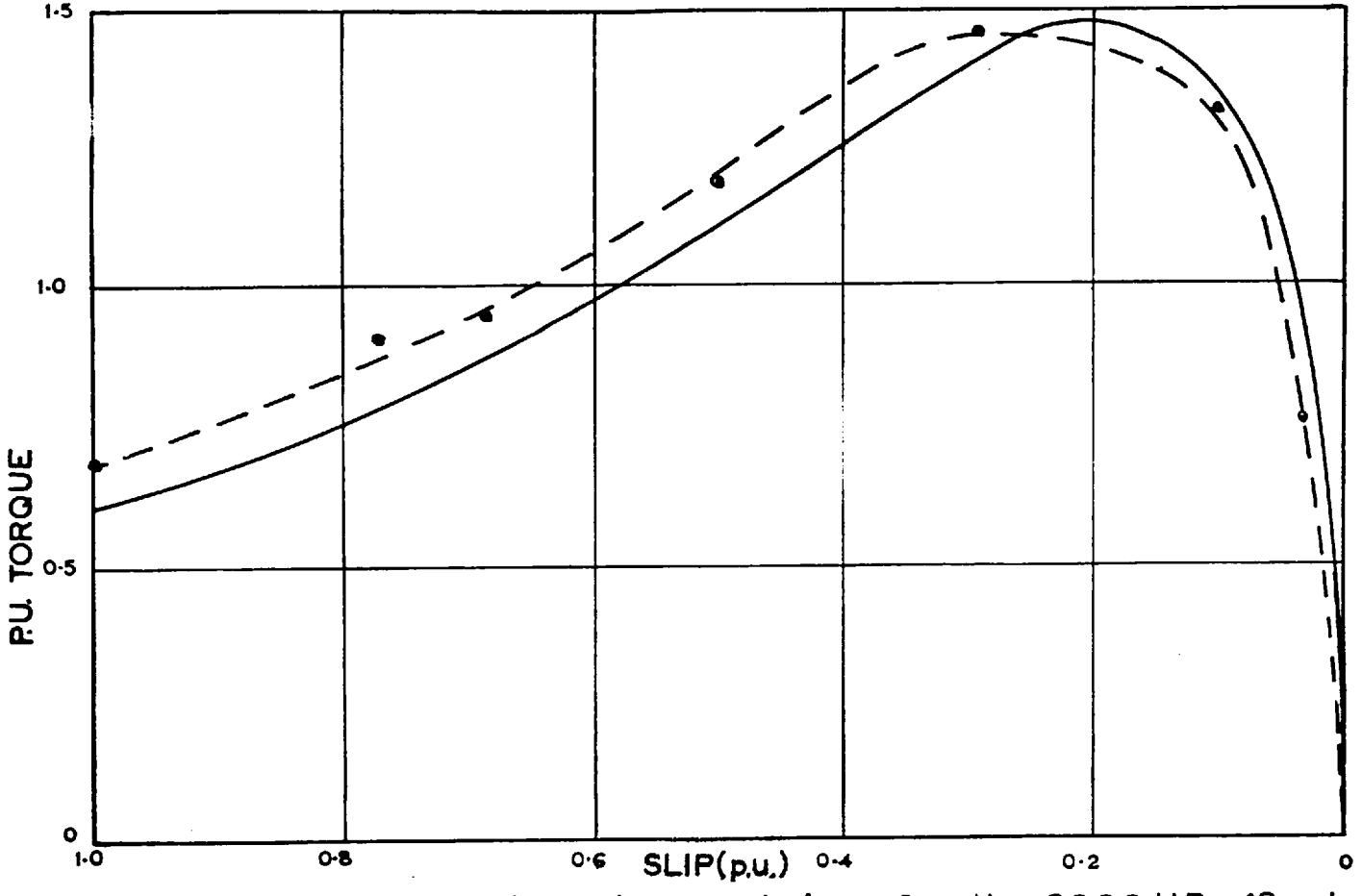

Fig. 37 Mean torque–slip characteristic for the 3000 HP, 18 pole synchronous motor. Voltage 1 p.u.

— — ● — — Measured by the accelerometer method

———— Calculated from design.

CHAPTER 8

CONCLUSIONS

8.1. ASSUMPTIONS IN THE THEORY

There are several assumptions made in the theory, and in the method of the two axis representation of the machine. It is worthwhile reviewing the assumptions before discussing reasons for discrepancy between measured and calculated results.

Saturation

In the idealised machine it is assumed that all voltages are proportional to the currents producing them, i.e. there is no saturation, or other non-linearity. The effect of a non-linearity such as saturation would upset the direct proportionality between the voltage and current, i.e. the reactances of the machine no longer remain constant but they are functions of the voltage across them, that is to say the reluctances of the machine are not constant but change with the flux linking them.

During starting the main flux is usually low, but, due to the high current in the windings, the leakage fluxes are high, and it is the value of reactances, representing the latter flux paths, that are liable to be in error due to saturation.

Harmonics

Space harmonics are neglected in the general theory, and since generally machines are designed to minimise the effects of space harmonics the assumption is justified.

Although the general machine equations apply to all possible manners of variation of the instantaneous values of current and voltage, it is assumed, when steady asynchronous running is considered, that the 'p' form of the general equations (2.2) to (2.7) transform to the '$js\omega_o$' equivalent. The effect of the presence of time harmonics is to make the 'p' to '$js\omega_o$' transformation invalid, and physically in the machine, to produce undesirable effects such as noise, voltage ripple, and parasitic torques.

Flux linkages

It is assumed, in the derivation of the equivalent circuits in Chapter 2, that the fluxes linking the various windings can be simplified to a main flux linking equally all stator and rotor windings, and to a leakage flux appropriate to each winding as shown in Fig. 3a.

The two axis representation

The rotating M.M.F. and flux waves are considered to be transformed to two pulsating M.M.F.'s and fluxes one on each axis of the machine. Even if there are no harmonics in the rotating M.M.F.

and flux waves it cannot necessarily be assumed that the axis quantities change perfectly sinusoidally at the slip frequency. Supporting evidence of this is seen by observation of the axis quantities, at low slip, in Fig. 10.

A further assumption is that the complete squirrel cage winding may be considered as two independent damper windings, one on each axis. The independence becomes very questionable, for example, when the current flowing in the cage is high and the temperature rise of a section common to both 'equivalent windings', due to one axis damper current, causes change of the resistance of the section to both axes damper currents.

The rotor circuits

The rotor is considered perfectly laminated and hence the only rotor current paths are in the discrete windings. The assumption is certainly invalid if there are any solid iron parts in the rotor, in which eddy currents are able to flow. In these circumstances the machine cannot be represented by a two secondary winding equivalent circuit for the direct axis and a single secondary winding equivalent circuit for the quadrature axis.

The operational admittances and stator iron loss

Iron loss in the stator, unlike that of the rotor, contributes no torque to the machine. Consequently if the torque is defined by the real part of the operational admittances, (Chapter 2) it is necessary to ignore the resistive part of the magnet-

ising branch (conventionally included in induction motor equivalent circuits) in the synchronous machine equivalent circuits. However when the operational admittances are determined by test, a proportion of the real part obtained is due to stator iron loss, and not an indication of output torque of the machine. It is possible that an allowance could be made for this, although usually, since it may only be of the order of 1% of the total real part obtained, it is justifiable to neglect it.

8.2. SUGGESTED REASONS FOR DISCREPANCIES BETWEEN MEASURED AND CALCULATED RESULTS

The comparisons of the measured torque and current characteristics with those estimated from static impedance test results show that the operational admittance loci calculated from static impedance tests can be satisfactorily used to predict accurately the torques and currents of the machine. It is observed that the measured torques are approximately 10% less than those predicted by static impedance test results. This can be accounted for by the stator iron loss, not allowed for in the calculation of results from static impedance test, and by load loss. The load loss is mainly produced by harmonics.[21]

It is shown for the micromachine that, although the calculated parameters of the machine agree well with the reactances and time constants calculated from sudden short circuit tests, the same parameters do not predict the torque with any satisfactory degree of accuracy at all. This is not surprising since the operational admittance frequency loci calculated directly from sudden short circuit parameters gave very pessimistic results compared to the static impedance tests, at high frequency. It was considered, at first, there was error in the estimation of both the calculated parameters and the parameters obtained from sudden short circuit results, and an attempt was made to find what values of standard reactances and time constants would produce a locus that agreed well with that measured by the static impedance test. However, it was found impossible with any values of the standard reactances and time constants to obtain a locus,

either for the direct or quadrature axis, that agreed with the loci obtained by static impedance test, over the whole frequency range. It was then concluded that the operational admittance frequency loci and hence the asynchronous performance of the laminated pole micromachine could not be accurately estimated from a direct axis equivalent circuit with two secondary branches and a quadrature axis equivalent circuit with a single secondary branch, but that at least one additional secondary branch was necessary in both cases. The additional secondary branch would then be representative of eddy current paths in the solid iron parts of the rotor, particularly in the large solid iron end clamps.

The results for the large machine show that agreement between calculated and measured results is much closer. This is because first of all the stray load loss of machinery reduces in proportion to the output as the size of the machine increases, and more important, because there is much less solid iron in the rotors of large machines tested, than in the micromachine.

8.3. THE ADDITION OF A FURTHER SECONDARY BRANCH TO THE EQUIVALENT CIRCUITS

The simplest addition to the equivalent circuits is a branch of resistance and reactance which, although not truly representative of eddy current paths, as is shown in the third part of this thesis, does at least show in principle how the addition of another secondary branch to the equivalent circuits improves the estimation of the operational admittance frequency loci of the micromachine, and hence more accurately allows prediction of performance.

Fig. 38 shows the almost frequency for frequency agreement between the loci determined from static impedance measurements, and that calculated from the direct axis equivalent circuit, with field short circuited, and with a third simple eddy current branch. Fig. 39 shows similar agreement for the quadrature axis.

The addition of another secondary branch to the equivalent circuits infers that the micromachine has a direct and quadrature axis sub-sub-transient reactance, and it is well known that the results of sudden short circuit tests applied to laminated pole machines often indicate the presence of such a reactance.

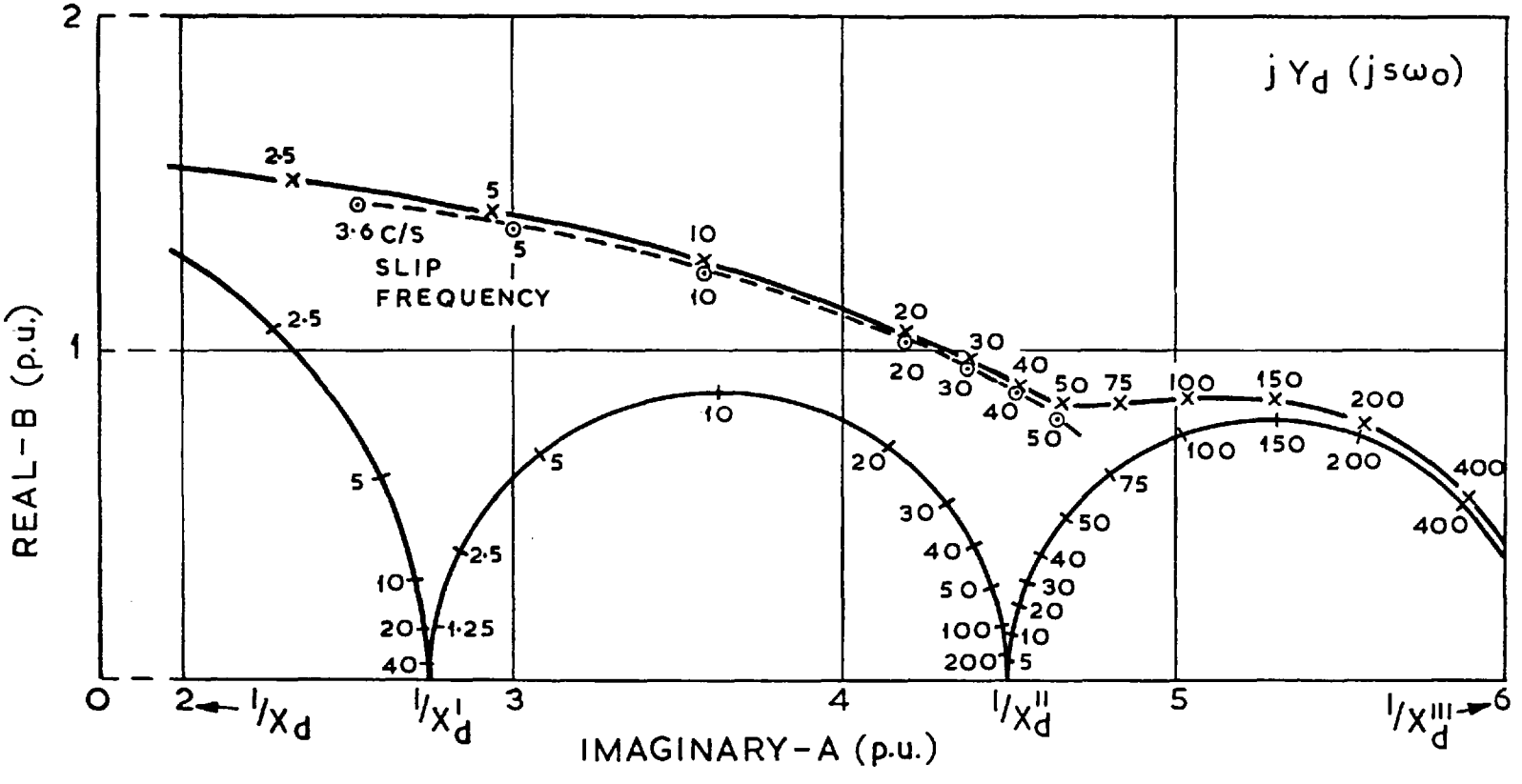

Fig. 38 Direct axis operational admittance frequency loci of the micromachine with field short circuited

---⊙--- Locus obtained from static impedance test results

——x—— Locus calculated from equivalent circuit with three secondary branches

——✓—— Construction circles

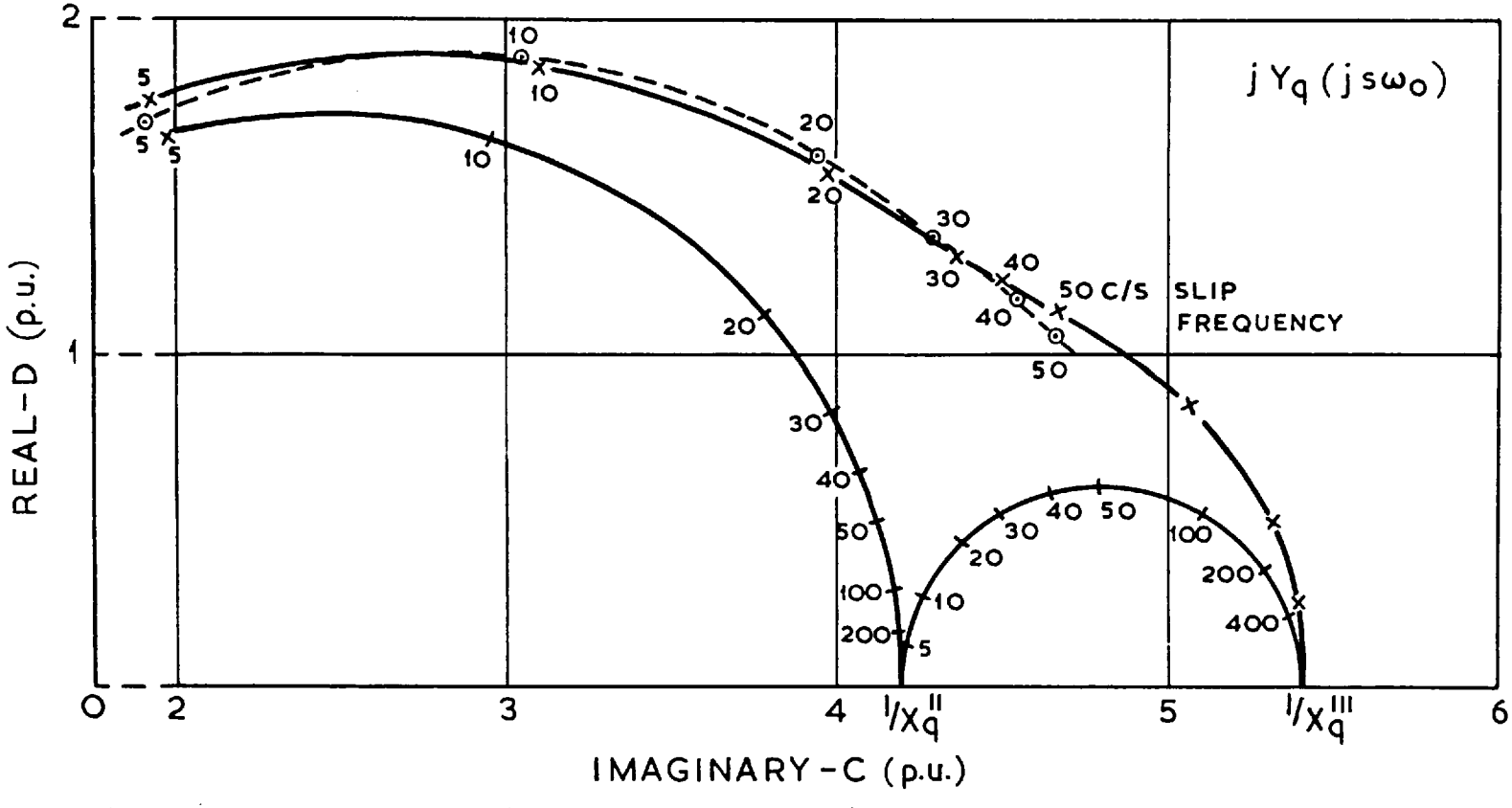

Fig. 39 Quadrature axis operational admittance frequency loci of the micromachine

—o— Locus obtained from static impedance test results

—x— Locus calculated from equivalent circuit with two secondary branches

—/— Construction circles

PART III

THE SOLID POLE SYNCHRONOUS MOTOR

CHAPTER 9

INTRODUCTION

9.1. THE FEATURES OF THE SOLID POLE MOTOR

The rotor of the solid pole type of synchronous motor is constructed entirely of unlaminated "solid" iron. The poles of the salient pole motor are fixed to the solid forged "spider" by radial bolts. The structure of large salient pole motors of this type is sufficiently robust to rotate at speeds of 1800 R.P.M. (4-pole, 60 c/s speed). Plate 4 shows a typical construction of such a rotor.

The motor has no separate starting winding on the rotor, but adequate starting torque is produced by the distributed flow of eddy currents, both in the pole shoe and, to a lesser extent, in the pole body of the rotor. The main field winding, as in the case of the laminated pole motor, is unexcited but closed through a discharge resistance. This discharge resistance both minimises the induced voltage across the main field winding during starting and also enables the winding to exert additional starting torque.

The advantages of the solid pole machine over the laminated counterpart are cheapness of construc-

tion, high speed operation, and, because of the high thermal capacity of the solid poles, particular suitability for the starting of high inertia loads. The main disadvantage of the solid pole type of motor is that very little can be done to vary the starting torque characteristics from the inherent high standstill, rapidly falling, characteristic found in all motors having poles of solid iron.

The distribution of the eddy currents, the very pronounced non-linearity of the solid iron, the change of iron resistance with temperature, the saliency, and the end effects, are all serious problems which make the calculation of the performance of a salient solid pole motor very difficult.

9.2. HISTORY OF THE EDDY CURRENT WORK

In earlier work, the eddy current starting problem was solved by the application of the traditional constant permeability eddy current theory; usually to the simple round rotor machines[5,6,8,9]. This linear theory gives a fixed rotor impedance angle of 45^{o}. Test results generally showed that this angle was incorrect and consequently earlier works attempted to justify a lower angle by considerations of hysteresis, end effects etc.[5,8].

In more recent years the non-linear eddy current theory has evolved. A very good interpretation of the theory is given by Agarwal[10]. It is based on the assumption of the saturation curve of the iron to be a constant value of positive flux density B_s, for all positive values of exciting M.M.F., and a constant $-B_s$ for all negative values of the M.M.F. (Fig.40). The non-linear theory gives a rotor impedance which is an inverse function of the voltage across it and has a fixed angle of 26.6^{o}. The non-linear theory has been applied recently to numerous problems with some success[10,11,14,15,16,19].

Shevel[17] derives a "modified non-linear theory", based on the representation of the saturation curve shown in Fig.40. The theoretical results of the modified non-linear theory are much more complicated than those of the non-linear theory and, although Shevel's approach is bound to yield more exact theoretical results, the difference is small under normal operating conditions. Thus it may be considered that the extra

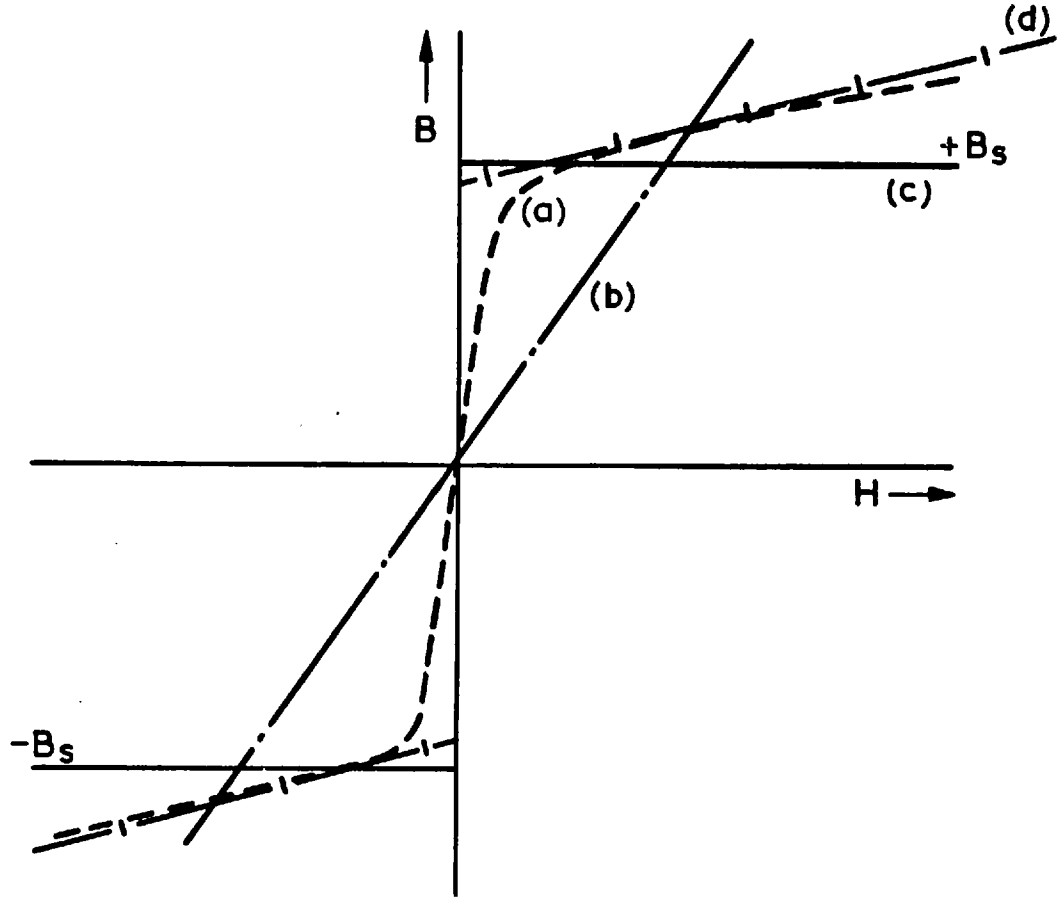

Fig. 40. Representation of the saturation curve

(a) – – – – True saturation curve

(b) — · — Linear representation

(c) ——— Non-linear representation

(d) —I— Modified non-linear representation (Shevel)

complication of Shevel's theoretical results would not always justify its use.

All past work has placed considerable emphasis on the mathematics of the eddy current problem and virtually no consideration has been given to the equivalent circuit representation of the machine. Without exception it has been assumed that the eddy current effects may be represented, in the equivalent circuit of both induction and synchronous motors, by a single secondary branch of resistance and reactance. Moreover, despite the abundance of theoretical work available, the comparative results of tests for a wide range of machines is unfortunately lacking.

9.3. THE PRESENT WORK

The present work is a completely new attempt to produce a sound practicable method of accurately calculating the starting performance of the solid pole synchronous motor, valid for machines of all sizes and number of poles.

The method may be divided into four parts. The first, and most important part, is a careful derivation of the direct and quadrature axis equivalent circuits. The second part is the determination of the impedances representing the eddy current effects and the insertion of the impedances into the equivalent circuits. The third part is the calculation of the two axis operational admittance functions, and the final part is the estimation of the asynchronous performance from the functions.

The derivation of the direct axis equivalent circuit takes particular account of the effect of the distribution of the flux entering the pole shoe; it separately accounts for the effect of eddy currents in the pole body; special consideration is given to the pole tips, when these become completely saturated with flux; and, of course, the effect of the main field winding is also included. The quadrature axis equivalent circuit, which is found to be the simpler of the two, also particularly accounts for the distribution of the flux entering the pole shoe.

The eddy current theory applied to the problem throughout is the non-linear theory. Using this theory impedances are obtained that have a fixed angle of

26.6^{o} and are direct inverse functions of the slip and the voltage across them. Non-linear impedances of this form satisfactorily represent the behaviour of the eddy currents in the iron, under normal operating conditions,[10, 11, 14] and yet are relatively easy to manipulate. A simple method of linearising the impedances has been applied when the permeability of the iron approaches the physical limits - that of air and that found by the initial slope of the saturation curve. The quadrature axis eddy current impedances are modified when the solid poles are provided with special end rings to connect them together at the ends of the machine. Although the angle of the eddy current impedance, obtained by the non-linear method, is 26.6^{o}, the effect of the distribution considered in this work is to modify the angle of the single effective pole-shoe eddy current impedance to a higher value. In fact, the pole-shoe impedance angle is shown to range between 26.6^{o} and 45^{o}; the value depending on the rotor frequency and flux.

Because of the non-linearity of the eddy current impedances, the method of calculating the operational admittance functions from the equivalent circuits is necessarily an iterative method. Furthermore, the effect of the distribution results in a double iterative process, and a fast computer is necessary to calculate the functions. The logic of the computer programme is clearly explained in the next chapter.

The calculation of the asynchronous performance from the two operational admittance functions is relatively easy, if it is assumed that the action of the eddy currents on the two axes of the machine is inde-

pendent. Adequate experimental results and theoretical reasons are given to justify this assumption. The method of calculating the asynchronous performance from the two axis operational admittance functions is fully explained in Chapter 2.

A detailed experimental study has been carried out on the micromachine, fitted with a solid salient pole rotor, at Imperial College. Measurements have also been made on many solid salient pole synchronous motors of sizes ranging from 100 to 5000 H.P., with numbers of poles from 4 to 8. Two machines were tested with, and without, copper end rings.

The following conclusions were obtained from the results of tests on the many machines:-

1. The asynchronous characteristics of all solid iron machines decrease steadily from a maximum value at standstill to zero at synchronous speed.

2. The presence of the main field winding on the direct axis is to increase very seriously the saliency of a machine that otherwise would not exhibit very serious saliency.

3. At standstill, and when the terminal voltage is 1 p.u., all machines behave as if they have a pole shoe impedance angle of approximately 40^{o} on both axes. (Recently Basta[18] suggested a rotor impedance angle of 31^{o} for a large synchronous motor.)

4. The effect of end rings, connecting the solid salient poles, is to increase the ratio of mean torque to oscillating torque, and to increase the mean torque/input current ratio. The latter is confirmed by Gibbs[8].

Very good agreement is obtained between measured and calculated results, for the solid pole micromachine at three different voltages with three different main field connections, both with and without end rings. Good agreement is also shown between the measured and calculated results for many large machines.

CHAPTER 10

THEORY OF THE SOLID POLE SYNCHRONOUS MOTOR

The theory of the solid pole motor is divided into four parts:-

1. The development of the two axis equivalent circuits.

2. The determination of the eddy current impedances and their insertion into the equivalent circuits.

3. The calculation of the two axis operational admittance functions.

4. The determination of the asynchronous performance from the derived operational admittance functions.

10.1. THE TWO AXIS EQUIVALENT CIRCUITS OF THE SOLID POLE MOTOR

The final equivalent circuits of the solid pole motor are complicated; particularly that of the direct axis. It is well, therefore, to derive first of all, very simple equivalent circuits, to explain their inadequacies, and consequently to show how they must be extended to agree more closely with the physical happenings within the machine.

10.1.1. Simple Equivalent Circuits

10.1.1.1. The equivalent circuit of a simple solid iron machine

The equivalent circuit of a simple solid iron machine such as shown in Fig.41a, may be derived in a similar manner to that explained in Chapter 2.3. The steps of the derivation are shown in Fig.41. Fig. 41c and d indicate that of the total flux Φ_g crossing the air-gap, Φ_{er} induces eddy currents in the solid iron, which in turn produces a leakage flux $\Phi_{e\ell}$ opposing the total flux crossing the gap.

The derivation of equivalent circuits of more complicated machines can be simplified if the solid iron is treated in a manner such as used by Bharali and Adkins[11]. Using this approach the flux paths of the simple machine (Fig.41a) may be drawn as in Fig.42a and the final equivalent circuit is shown in Fig.42b.

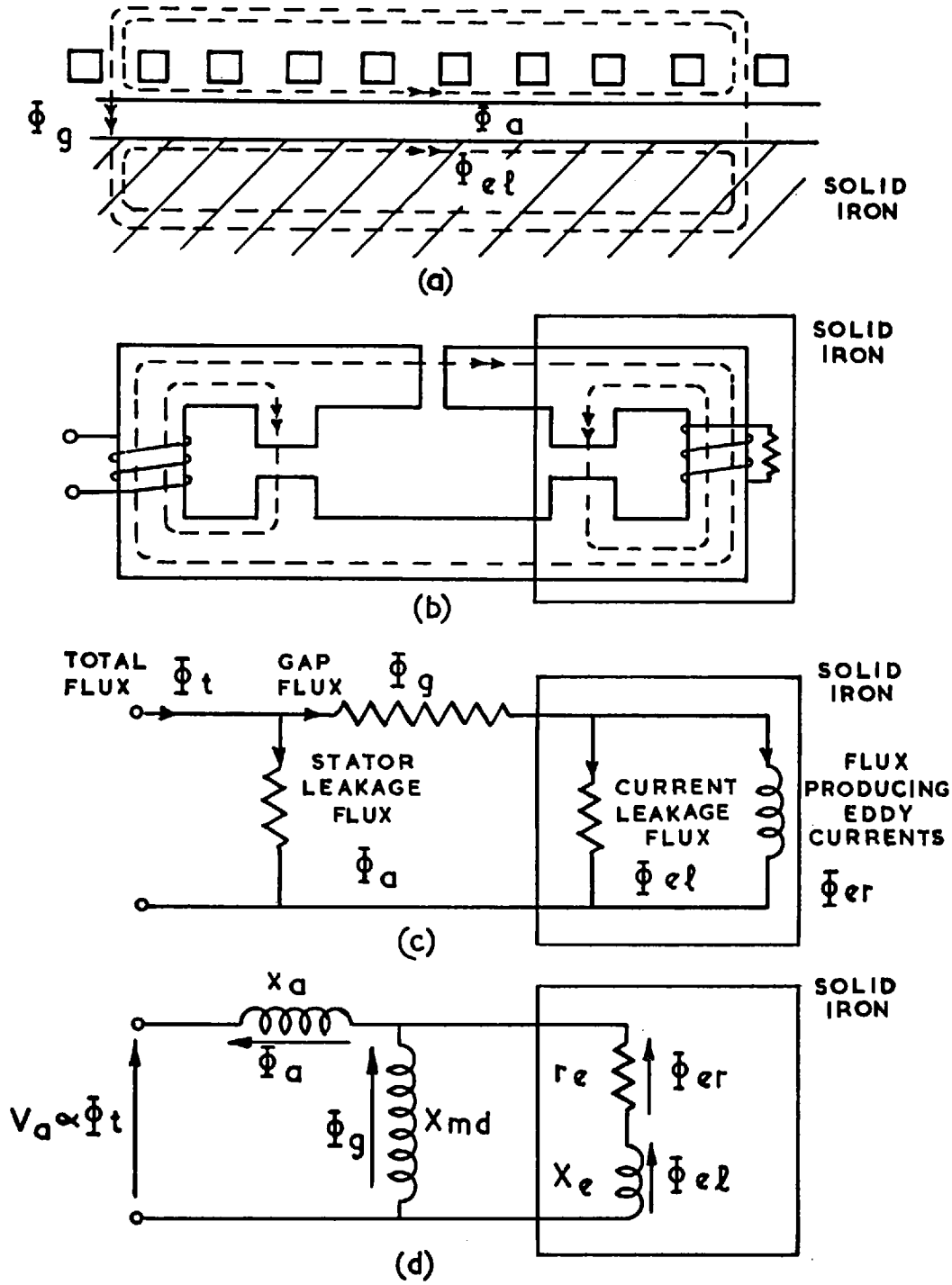

Fig. 41. Equivalent circuit of simple solid iron machine.

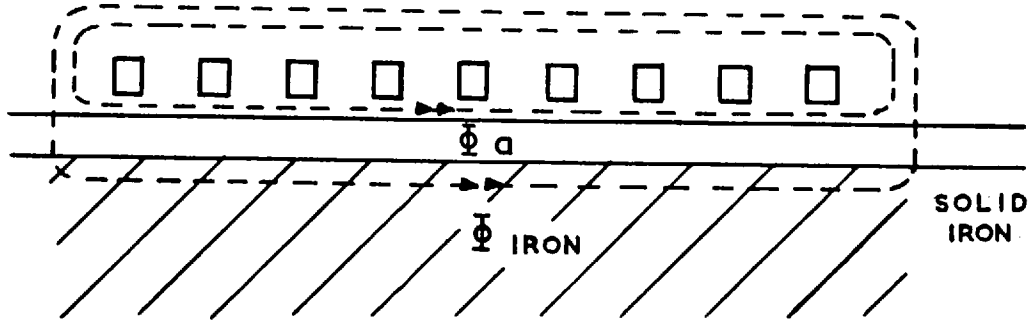

(a)

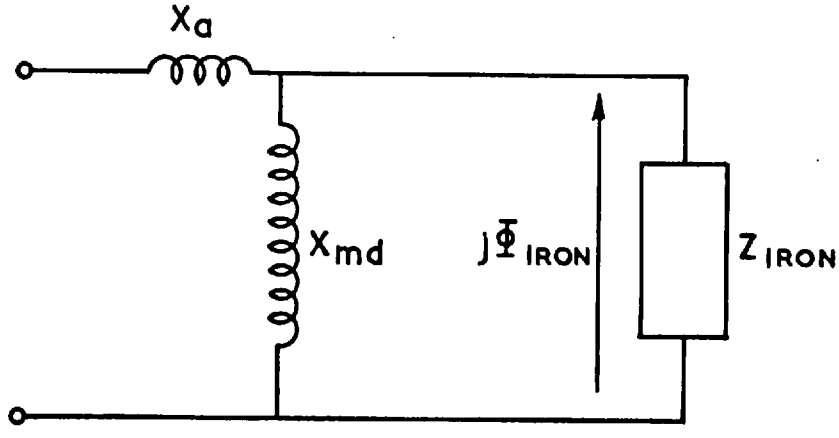

(b)

Fig. 42. Equivalent circuit of simple solid iron machine.

The solid iron impedance, Z, has resistive and reactive components, r_e, x_e, the voltages across which, represent the linkage and leakage components, respectively, of the solid iron flux. With Z replaced by r_e, x_e it is clear that the final equivalent circuits of Figs. 41 and 42 are the same.

It is observed that fluxes are shown across components of the equivalent circuit instead of voltages. This is to act as a reminder that the voltage across a component of an equivalent circuit is directly representative of the flux linking that part of the machine represented by the equivalent circuit component (refer to Chapter 2.3).

An equivalent circuit of the type shown in Figs. 41 and 42 is that which, in the past, has been assumed, incorrectly, to represent both solid rotor induction motors and solid rotor synchronous motors.

10.1.1.2. The simple direct axis equivalent circuit of the solid pole synchronous motor

Figs. 43 and 44 show the diagrammatical development of the direct axis equivalent circuit of the solid pole synchronous motor. The full details of such a diagrammatical development are given in Chapter 2.3.

It is known that all oscillating flux in solid iron is confined to a skin by the reaction of the

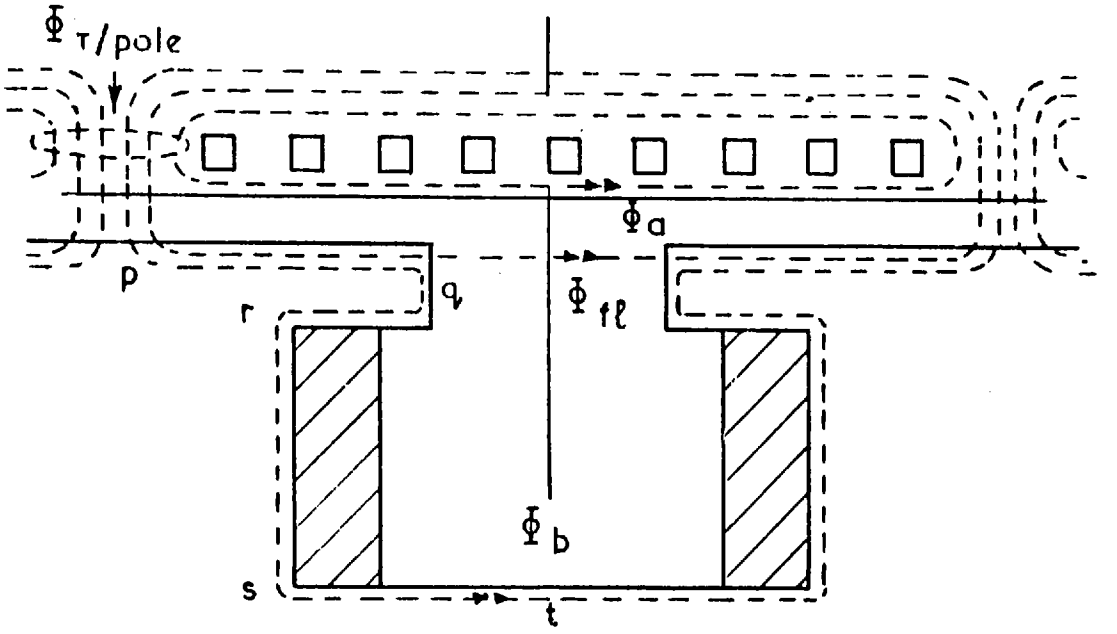

(a)

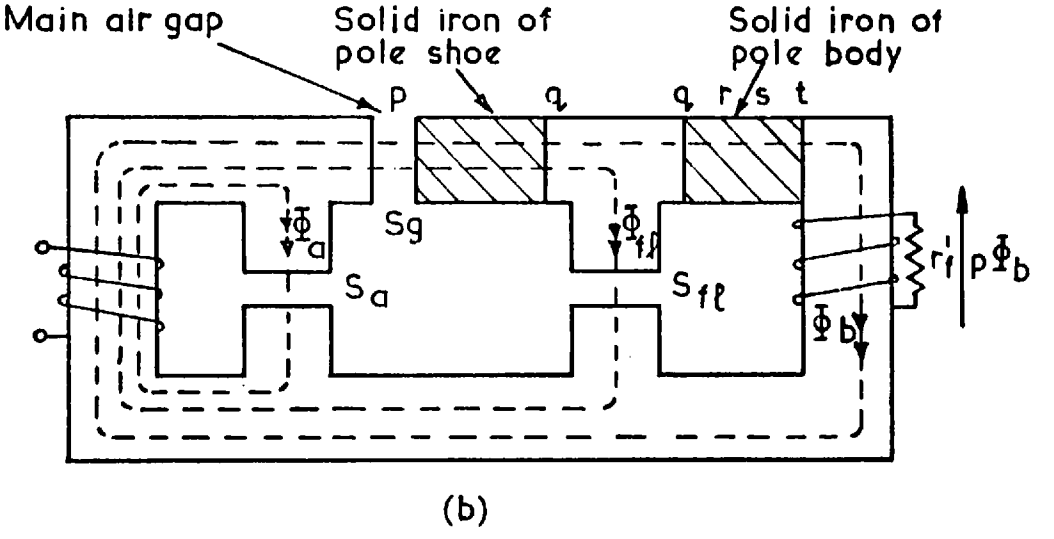

(b)

Fig. 43 Development of the simple direct axis equivalent circuit of the solid pole motor.

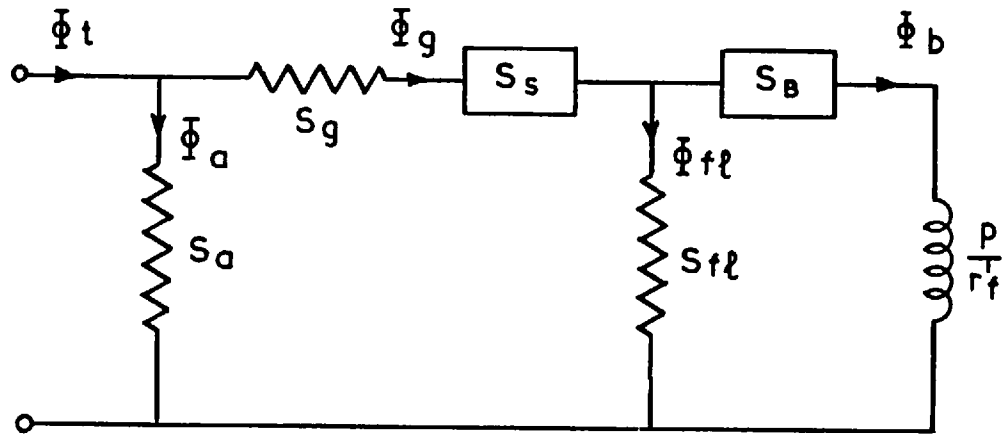

(a)

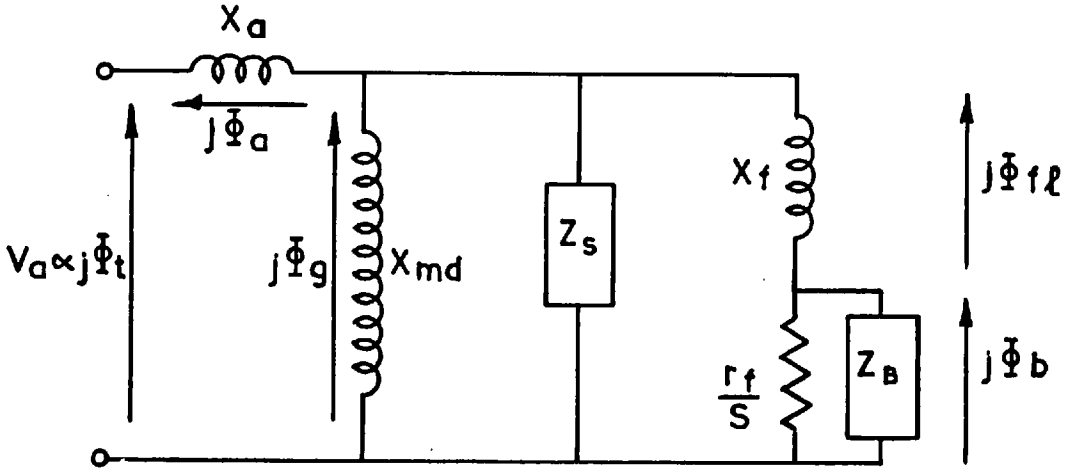

(b)

Fig.44. Development of the simple direct axis equivalent circuit of the solid pole motor (cont)

eddy currents produced. Hence all presupposed flux paths in the solid iron of the synchronous motor are shown, in Fig.43a, to be confined to the surface of the iron.

The direct axis fluxes of the synchronous motor are considered to be stator leakage flux Φ_a, which links only the stator winding; a component of main flux $\Phi_{f\ell}$, which links the stator winding, the main air-gap, the complete pole shoe iron, and the interpole leakage path; and a component of main flux Φ_b, which links the stator winding, main air-gap, the pole shoe iron, the pole body iron, and the main field winding.

Fig. 43b shows these same components of flux in a simplified iron diagram. The shaded sections correspond to solid iron portions of the iron circuit. Unshaded iron sections are considered to be perfectly laminated iron of zero reluctance. The complete reluctance of a path, part in laminated iron, part in air, is represented by a single air-gap, e.g. the length of the main air-gap is slightly extended to include the reluctance of the laminated stator iron in the path of the main air-gap fluxes.

Fig. 44a shows the iron circuit replaced by an electric circuit. The current in the circuit represents the flux, and resistances, the equivalent air-gap reluctances. The unknown reluctances, in the boxes, which are complex, represent the effect of the pole shoe and body solid iron. The field winding resistance, r_f, is drawn reac-

tive because of the 'p', which was introduced by the voltage induced across the winding being $p\Phi_b$.

Fig. 44b, is obtained by the inversion of the circuit above, for steady asynchronous running conditions at slip s. The reluctances are replaced, after inversion, by the corresponding reactances, defined at base frequency ω_o.

The division of flux in the machine is still evident, since the voltage across a component of the equivalent circuit is a measure of the flux in that part of the machine. This is emphasised in Fig.44b by showing the voltages in the equivalent circuit as the fluxes they represent. In Fig. 44b:-

> The phase voltage, V_a is a measure of the total flux, Φ_t, produced. The voltage drop across the stator leakage reactance, X_a, is a measure of the stator leakage flux, Φ_a, and the remaining voltage across the magnetising reactance, X_{md}, is a measure of the flux, Φ_g, crossing the main air-gap. Since Φ_g also links the pole shoe iron, the voltage across X_{md} is also applied to the impedance, Z_S. After passing through the pole shoe iron the flux, and hence the voltage, divides; $\Phi_{f\ell}$ leaks across the interpole gap, represented by X_f, and the remainder, Φ_b, links both the field winding and the pole body iron.

The final equivalent circuit representing the direct axis of the solid pole synchronous motor, Fig.44b, is still quite simple, and in particular, it is seen to represent, separately the eddy current effects in the solid iron of the pole shoe and the pole body.

It is interesting to note, at this point, the form of the direct axis equivalent circuit with main field winding on open-circuit. In this situation $r_f = \infty$ in Fig.44b and the tertiary branch, unlike the case of the laminated pole machine, still remains. The tertiary branch becomes a series combination of the field leakage reactance, X_f, and the pole body impedance, Z_B.

10.1.1.3. The simple quadrature axis circuit of the solid pole synchronous motor

The flux paths of the quadrature axis may be simply represented by those shown in Fig. 45a. It is clear that the simple configuration may be represented by a simple equivalent circuit, Fig.45b. Of the total flux, Φ_t, which is proportional to V_a, Φ_a leaks in the stator and the remainder, Φ_g, cross the main air-gap and links the solid iron of the rotor. Thus the voltage across X_{mq}, which is proportional to Φ_g, is also applied to Z_s.

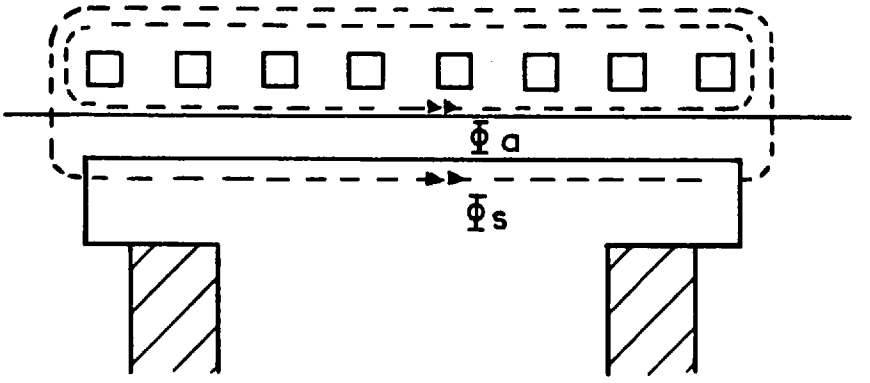

(a)

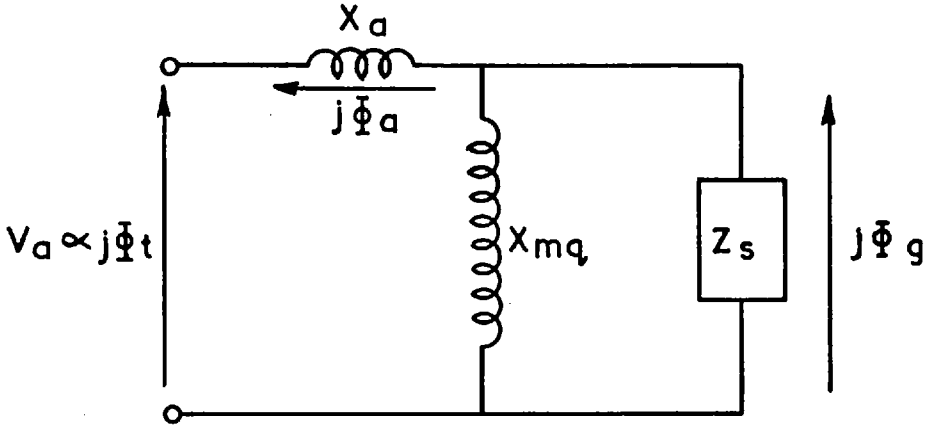

(b)

Fig. 45. The simple quadrature axis equivalent circuit of the solid pole motor.

10.1.2. The More Exact Equivalent Circuits of the Solid Pole Synchronous Motor

It was decided, on grounds given later, that the most appropriate impedances representing the solid iron sections, were those derived by the "Non-linear theory[10]". With the impedances inserted into the equivalent circuits, operational admittance functions were calculated over a wide range of slip. However, it was found from the results of tests on many machines that there was serious difference between the operational admittances measured and calculated, and it was deduced that the impedances, representing the pole shoe iron, were incorrect in both magnitude and angle. The magnitude of the impedance was found to be out by several times and the angular error of the order 10^{o} too low. It was decided, after a great deal of consideration, that the error in the method lay in the assumptions of the derivation of the equivalent circuit, rather than in the derivation of the impedances from the 'non-linear theory'. The greatest single error in the method of derivation of the equivalent circuits lies in the assumption that all the direct axis rotor flux of the machine enters the centre of the pole, and all the quadrature axis flux enters the tip of the pole. It is clear that the flux crossing the main air-gap must cross it in some distributed fashion, Fig. 46, otherwise there would be severe saturation in certain stator teeth opposite the point of crossing. This was confirmed by search coil tests, described in section 10.3.2.2.

The distribution of the flux entering the pole shoe is now considered.

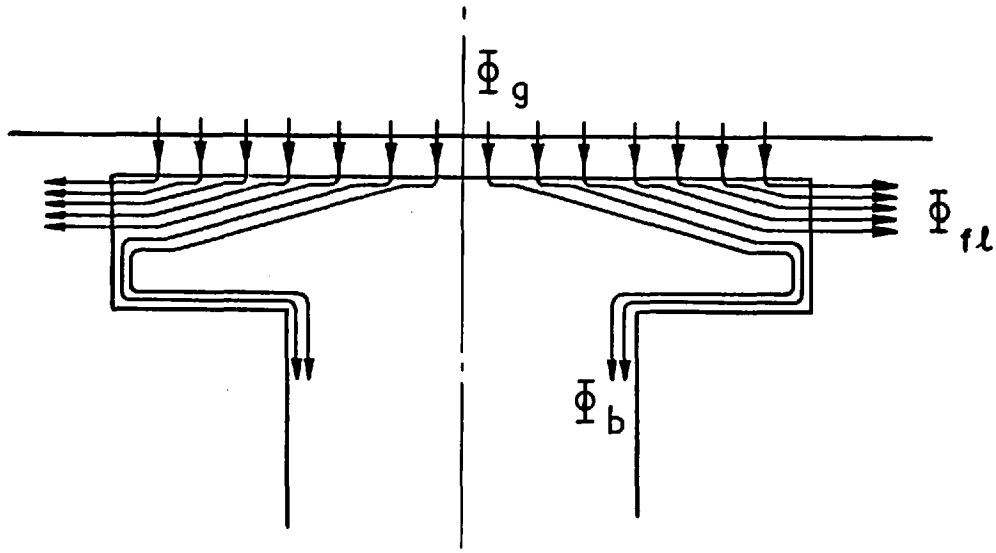

(a) The direct axis flux.

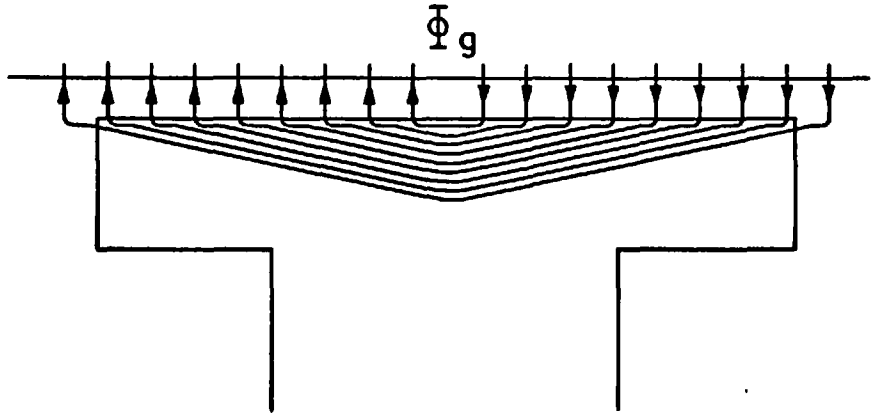

(b) The quadrature axis flux

Fig. 46 The distribution of flux in the solid iron

10.1.2.1. An equivalent circuit account of flux distribution in the solid iron

The effect of flux distribution may be accounted for directly in an equivalent circuit manner.

Consider a section of the pole shoe of a machine shown in Fig.47a. Consider the total flux crossing the air-gap to be divided into seven parts, Φ_{a-g}, at equal intervals of space. Consider the seven equal parts of the main air-gap, through which the fluxes pass to be denoted a to g. The reactances representing the reluctances to the flux, of the seven sections of air-gap are x_{a-g}. The impedances of the solid iron sections A to G representing the reluctance to the flux and the resistance to the eddy currents produced are denoted Z_{A-G}. The configuration of Fig.47a may then be represented by the equivalent circuit of Fig.47b. If the fluxes, $j\Phi$, are multiplied by certain constants they become voltages (eqn. 2.14), and the equivalent circuit is representative of sinusoidal conditions in terms of machine voltage and current.

It is worthwhile comparing the equivalent circuit of Fig.47b with the configuration of Fig. 47a:-

In (a), Φ_a crosses the air-gap section a, turns at right angles to keep to the surface, and links solid iron section A.

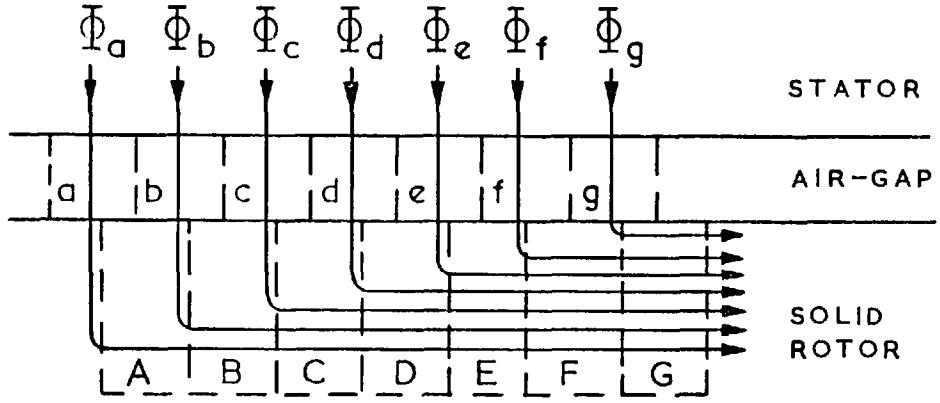

(a)

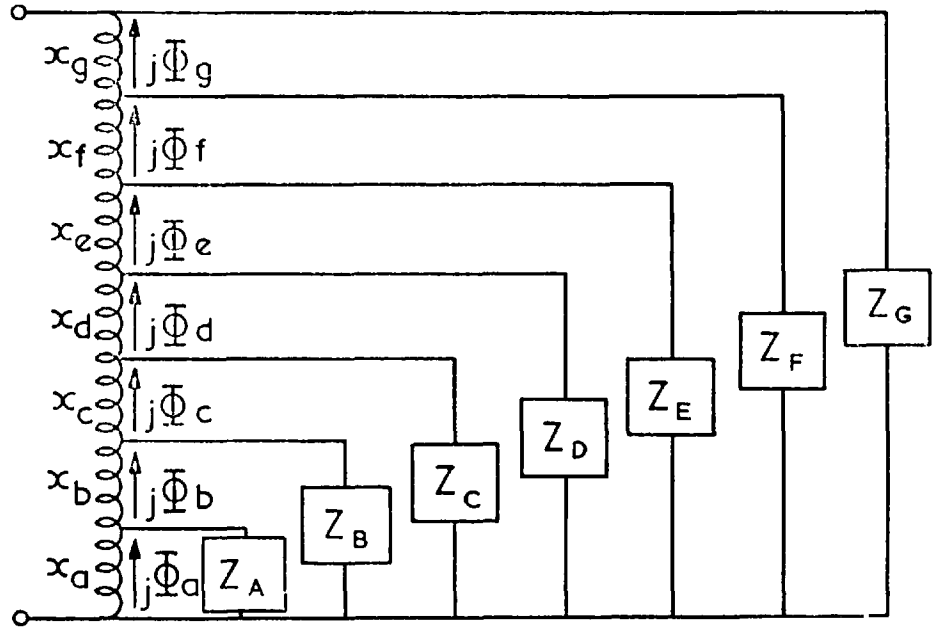

(b)

Fig. 47 Representation of flux distribution in an equivalent circuit

In (b), The voltage, $j\Phi_a$, is applied first to x_a, representing the air-gap section a, then to Z_A representing solid iron section A.

In (a), Φ_b crosses the air-gap section b, turns at right angles to keep to the surface, combines with Φ_a and together they pass into solid iron section B.

In (b), The voltage, $j\Phi_b$, is applied to x_b, representing the air-gap section b, it then adds (phase inclusive) to voltage $j\Phi_a$, and the total voltage is applied across Z_B representing solid iron section B.

In (a), Φ_c crosses the air-gap section c, again turns at right angles to keep the surface, combines with $(\Phi_a + \Phi_b)$ and together they pass into solid iron section C.

In (b), The voltage, $j\Phi_c$, is applied to x_c, representing the air-gap section c, it then adds (phase inclusive) to voltage $j(\overline{\Phi}_a + \overline{\Phi}_b)$, already combined, and the total voltage is applied across Z_C representing the solid iron section C.

So the process continues until eventually all the flux has crossed the main air-gap, and has passed through the final iron section in the configuration, G.

It appears, therefore, that the effect of flux distribution in the solid iron, can easily be taken account of in the manner explained. However,

certain assumptions must be made before the equivalent circuit can be solved - that is, an assumption must be made as to the nature of the flux distribution in the air-gap, e.g. sinusoidal distribution, uniform distribution, free distribution. The nature of the air-gap flux distribution is dealt with later.

10.1.2.2. An equivalent circuit account of complete pole tip saturation

Fig. 46a shows a suggested distribution of the direct axis flux in the pole. If the eddy currents in the iron cause the flux to follow the surface path shown, then it is clear that the pole tips are liable, under certain conditions, to become completely saturated with flux. Should this occur the pole body flux, Φ_b, or some part of it, is unable to follow the surface path shown but would proceed directly to the body of the pole without linking the pole shoe system of distributed flux.

This latter effect may be easily accounted for in the equivalent circuit. In the following explanation it is much simpler to ignore the effect of the distribution and to consider the original incorrect assumption of all the direct axis rotor flux entering the centre of the pole shoe, turning at right angles, and following the surface path to the tip. At the tip the flux divides into the two components, the field leakage component, $\Phi_{f\ell}$, and the pole body component, Φ_b.

Fig. 48a shows how the flux must divide when the tip becomes completely saturated, i.e. when the penetration of flux from the top of the pole tip meets the penetration of flux up from the bottom. The section of the body flux, Φ_{b1}, penetrates the solid iron and passes straight to the pole body. Fig. 48b shows the fluxes simplified to line paths, and (c) the equivalent circuit of the latter configuration.

Comparing (b) and (c) of Fig. 48:-

In (b), Flux Φ_g , crosses the main air-gap.

In (c), Voltage, $j\Phi_g$, is applied to the magnetising reactance X_{md}.

In (b), Flux $(\Phi_{f\ell} + \Phi_{b2})$ links the surface iron of the pole shoe.

In (c), Voltage $j(\overline{\Phi}_{f\ell} + \overline{\Phi}_{b2})$ is applied across the shoe impedance Z_S.

In (b), Flux, Φ_{b1}, passes straight to the pole body without linking the pole shoe surface.

In (c), Voltage, $j\Phi_{b1}$, is not applied to the shoe impedance, Z_S.

In (b), The shoe flux divides into an interpole leakage flux, $\Phi_{f\ell}$, and a pole body flux, Φ_{b2}.

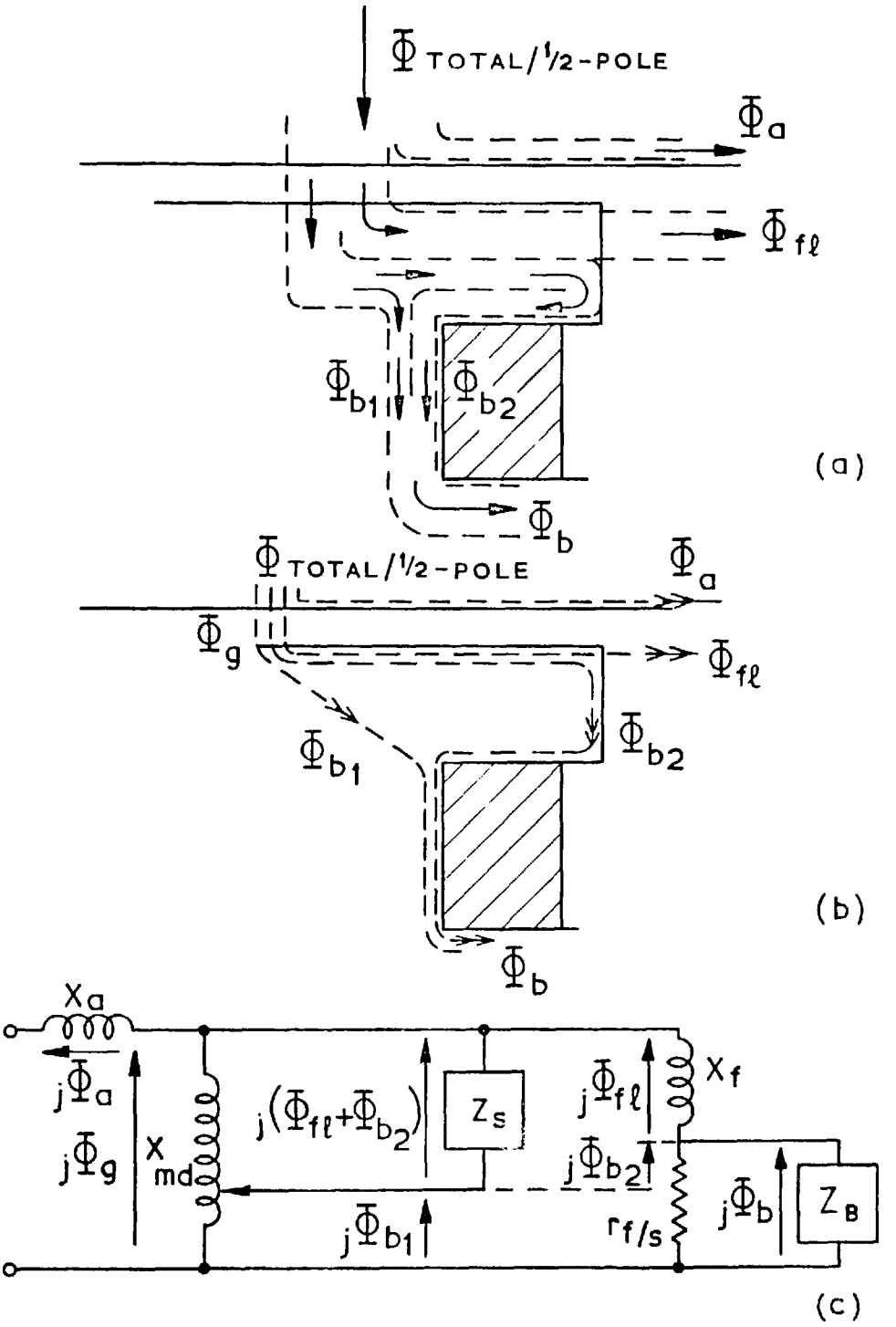

Fig. 48 Equivalent circuit representation of complete pole-tip saturation

In (c), The voltage $j(\overline{\Phi}_{f\ell} + \overline{\Phi}_{b2})$ divides to a voltage, $j\Phi_{f\ell}$, applied to X_f, representing the interpole leakage reluctance, and to a voltage, $j\Phi_{b2}$.

In (b), Fluxes Φ_{b1} and Φ_{b2} combine to form a single flux, Φ_b, linking both the field winding and the pole body iron.

In (c), Voltages $j\Phi_{b1}$ and $j\Phi_{b2}$ add and are applied to both the field winding, r_f, and to the pole body iron represented by Z_B.

The point at which Z_S divides X_{md} is determined by the calculation of the flux conditions in the pole tip. Care must be taken that a dividing point is never obtained that indicates the voltage $j\Phi_{b1}$ exceeds $j\Phi_b$. The physical interpretation of Φ_{b1} being greater than Φ_b is not only that there is some of the body flux, Φ_b, which does not link the pole shoe, but also some of the interpole leakage flux, $\Phi_{f\ell}$; the latter is not possible.

Using the non-linear eddy current impedance to represent the solid iron, the meaning of complete pole tip saturation is made much clearer. This is because the flux density in the iron, everywhere where eddy currents flow, is assumed to be equal to a constant saturated level B_s. Because in a machine, the flux is distributed in the tip (Fig. 46a), and the tip itself is tapered, the check on the saturation calculation for the tip must be made at a point half way along the tip. In the

saturation calculation for the tip, full account must be taken of phase as well as magnitude. The calculation is explained in Appendix III.

10.1.2.3. The final equivalent circuits

Fig. 49a shows the direct axis equivalent circuit representing high slip, low flux conditions. The paths of the rotor flux are shown. At low slip, high flux conditions, the paths of the flux are modified, due to pole tip saturation, to that shown in Fig.49b. The equivalent circuit representing the latter conditions is then modified as shown, as explained in the previous section. Fig. 50 shows the quadrature axis equivalent circuit and corresponding flux paths.

The equivalent circuits are drawn for a complete pole, each half representing the effects of half the flux per pole in half a pole pitch. The comparison between the flux diagrams and equivalent circuits is then more obvious.

It is considered that the equivalent circuits shown represent adequately, yet without undue complication, the solid salient pole synchronous motor. They are used later in the calculation of the two axis operational admittance functions of the motor.

It is convenient, however, to replace the whole chain of series/parallel branches, representing the distribution of flux in the iron, by a

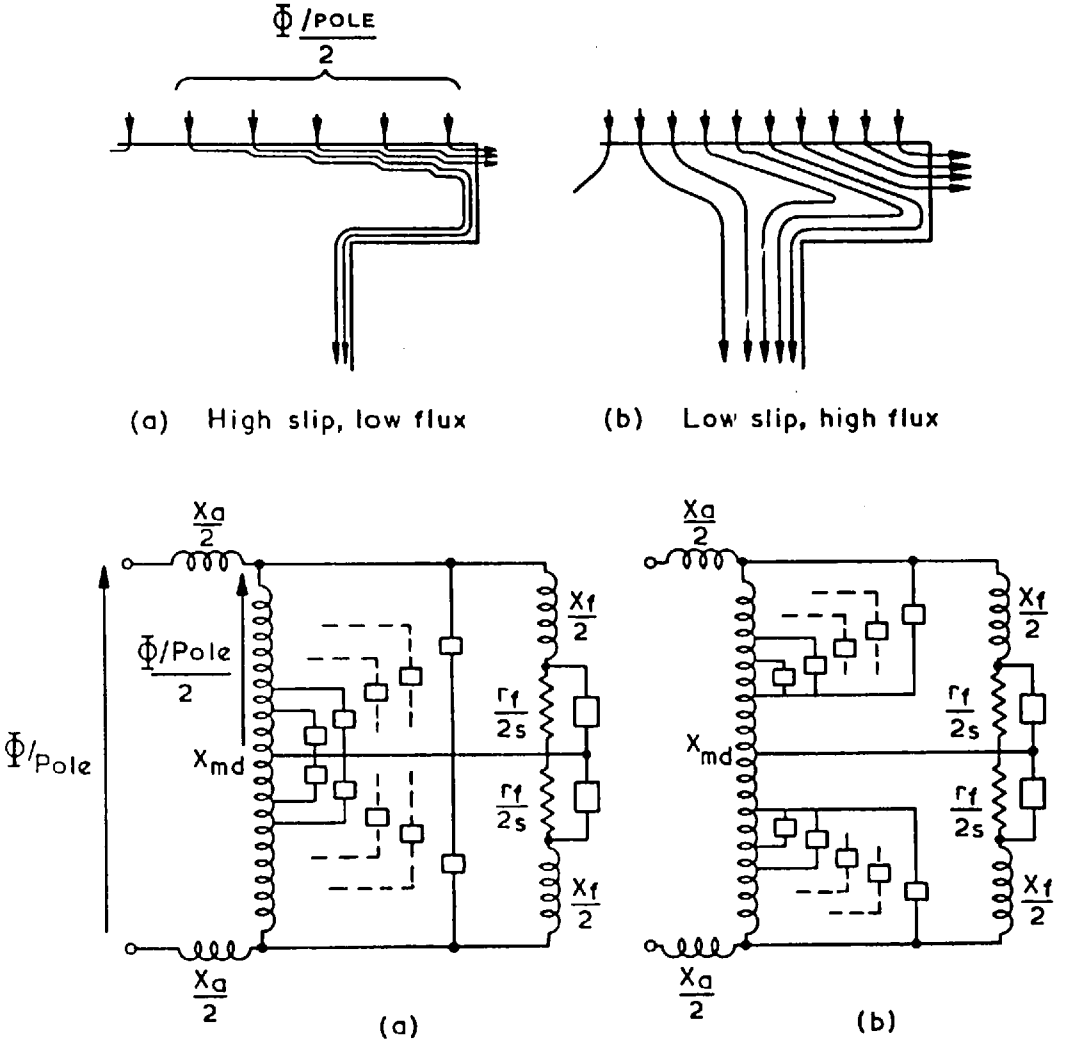

Fig. 49 Direct axis flux paths and their representative equivalent circuits

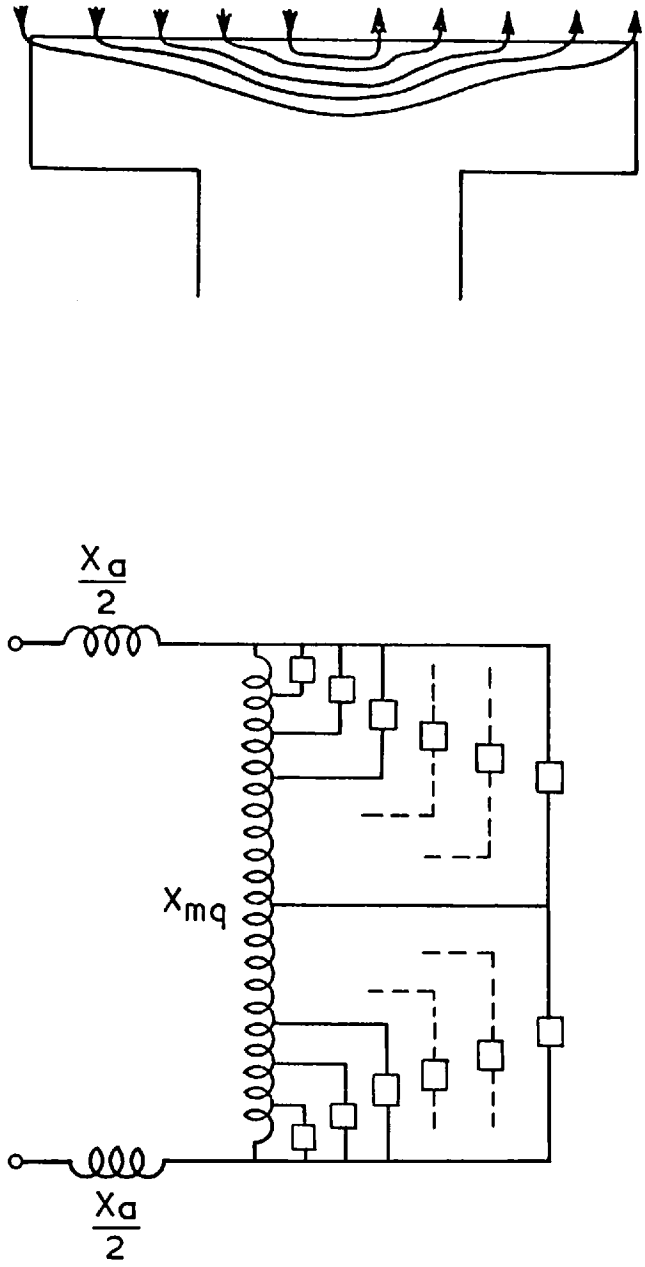

Fig. 50. The quadrature axis flux paths and the representative equivalent circuits

single equivalent pole shoe impedance. In this way the separate effects of pole shoe and pole body are isolated. The equivalent circuits then become similar in appearance to the simple ones first derived (Fig.51). The equivalent pole shoe impedance, Z'_S, however, is no longer a simple impedance, derived directly from the dimensions of the machine, but is calculated, as shown later, by a complicated iterative method.

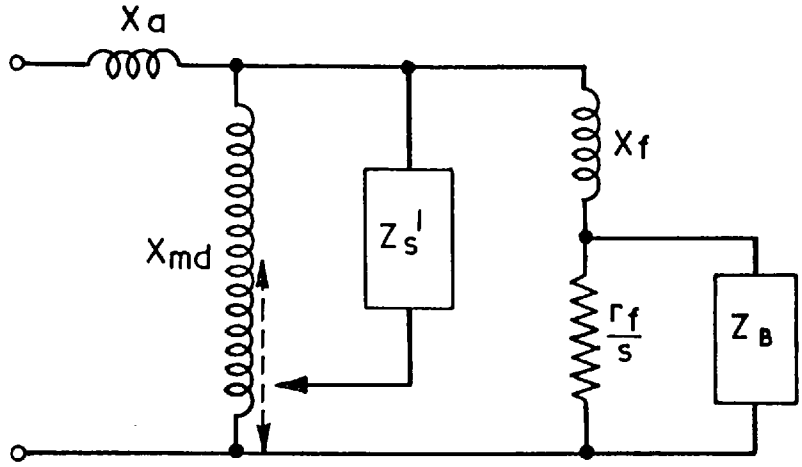

(a) Direct axis

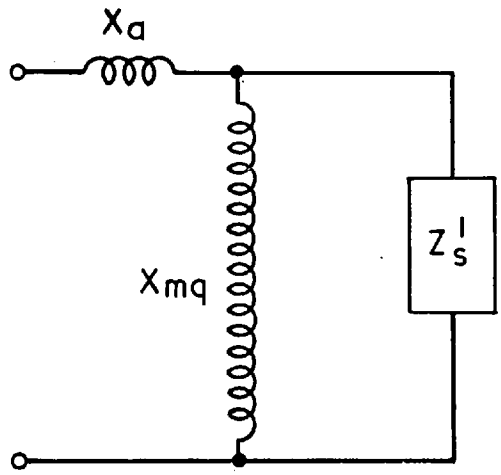

(b) Quadrature axis

Fig. 51 The final two axis equivalent circuits of the solid pole motor with equivalent single pole shoe impedance.

10.2. THE THEORY OF THE SOLID IRON

Maxwell's field equations, neglecting displacement current, are:-

$$\left.\begin{aligned} \text{Curl } \overline{H} &= \overline{J} = \frac{1}{\rho}\overline{E} \\ \text{Curl } \overline{E} &= -\frac{\partial \overline{B}}{\partial t} \end{aligned}\right\} \qquad (10.2)$$

The machine is considered to be of infinite dimensions. In particular the solid rotor is of infinite radial depth and of infinite axial length. The magnetic field intensity, $\overline{H}$, and flux density, $\overline{B}$, are considered to have a magnitude only in the y direction shown in Fig.52. The electric field, i.e. the flow of eddy currents, is then only in the z direction.

Equations 10.2 with the above assumptions may be combined and written

$$\frac{\partial^2 H_y}{\partial x^2} = \frac{1}{\rho}\frac{\partial B_y}{\partial t} \qquad (10.3)$$

10.2.1. The Linear Theory

The linear eddy current theory is obtained from the solution of the equation 10.3 with the assumption that

$$B_y = \mu_r \mu_o H_y \qquad (10.4)$$

where μ_r is a constant value of relative permeability assumed for the solid iron.

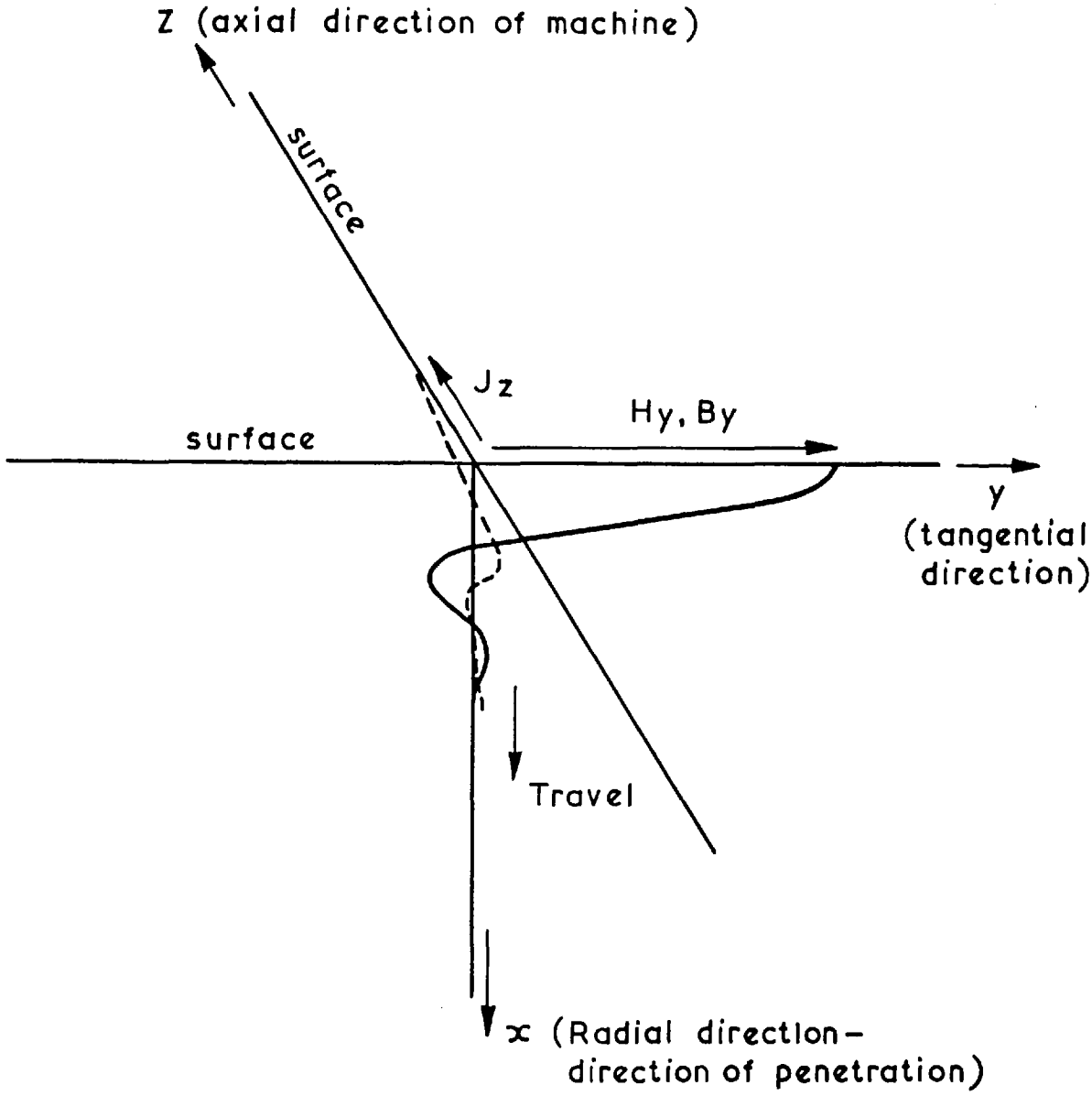

Fig. 52. Hy, By, Jz, predicted by the linear theory at time zero

10.2.1.1. General results of the linear theory

During asynchronous running the fictitious axis armature coils are stationary relative to the solid iron rotor and carry currents pulsating sinusoidally at slip frequency, i.e. the magnetic field intensity at the iron surface is considered not to vary with y, or z, and is given by:-

$$H_y = H_{mo} \sin s\omega_o t \qquad (10.5)$$

The solution of equation 10.3, with a substitution of 10.4 and 10.5 is:-

$$H_y = H_{mo} e^{-x/\delta} \sin(s\omega_o t - x/\delta) \qquad (10.6)$$

$$\text{where } \delta = \sqrt{\frac{2\rho}{s\omega_o \mu_r \mu_o}} \qquad (10.7)$$

the depth of penetration

Similarly

$$B_y = B_{mo} e^{-x/\delta} \sin(s\omega_o t - x/\delta) \qquad (10.8)$$

$$B_{mo} = \mu_r \mu_o H_{mo} \qquad (10.9)$$

Also the eddy current density, J_z, is given by $\frac{\partial H_y}{\partial x}$. It is:-

$$J_z = \frac{H_{mo}}{\delta} e^{-x/\delta} \sin(s\omega_o t - x/\delta + \pi/4) \qquad (10.10)$$

Fig.52 describes equations 10.6, 10.8, 10.10, in the semi-infinite slab of solid iron, at time

zero when H_y, B_y at the surface is a maximum. Clearly as H_y, B_y pulsate at slip frequency, the wave shape travels into the solid iron, within the bounds of the exponential $y = H_y e^{-x/\delta}$. The time constant of the exponential is exaggerated, in the figure, to show the wave propagation more clearly. In fact the amplitude of successive peaks decreases in the ratio of approximately 25 : 1. J_z behaves in a similar manner to H_y, B_y.

10.2.1.2. The linear solid iron impedance

The solid iron impedance of a machine may be derived from the reluctance of the solid iron per pole:-

Reluctance/pole =

$$= \frac{\text{M.M.F. applied to the solid iron pole}}{\text{Total flux in the solid iron of the pole}}$$

The M.M.F. applied to the solid iron pole is given by:-

$$H_{mo} L \sin s\omega_o t \qquad (10.11)$$

where L is the length of flux path in the solid iron pole.
The total flux in the solid iron of the pole is:-

$$2W \int_o^\infty B_{mo}\, e^{-x/\delta} \sin(s\omega_o t - \frac{x}{\delta}).dx$$

where W is the axial length of the pole.

$$= 2WB_{mo}\,\delta\,\sin(s\omega_o t + \frac{\pi}{4}) \qquad (10.12)$$

The total reluctance/pole is therefore:-

$$S = \frac{H_{mo}L}{2WB_{mo}\delta}\; e^{j45^o}$$

$$= \frac{L}{2W} \cdot \frac{1}{\mu_r\mu_o\delta}\; e^{j45^o}$$

$$= \frac{L}{2W}\sqrt{\frac{s\omega_o}{2\rho\mu_r\mu_o}}\; e^{j45^o} \qquad (10.13)$$

using equation (10.7)

The impedance in the equivalent circuit representing the iron reluctance is:-

$$Z = jK.\ 1/S$$

where K is the constant including stator turns, base frequency, and winding factors (eq. 2.18).

The linear impedance, Z_L, representing the eddy current effects, therefore, is:-

$$Z_L = \frac{2KW}{L}\sqrt{\frac{2\rho\mu_r\mu_o}{s\omega_o}}\; e^{j45^o} \qquad (10.14)$$

Thus, the linear theory gives an impedance, which varies inversely with the square-root of slip, and which has a fixed angle of 45^o.

Although the results of the linear theory are relatively simple, the 45^{o} angle impedance obtained does not yield correct results and, moreover, predicts very high flux densities at the surface of the iron. An example of the iron surface flux density predicted, by the linear theory, for a 3000 H.P. machine, is approximately 50 webers/metre^{2}.

It is clear that the flux density would be unlikely to exceed about 2 webers/metre^{2}, a value of flux density just over the knee of the saturation curve. If the actual saturation curve was used to calculate the iron surface density, as the magnetic field intensity, in one direction, changed sinusoidally through a half cycle, it would be found that the surface density would remain, over most of the half cycle, at a value a little above the knee of the saturation curve.

The method of solving the eddy current problem, using the non-linear approach[10], assumes a constant surface density $+B_s$ for the whole half cycle that the surface M.M.F. is positive, and $-B_s$ for the whole negative half cycle. Hence it is clear that the non-linear approach is a more realistic approach than that of the linear.

10.2.2. The Non-linear Theory

The saturation curve assumed to represent the magnetic characteristics of the iron is (c), shown in Fig.40. Physically in the iron, it is assumed that, as the M.M.F. at the surface increases from zero to a

positive maximum and decreases again to zero, a constant saturated wavefront of flux density $+B_s$ propagates into the iron. At the end of the half cycle the surface of the iron is saturated with flux density, B_s, to a depth δ. During the following negative half cycle the negative surface M.M.F. drives a negative saturated flux density $-B_s$ into the iron, which demagnetizes the density $+B_s$ as it progresses. Fig. 53 shows the flux in the iron at different instants of time in the cycle. Eddy currents flow in the iron as a result of the changing flux.

10.2.2.1. General results of the non-linear theory

The flux only changes to the left of the wavefront (Fig.53), and, hence, eddy currents are only induced in this region. The current density, J, which flows only in the Z direction, at distance x from the surface, is given by:-

$$J = \frac{1}{\rho} \frac{d}{dt}[B_s(\xi - x) - B_s(\delta - \xi)]$$

$$= \frac{2}{\rho} B_s \frac{d\xi}{dt} \qquad x < \xi$$

$$= 0 \qquad x > \xi$$

The current distribution at time t is therefore a uniform current density up to the wavefront and zero beyond. Thus, H is zero at the wavefront and increases linearly to the surface value of H at that instant of time. In particular,

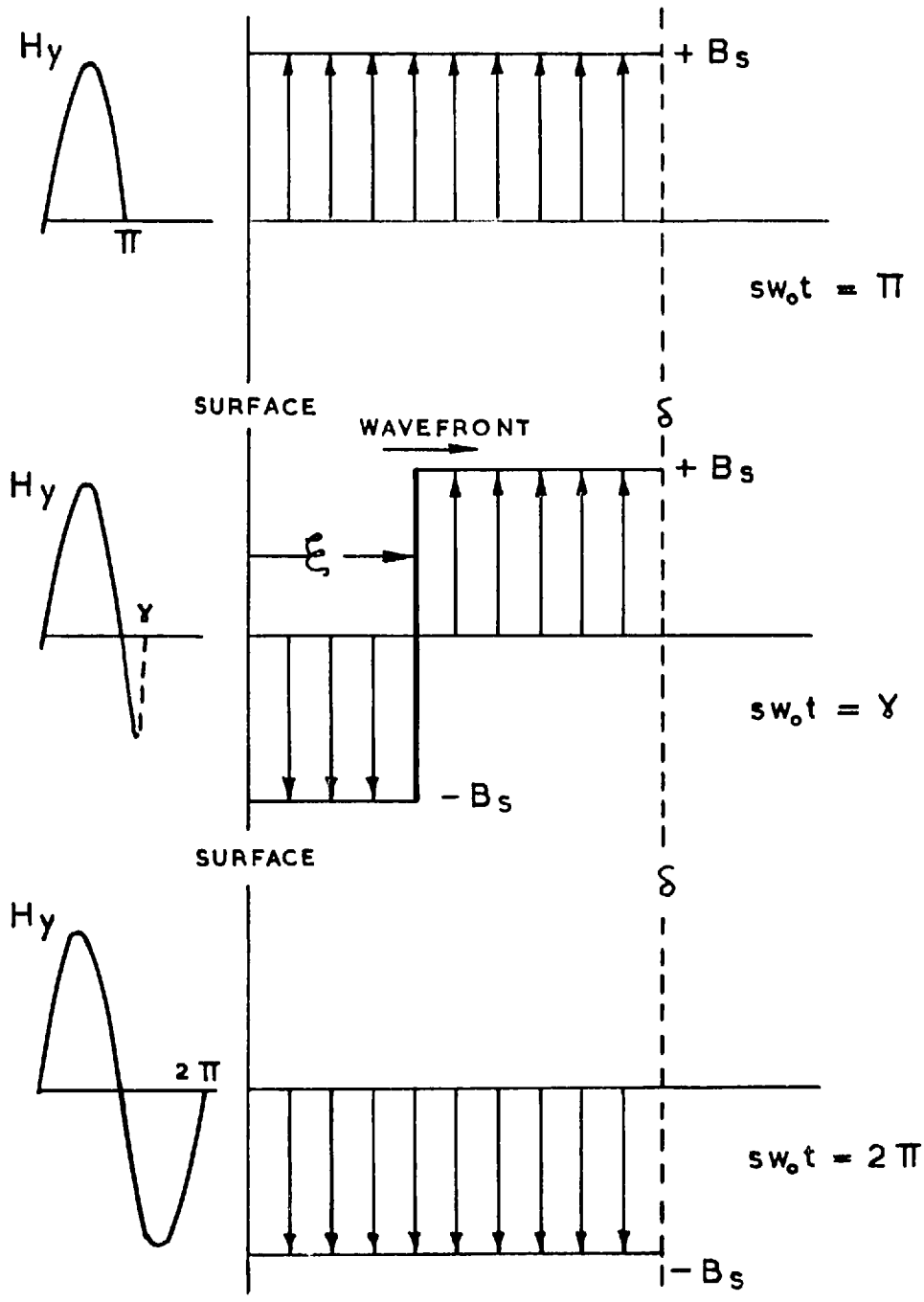

Fig. 53. Flux in the iron at different instants in the cycle.

from Maxwell's first equation (10.2):-

$$H_y = H_{mo} \sin s\omega_o t \cdot = \frac{2}{\rho} \xi \frac{d\xi}{dt} B_s$$

$$= \frac{B_s}{\rho} \frac{d}{dt} (\xi)^2 \qquad (10.15)$$

Hence $\xi = \sqrt{\frac{2 H_{mo}}{s\omega_o B_s}} \sin \frac{s\omega_o t}{2}$ over the period

$$0 < t < \frac{\pi}{s\omega_o}$$

The maximum value of ξ is δ when $t = \frac{\pi}{s\omega_o}$

$$\text{i.e.} \quad \delta = \sqrt{\frac{2 H_{mo}}{s\omega_o B_s}} \qquad (10.16)$$

The total flux linking the solid iron of width, W, at the same time, t, is given by:-

$$\Phi = W B_s \delta (2\sin s\omega_o t/2 - 1) \qquad (10.17)$$

$$0 < t < \frac{\pi}{s\omega_o}$$

Similarly for the second half cycle of the M.M.F. $(\frac{\pi}{s\omega_o} < t < \frac{2\pi}{s\omega_o})$

$$\Phi = W B_s \delta (1 - 2\cos s\omega_o t/2) \qquad (10.18)$$

Fig. 54 shows the total flux plotted out over one cycle of the surface M.M.F. The fundamental component of flux is also shown.

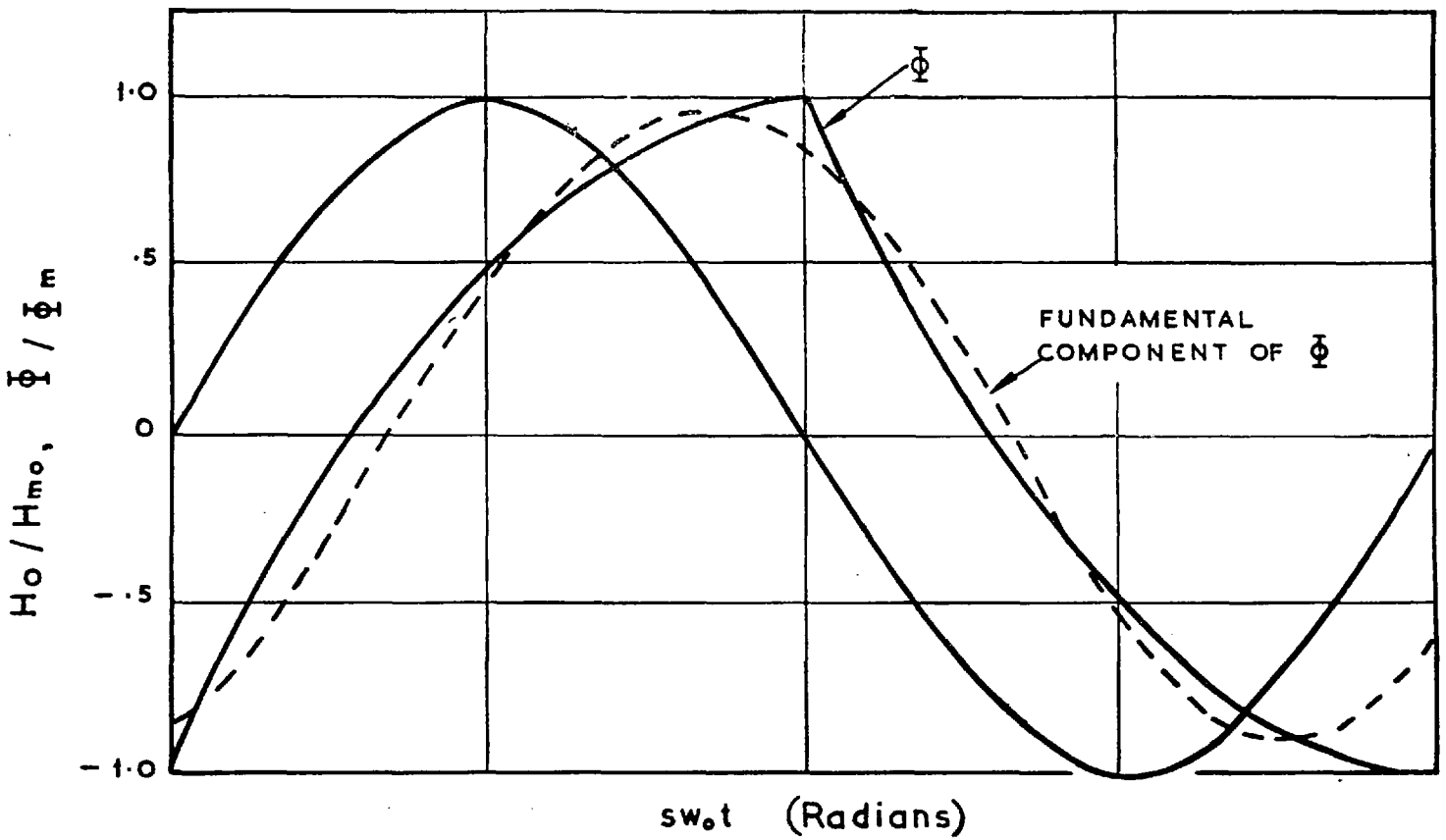

Fig. 54. Flux and M.M.F. waveforms based on the non-linear theory.

It is found to be:-

$$= \Phi_m \sin (s\omega_o t - \gamma)$$

where $$\Phi_m = \frac{4\sqrt{5}}{3\pi} W B_s \delta \qquad (10.19)$$

and $$\gamma = \tan^{-1} 2 = 63.4^o \qquad (10.20)$$

The effective reluctance representing the eddy currents in both halves of a pole is:-

$$S_{NL} = \frac{H_{mo} L}{2\Phi_m}$$

$$= \frac{3\pi}{4\sqrt{5}} \frac{H_{mo} L}{2WB_s\delta} e^{j63.4^o} \qquad (10.21)$$

Replacing δ by that given in equation (10.16), the expression for the non-linear reluctance, first derived by Bharali and Adkins[11], is obtained:-

$$S_{NL} = \frac{3\pi}{8\sqrt{5}} \frac{L}{W} \sqrt{\frac{H_{mo}}{B_s} \cdot \frac{s\omega_o}{2\rho}} e^{j63.4^o} \qquad (10.22)$$

Comparing the above expression with that derived by the linear theory (eqn. 10.13) it is observed that if the effective permeability ($=B_s/H_{mo}$) in equation (10.22) is the same as that in (10.13) then the magnitude of the non-linear reluctance is only slightly higher than the linear reluctance. The angles, however, of the two reluctances are different.

10.2.2.2. The non-linear solid iron impedance

The impedance in the equivalent circuit representing the non-linear reluctance of equation (10.22) is:-

$$Z_{NL} = K \frac{8\sqrt{5}}{3\pi} \frac{W}{L} \sqrt{\frac{2 B_s \rho}{H_{mo} s\omega_o}} \; e^{j26.6^o} \qquad (10.23)$$

where K is the constant including stator turns, base frequency, and winding factors (eqn. 2.18).

The impedance is seen to be a function of H_{mo}, i.e. is a function of the M.M.F. applied to the iron, that is, a function of the current through the impedance. Alternatively, $\sqrt{H_{mo}}$ may be replaced in equation (10.23) using equations (10.16) and (10.19). i.e.

$$\sqrt{H_{mo}} = \frac{\Phi_m}{W} \frac{3\pi}{8\sqrt{5}} \sqrt{\frac{s\omega_o}{2\rho B_s}} \qquad (10.24)$$

The impedance, representing the solid iron may then be written:-

$$Z_{NL} = K \frac{640}{9\pi^2} \frac{W^2}{L} \frac{B_s \rho}{\omega_o} \cdot \frac{1}{s\Phi_m} e^{j26.6^o} \qquad (10.25)$$

The magnitude of the voltage across the impedance V_{NL} is directly proportional to the flux Φ_m, (eq. 2.14).

Thus:-

$$Z_{NL} = K' \frac{640}{9\pi^2} \frac{W^2}{L} \frac{B_s \rho}{\omega_o} \cdot \frac{1}{s|V_{NL}|} e^{j26.6^\circ} \quad \ldots (10.26)$$

where

$$K' = \frac{41.8\ K_{w1}\ K_{w2}^2\ f_o^2\ T^3}{P} \quad (10.27)$$

from eqns. 2.14 and 2.18

The impedance representing the non-linear eddy current effects in the solid iron is, itself, non-linear. It is a direct inverse function of both the slip, and the voltage across it V_{NL}, and has a fixed angle of 26.6°; that is to say, the reluctance of the solid iron changes in direct proportion to the slip frequency and the flux through it, and has a fixed angle of 63.4°.

10.3. DETERMINATION OF THE NON-LINEAR SOLID IRON IMPEDANCES

10.3.1. Determination of the Simple Pole Shoe Impedance

The general expression for the non-linear solid iron impedance is given by equation 10.26.

The simple pole shoe impedance is that impedance representing the effect of eddy currents in the pole shoe, if the flux distribution is neglected, i.e. if it is assumed that all the rotor flux enters the centre of the pole and follows the whole surface path to the tip (Fig. 43a). The simple pole shoe impedance is given by:-

$$Z_S = 1.15\ K' \frac{B_s\ \rho\ W^2}{L_S\ f_o} \cdot \frac{1}{S|V_S|}\ e^{j26.6^o} \qquad (10.28)$$

where L_S is the length of the pole arc from tip to tip.

W is the gross core length, plus two mean air gap lengths to allow for flux fringing at the ends.

V_S is the voltage across the impedance, Z_S, (V_S is directly proportional to the flux through the solid iron represented by Z_S).

B_s is taken as 1.75 webers/m^2.

ρ is chosen according to the size of machine. For the largest machines 30 x 10^{-8}, and for the smallest 20 x 10^{-8} ohm-m.

The material is always mild steel but different values of iron resistivity must be used because of the variation of iron temperature. As the machine size increases, the total quantity of eddy currents increases, and the ability to conduct away the heat generated in the solid iron decreases. Consequently, the surface temperature of the solid iron rises, for a given operating condition, as machine size increases. Plate 4 shows how hot the solid pole shoes of a 5000 H.P. motor became after a 30 second application of a quadrature axis static impedance test at half voltage. The estimated temperature rise, in places, was as much as 300-400°C, causing a local increase in iron resistivity to more than twice its cold value. Similar tests applied to a 1000 H.P. machine resulted in no discolouration of the pole shoes. It is clear, therefore, that the value chosen for the iron resistivity depends on both the machine size, and on the conditions of operation.

Moreover the iron resistivity must be multiplied by a factor depending on end effects. The path factor allows for the extra distance, and hence the extra resistance, through which the eddy currents must pass at the ends of the poles, in order to complete their closed circuit in the surface of the pole shoe. The factor for the direct axis is:-

$$\frac{W + .5\, L_S}{W} \qquad (10.29)$$

If there are no end rings connecting together adjacent pole shoes, the quadrature axis pole shoe eddy currents, in order to complete the closed circuit, must

penetrate through the pole body and link up in the spider construction at the base of the pole bodies. The increase in path resistance is considerable in this situation and the iron resistivity must be multiplied by a quadrature axis path factor:-

$$\frac{W + L_B}{W} \qquad (10.30)$$

where L_B is the minimum surface distance between adjacent poles.

If end rings are present connecting together the iron of adjacent pole shoes (Plate 3), the latter path factor is taken as unity.

The path factors are similar to those suggested by Gibbs[8].

The choice of the value of the saturated iron density, B_s, which has received a good deal of attention in earlier writings, is less critical than the choice of resistivity, since the range of variation is less, and is less dependent on unknown factors.

10.3.2. Determination of the Equivalent Pole Shoe Impedance accounting for the effect of Flux Distribution in the Solid Iron

It is convenient to replace the distributed representation of eddy current effects, shown in Fig.55a, by a single equivalent pole shoe impedance, Z'_S, shown in Fig.55b.

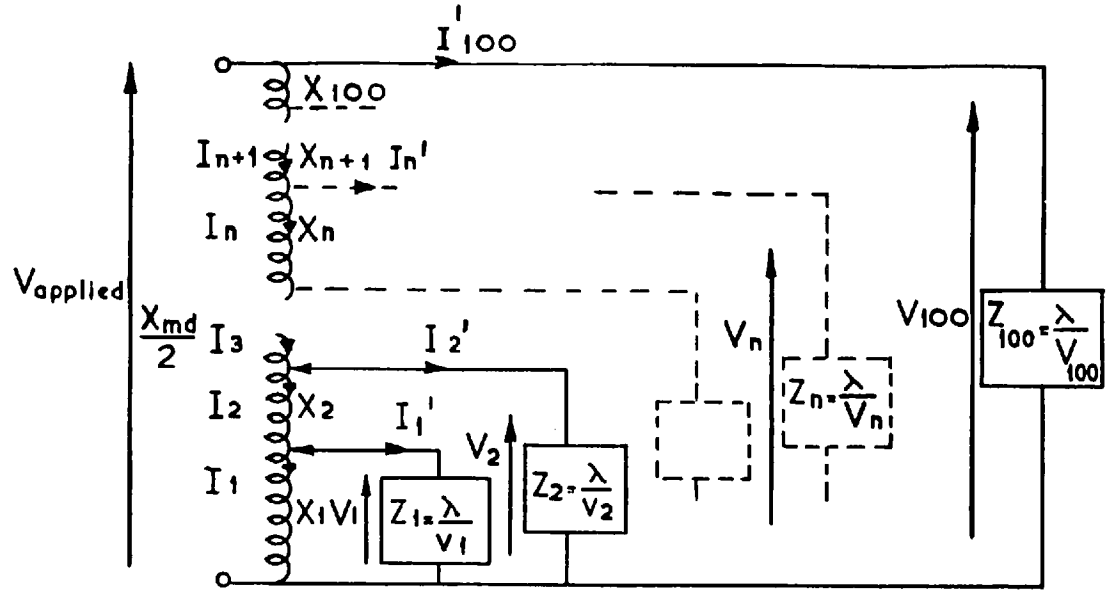

(a)

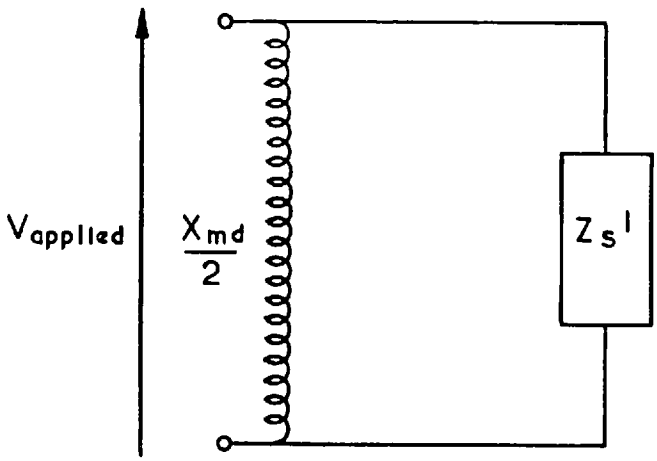

(b)

Fig. 55. The single equivalent pole shoe impedance representing the distribution.

Before any calculation can be made it is necessary to make assumptions as to the nature of the flux distribution in the air gap - and hence in the iron. There are three practicable assumptions that can be made:-

1. Free space distribution of air gap flux. The distribution is not assumed but is determined from the solution of the equivalent circuit.

2. Sinusoidal space distribution of air gap flux. This is what is ideally assumed in machines.

3. Uniform space distribution of air gap flux. This is easier to manage than a sinusoidal distribution and only gives marginally different results.

The nature of the flux distribution is realised from the solution of the equivalent circuit (Fig.55a), by the consideration of the voltages across the components of air gap reactance, X_1, X_2, X_3, ... e.g. If the magnitudes of the voltages across successive reactance components are all equal, the air gap flux distribution is uniform. The phase of successive voltages may, of course, differ.

10.3.2.1. Free air gap distribution

The length of pole arc from the pole centre to pole tip is divided into 100 equal sections, as shown in Fig.47a. It is then assumed that each section of the air gap has equal reluctance and hence is represented by equal portions

of $X_{md}/2$, i.e. in Fig.55a $X_1 = X_2 = X_3 = \ldots = X_n = \ldots = X_{100}$.

The voltage across $X_{md}/2$, i.e. V_{100} is assumed to be known. (It would, in fact, be obtained from the last iterative calculation of the complete equivalent circuit.) Since the flux distribution is unknown none of the voltages $V_1 - V_{99}$ are known.

The solid iron impedances, representing equal lengths of solid iron of the pole shoe (Fig.47b) are:-

$$Z_n = \lambda / |V_n| \qquad (10.31)$$

where λ is given by:-

$$\lambda = 1.15\ K' \frac{B_s \rho\ W^2}{s f_o L}\ e^{j26.6^o} \qquad (10.32)$$

from eqn. 10.27.

where $L = L_S/200$

Since the voltages V_1-V_{99} are all unknown, so, too are all the solid iron impedances Z_1-Z_{99}. Consequently the equivalent circuit representation, Fig.55a, cannot be solved directly but an iterative process must be employed, and it is necessary, because of the many branches, to use a computer.

The circuit (Fig.55a) was solved by first assuming a value for the unknown voltage, V_1, and then working up the ladder network until the voltage V_{100} was found. Since V_1 was incorrectly

assumed the voltage V_{100} was found not to equal the applied voltage. Thus V_1 was modified and the calculation repeated successively until the voltage V_{100} agreed with the applied voltage to within 1%. The rate of convergence to the solution is determined by how V_1 is modified before successive calculations of the network.

The magnitude of the voltages across the reactances X_1, X_2, ... X_{100}, after the final iterative cycle, are a measure of the magnitude of flux crossing the air gap at the equal sections 1-100 (c.f. Fig.47). Hence the air gap flux distribution is evident at the completion of the equivalent circuit calculation.

A typical air gap distribution, for the direct axis of the solid pole micromachine, calculated with 50 c/s rotor frequency and 1 p.u. terminal voltage, is given:-

Position on pole arc		% Total flux/half pole crossing main air gap
centre of pole	1	.637
	10	.638
	20	.644
	30	.662
	40	.701
	50	.778
	60	.917
	70	1.15
	80	1.54
	90	2.17
pole tip	100	3.20

It is clear that the effect of the eddy currents is to oppose the flux linking the rotor, and to encourage that which does, to cross the main air gap at such position that it links least length of the rotor solid iron.

The table shows that about .5% of the total rotor flux crosses the main air gap section 1, whereas 3% crosses the main air gap section 100, the pole tip; both sections being equal width of pole arc. In fact, the complete computer output shows that approximately 25% of the total flux/pole crosses the gap in the 10% of the pole arc at the tips.

Once the equivalent circuit is solved, it is an easy matter to calculate the value of the single equivalent impedance, Z'_S, which in parallel with the complete magnetising reactance, $X_{md}/2$, represents the distributed system of eddy current impedances. (Fig.55b). For the conditions above the single equivalent pole shoe impedance, Z'_S, is found to be 5.80 times the magnitude of the simple pole shoe impedance (neglecting distribution), and to have an angle of 39.6^{o}.

It was considered that should the distribution of flux be as calculated above, the stator teeth opposite the pole tips, at any instant, would be severely saturated, and conversely the teeth opposite the centre of the pole would be very much under-saturated. The stator tooth saturation, opposite the pole tips, would encourage the flux to redistribute itself into a more uniform manner, in the air gap.

10.3.2.2. Search coil tests

At this point, in the work, it was considered necessary to attempt to measure the distribution of flux in the air gap, just prior to entry into the solid iron of the pole. A series of search coils of six turns of two 'thou' wire was wound in loops on the pole surface of the micromachine, as shown in Fig.56b. Since the voltage induced in the search coils is a measure of the alternating flux linking the coils, an approximate measure of the magnitude of flux entering the pole shoe, at six sections, is obtained. Fig.56a shows the comparison between the air gap distribution determined from the induced voltage in the search coils, and the distribution calculated by the free distribution method. It is apparent that, although the eddy currents in the solid iron tend to encourage the rotor flux to enter the pole near the pole tips, the resulting stator tooth saturation does redistribute the air gap flux in a more uniform fashion. It is clear from the figure that an assumption of uniform air gap distribution gives the best approximation to the actual distribution in the air gap. This assumption is, in fact, adopted in the final method of calculation.

10.3.2.3. Uniform air gap flux distribution

The assumption of uniform air gap distribution immediately necessitates a restraint on

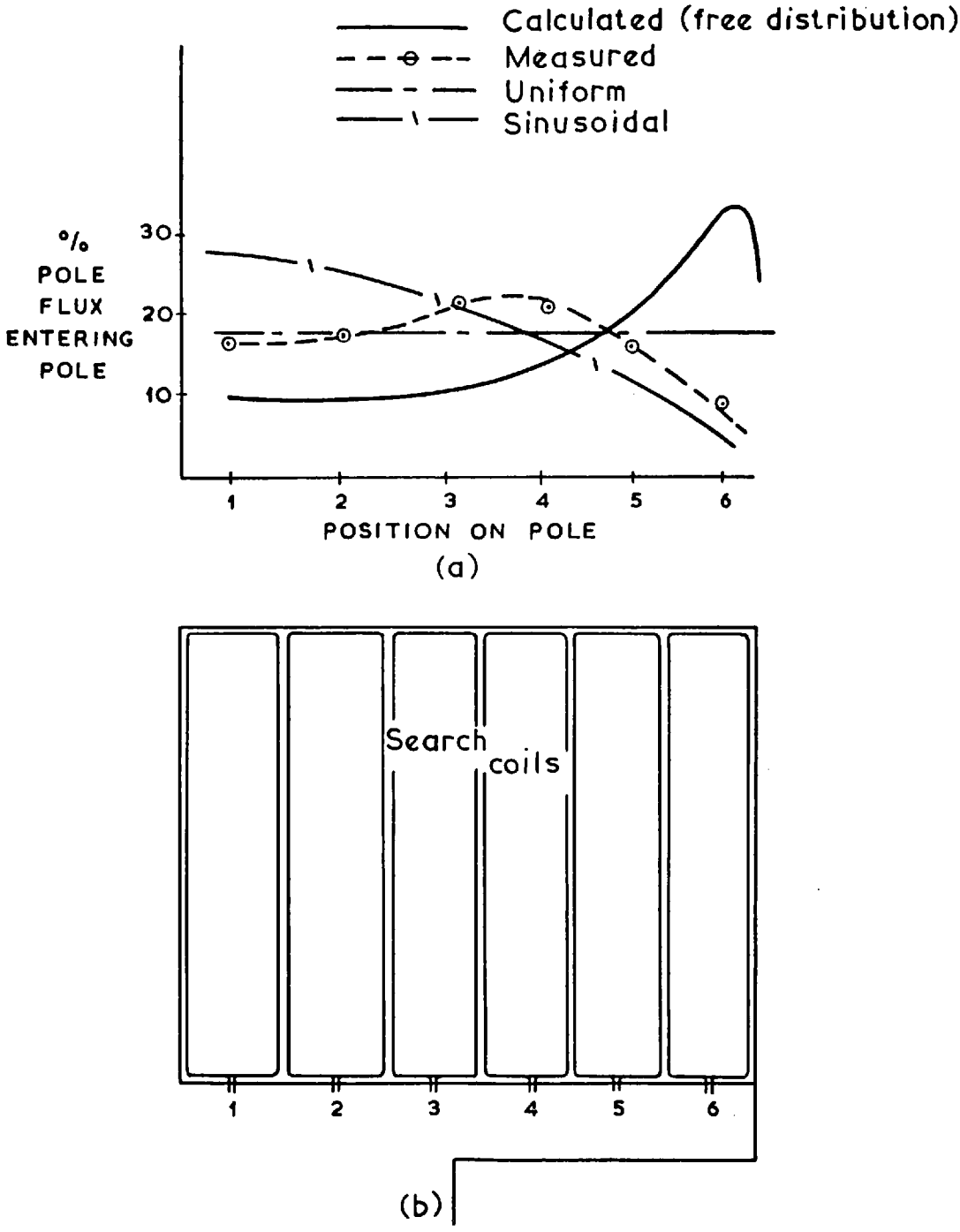

Fig. 56. Comparison of direct axis flux distribution measured by search coils, with that calculated (Rotor freq. 50 c/s)

the calculation that the magnitude of the voltages across the sections of $X_{md}/2$, i.e. X_1, X_2, X_3, ... X_n, ... X_{100}, must all be equal. Referring to Fig.55, it is clear that I_{n+1} must always be greater than I_n since:-

$$\overline{I}_{n+1} = \overline{I}_n + \overline{I}'_n$$

and if the equal voltage constraint is applied:-

$$|I_{n+1}|.X_{n+1} = |I_n|.X_n .$$

Thus $X_{n+1} < X_n$

The interpretation of this result is that different equal air gap sections must be represented by different unequal sections of the magnetising reactance, since the effective air gap is increased by saturation.

The method of solving the distributed equivalent circuit, for the uniform air gap distribution constraint, is much more difficult than that for free distribution since:-

(a) Although the voltages across the sections of X_{md} must all be of equal magnitude, they are not equal to $1/100^{th}$ of the voltage applied to the complete circuit, since the sectional voltages are not all in phase.

(b) Although $\sum_{1}^{100} X_n = X_{md}/2$ the values of X_{1-100} are different for the reasons ex-

plained earlier, and hence each value, X_{1-100}, is unknown.

(c) If the voltages in the circuit are unknown, the solid iron impedances Z_{1-100} $(= \lambda/|V_{1-100}|)$ are all unknown.

The equivalent circuit is solved, using the computer, by the following iterative method:-

First attempt. (Refer to Fig.55a)

1. V_1 is incorrectly assumed equal to $V_{applied/100}$.

2. X_1 is incorrectly assumed equal to $X_{md/200}$.

3. Z_1 $(= \lambda/|V_1|)$ is calculated.

4. The parallel combination of X_1 and Z_1 is calculated.

5. The currents $\overline{I}_1$ and $\overline{I}'_1$ are calculated.

$$\overline{I}_1 = \overline{V}_1/X_1, \quad \overline{I}'_1 = \overline{V}_1/Z_1$$

6. The current, I_2, is calculated.

$$\overline{I}_2 = \overline{I}_1 + \overline{I}'_1$$

7. The voltage across X_2 must be of equal magnitude to that across X_1. Therefore X_2 is calculated by:-

$$X_2 = |V_1|/|I_2|$$

8. The voltage V_2 is calculated by:-

$$\overline{V}_2 = \overline{V}_1 + \overline{I}_2 X_2$$

9. The impedance, $Z_2 (= \lambda / |V_2|)$ is calculated.

10. X_2 is added to the parallel combination of X_1 and Z_1 and the whole paralleled with Z_2.

11. The current, $\overline{I}_3$ is calculated etc., until the whole equivalent circuit is solved from Z_1 to Z_{100}. At the end of the calculation V_{100} is obtained and is found to be less than $V_{applied}$ because of the phase difference between successive voltages. Furthermore, the sum $\sum_{1}^{100} X_n$ is found to be much less than $X_{md}/2$.

Second attempt

1. Voltage, V_1, is corrected to:-

$$V_{1\ Old} \times |V_{applied}| / |V_{100}|$$

2. X_1 is corrected to:-

$$(X_{1\ Old} \times X_{md}/2) \Big/ \sum_{1}^{100} X_n$$

- the whole calculation is repeated as before.

Further attempts are applied until <u>both</u> V_{100} equals $V_{applied}$ to within 1%, and $\sum_{1}^{100} X_n$ equals $X_{md}/2$ to within 1%.

The single equivalent pole shoe impedance, Z'_s, representing the distributed effect of the eddy currents in the pole shoe is now easily obtained.

The value of the equivalent pole shoe impedance, Z'_s, for the micromachine, with 50 c/s rotor frequency and 1 p.u. terminal voltage, is 3.055 times the magnitude of the simple pole shoe impedance (neglecting distribution), and is found to have an angle of 38.0^{o}.

The extent of the artificial modification of the air gap, in the calculation, assuming uniform air gap flux distribution, is shown, to scale in Fig.57, for the micromachine. The rotor frequency and terminal voltage are, again, 50 c/s and 1 p.u. respectively.

Throughout the work on the effect of flux distribution in the iron it has been assumed that the division of the half pole into 100 sections is adequate to represent the ideal infinite number of sections.

The table below shows the difference in results obtained for the equivalent pole shoe impedance using 3, 20, 100, 500 and 1000 sections to represent the uniform air gap flux distribution of the solid pole micromachine, with 1 p.u. terminal

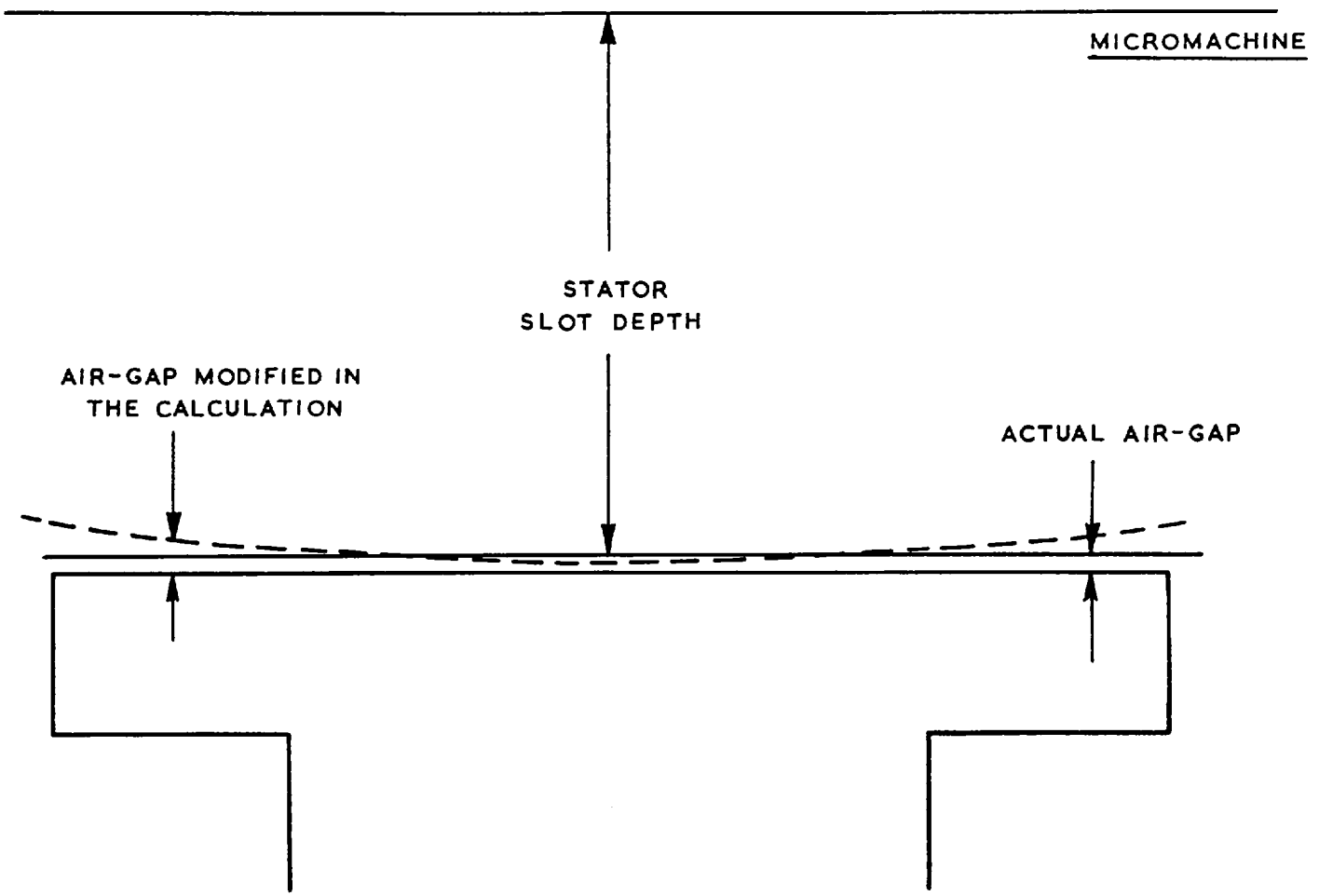

Fig. 57 Scale drawing showing the extent of air gap modification
(Rotor frequency 50 c/s, 1 p.u. terminal voltage)

voltage and 50 c/s rotor frequency.

Sections/Half Pole	$\frac{\lvert Z'_s \rvert}{\lvert Z_s \rvert}$	Angle $\lvert Z'_s \rvert$
1 ($Z'_s = Z_s$)	1.00	26.6°
3	1.985	33.0°
20	2.88	37.4°
100	3.055	38.0°
500	3.090	38.2°
1000	3.092	38.2°

Z'_s is the equivalent pole shoe impedance, including distribution.

Z_s is the simple pole shoe impedance, neglecting distribution.

The conclusion is that 100 sections are adequate to represent uniform flux distribution. The error in the angle of the equivalent pole shoe impedance, obtained using 100 sections, is less than .5%, compared with that obtained using 1000, i.e. infinite, sections. The error in magnitude is 1%. 1%, in any case, is the limiting factor to the iteration cycling in the calculation of the equivalent impedance.

As the slip of the machine changes from zero to infinity, the ratio, $\frac{\lvert Z'_s \rvert}{\lvert Z_s \rvert}$, changes from approximately 3.0 to 4.0, and the angle of the equivalent impedance from 26.6°, to 45°.

10.3.3. Determination of the Pole Body Impedance

The pole body impedance, Z_B, unlike the pole shoe impedances has no complications, due to flux entering the iron along its length.

10.3.3.1. The non-linear pole body impedance

The non-linear pole body impedance, is calculated from:-

$$Z_B = 1.15\ K' \frac{B_s \rho W^2}{L_B f_o} \cdot \frac{1}{s|V_B|} e^{j26.6^o} \qquad (10.33)$$

where L_B is the minimum surface distance between pole tips of adjacent poles.

- V_B is the voltage across the pole body impedance, i.e. across the field winding resistance.

- W and B_s are the same values as used in the expressions for pole shoe impedance.

- ρ, the effective resistivity, also is the same value as used in the expressions for pole shoe impedance; i.e. is multiplied by the direct axis path factor (10.29).

10.3.3.2. Linearization of the pole body impedance at limiting permeabilities

Fig. 58a shows the field winding section of the direct axis equivalent circuit.

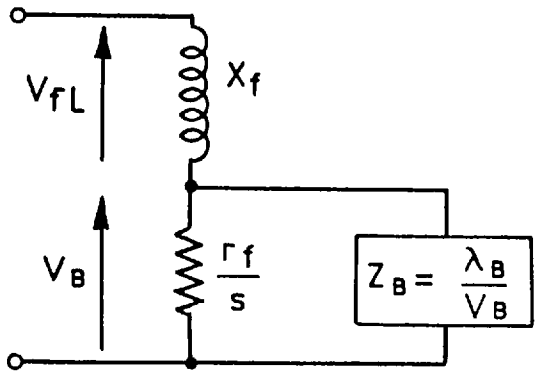

(a)

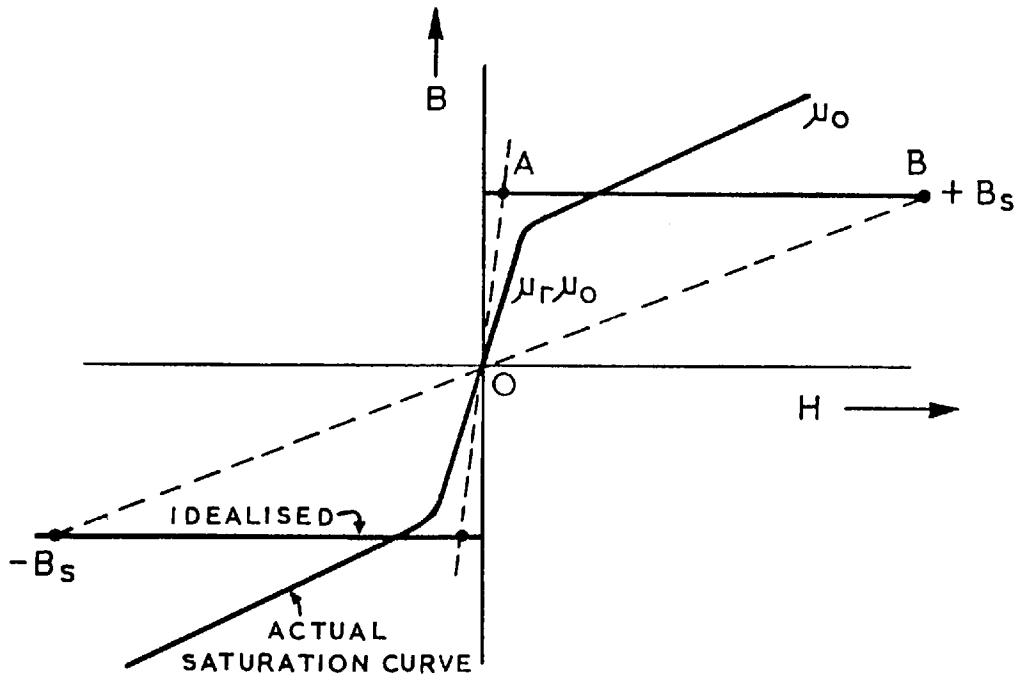

(b)

Fig. 58 Operation at limiting conditions

At high slips $\frac{r_f}{s} << X_f$, and the voltage, V_B, is very much smaller than V_{FL}. The voltage, V_B, in fact may be so small that Z_B, which is an inverse function of the voltage across it, may attain a value less than that which would be obtained by the linear theory, with relative permeability equal to the initial slope of the saturation curve; i.e. the magnitude of the non-linear pole body impedance corresponds to operation at a point A, say, on the non-linear saturation curve in Fig. 58b. (Compare eqns. 10.14 and 10.23.) Conversely, at very low slips, $\frac{r_f}{s} > X_f$ and the voltage, V_B, may, in certain instances, rise to such a value that the pole body impedance becomes less than the linear impedance with air permeability; an operating point, B, say, on the idealised saturation curve in Fig. 58b.

The non-linear pole body impedance, Z_B, may be very easily linearised, at these extreme conditions, by replacing it in the equivalent circuit by the combination of impedances shown in Fig.59a. Clearly, the magnitude of the combination can never exceed the fixed magnitude of the parallel branch - the linear impedance with relative permeability equal to the initial slope of the saturation curve; and the magnitude of the combination can never fall below the magnitude of the series impedance - the linear impedance, with permeability equal to that of air. The linear impedances are determined from equation 10.14.

The chain-dotted line in Fig.58b shows that, without linearisation, the magnitude of the pole

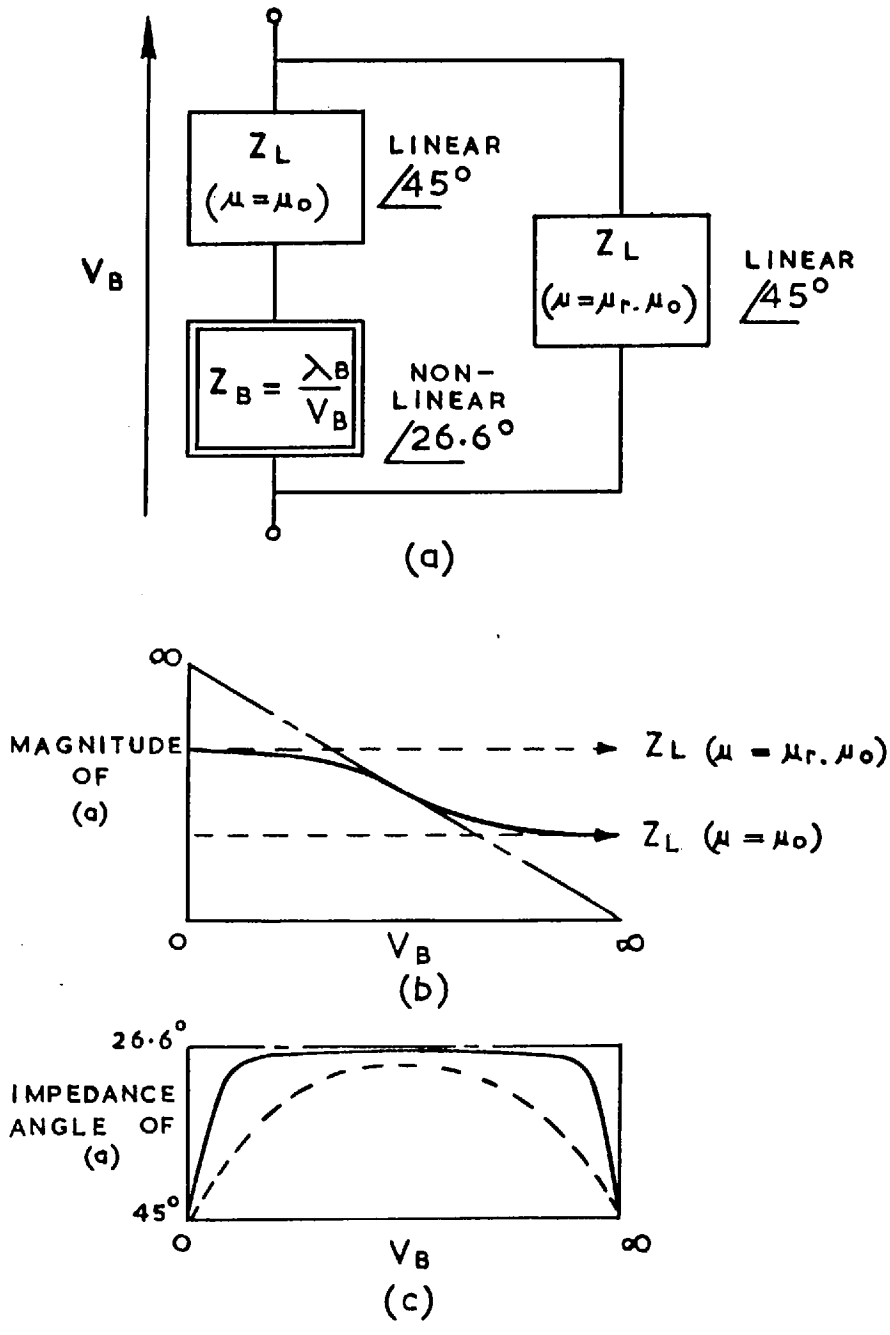

Fig. 59. Linearization of the pole body impedance at limiting permeabilities.

body impedance may change from zero to infinity as the pole body voltage changes from infinity to zero. With limiting linearisation in the form of series and parallel limiting impedances, the magnitude of the effective pole body impedance is limited within the two values of Z_L, as the pole body voltage changes from zero to infinity. The angle of the pole body impedance, without limiting linearisation, is shown in Fig.59c, by the half dotted line, to be 26.6^{o} for all voltage, V_B. If the limiting linearisation is applied the angle of the combination tends to limits of 45^{o}, and is shown by the full dotted line in Fig.59c. This angular characteristic was found to be unsatisfactory in practice. A more satisfactory, empirical, characteristic is obtained by squaring, first, all the impedances in Fig.59a, calculating their combination, and square-rooting the result. The angular characteristic then obtained is the full line in Fig.59c.

10.4. THE DETERMINATION OF THE TWO AXIS OPERATIONAL ADMITTANCE FREQUENCY LOCI

10.4.1. Calculation of the Operational Admittances

The two axis operational admittances are determined as the value of input admittance to the two axis equivalent circuits shown in Fig.51, with eddy current effects represented by the impedances, obtained by the non-linear theory. Since all the impedances are functions of the voltage across them, the solution of the circuit is necessarily an iterative process. Further complex calculation is required, which also requires an iterative method, to obtain the equivalent pole shoe impedances representing flux distribution in the pole shoe.

The equivalent circuit is actually split into two parts, for the calculation, as shown in Fig.49, to clarify the process. The admittance of one half is obtained, and is halved to give the operational admittances.

The method of calculating the operational admittance of the direct axis equivalent circuit is as follows:- (Refer to Fig.51a)

First attempt:-

1. It is assumed that the magnitude of the voltage across X_{md} and Z_B is equal to the terminal voltage.

2. It is assumed that the pole tips are not saturated and hence the equivalent pole shoe impedance, Z'_S, is fully paralleled with X_{md}.

3. The equivalent pole shoe impedance, Z'_S, is determined, using the 100 series/parallel branch iterative method described in 10.3.2.3.

4. The pole body impedance, Z_B, is calculated using the terminal voltage, as the voltage across it. Limiting linearisation is applied.

5. The complex admittance of the complete equivalent circuit is calculated.

6. The magnitude of the voltage across Z'_S and Z_B are calculated and are, of course, found to be different from the initial assumed value.

Second and Further attempts:-

Items 3 to 6 are repeated using the new voltages. The iteration is repeated until successive voltages are within 1%.

The flux in the pole tips is then calculated to see whether, at saturated level B_s, all the flux that needs to pass through the tip is able to do so.

If the tip is not over-filled then the calculation is complete for that terminal voltage and slip. If the

pole tip is over-filled the equivalent circuit is modified, by changing the coupling of Z_S' with X_{md} as shown in Fig.48 and the circuit iterative calculating process repeated.

The method of determining the quadrature axis operational admittance, which is simpler, is carried out in a similar iterative manner to that of the direct axis.

The operational admittance frequency loci of the solid pole motor are obtained by plotting out the real and imaginary parts of the admittances, calculated over a slip frequency range from zero to infinity, in the complex plane. Since both the resistive and reactive components of the solid pole impedances are inverse functions of the slip, it is evident that, at infinite slip, the solid iron impedances are zero, and therefore it is clear that the sub-transient reactance of a solid pole machine is equal to the stator leakage reactance.

10.4.2. The Frequency Locus of a Simple Equivalent Circuit having Different Fixed Rotor Impedance Angles

Fig. 60 shows the operational admittance frequency loci, of the simple equivalent circuit, shown in Fig.42, with the rotor impedance having different fixed angles. The curves drawn in full lines are all arcs of circles of different diameters, since they all may be obtained by the inversion of straight lines, having different angles to the real axis. The locus for a rotor impedance, with fixed angle of 45^{o} - that predicted by the simple linear theory - is shown; and also the locus for a rotor impedance, with fixed angle

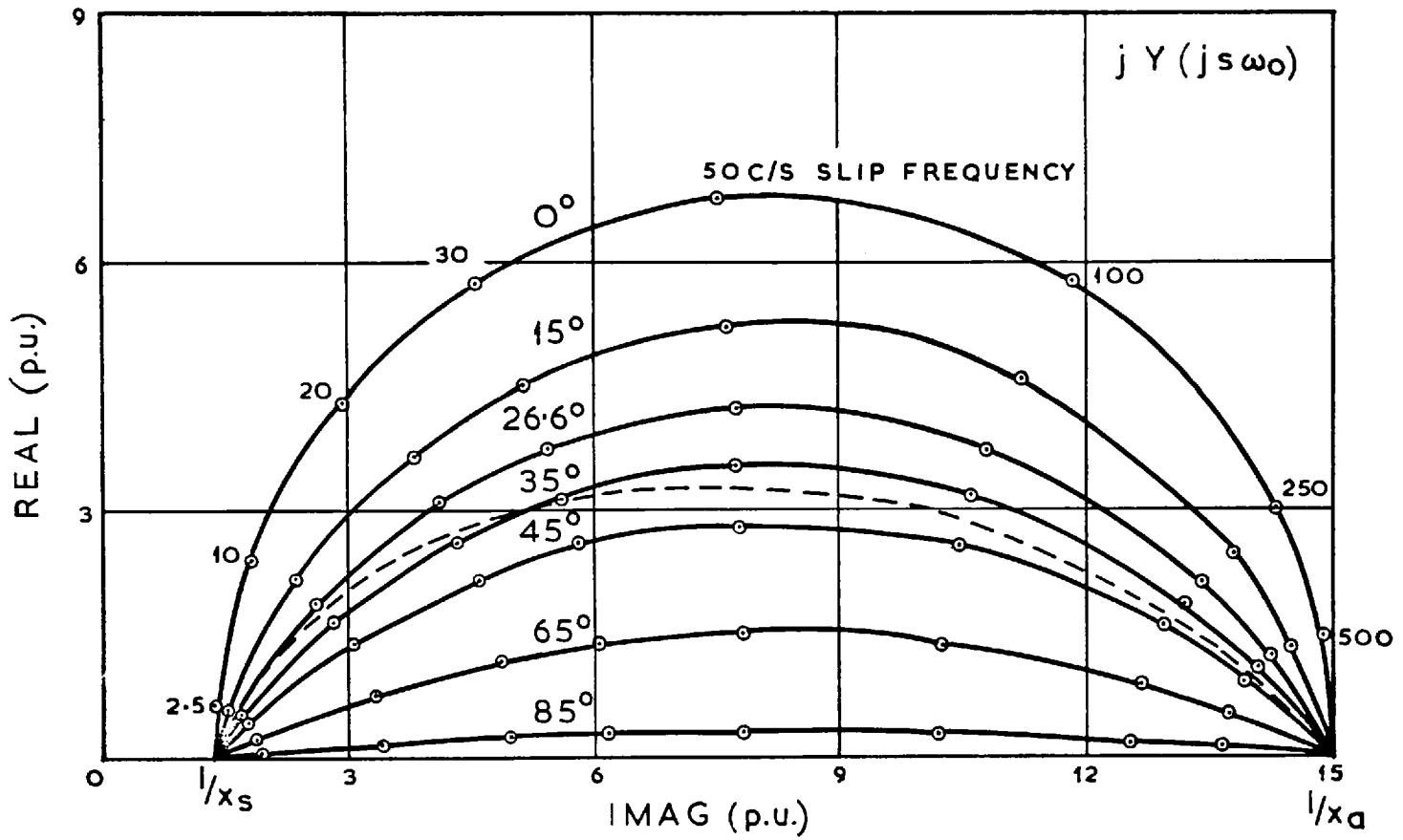

Fig. 60. Operational admittance frequency loci of a simple solid iron machine with different fixed rotor impedance angles

– – – – – Impedance angle 26·6°, but including flux distribution effect

of 26.6^{o} - that predicted by the non-linear theory, neglecting distribution. The dotted line is the operational admittance frequency locus of the simple solid iron machine, (Fig.42) including the effect of flux entering the solid iron, in a distributed manner (each solid iron section - Fig.47 - is represented by a non-linear solid iron impedance, having a fixed angle of 26.6^{o}). The machine is seen to behave as having a rotor impedance angle of 26.6^{o} at low slip, changing steadily to 45^{o} at high slip. The dotted locus (Fig. 60) is clearly not an arc of a semi-circle, and is not the inversion of a straight line, but of a curve.

10.4.3. The Quadrature Axis Operational Admittance Frequency Locus

Fig.61 shows the quadrature axis admittance locus, of a typical solid pole machine, calculated at two different terminal voltages by the method described. The path traced by the quadrature axis locus, at each voltage, is the same, although the frequency scale is different. This is because the only variables in the equivalent circuit are the solid iron impedances, which are all of the form $\lambda'/s|V|$, and hence the same result will be obtained whether, for example, s = .7 and V = 1.0, or s = 1.0 and V = .7.

10.4.4. The Direct Axis Operational Admittance Frequency Locus

Fig.62 shows the direct axis admittance locus of a typical solid pole machine, with field short circuited, calculated at two different terminal vol-

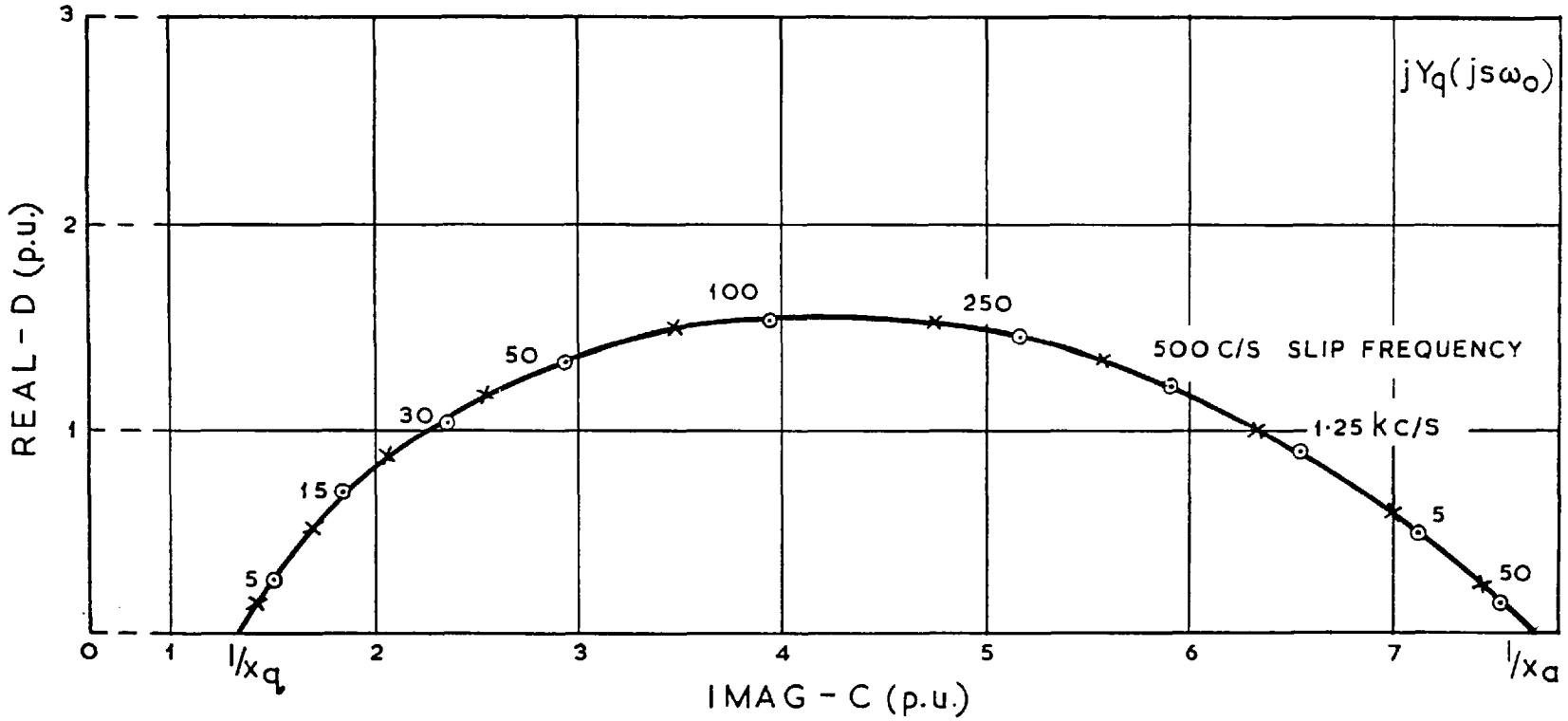

Fig. 61. Typical quadrature axis operational admittance frequency loci, of a solid pole motor, calculated at different voltages

—⊙— Calculated at 1 p.u. voltage

—×— Calculated at ·7 p.u. voltage

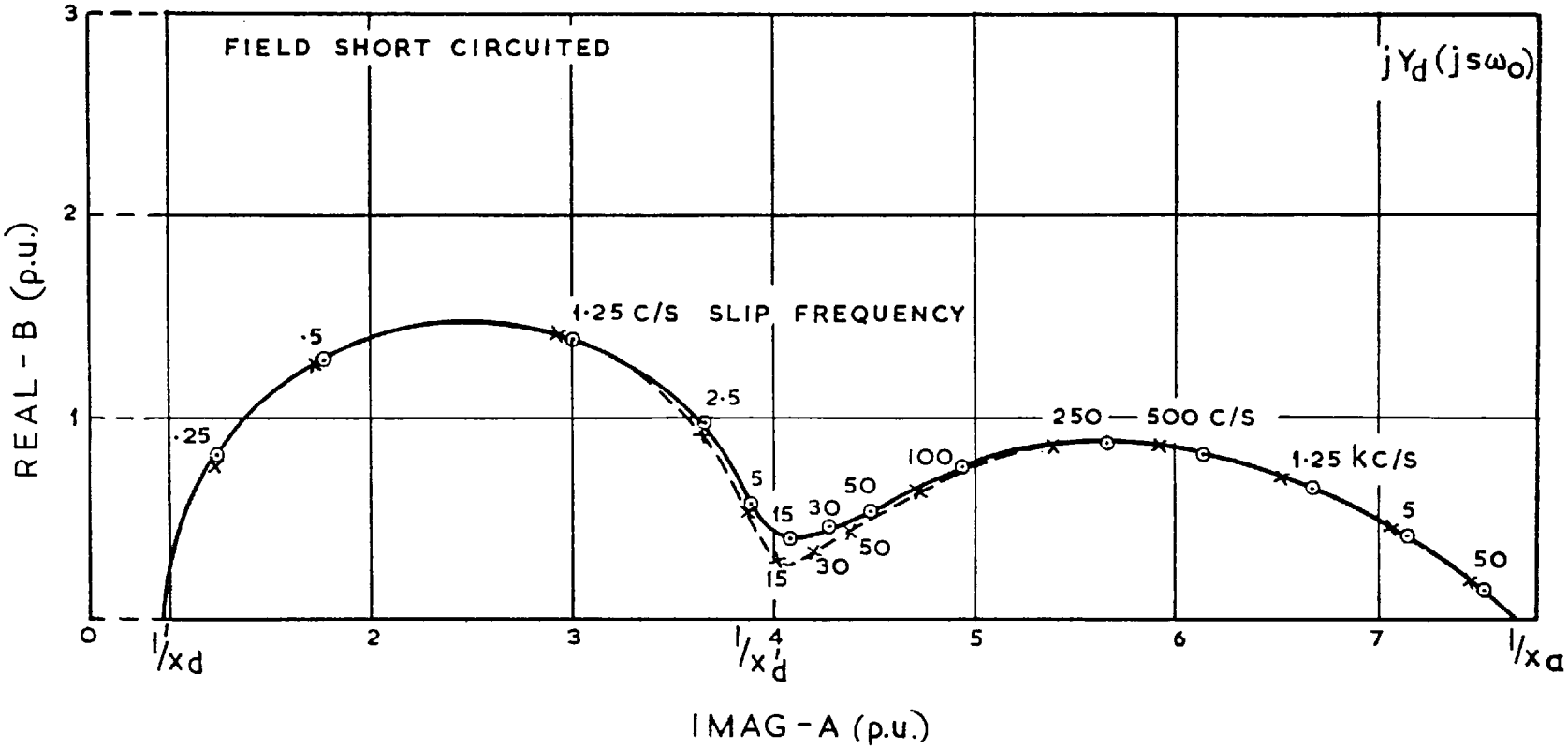

Fig. 62. Typical direct axis operational admittance frequency loci, of a solid pole motor calculated at different voltages

——o—— Calculated at 1 p.u. voltage

– – –x– – Calculated at ·7 p u voltage

tages by the method described. The paths traced by the direct axis loci, calculated at each voltage, are different since the variables in the direct axis equivalent circuit are not only solid iron impedances.

10.4.5. The Direct Axis Computer Programme

Because of both the complexity of the flux distribution in the solid iron, and the iterations necessary, because of the non-linearity of the impedances, the solution of both the direct and quadrature axis equivalent circuit was obtained using a fast computer. The computer used was the IBM 7090 at Imperial College.

The logic of the direct axis computer programme is shown, as a flow diagram, in Fig.63.

Because of the many loops within loops, including a double iterative procedure, the calculating time for obtaining the direct axis operational admittances of a solid pole machine, with two field connections, twenty-one slip frequencies at two voltages, was approximately 15 minutes. It was found, later, however that the complicated iterative sub-routine, for calculating the equivalent pole shoe impedance, that accounts for the flux distribution in the iron, may be replaced by a pair of curves. Using the curves, instead of the complex series/parallel iterative calculation, the programme running time was found to reduce by as much as fifteen times. Appendix IV explains how the sub-routine may be replaced by tables.

Part of an output sheet of the direct axis programme is shown in Fig.64. It is particularly inter-

DIRECT AXIS PROGRAMME OF SOLID SALIENT POLE SYNCHRONOUS MOTOR (FORTRAN - 4)

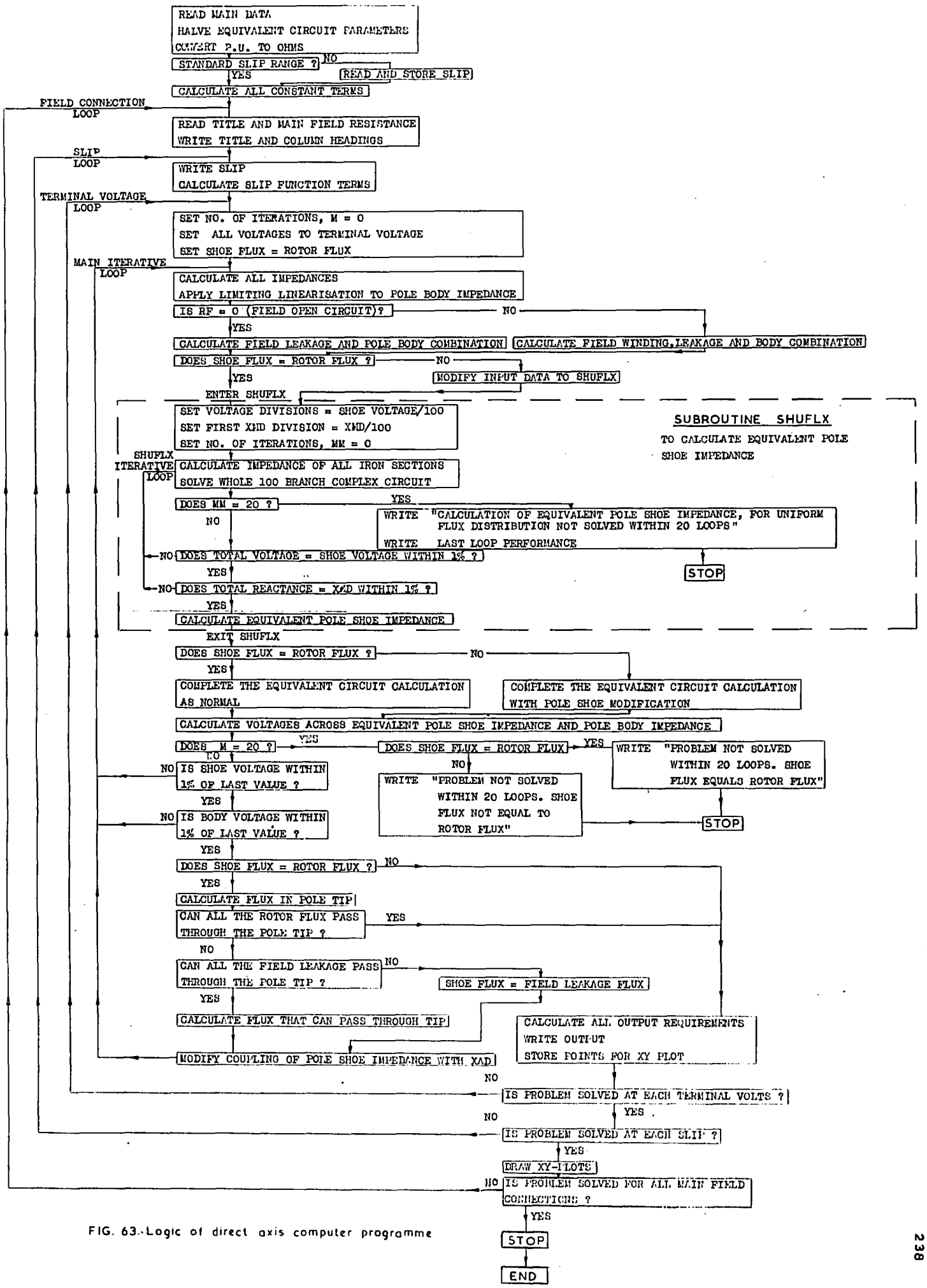

FIG. 63.-Logic of direct axis computer programme

esting to see the point at which the equivalent circuit is modified to allow for complete pole tip saturation. At slip .05, 1 p.u. terminal voltage, the shoe flux equals the rotor flux (both expressed as a percentage of the total flux produced in the machine), indicating that all rotor flux is able to link the pole tips. At slip .025, 1 p.u. terminal voltage, the shoe flux does not equal the rotor flux, indicating that the pole tip has become completely saturated, and hence some rotor flux must pass straight to the pole body. The equivalent circuit is then modified, as explained in 10.1.2.2. It is observed that, at .7 p.u. terminal voltage, the pole tips never become completely saturated.

A further point of interest, in the output shown, is the effect of limiting linearisation of the pole body impedance. The angle of the pole body impedance is retained at the linear angle of 45^{o} until the pole body flux has grown to a saturable magnitude.

MICROMACHINE - SOLID ROTOR - FIELD ONTO DISCHARGE RESISTANCE

OPER.L IMAG-A (P.U.)	ADMITT. REAL-B (P.U.)	SHOE IMPEDANCE (P.U.)	DISTR. N	SHOE ANGLE (EFFECT)	ROTOR FLUX (O/O)	EQUIV. B/H (REL)	SHOE PENETR. (EFFECT)	BODY IMPED. (P.U.)	BODY ANGLE	BODY FLUX	BODY B/H	BODY PENETR. (CMS)	ITERATIONS (INT)	ITERATIONS (EXT)	SHOE FLUX (O/O)	PHASE VOLTS (P.U.)
SLIP-	1000.0000															
7.5252	0.1557	0.0040	3.02	44.5	3.0	21.2	0.039	4.5438	45.0	0.001	2025.6	0.0000	7	11	2.97	1.00
7.4924	0.1835	0.0048	3.02	44.5	3.5	30.5	0.032	5.4621	45.0	0.001	2025.6	0.0000	7	11	3.53	0.70
SLIP-	100.0000															
7.1597	0.4225	0.0133	2.96	44.1	8.8	23.0	0.113	1.5324	44.9	0.023	2015.3	0.0003	7	11	8.84	1.00
7.0559	0.4833	0.0161	2.95	44.0	10.4	33.7	0.093	1.8623	44.9	0.027	2018.7	0.0002	7	11	10.39	0.70
SLIP-	25.0000															
6.6412	0.6744	0.0285	2.92	43.3	16.2	26.5	0.207	0.8341	43.8	0.171	1893.7	0.0022	7	10	16.23	1.00
6.4498	0.7369	0.0351	2.91	43.0	18.8	40.1	0.168	1.0300	44.2	0.198	1937.2	0.0018	6	10	18.78	0.70
SLIP-	5.0000															
5.3981	0.8622	0.0786	2.92	41.1	29.4	40.2	0.376	0.4664	35.0	1.532	945.4	0.0196	6	9	29.44	1.00
5.3191	0.8419	0.1018	2.94	40.3	32.7	67.4	0.293	0.5976	37.3	1.707	1197.4	0.0153	6	9	32.74	0.70
SLIP-	2.0000															
4.9168	0.8132	0.1588	3.02	38.7	37.6	65.7	0.481	0.3789	29.9	4.712	376.1	0.0602	5	8	37.63	1.00
4.6740	0.7418	0.2165	3.09	37.5	40.4	122.0	0.362	0.5012	31.8	5.100	579.4	0.0456	5	9	40.42	0.70
SLIP-	1.0000															
4.4848	0.7977	0.2930	3.18	36.2	43.0	111.8	0.550	0.3590	28.3	9.972	187.6	0.1274	5	8	43.01	1.00
4.3096	0.7244	0.4152	3.31	34.7	45.0	224.4	0.403	0.4787	29.4	10.673	311.5	0.0955	4	8	45.03	0.70
SLIP-	0.8000															
4.3630	0.8168	0.3603	3.26	35.3	44.7	135.2	0.572	0.3386	28.0	12.453	152.7	0.1591	4	7	44.67	1.00
4.2091	0.7538	0.5154	3.38	33.8	46.4	276.7	0.416	0.4813	28.9	13.276	259.5	0.1188	4	8	46.40	0.70
SLIP-	0.6000															
4.2087	0.8675	0.4718	3.35	34.2	46.8	173.8	0.600	0.3664	27.8	16.266	121.7	0.2079	4	7	46.80	1.00
4.0793	0.8229	0.6772	3.48	32.8	48.3	358.2	0.434	0.4893	28.5	17.374	207.0	0.1554	4	7	48.33	0.70
SLIP-	0.5000															
4.1076	0.9149	0.5592	3.41	33.5	48.2	203.6	0.618	0.3751	27.7	19.079	107.1	0.2438	4	7	48.23	1.00
3.9890	0.8834	0.8052	3.54	32.1	49.7	422.0	0.446	0.5007	28.3	20.393	183.0	0.1824	3	7	49.66	0.70
SLIP-	0.4000															
3.9743	0.9872	0.6865	3.49	32.7	50.2	245.4	0.643	0.3900	27.6	22.951	93.4	0.2933	4	7	50.15	1.00
3.8649	0.9726	0.9876	3.61	31.4	51.5	507.9	0.462	0.5200	28.1	24.563	159.9	0.2197	3	7	51.51	0.70
SLIP-	0.3000															
3.7776	1.0959	0.8886	3.57	31.7	53.0	308.4	0.679	0.4173	27.5	28.613	80.8	0.3657	3	7	52.99	1.00
3.6712	1.1022	1.2717	3.67	30.6	54.4	631.6	0.488	0.5654	27.9	30.689	138.4	0.2745	3	7	54.37	0.70
SLIP-	0.2000															
3.4383	1.2502	1.2493	3.67	30.6	57.9	406.4	0.744	0.4740	27.4	37.725	70.0	0.4821	3	6	57.92	1.00
3.3162	1.2771	1.7819	3.75	29.6	59.4	826.8	0.533	0.6319	27.8	40.489	120.7	0.3622	3	7	59.40	0.70
SLIP-	0.1000															
2.6864	1.3731	2.2106	3.79	29.1	67.7	636.2	0.868	0.6552	27.4	54.543	67.2	0.6970	2	6	67.70	1.00
2.5235	1.3840	3.0965	3.83	28.5	69.8	1248.2	0.626	0.8774	27.7	58.235	116.6	0.5209	2	6	69.80	0.70
SLIP-	0.0500															
1.9192	1.1813	3.9659	3.85	28.1	76.8	1023.8	0.984	1.0339	27.5	69.236	82.6	0.8848	2	6	76.80	1.00
1.7633	1.1322	5.5615	3.88	27.7	78.7	2013.3	0.706	1.4105	28.0	72.479	148.0	0.6493	2	6	78.68	0.70
SLIP-	0.0250															
1.3787	0.7791	9.9909	3.90	27.2	82.7	2196.5	0.968	1.8233	27.8	78.725	125.3	1.0061	2	7	78.37	1.00
1.3025	0.7279	10.9106	3.90	27.1	83.8	3595.5	0.751	2.3343	28.7	80.695	228.6	0.7219	2	6	83.80	0.70
SLIP-	0.0100															
1.0877	0.3456	24.5732	3.91	26.8	86.1	5734.4	0.943	4.2404	28.9	84.491	252.7	110796	1	6	73.79	1.00
1.0644	0.3356	25.4523	3.91	26.8	86.7	8427.7	0.779	5.9759	30.6	85.369	448.0	0.7637	2	5	86.66	0.70

Fig.64. Output of Direct Axis Computer Programme

10.5. THE ESTIMATION OF THE SOLID POLE SYNCHRONOUS MOTOR STARTING PERFORMANCE FROM THE ADMITTANCE FUNCTIONS

If the eddy current actions on the two axes of the solid pole motor may be considered independent, the torques, input power, current, p.f., etc., may be accurately determined from the two axis operational admittance frequency functions, in a manner fully explained in Chapter 2.

The assumption of independent eddy current action on the two axes is shown to be a valid one by comparison of results obtained from both the micromachine and two large machines. For both machines, the two axis operational admittances were obtained, at several frequencies, by the single phase static impedance test - a test in which the effects on each axis are determined separately and independently. Asynchronous running performance, (with flux on both axes) was determined. The agreement between the running performance, estimated from the measured single axis tests, and that directly measured, was found to be good, in the case of both machines.

Consideration of flux and current distribution in the solid iron also lends reason to the assumption that the two axis eddy current effects may be considered independent actions. Fig.46 shows the suggested flux and, hence, eddy current distribution, in the solid iron, on the two axes of the machine. It is observed that, where the flux is the greatest on the direct axis, it is least on the quadrature axis, and vice-versa. Furthermore, the pulsation of flux and current, on the two axes of the machine, is out of time phase by approximately 90^{o}.

If the running characteristics are to be calculated at 1 p.u. voltage it is assumed that the operational admittance functions, estimated at the same voltage, may be used in the calculation. This is not perfectly correct since the voltage applied to the two axis equivalent circuits is slightly less than 1 p.u. due to the armature resistance volt drop. However, since the armature resistance volt drop is very small, and in any case is almost in quadrature with the terminal voltage, since the power factor is very low during starting, the error in above assumption is considered negligible.

CHAPTER 11

COMPARISON OF THE MEASURED AND CALCULATED RESULTS OF SOLID POLE MACHINES

Table 1 shows a list of the eleven machines for which test results are available. Information is given regarding numbers of poles, horse power, and main dimensions.

Abundant comparison between measured and calculated results is available for the solid pole micromachine. Tests have been carried out at several voltages, with and without end-rings, and with three different connections of the main field winding. The tests applied were variable frequency static impedance tests to determine the operational admittance functions, and measurements were made of mean torque and current during steady asynchronous running. The performance of the machine has been calculated for all these conditions and is compared with test results.

The methods of calculation have been applied to several large machines of different sizes and of different numbers of poles, and although the test results are more sparse than on the micromachine, adequate verification of the methods of calculation is evident. The tests applied to the large machines were the axis reso-

Machine No.	Horse Power H.P.	No. of poles p	Effective Axial Core Length W metres	Stator Core Diameter metres	Pole Arc Length L_s metres	Iron Resistivity used in the Calculation ρ ohm-metres
Micro-machine	2.5	4	.109	.367	.107	20×10^{-8}
1	2500	6	.74	1.32	.33	28
2	4000	4	.80	1.37	.43	30
3	100	4	.213	.56	.197	21
4	800	8	.42	.91	.190	22
5	5000	6	1.05	1.60	.400	31
6	75	6	.311	.457	.127	23
7	7500	4	1.39	1.32	.42	32
8	3500	4	.915	1.20	.41	32
9 (2 machines)	5000	4	1.45	1.32	.39	31
10 (2 machines)	1650	4	.54	1.07	.34	28

TABLE 1. List of machines tested.

lution method, or the variable frequency static impedance test - over a limited frequency range. Torque-time characteristics were obtained, by the acceleration method, for two large machines.

11.1. THE SOLID POLE MICROMACHINE

The stator of the solid pole micromachine is the same as that with laminated poles. The rotor of the machine has four solid salient poles around which the main field winding is wound (Plate 3.). The field winding has an overall resistance of 19.7 ohms and 660 turns/pole. The primary referred field winding resistance, r_f, was found to be less than that of the corresponding laminated rotor micromachine, because it was found possible to wind the solid pole field winding with larger section copper wire (same number of turns as for the laminated rotor). The mean air-gap of the solid pole machine is not the same as that of the laminated pole machine, and thus both the direct and quadrature axis synchronous reactance, X_d, X_q, of the two forms of the micromachine are different. The field leakage reactances, X_f, also differ since the pole-arc to pole pitch ratio of the two machines is quite different.

The p.u. values of calculated parameters used in the solid pole equivalent circuits are as follows:-

		Corresponding Transient Parameters		
X_a	= .130	X_d	=	1.10
X_{md}	= .97	X_q	=	.77
X_f	= .15	X'_d	=	.257
r_f	= .0040	T'_d	=	.212 secs

The transient parameters were confirmed by test.

11.1.1. Comparison of the Measured and Calculated Operational Admittance Frequency Loci

Fig. 65 shows the comparison of the direct axis operational admittance frequency loci calculated for three different connections of the main field winding. Since the direct axis mean torque is approximately obtained by the real part of the admittance, B, and the direct axis current by the magnitude $\sqrt{A^2 + B^2}$, (fully explained in Chapter 2), it is clear that at standstill the greatest torque and the minimum current is obtained with the main field winding on open circuit. The explanation for this is that, at 50 c/s rotor frequency, the contribution of torque by the closed field winding is very small, but the reduction of eddy current torque, caused by the reduction of rotor flux due to the reaction of the closed main field winding is very large.

Fig. 66 shows comparison between the direct axis locus calculated with field winding open circuited, and that measured by the variable frequency static impedance test. Comparison is shown at two voltages - .7 and .4 p.u. The measurements were at equal voltage - frequency ratios of .7 and .4 p.u. in order that the tests corresponded correctly at the same p.u. flux. The agreement between measured and calculated results is particularly good at .4 p.u. voltage. Since the direct axis equivalent circuit, with field winding open circuited, derived in the previous chapter, still includes the field leakage reactance, X_f, the angle of the effective impedance representing the complete rotor effects is high - as much as 55^o at 50 c/s rotor frequency. The direct axis locus, hence, is seen to

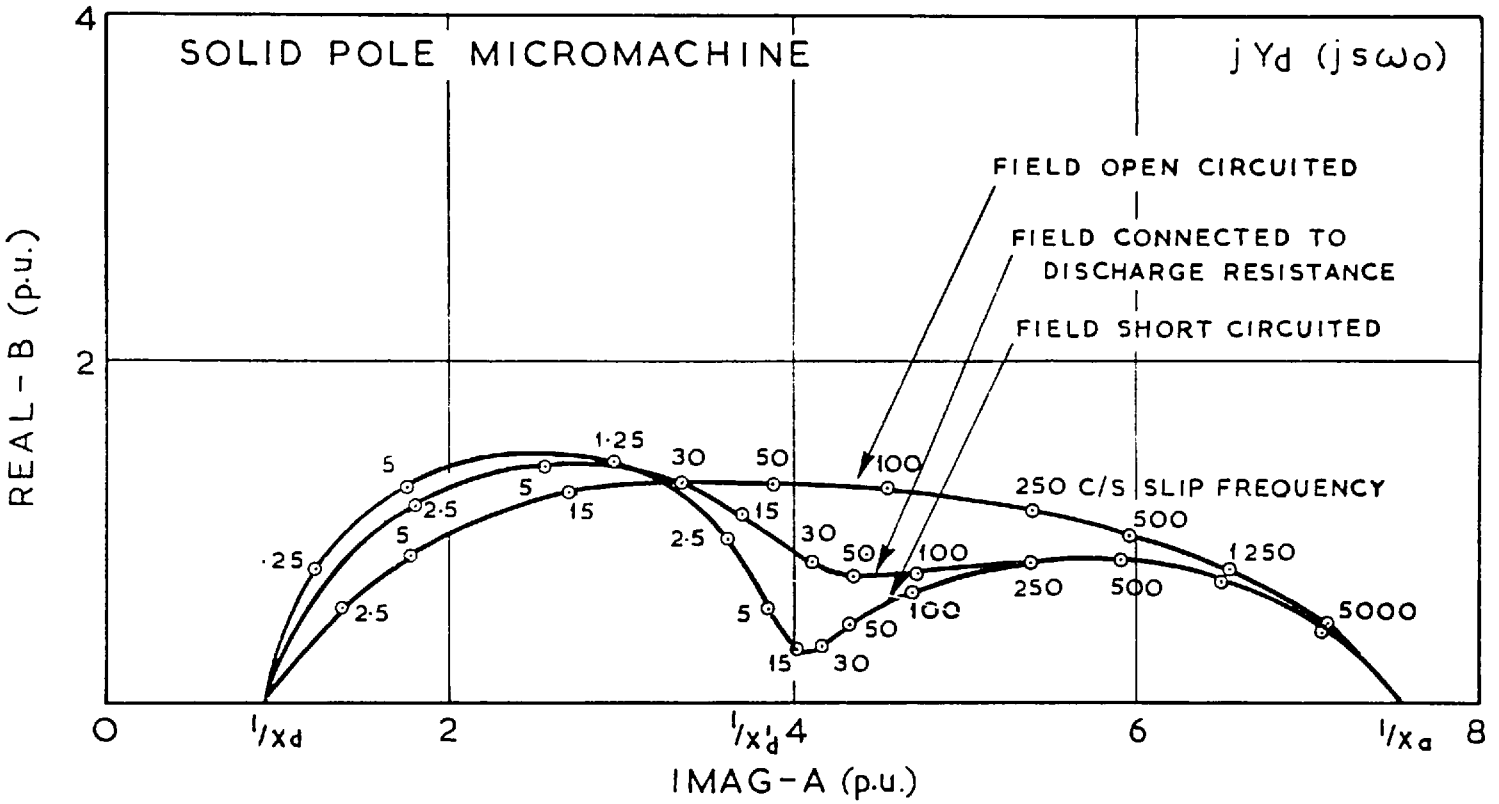

Fig. 65 Comparison of direct axis operational admittance frequency loci calculated with different main field connections (Voltage ·7 p.u.)

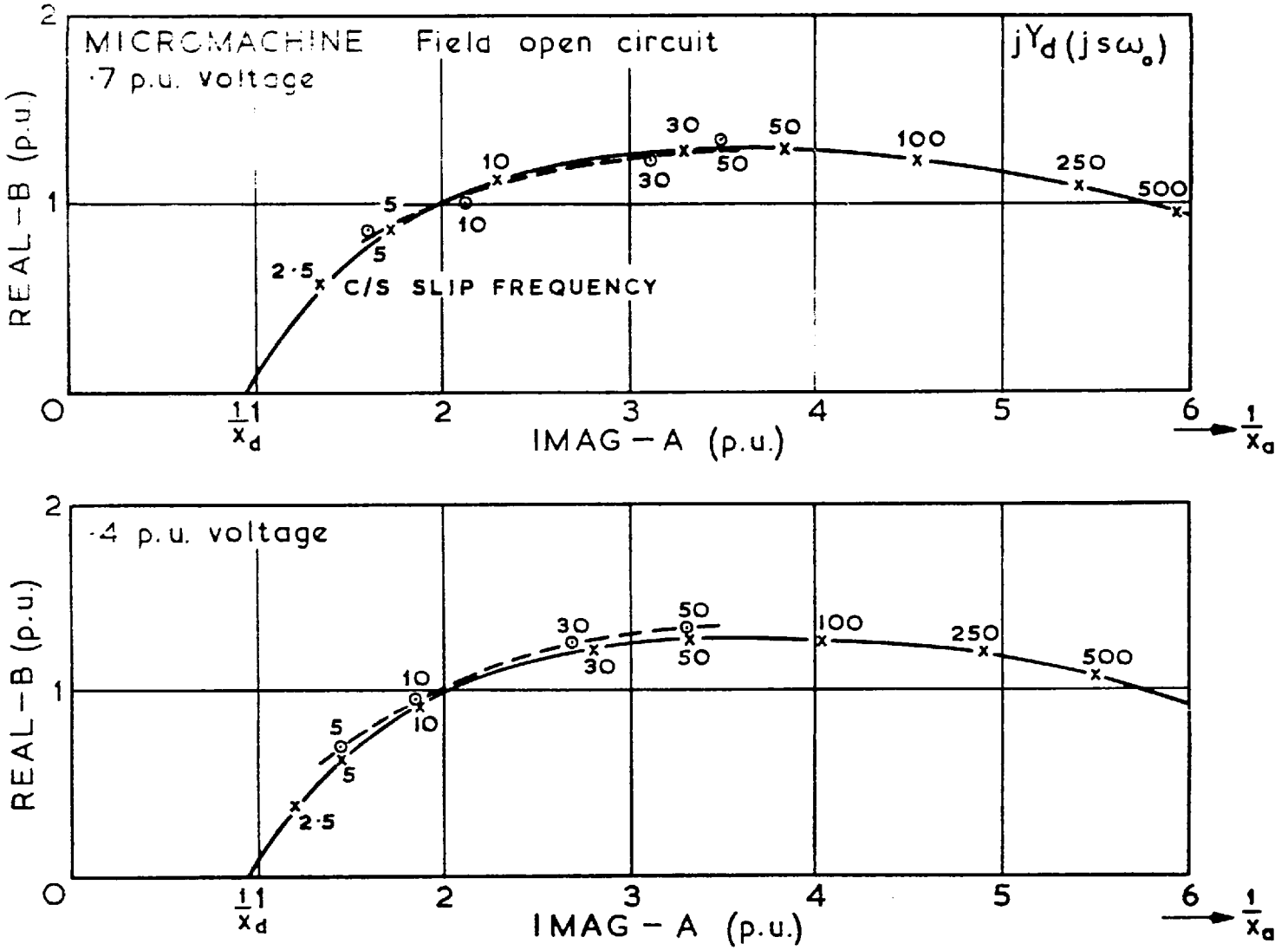

Fig. 66 Comparison of direct axis operational admittance loci

——x——Calculated

– –o– –Measured by static impedance test

be very much flatter than that of the quadrature axis.

Figs. 67 and 68 show similar comparison for the direct axis with the field connected to a discharge resistance and with the field short circuited. The agreement is not so good in the latter case. A possible reason for this is that the measurements were made at very low power factor, when the real part of the measured impedance is small; the real part of the operational admittance is obtained by the subtraction of the uncertain value of armature resistance (equation 3.1) which in this case is a major proportion of the real part of the measured impedance.

Fig. 69 shows the comparison between the measured and calculated quadrature axis operational admittance frequency locus of the micromachine without end rings connecting adjacent poles. Fig. 70 shows the comparison of the locus with end rings connecting adjacent poles. Good connection to the solid iron was achieved by screw thread contact. The rings were attached to each pole by five 2BA brass screws, spaced equally over the pole arc, as shown in Plate 3. (The 'rings' are actually polygonal in this case.) It is observed, in Figs. 69 and 70, that the agreement between measured and calculated results is very good, in both cases, indicating that the simple allowance of end effects in the solid iron, by a path factor (eqn. 10.30) is perfectly adequate without further complication.

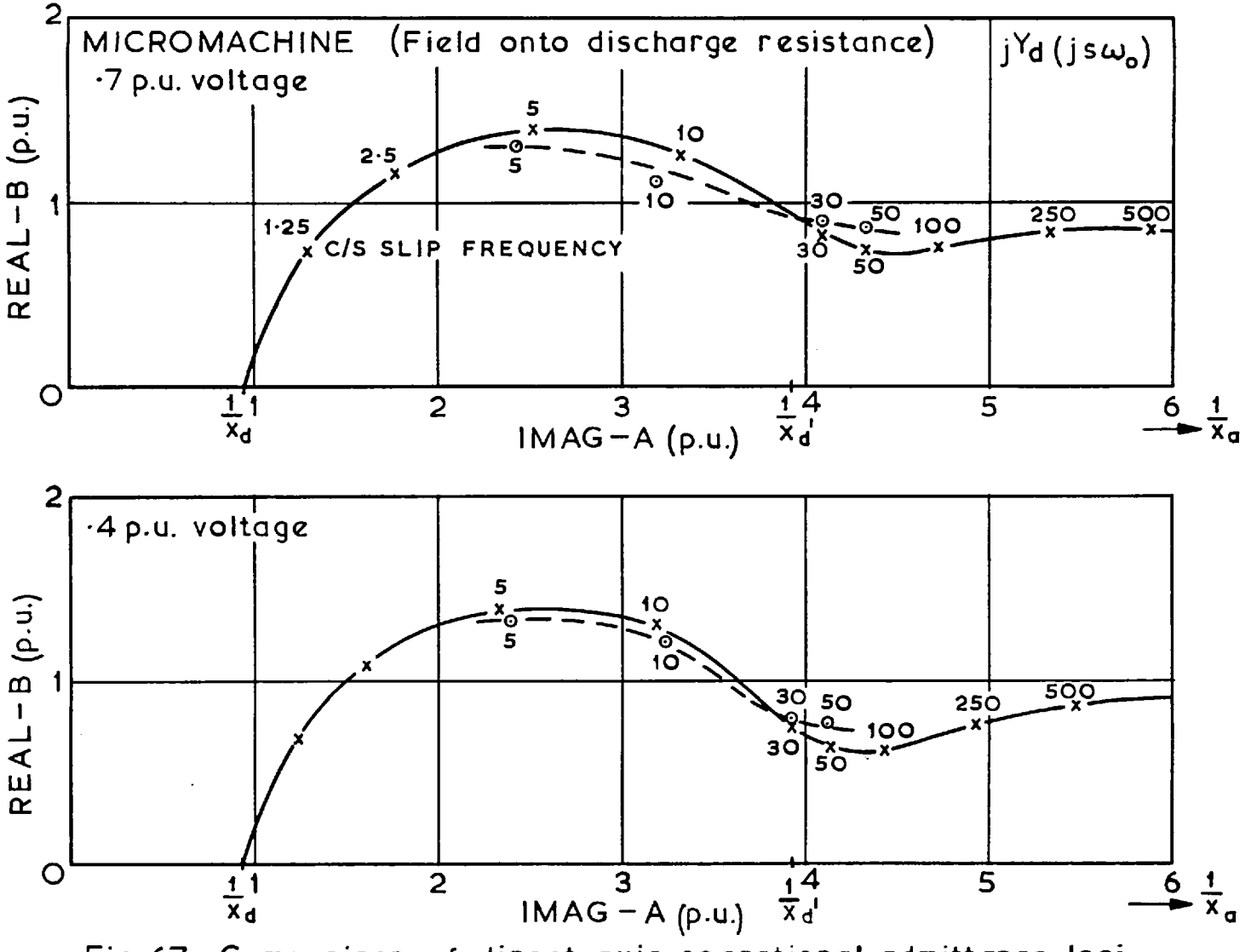

Fig. 67 Comparison of direct axis operational admittance loci

——x—— Calculated

– – ⊙ – – Measured by static impedance test

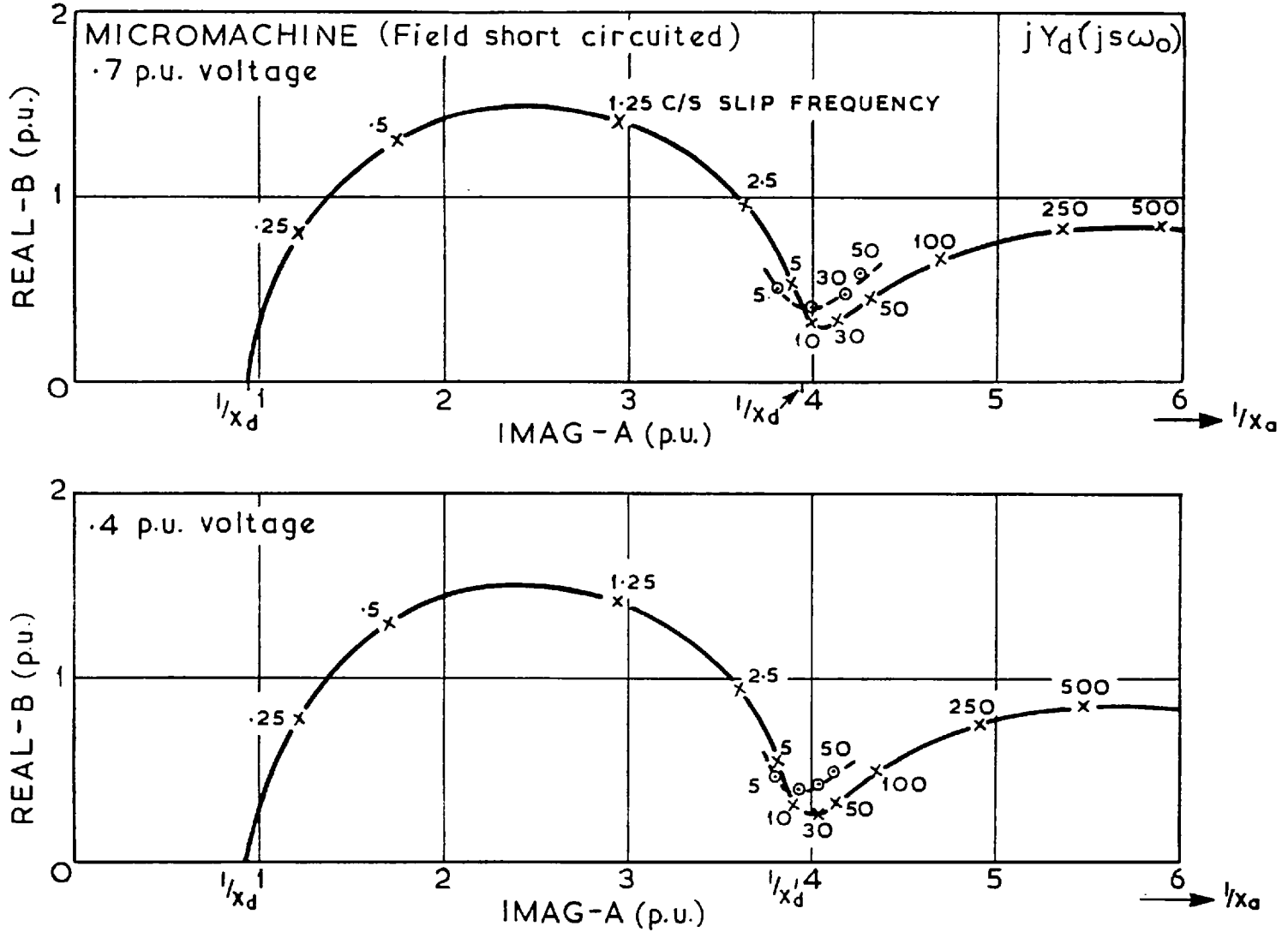

Fig. 68. Comparision of direct axis operational admittance loci

——×—— Calculated

– – –⊙– – – Measured by static impedance test

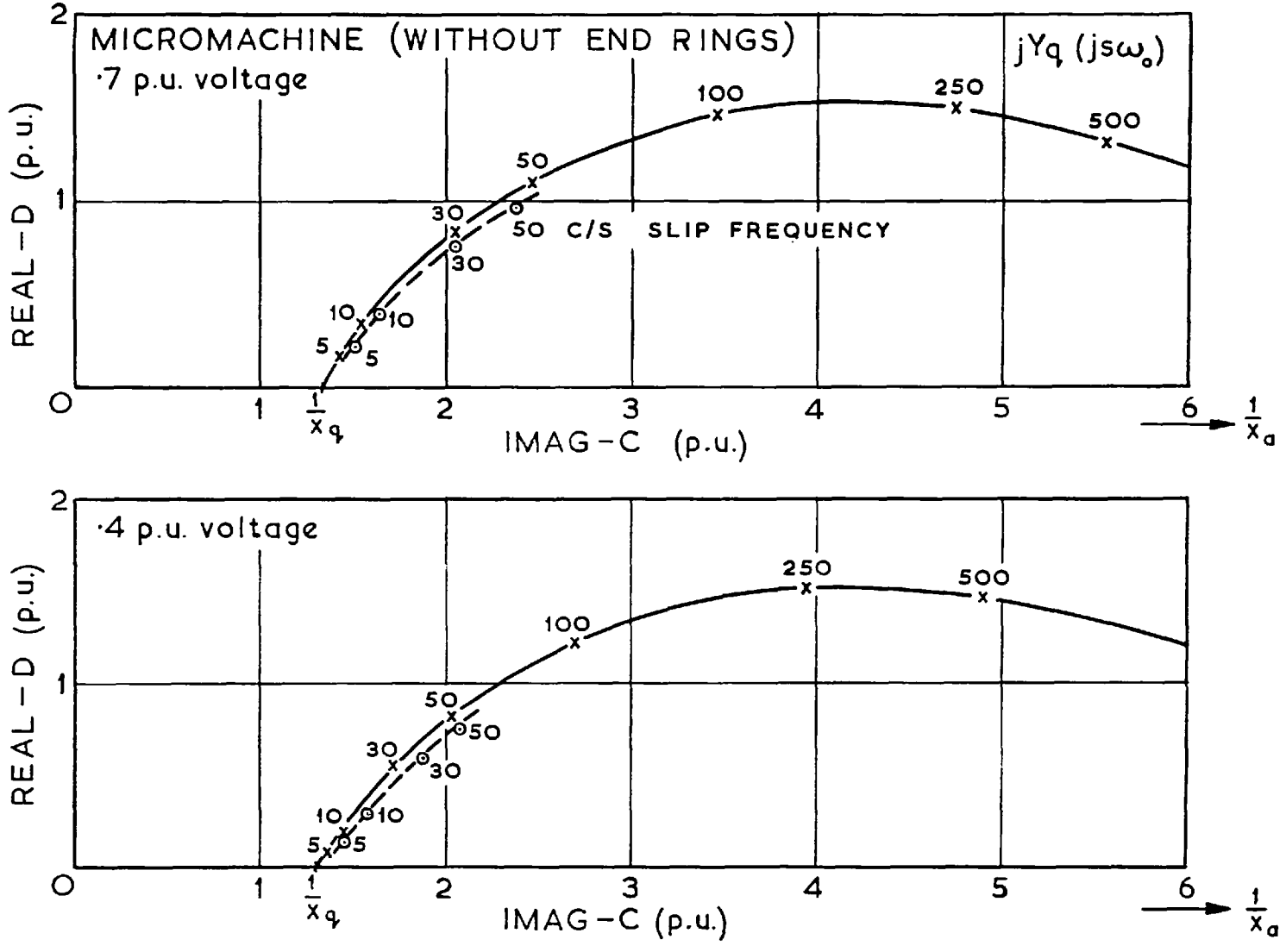

Fig. 69 Comparison of quadrature axis operational admittance loci

——x—— Calculated

– – ⊙ – – – Measured by static impedance test

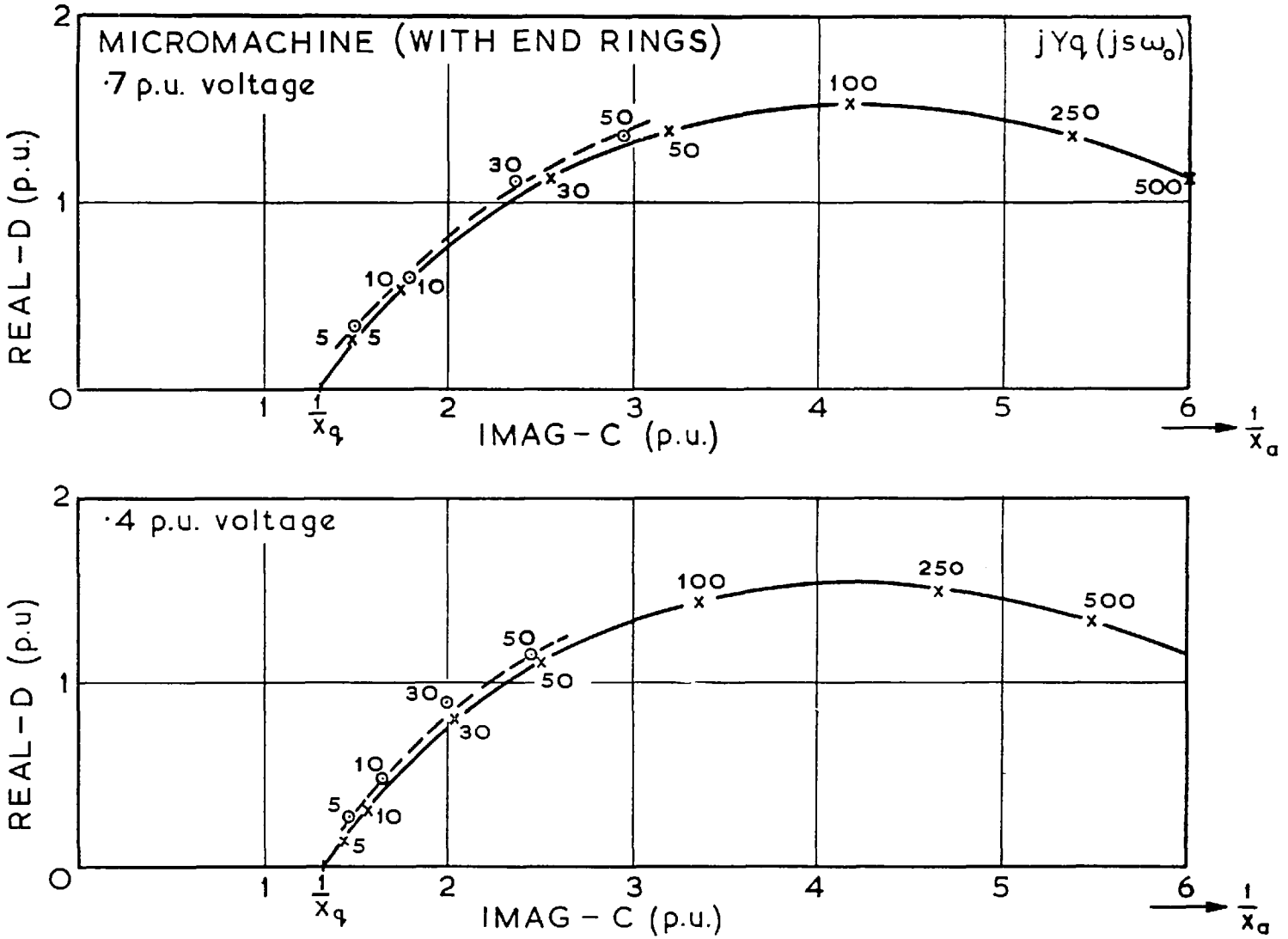

Fig. 70 Comparison of quadrature axis operational admittance loci

——x—— Calculated

– – ⊙ – – Measured by static impedance test

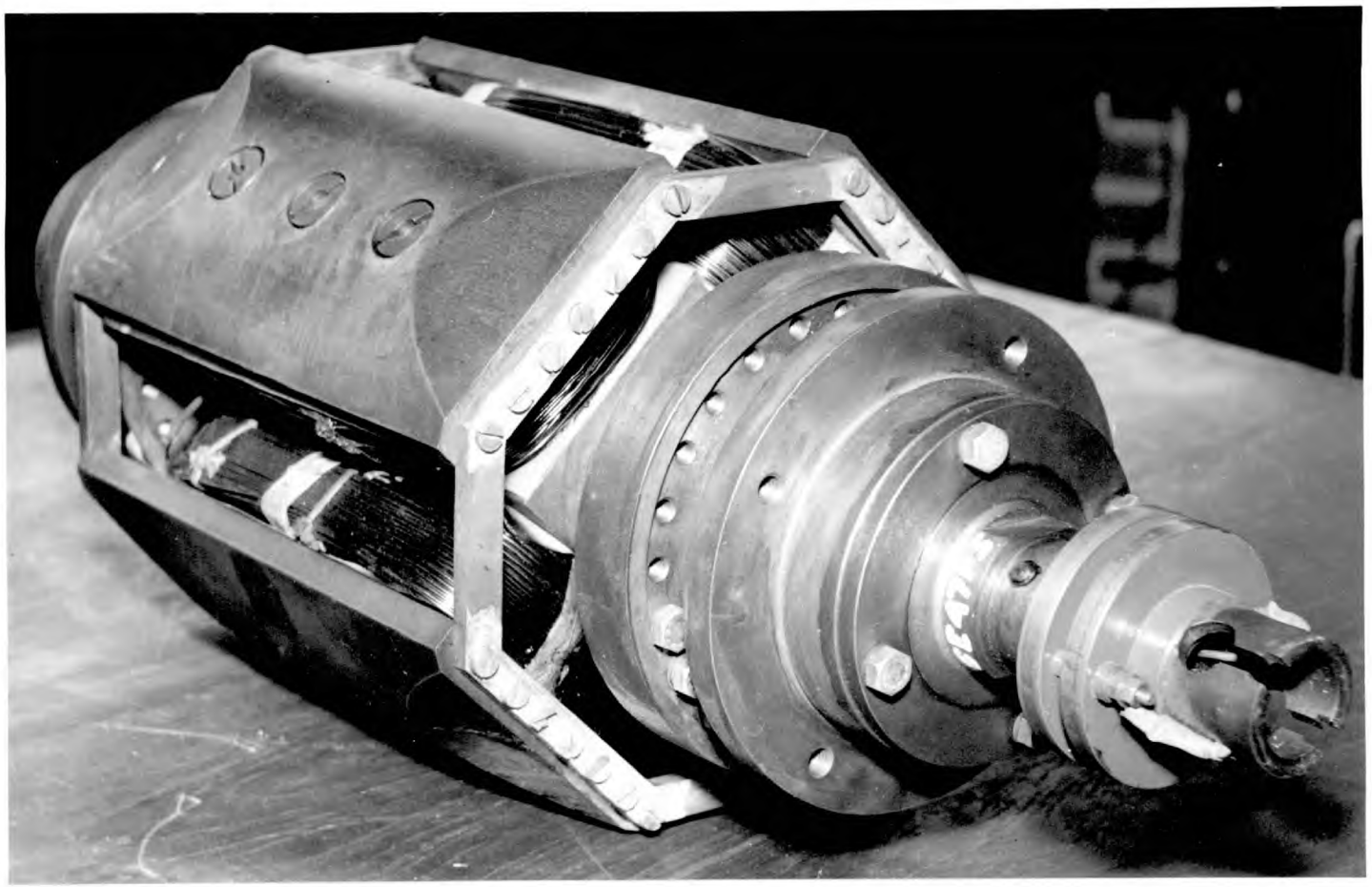

Plate 3. The solid pole micromachine rotor, with end rings connected.

11.1.2. Comparison of Measured and Calculated Starting Perfcrmance

Because of difficulties found in accurately determining the oscillating component of torque, comparisons are only given for mean torque and phase current. It was verified, on the laminated pole micromachine and on one large solid pole machine (Machine 3) that, if accurate determination of the two axis operational admittance frequency loci was obtained, the value of oscillating component of torque, calculated from the admittance loci was also accurately determined.

Figs. 71 and 72, show comparisons between the mean torque-slip characteristics, measured at three voltages, 1, .7, .4 p.u. and those calculated directly by the new method. The characteristics are all plotted, scaled to 1 p.u. voltage to demonstrate the non-linearity of the solid iron. (If there were no non-linearity all the characteristics would be identical.)

Fig. 73 shows comparison between the mean torque-slip characteristics of the micromachine, with and without end-rings, both measured and calculated at .7 p.u. voltage. The effect of end-rings is seen to both increase the mean torque, and to reduce the saliency at half speed, i.e. to reduce the half speed dip.

Fig. 74 shows the comparison between measured and calculated phase current-slip characteristics at the three voltages.

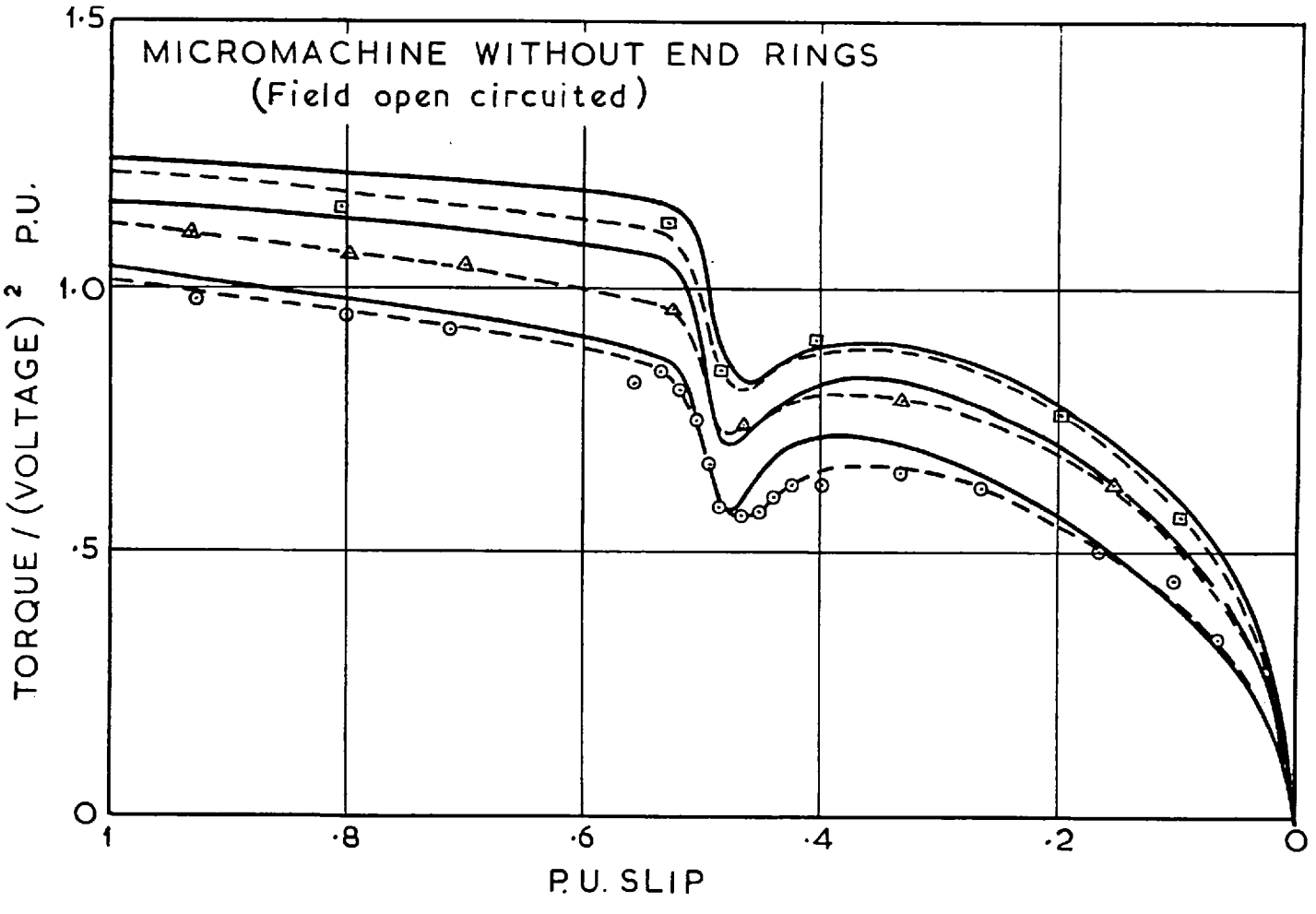

Fig. 71. Comparison of Mean Torque-slip characteristics at different voltages

—⊡—△—⊙— Measured at 1·0, ·7, ·4 p.u. voltage
——————— Calculated at same voltages

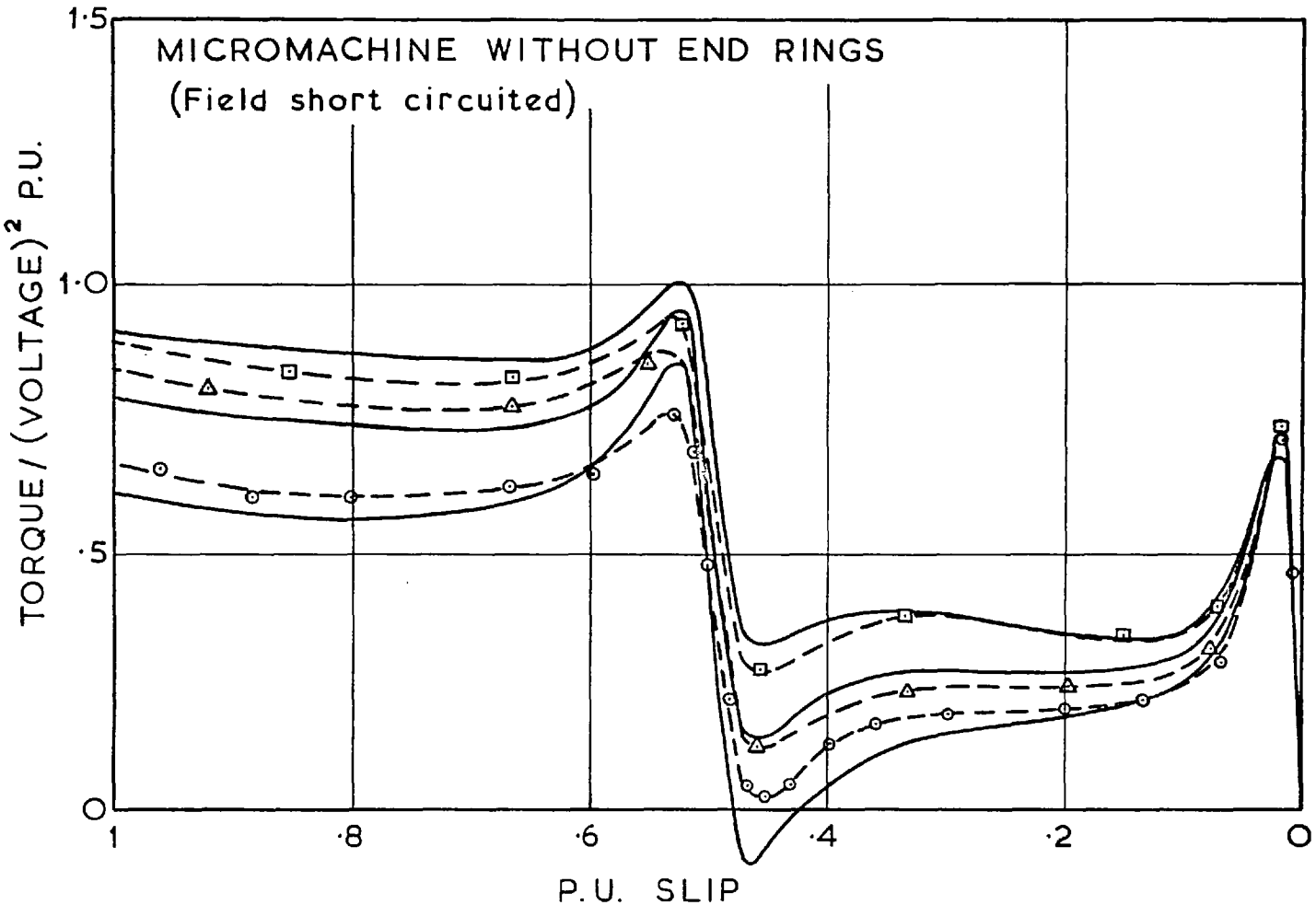

Fig. 72 Comparison of Mean Torque-slip characteristics at different voltages

—□—△—○— Measured at 1·0, ·7, ·4 p.u. voltage

——— Calculated at same voltages

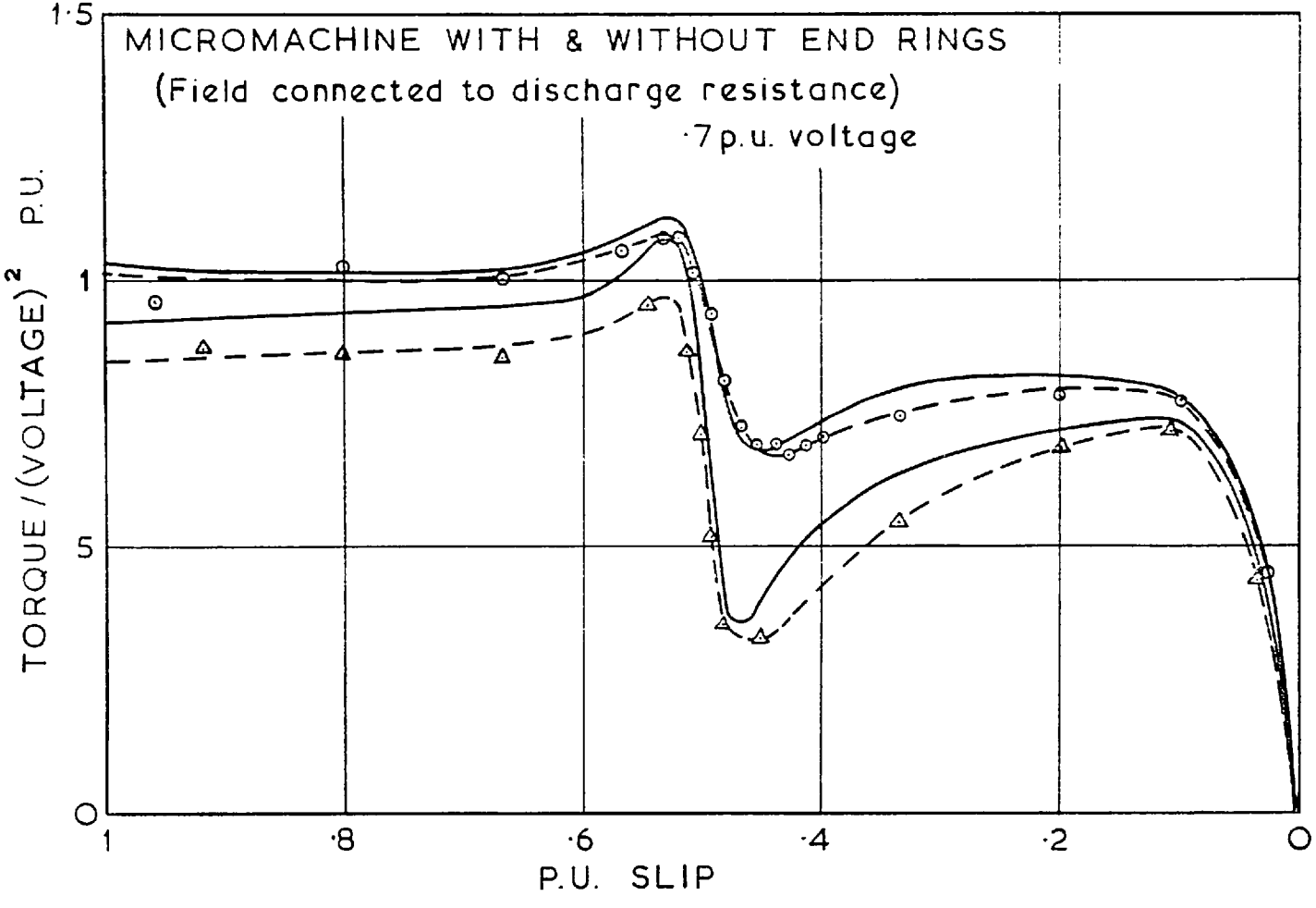

Fig. 73 Comparison of Mean Torque-slip characteristics, with and without end rings

——— Calculated (top curve end rings connected)
– –⊙– – Measured (end rings connected)
– –△– – Measured (no end rings)

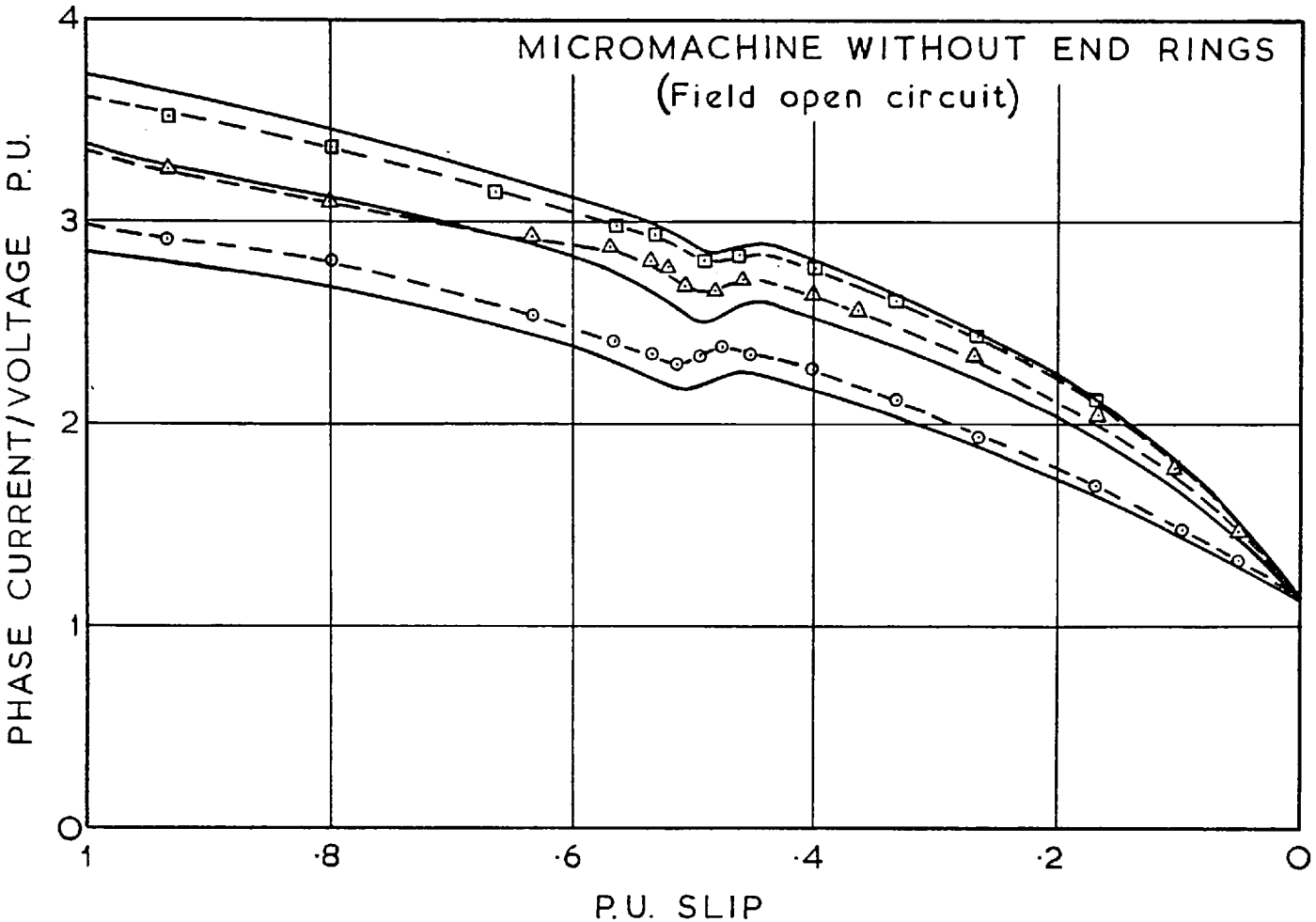

Fig. 74 Comparison of Mean phase current–slip characteristics at different voltages.

–□–△–○– Measured at 1·0, ·7, ·4 p.u. voltage

——— Calculated at same voltages

11.2. THE LARGE SOLID POLE MACHINES

The volume of test results available on each of the large solid pole machines, tested, varies considerably. The most test information is available on the machines 1 - 6, and the least on machines 7 - 10. The machines are considered in order of most availability of test results.

11.2.1. The 2500 HP, 6 Pole Motor (Machine 1)

The most reliable test, the single phase static impedance test, was applied at three frequencies and at .4 p.u. flux to this machine. The agreement between the operational admittances determined from the test results and those calculated by the new method is seen in Fig.75 to be extremely good, at all frequencies.

A starting test was also supplied to the machine at the same voltage and a recording taken of the acceleration, using the accelerometer method. The comparison between calculated and measured torque-slip characteristics is shown in Fig.76.

11.2.2. The 4000 HP, 4 Pole Motor (Machine 2)

Machine 2 is another machine for which static impedance results are available over an even wider frequency range. Agreement is seen in Fig.77 to be good over the whole frequency range. However, it is observed that the calculated frequency values from 10 c/s to 50 c/s extend over a greater part of the loci than the corresponding measurements would suggest.

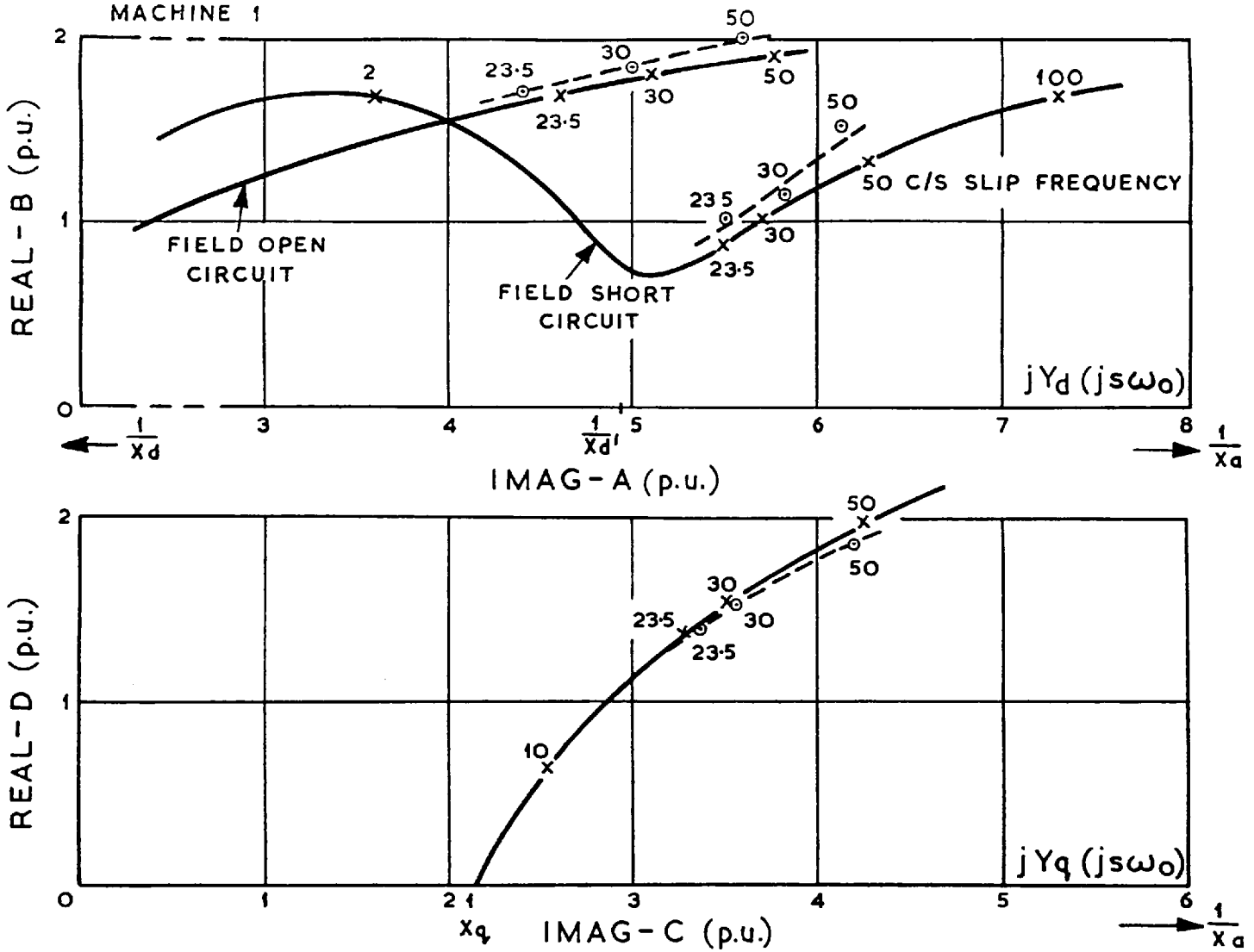

Fig. 75. The two axis operational admittance loci of the 2500 H.P., 6 pole, solid pole motor (·4 p.u. voltage)

---o--- Measured by variable frequency static impedance test

———×——— Calculated

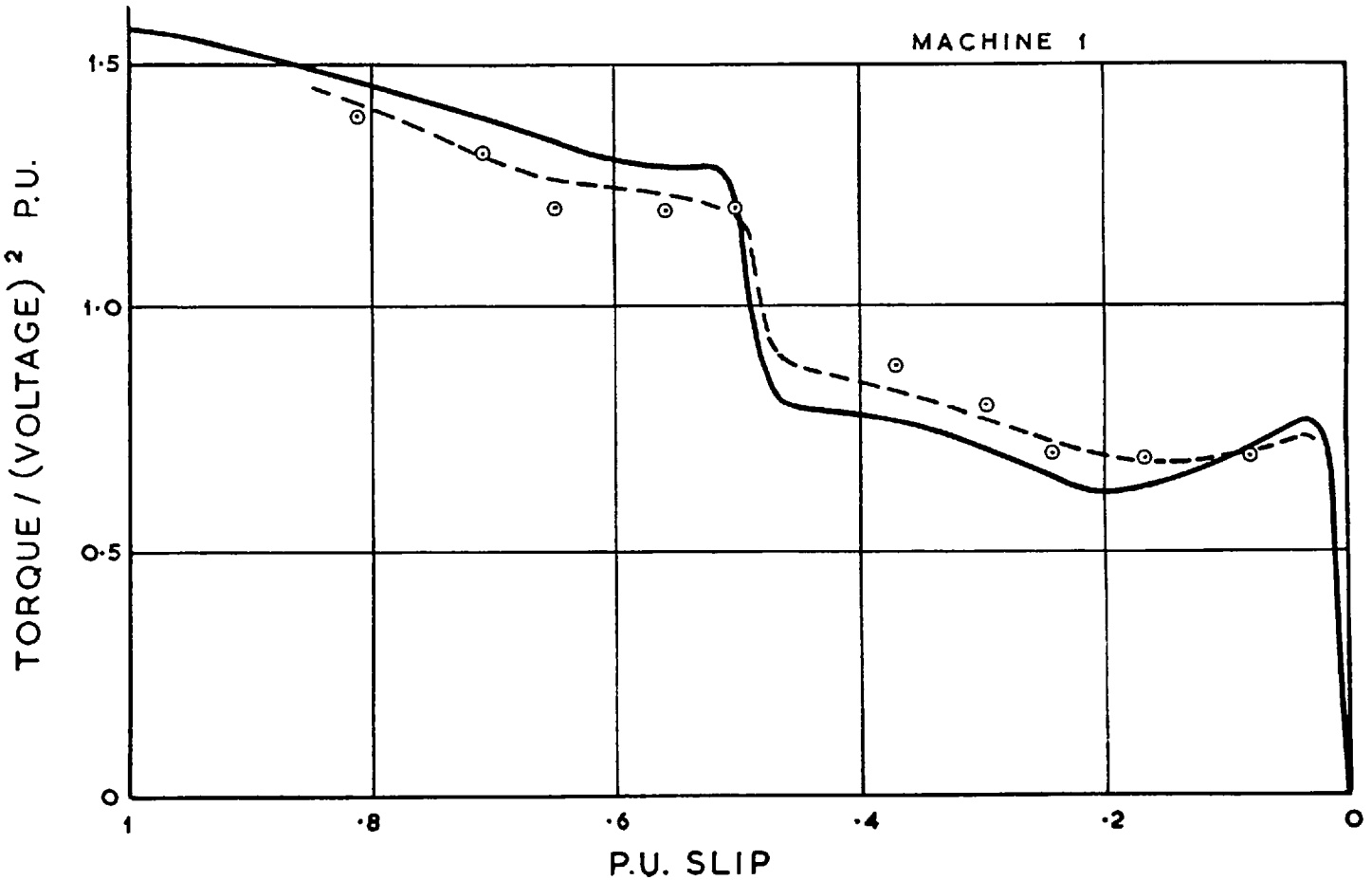

Fig. 76 Mean torque slip characteristic of the 2500 H.P., 6 pole, solid pole motor with field short circuited (·4 p.u. voltage)

---⊖--- Measured by accelerometer method

——— Calculated

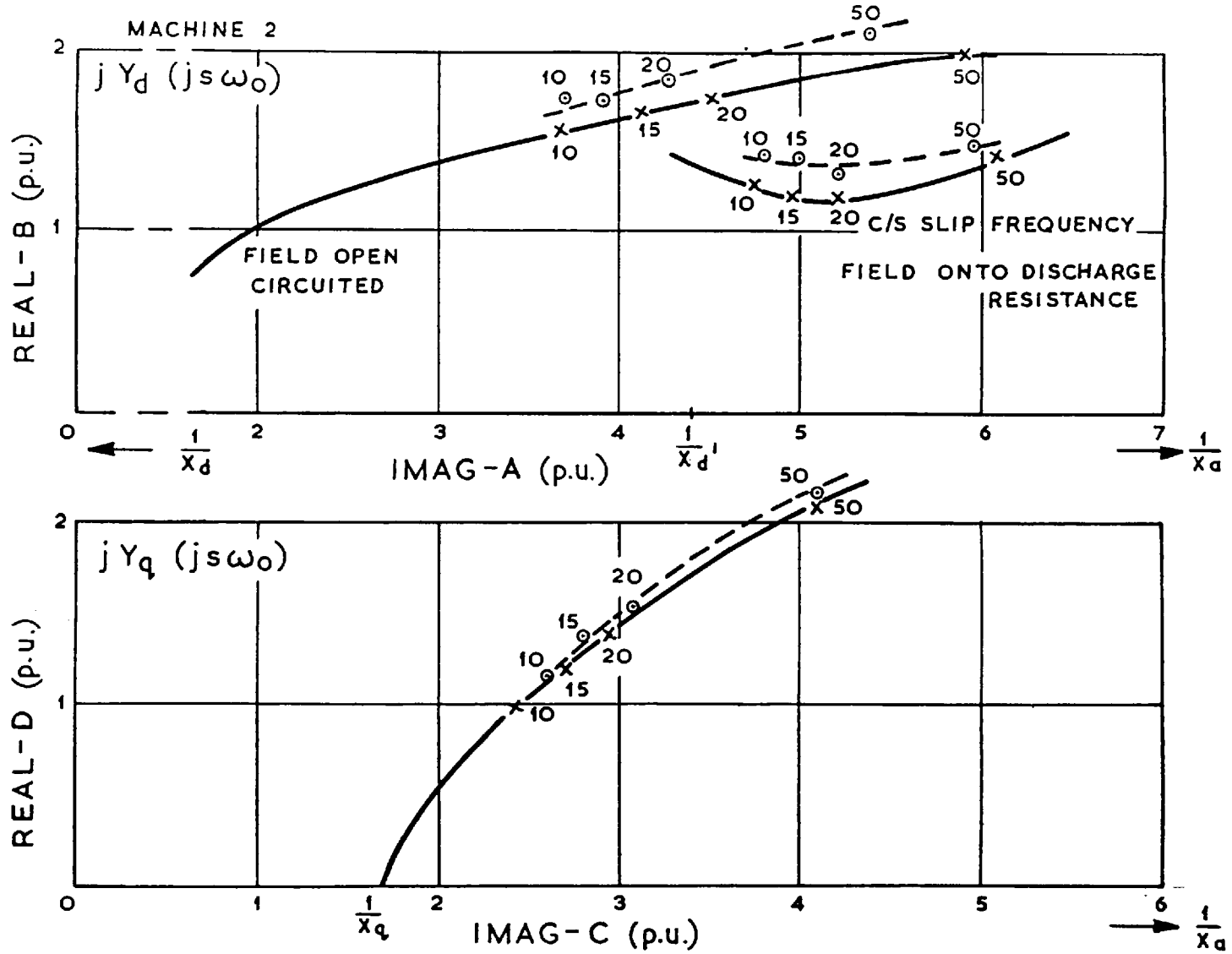

Fig. 77. The two axis operational admittance loci of the 4000 H.P., 4 pole machine (·3 p.u. voltage)

---⊙--- Measured by the variable frequency static impedance test

——×—— Calculated

11.2.3. The 100 HP, 4 Pole Motor (Machine 3)

The axis resolution method was used to obtain the operational admittance loci of this machine. The undesirable half speed effects in the method of measurement cause serious scatter in the measured points (Refer to Chapter 3). Consequently, in Fig. 78, only the frequency of measured points, well away from the half speed region, is indicated. The 50 c/s static impedance test was applied to this machine and is shown as an additional check.

Fig.79 shows the record of instantaneous input power and acceleration taken during a starting test. It should be noted that the instantaneous input power includes the stator resistance and iron loss, and hence has a false zero with respect to the estimation of instantaneous output torque from the instantaneous input power. The mean torque estimated from the recording of acceleration is compared with that calculated by the new method in Fig.80.

The component of oscillating torque was estimated from the recording of total instantaneous input power seen in Fig.79. The comparison between the measured and calculated oscillating component is shown in Fig. 81.

11.2.4. The 800 HP, 8 Pole Motor (Machine 4)

Comparison is shown in Fig.82 between the loci calculated by the new method and those estimated by the axis resolution method. Agreement is not so good for

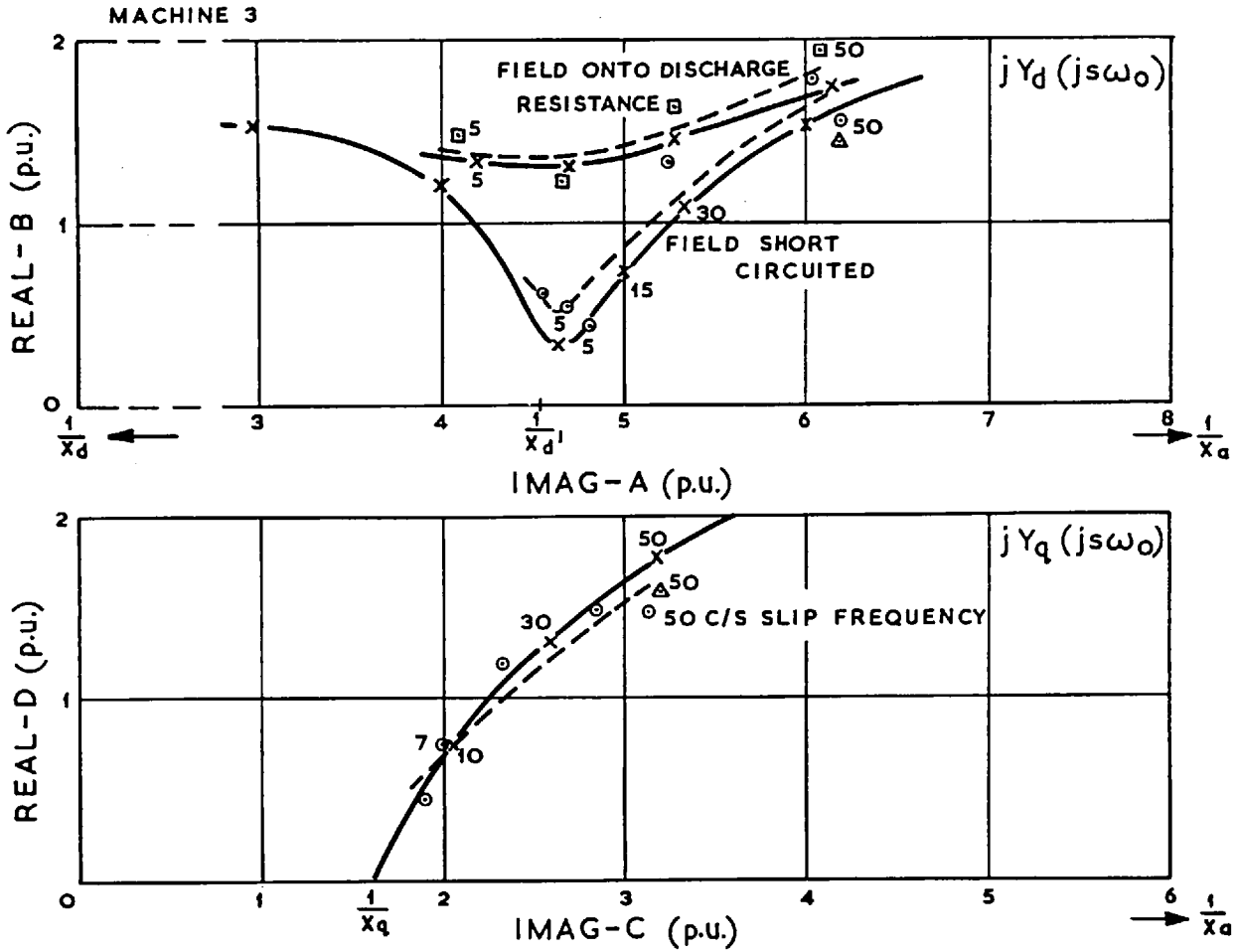

Fig. 78. The two axis operational admittance frequency loci of the 100 H.P, 4 pole motor (·45 p.u. voltage)
- —⊙— ⊡ — Measured by axis resolution method
△ 50 c/s static impedance measurement
——×—— Calculated

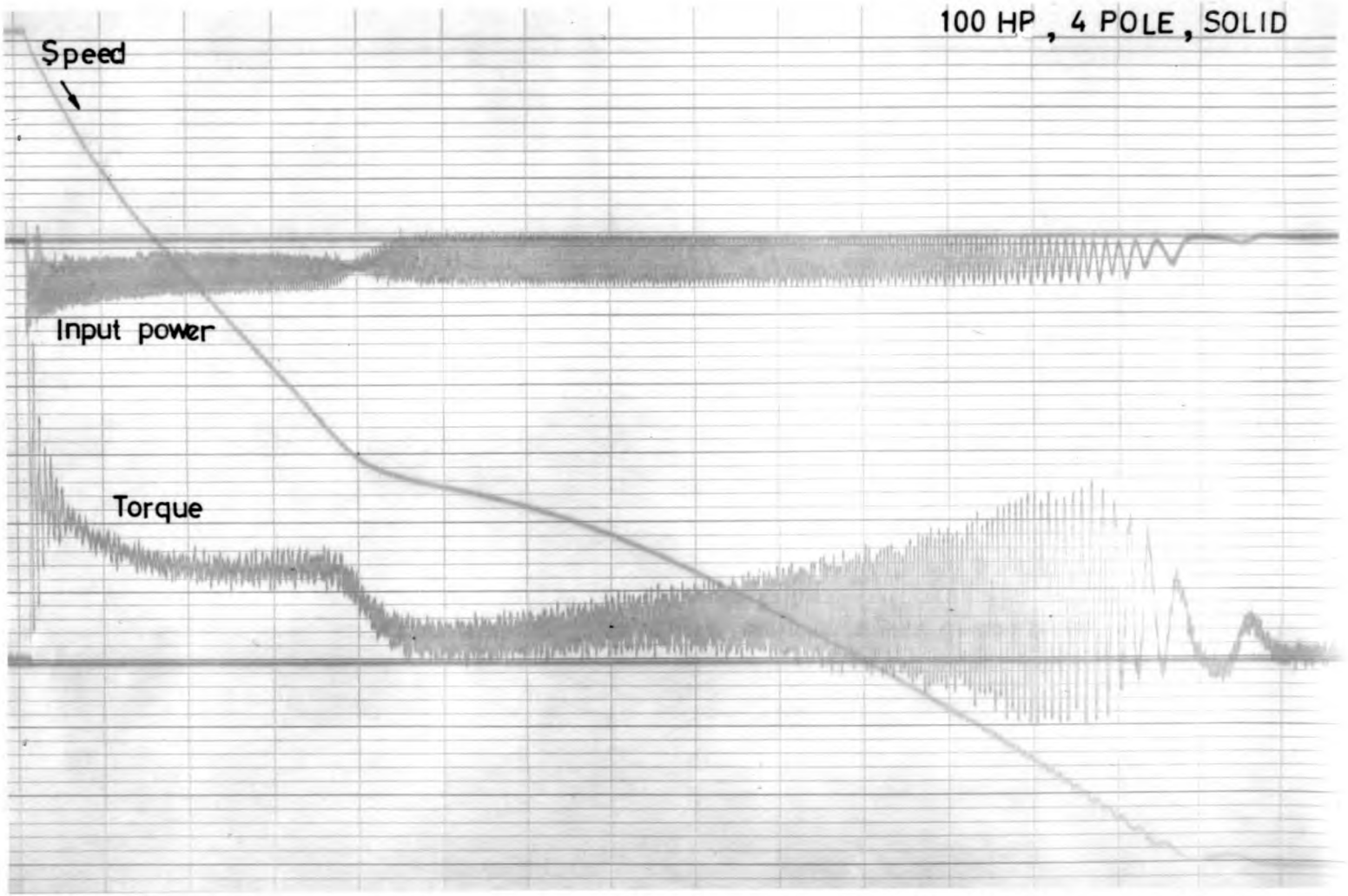

Fig.79. Instantaneous input power and acceleration during a starting test.

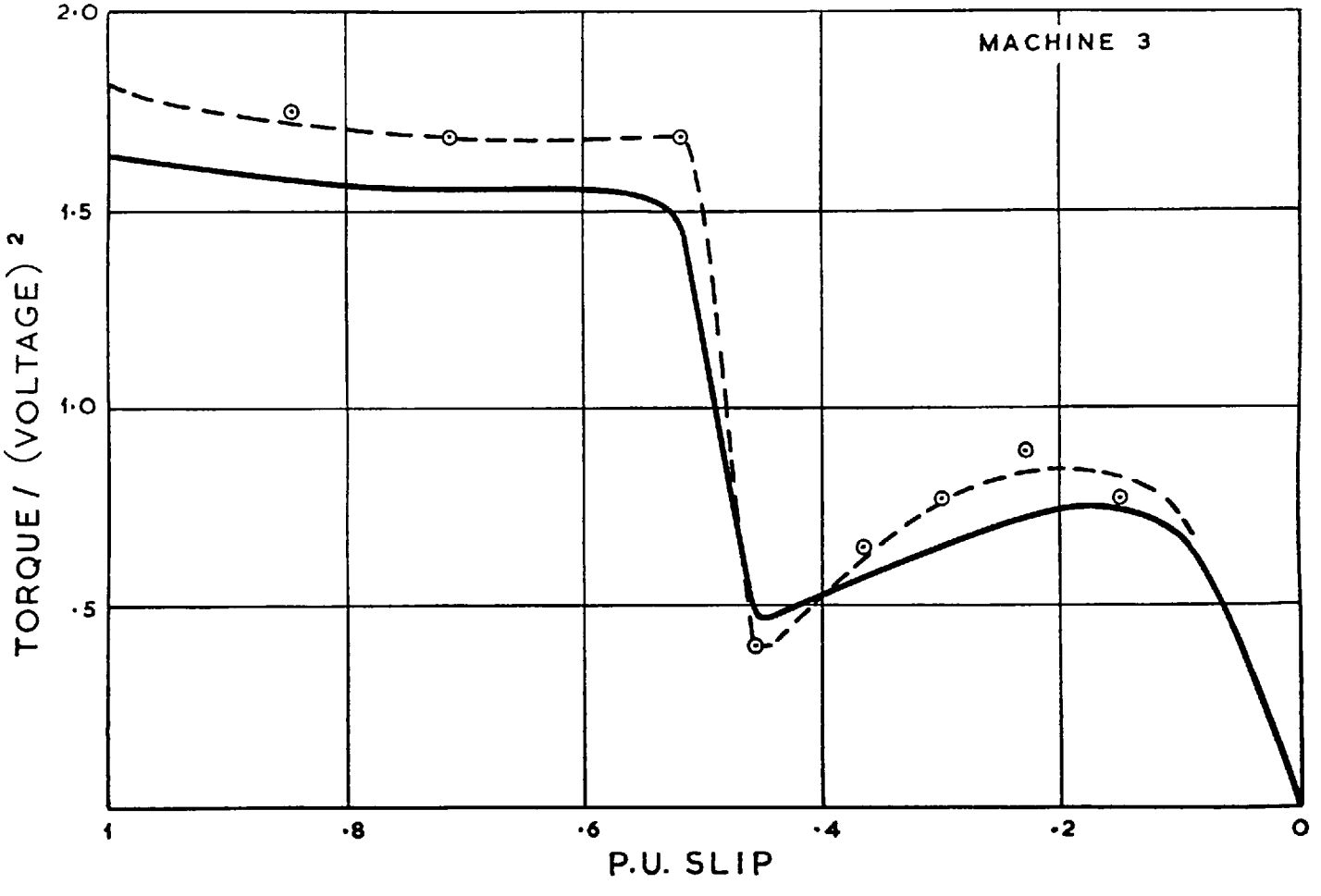

Fig. 80. Mean torque-slip characteristic of the 100 H.P., 4 pole, solid pole motor ·45 p.u. voltage

– – –⊙– – – Measured by accelerometer method

——— Calculated.

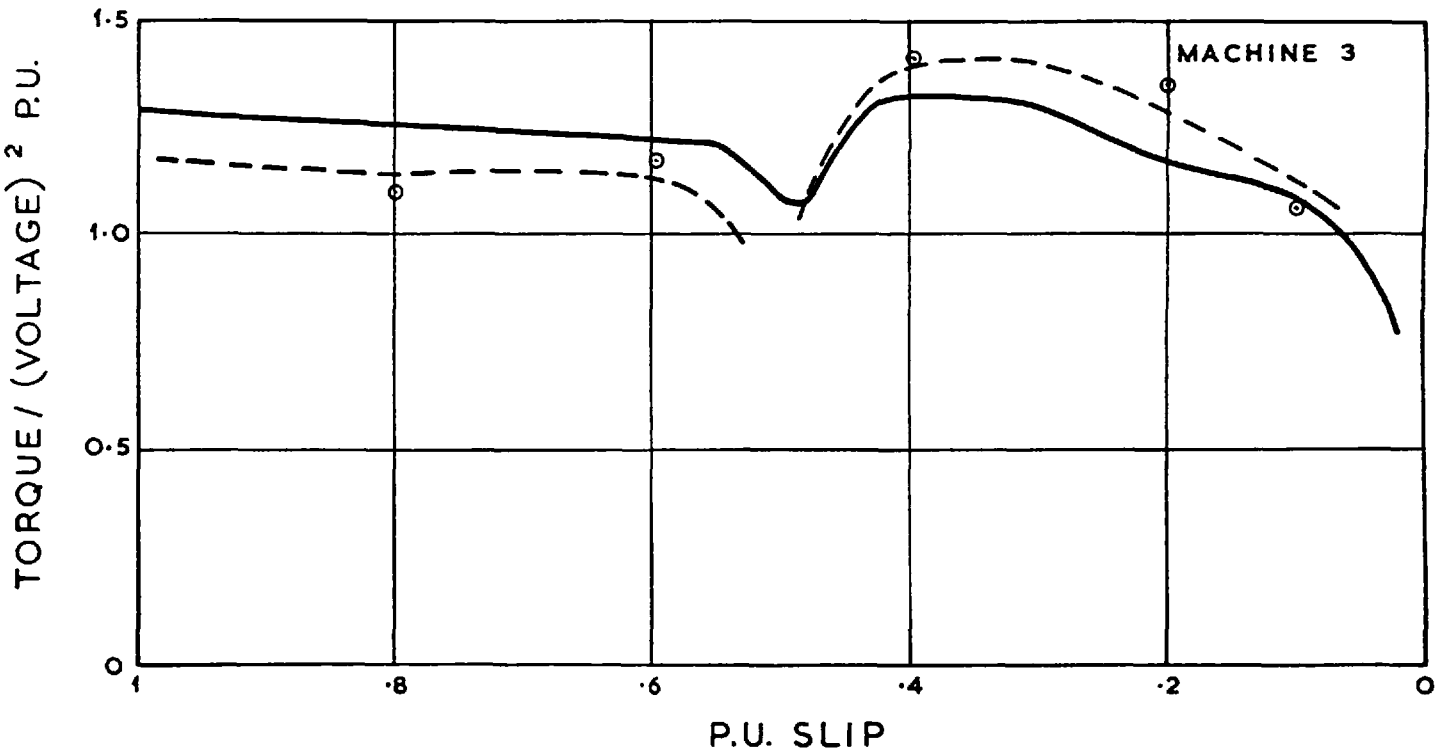

Fig. 81 Zero-peak oscillating torque-slip characteristic of the 100 H.P., 4 pole, solid pole motor (·45 p.u. voltage)

– – ⊖ – – Measured by input power method

——— Calculated

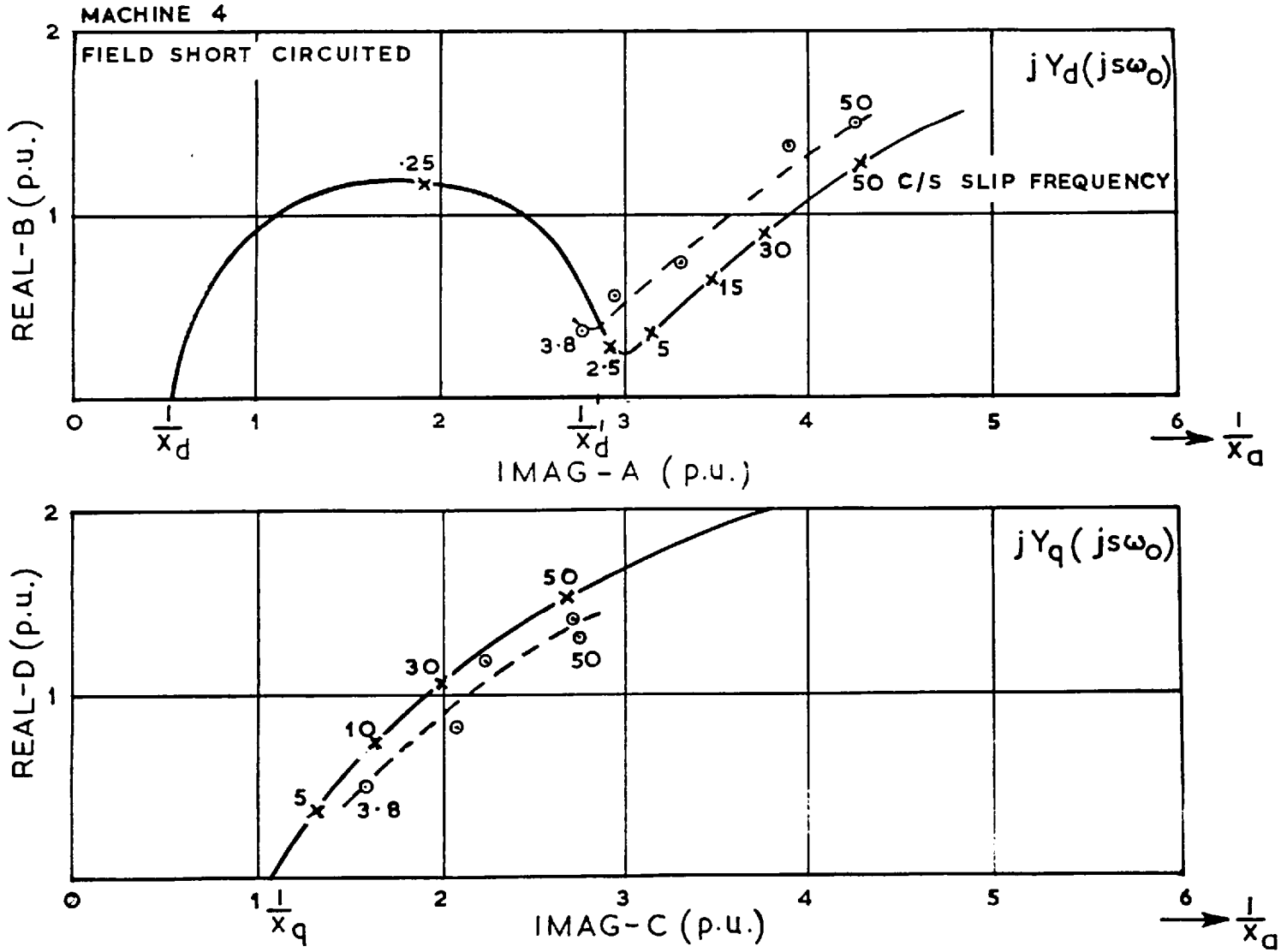

Fig. 82 The two axis operational admittance loci of the 800 H.P., 8 pole solid pole motor (·3 p.u. voltage)

– – –⊙– – – Measured by axis resolution method

——×—— Calculated

this machine. No confirmatory static impedance results were available.

11.2.5. The 5000 HP, 6 Pole Motor (Machine 5)

Fig. 83 shows the comparison between the measured and calculated direct axis operational admittances with the field winding short circuited, and that of the quadrature axis. Measurement was made using the axis resolution method, but a confirmatory 50 c/s static impedance test result is also shown. It appears, here, as well as in other comparisons, that the calculation of the real part of the direct axis operational admittance appears to be pessimistic, and conversely the calculation of the real part of the quadrature axis operational admittance to be optimistic.

11.2.6. The 75 HP, 6 Pole Motor (Machine 6)

Comparison (Fig.84) is only given between the measured and calculated quadrature axis operational admittance, for the machine with and without end-rings connecting adjacent pole shoes. Contact between the iron and copper was achieved in a similar manner to the micromachine, using screw thread contact. The magnitude of the admittances is abnormally high due to the extremely low designed stator leakage reactance of the machine (2.5%).

Agreement is seen to be good for the comparison without end-rings, and, although the agreement with end-rings connected is not quite as good, it is again confirmed that the simple method of allowing for end effects

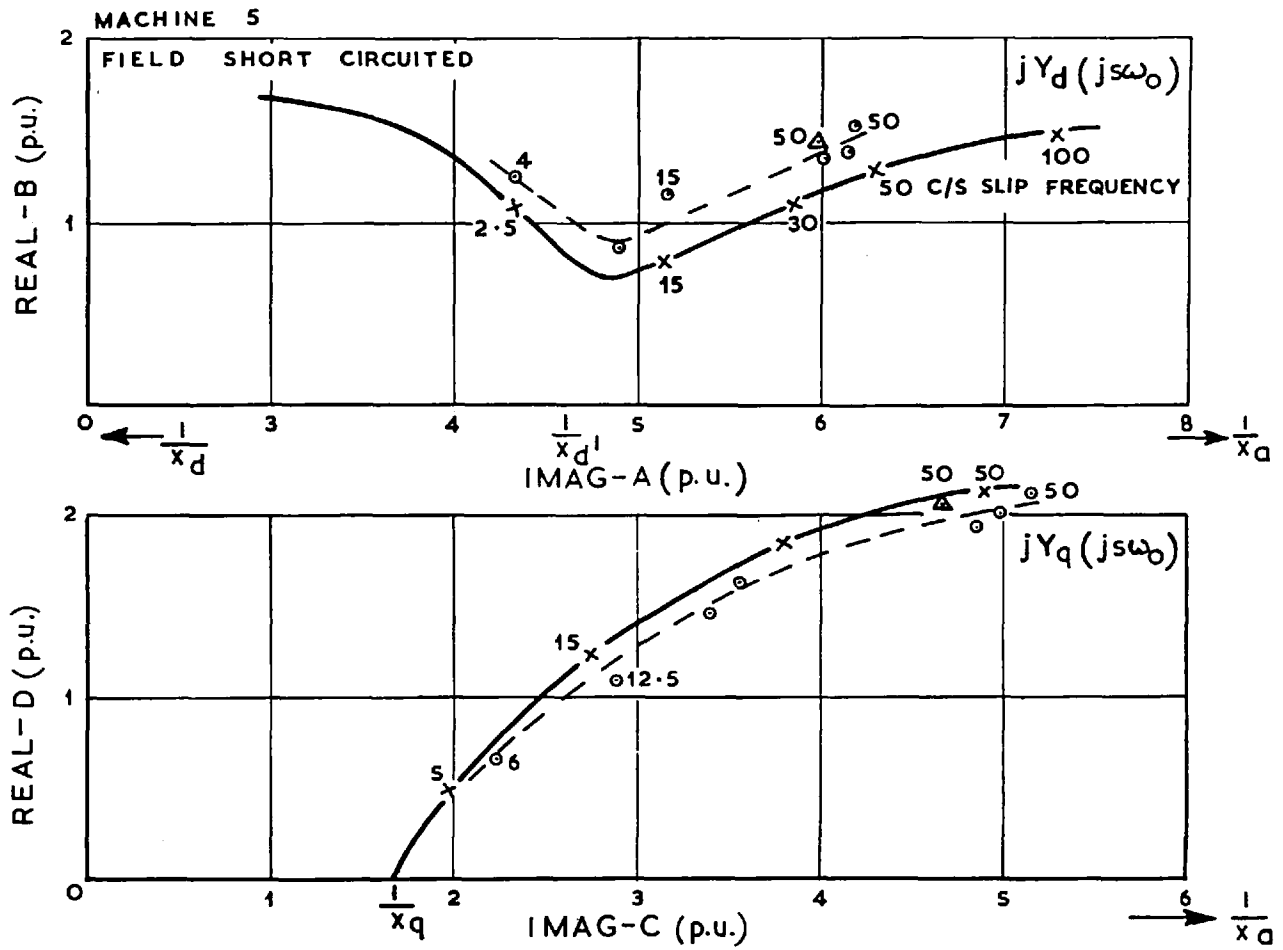

Fig. 83 The two axis operational admittance loci of the 5000 H.P., 6 Pole, solid pole motor (·4 p.u. voltage)
——⊙—— Measured by axis resolution method
△ 50 c/s static impedance measurement
——×—— Calculated

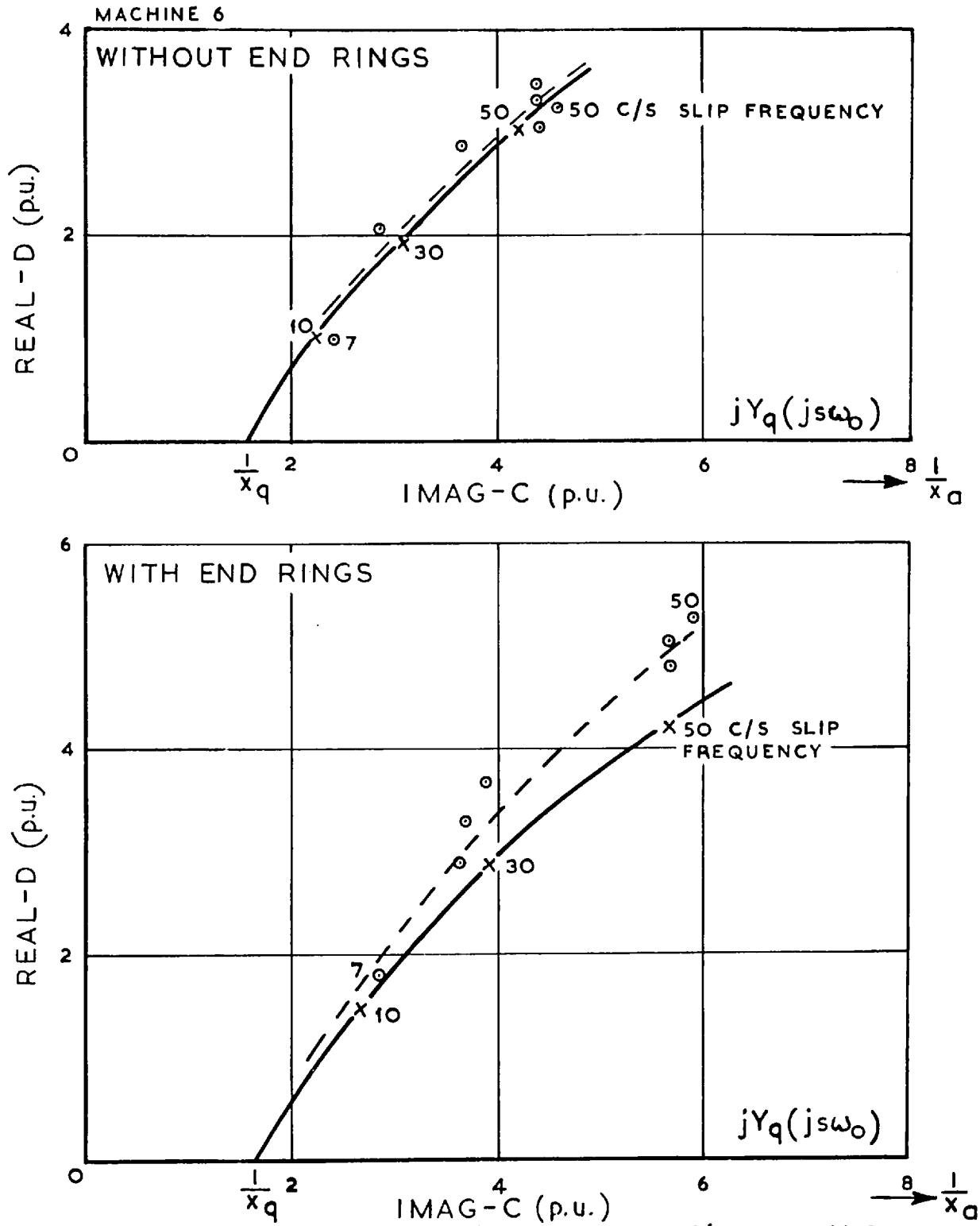

Fig. 84 The quadrature axis locus of the 75 H.P., 6 pole solid pole motor

---⊙--- Measured by the axis resolution method

——×—— Calculated

by the quadrature axis path factor (eqn. 10.30), is a satisfactory one.

11.2.7. The Other Machines (Machines 7, 8, 9, 10)

Table 2 gives comparison of the measured and calculated operational admittance values for machines 7, 8, 9, 10. The measured values were obtained from 50 c/s static impedance test results. Results for duplicate machines of types 9 and 10 are shown. Agreement is seen to be within 5% for all the machines, and in most cases is within 3%.

11.2.8. Comparison of Measured and Calculated 50 c/s Operational Admittance Voltage Functions

Further information is available for machine 10. 50 c/s static impedance test results are available over a range of voltages from .5 to .2 p.u., and it is possible to plot these as shown on the complex plot in Fig.85.

If the operational admittance, at 50 c/s, is calculated for voltages from zero to infinity, and the values obtained plotted in the complex plane, an operational admittance voltage loci is obtained. The quadrature axis locus varies from $1/X_q$ to $1/X_a$ in an identical manner to the frequency locus. (This is hardly surprising since the impedances in the equivalent circuit are of the form λ/sV, and hence variation of slip or voltage produce the same result.) The direct axis voltage locus, with field winding short circuited, goes from $1/X_a$ to a point near to $1/X'_d$,

	MACHINE 7 7500 H.P.		MACHINE 8 3500 H.P.		MACHINE 9 5000 H.P.			MACHINE 10 1650 H.P.		
	Measured/Calculated		Measured/Calculated		Measured/Calculated			Measured/Calculated		
50 c/s Q.A. OPERATIONAL ADMITTANCE (P.U.)	.45 p.u. voltage		.40 p.u. voltage		.45 p.u. voltage			.45 p.u. voltage		
					(a)	(b)		(a)	(b)	
REAL - D	1.63	1.73	2.36	2.38	1.52	1.49	1.52	1.37	1.42	1.52
IMAG - C	3.81	3.86	4.25	4.21	3.40	3.36	3.44	2.96	3.00	3.12
50 c/s D.A. OPERATIONAL ADMITTANCE (P.U.)										
Field open REAL - B	1.53	1.52	2.30	2.12	1.37	1.43	1.34	1.56	1.57	1.49
Field open IMAG - A	4.51	4.71	5.47	5.70	4.30	4.32	4.33	4.13	4.18	4.45
Field closed REAL - B	1.12	1.16	1.88	1.61	1.01	.99	.95	1.10	1.08	1.13
Field closed IMAG - A	4.85	4.83	6.35	6.21	4.75	4.67	4.49	4.43	4.45	4.60

TABLE 2. Comparison of p.u. 50 c/s operational admittances obtained by calculation, with those obtained by the static impedance test.

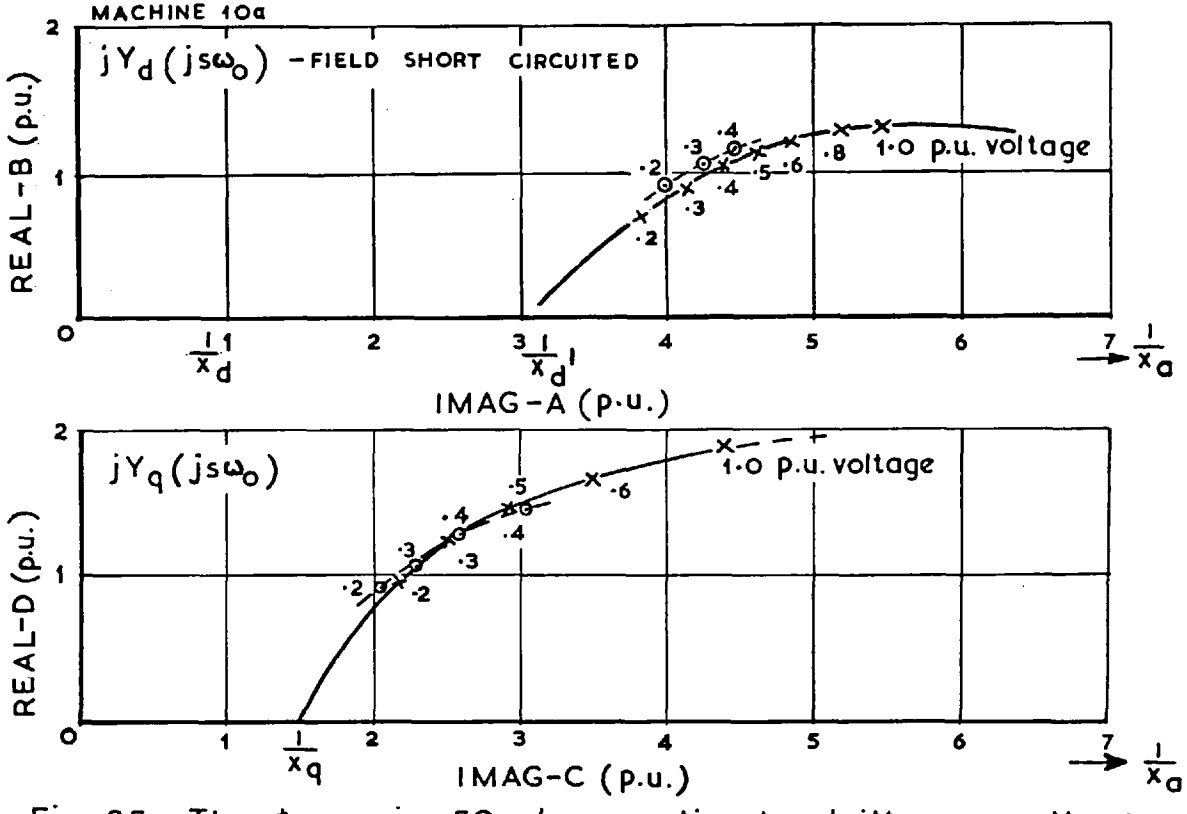

Fig. 85 The two axis 50 c/s operational admittance voltage loci of the 1650 H.P., 4 pole solid pole motor

——x—— Calculated

– – –o– – – Measured by static impedance test

- in fact, the 50 c/s point on the field winding semi-circle. (The field winding parameters are assumed to be independent of voltage.) In practice, the operational admittance voltage loci would not range over such wide limits since the non-linear impedances would linearise to fixed values, independent of further change of voltage, when the permeability of the iron reaches that of the initial slope of the saturation curve, or that of air.

It is seen, in Fig.85, that the loci of points obtained by the 50 c/s static impedance test at varying voltages agree well with the voltage loci calculated.

An alternative method of displaying static impedance test results, at various voltages, is by plotting V cos φ/I and V sin φ/I, where V and I are the terminal voltage and current, and cos φ the power factor, during the single phase static impedance test, at fixed frequency. The full lines in Fig.86 correspond to the direct axis functions V cos φ/I and V sin φ/I, calculated by the new method for the 1650 H.P., 4 pole machine (Machine 10a), with field short circuited. The circles are points obtained from the static impedance test results. Agreement is seen to be very good.

It has been proposed that this latter method of plotting static impedance test results should be the standard way, and that the 1 p.u. voltage values of static impedance should be deduced from the best slope, slope A, through the points obtained by measurement at lower voltage. However, it is clear, from the calculation at 1 p.u. voltage, that slope A is not the correct slope to deduce the 1 p.u. voltage static impe-

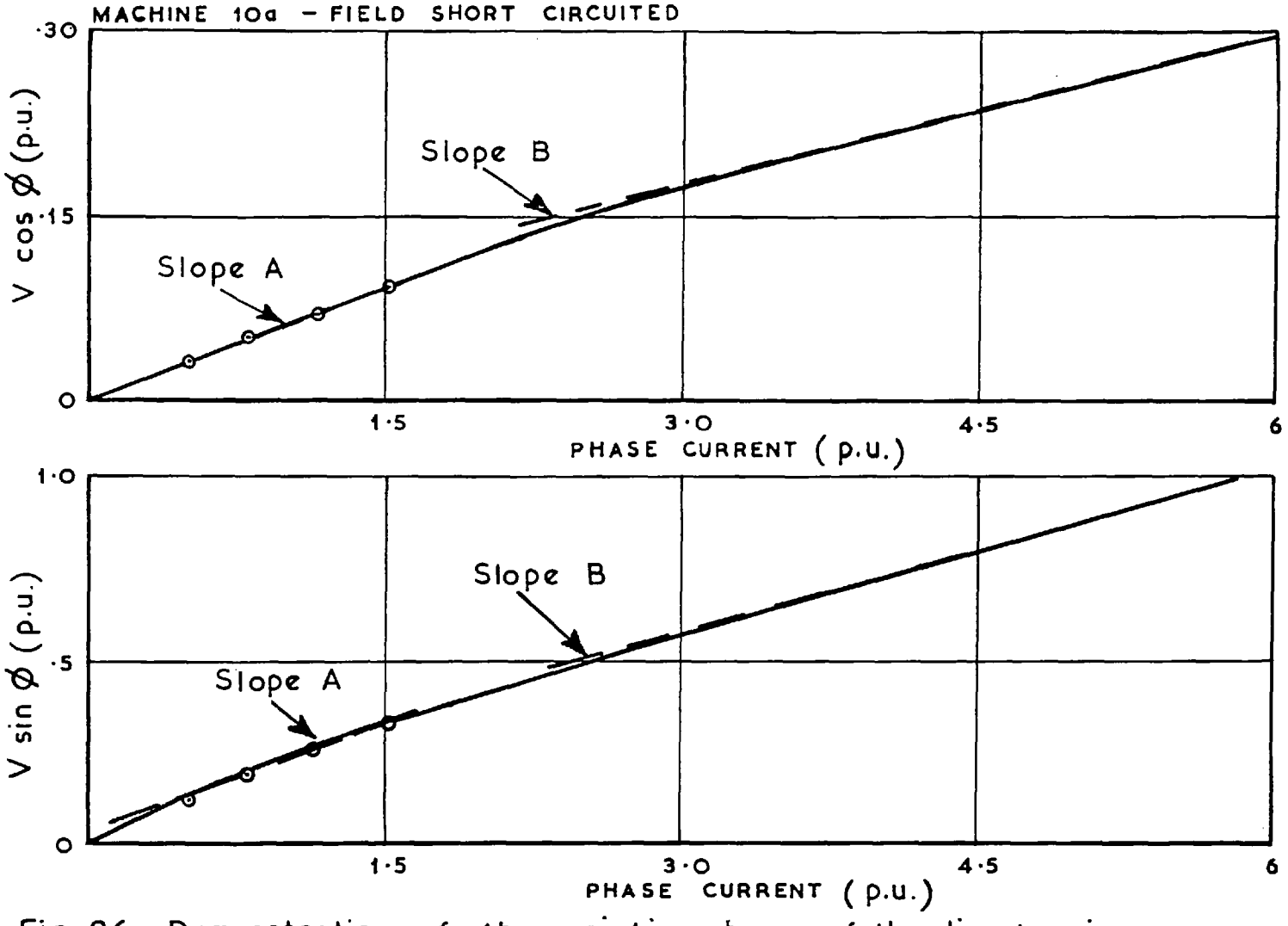

Fig. 86 Demonstration of the variation change of the direct axis static impedance with voltage for the 1650 H.P., 4 pole solid pole motor.

——— Calculated

⊙ Measured at 50 c/s

dance values, but that a shallower slope should be used - slope B.

11.2.9. The Pictorial Demonstration of the Flow of Quadrature Axis Eddy Currents in a Large Machine

Plate 4 indicates the distribution of the eddy currents in the solid pole shoe, when the machine was subjected to the single phase 50 c/s static impedance test on the quadrature axis, at half voltage, for too long a period. The discolouring of the steel, due to overheating of the solid iron, gives a direct indication of the density of eddy currents in the pole shoe.

It is observed that:-

1. The centre of the pole, over the whole axial length, was the hottest, with local spots, between the pole bolts, even hotter, where the eddy current paths were restricted. Fig. 46b shows that the quadrature axis flux is greatest in the centre of the pole, confirming that the eddy current density should be greatest, i.e. heating greatest along the centre of the pole.

2. The temperature of the iron was greatest between the pole bolts, i.e. the current density was greatest between the pole bolts, indicating that the eddy currents did not penetrate to a greater depth in the iron, when their path was restricted by the bolts, but that they remained in the surface with increased density.

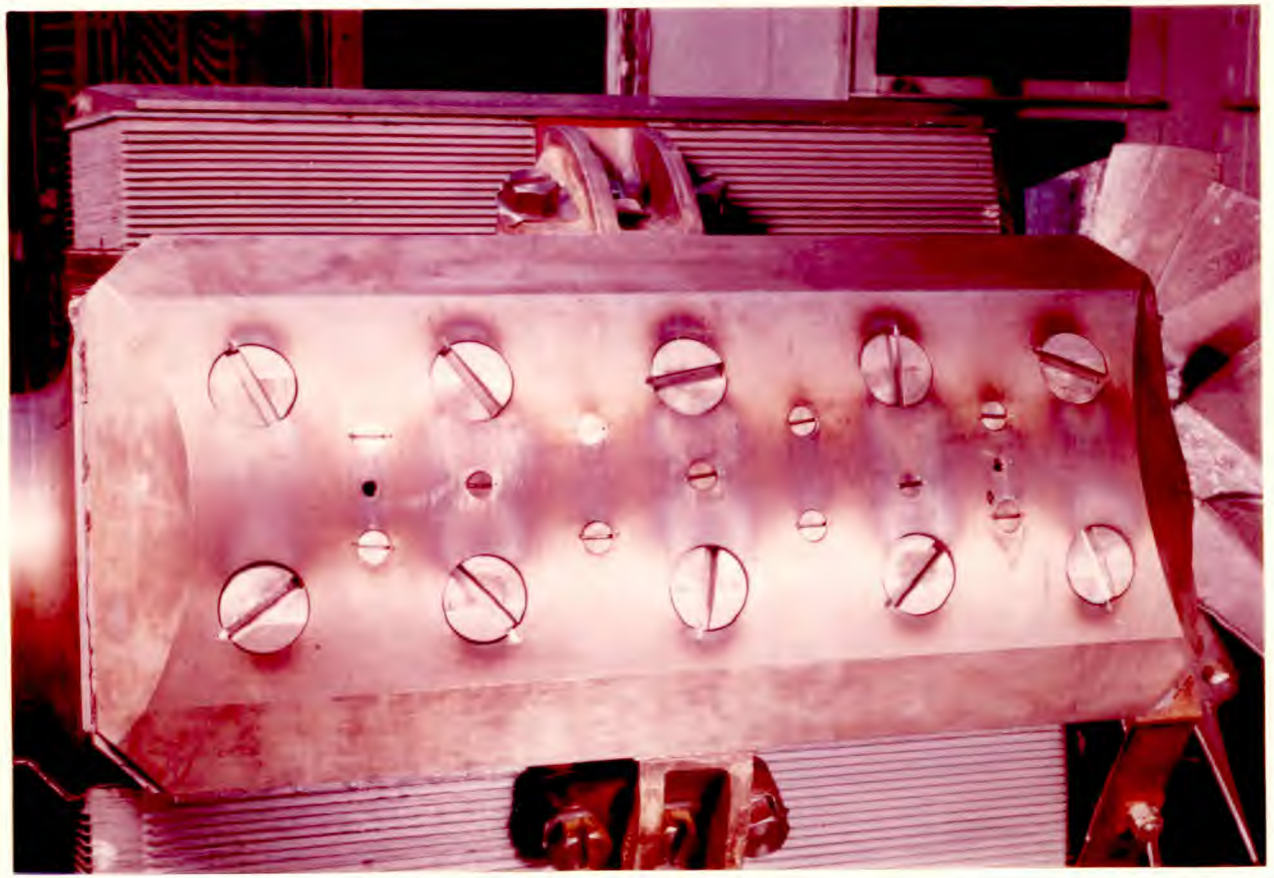

Plate 4. The rotor of a 5000 H.P. motor, following a prolonged quadrature axis static impedance test.

3. The temperature, hence current densities, reduced at the ends of the pole, as the currents began to part off and make their way, via the pole body, to the adjacent pole.

CHAPTER 12

CONCLUSIONS

12.1. A SUMMARY OF THE FEATURES OF THE NEW WORK

The method of determining the starting performance of a solid pole synchronous motor from the operational admittance functions has been described. The functions for torque and current are calculated from the two axis equivalent circuits. Completely new two-axis equivalent circuits are derived from considerations of the flux paths in the machine.

The salient features of the new direct axis equivalent circuit are:-

1. The circuit accounts, separately, for the eddy current effects in the pole body and in the pole shoe, by a complex impedance representing each. The pole shoe impedance is an equivalent impedance representing the effects of the flux entering in a distributed fashion along its surface.

2. The circuit is modified when the pole tips become completely saturated with flux.

3. Unlike the direct axis equivalent circuit of the laminated pole machine, that of the

solid pole machine still includes the field leakage reactance when it represents field open circuit conditions.

The salient features of the quadrature axis equivalent circuit are:-

1. The eddy current effects are represented in the circuit by an equivalent pole shoe impedance, representing the flux entering the pole shoe in a distributed fashion along its surface.

2. The eddy current pole shoe impedance is modified to include the effect of end-rings, when these are present.

In all past work a very simple equivalent circuit has been assumed to represent both the direct and quadrature axes without prior consideration of the flux paths in the machine.

The impedance representing the effects of eddy currents in solid iron may be derived from the linear theory (Chapter 10.2.1.) or from the non-linear theory (Chapter 10.2.2.). The linear impedance is an inverse function of the square root of slip and has a constant angle of 45^{o}. The non-linear impedance is an inverse function of the slip and the voltage across it, and has a constant angle of 26.6^{o}. In all past work one of these two results has been applied to the simple equivalent circuits. The former result gives pessimistic prediction of torque and power, the latter optimistic, when comparisons are made with test results.

Although the non-linear theory has been applied in this work, the account taken of flux entering the pole shoe in a distributed manner along its length increases the angle of the effective pole shoe impedance. The angle is found to vary from 26.6^{o} at zero slip to 45^{o} at infinite slip. At standstill slip the effective pole shoe impedance angle is found to be between 35^{o} and 40^{o}. Test results agree well with this calculated result.

Since the non-linear impedances, used in the new equivalent circuits, are inverse functions of the voltage across them, as well as the slip, the operational admittances derived from them are both slip and voltage functions, i.e. they account for saturation in the solid iron.

Both the equivalent pole shoe impedances, representing the distributed pole shoe effects, and the operational admittance functions, are calculated by iterative methods because of the non-linearity of the solid iron impedances.

12.2. CONCLUSIONS AS TO THE NATURE OF THE ASYNCHRONOUS CHARACTERISTICS OF SOLID POLE MOTORS

The following conclusions as to the nature of the asynchronous characteristics of solid pole motors are drawn:-

1. The mean torque-slip characteristic is a maximum at standstill and falls steadily to zero at full speed.

2. The component of oscillating torque is small over the whole slip range when the main field winding is on open circuit.

3. The component of oscillating torque is large, and the half speed dip in the mean torque is large, when the main field winding is closed either through a discharge resistance or short circuited.

4. Both the oscillating torque and the half speed dip decrease in proportion to the mean torque as the size of the machine increases.

5. The effect of end-rings connecting adjacent solid poles is to increase the mean torque and to decrease both the oscillating component and the half speed dip, i.e. they reduce the saliency of the machine during asynchronous running. A further effect is to increase slightly the mean phase current at a given slip.

6. Very little can be done to modify the solid pole characteristics, either at the design stage, or after the machine has been constructed. Addition of end-rings, or adjustment of the field winding discharge resistance do not make a great deal of difference to the characteristics.

12.3. ASSUMPTIONS IN THE NEW METHOD

The assumptions applicable to the principles of the two axis theory also apply to the solid pole motor. (See Chapter 8.) The most important of these assumptions is the consideration that the two axis eddy current effects are independent.

Assumption of independent eddy current action

Clearly, since the eddy currents, and solid iron fluxes of both axes pass through common solid iron material, the assumption of complete independence is incorrect. However if the distribution of the solid iron pole shoe flux, and hence eddy currents, is of the nature suggested in Fig.46, then the assumption of independent action is a reasonable one. This is so, since the quadrature axis flux, and hence eddy currents, are most dense in the centre of the pole and the least at the pole tips, while the direct axis flux and currents are conversely most at the tips and the least in the centre. Moreover, the pulsation of flux and current in the solid iron of the direct axis is out of time phase, by approximately 90^{o}, with that of the quadrature axis. Further evidence that the assumption of independent eddy current action is a sound one is borne out by experimental results, i.e. the two axis operational admittances, determined by a single axis test - the static impedance test - may be used to determine accurately the asynchronous operation, when both axis effects are present together.

Derivation of the equivalent circuits

The derivation of the two axis equivalent circuits are based on the assumption that the paths taken by the flux in the rotor are known.

It is assumed that the direct axis rotor flux crosses the main air gap in a uniformly distributed manner along the length of the pole shoe, and that the flux divides, at the tip, into a tip to tip leakage flux, and a pole body flux. The flux that links the pole body links equally the main field winding. It is assumed, in the estimation of the pole body eddy current impedance, that no flux leaves the iron in the path around the main field winding. However, the value of the field leakage reactance, X_f, representing the reluctance of the air gap leakage path between poles does include the reluctance of the air gap between both the pole tips and the pole bodies. It is assumed that the flux paths, and hence the direct axis equivalent circuit may be modified, as shown in Fig.48, when the pole tips become completely saturated.

It is assumed that the quadrature axis rotor flux crosses the main air gap in a uniformly distributed manner.

The solid iron impedances

The solid iron impedances inserted into the equivalent circuit are those derived using the non-linear saturation curve shown in Fig.40c. Although the values of impedances obtained are reasonable at normal operating magnetising forces they become unsound at very low or very high magnetising forces. Limiting linearisation is

applied to the impedances representing the pole body iron, which is often subjected to very low magnetising forces, but not to the pole shoe impedances. Thus it is apparent that at very low or very high terminal voltages (e.g. less than .1 p.u. or greater than 3 p.u.) the pole shoe impedances may become excessively high or low. It is clear, in fact, that since the non-linear impedances are of the form $\lambda'/s|V|$ they become zero at infinite voltage, and infinite at zero voltage, when in practice the upper and lower limits of the impedance are determined by the insertion of the maximum ($\mu_r\mu_o$) and minimum (μ_o) slopes of the actual iron saturation curve into equation 10.14. It is clear therefore that without limiting linearisation applied to all solid iron impedances, the method accounts for saturation in too coarse a manner.

The flux distribution in the solid iron

The method of representing, in the equivalent circuit, the effect of distributed flux entering the pole shoe (Fig.47) appears to be a good one, although an important assumption is made with regard to the nature of the distribution. Fig. 56a shows that the nature of the direct axis air gap flux distribution, determined by the method of calculation allowing free distribution, is very dense at the pole tips and correspondingly sparse at the pole centre. Stator tooth saturation modifies the distribution to a more uniform air gap distribution, and the assumption of uniform air gap distribution is the one used. However, at very high slip, (e.g. $s > 10$) the rotor flux may become so reduced that the stator teeth opposite the pole tips can carry more flux than the proportional amount. The actual air gap flux distribution

is then able to attain the "free distributed" condition - the full line shown in Fig. 56a.

A further assumption made is that all the iron section impedances may be represented by the non-linear impedances, λ'/sV, even though the iron sections at the centre of the pole (in the direct axis case - Fig.46a) carry extremely low flux and ought strictly to be represented by a linear impedance - even at normal machine operating voltage.

End effects

It is assumed, in this work, that the increase in path resistance, caused by the necessity of the eddy currents to close their circuits at the ends of the pole, can be simply accounted for by a path factor (Eqn. 10.28 for the direct axis, and Eqn. 10.29 for the quadrature axis). The iron resistivity, ρ, is simply multiplied by the appropriate path factor.

Clearly, this simple method of allowing for end effects is not consistent with the use of Maxwell's equations at the ends, since it has been assumed that the tangential components of magnetising force, and flux density are zero over all the solid iron. However, experimental results with and without the connection of end-rings, serve to justify this simple assumption.

Discontinuities in the rotor surface

All solid pole shoes are attached to the "spider" of the rotor by large radial screws as shown in Plates 3 and 4. It is clear that, since there is a small clear-

ance around the heads of the screws, neither the rotor flux nor the eddy currents produced by it penetrate the screw heads. This is confirmed by the discolouring patterns seen in Plate 4. It is assumed that the presence of the screw heads in no way affects the eddy current performance of the machine, i.e. it is assumed that the effective axial length of the rotor, W, and the length of the main flux pole-shoe path, L, in the solid iron, are increased by a negligible amount, due to the diversion of both the eddy currents and the flux around the screw heads.

12.4. SUGGESTED REASONS FOR DISCREPANCIES BETWEEN MEASURED AND CALCULATED PERFORMANCE

12.4.1. The Operational Admittance Frequency Loci

The agreement between measured and calculated operational admittances, in general, is good. However, the tendency is that the calculated real parts of the direct axis admittances are slightly lower than those measured, and the converse in the case of the quadrature axis. This, in the main, can be explained most probably by the error in the assumption of uniform air gap distribution which leads to error in the angle of the equivalent pole shoe impedance derived. Any error in magnitude of the operational admittances can be accounted for by the rather uncertain value of iron resistivity, which is inserted in the calculation. It was related, in Chapter 10 how the temperature rise in the solid poles is quite considerable, and, for a given running condition, is greater for larger machines.

12.4.2. The Asynchronous Performance

Calculation of the asynchronous running performance also compares very well with that measured, indicating that the assumption of superposition of the independent eddy current action is valid.

It is seen (Figs. 66-74) that if the operational admittance frequency loci are estimated accurately, the asynchronpus performance is also predicted accurately. It is noticed that the slightly high prediction of the real part of quadrature axis admittance compensates the slightly low prediction of real part of direct

axis admittance in the mean torque calculation.

Figs. 72 and 74, giving a comparison between measured and calculated asynchronous performance of the solid pole micromachine, show that the new method accounts for saturation in too coarse a manner (as indicated in 12.3) i.e. the calculated effects of saturation are more severe than measurements suggest.

12.5. SUGGESTIONS FOR NEW WORK

Probably the first extension of the present work should be a more thorough experimental investigation of the flux paths on both axes of the machine over a greater range of frequency, flux levels, and with different connections of the main field. By measurement of the phase as well as the magnitude of voltage induced in search coils, much more detail of the distribution of flux in the machine would be obtained. At present, it is uncertain as whether the flux enters the pole shoe over its whole pole arc length, while the tip to tip leakage flux leaves only from the tip, or whether the tip leakage flux starts to leave in a distributed fashion before the tip. In other words, is the interpole tip leakage path entirely an air path, presented by X_f?

Once this matter has been thoroughly checked, it would be a sound idea to attempt to verify the agreement between measured and calculated values of operational admittance at higher frequencies. The easiest way of doing this would be to use a high frequency alternator of suitable capacity. Although the operational admittances are only required to be known over a frequency range from supply frequency to zero in order to calculate the starting performance, if transient performance, at rates of change corresponding to higher frequencies, is to be considered, it is necessary to be able to check the operational admittance frequency functions over a much greater frequency range.

If the operational admittance frequency functions are known over the complete frequency range, it is possible to find the corresponding functions $Y_d(p)$, $Y_q(p)$. A further field for extension of the work, then, is to use the operational functions in "p" form to calculate transient performance of the solid pole motor, e.g. sudden direct-on-line application of the line voltage on starting, sudden short circuits, or sudden application of excitation etc.

If the operational admittance functions could be extended to include rectifiers in the main field circuit, it would be possible to determine losses in the solid iron during steady synchronous operation, due to harmonics in the field current, and also such transient performance as sudden short circuits or sudden changes in the field excitation.

REFERENCES

1. Park, R.H. "Definition of an ideal synchronous machine and formula for the armature flux linkages". G.E. Review 1928, Vol. 31, p.332.

2. Park, R.H. "Two reaction theory of the synchronous machine". Trans. A.I.E.E., Pt.1, 1929, Vol.48. Pt. 2, 1933, Vol.52.

3. Adkins, B. "The general theory of electrical machines". (book) Chapman & Hall, 1957.

4. Edwards, J.D. "The measurement of the direct and quadrature axis components of voltage and current with particular applications to synchronous machines". A.E.I. Internal report EFQ 24 1967.

5. Pohl, R. Electromagnetic and mechanical effects in solid iron due to an alternating or rotating magnetic field". J.I.E.E. 1944, Vol.91, Pt.II.

6. Poritsky, H. and Concordia, C. "Synchronous machines with solid cylindrical rotors". A.I.E.E. Trans. Vol.56, 1937.

7. Gibbs, W.J. "Tooth ripple losses in unwound pole shoes". J.I.E.E., 1947, Vol.94, Pt.II.

8. Gibbs, W.J. "Induction and synchronous motors with unlaminated rotors". J.I.E.E., 1948, August.

9. Postnikov, I.M. "Eddy currents in synchronous and asynchronous machines with unlaminated rotors". Elecktrikchestvo, No.10, 1958.

10. Agarwal, P.D. "Eddy current losses in solid and laminated iron". A.I.E.E. Trans. 1959, Vol.78, Pt. II.

11. Bharali, P., and Adkins, B. "Operational impedances of turbogenerators with solid rotors". Proc. I.E.E., Vol.110, 1963.

12. Khosla, S.K. "A development of synchronous m/c theory by frequency response and Laplace transform methods". M.Sc.(Eng.) thesis, University of London, 1961.

13. Wright, S.H. "Determination of synchronous machine constants". Trans. A.I.E.E., 1930.

14. McConnell, H.M., and Sverdrup, E.F. "The induction machine with solid iron rotor". Trans. A.I.E.E., Pt.III, P.A.S.1955.

15. Angst. G. "Polyphase induction motor with solid rotor; effects of saturation

and finite length." Trans. A.I.E.E. P.A.S. No.58, Feb. 1962.

16. Wood, A.J. and Concordia, C. "An analysis of solid rotor machines". Trans. I.E.E., Pt.III P.A.S. 1959-60.

17. Shevel, W.L. "A modified limiting non-linear theory of eddy current phenomena in solid iron". Trans. A.I.E.E. Commun. & Electronics No.59, March 1962.

18. Basta, J. "Anlauf eines Synchonmotors mit massiven Schenkelpolen". Elektrotecknik Ilmenau Jg. 9 (1963), Heft. 2.

19. Chalmers, B.J. "Asynchronous performance characteristics of turbo-alternators". Proc. I.E.E. Vol.109 Aug. 1962.

20. Sen S.K. and Adkins, B. "The application of the frequency response method to electrical machines". I.E.E. Monograph No.178S May 1956.

21. Christofides, N. "The origins of load losses in induction motors". Proc. I.E.E. Vol. 112, Dec. 1965.

APPENDIX I

The Measurement of Axis Phase Angle from the Recording of Instantaneous Axis Power

The equations for the direct axis voltage and current at slip frequency $s\omega_o$ are:-

$$v_d = V_m \cos s\omega_o t$$

$$i_d = I_{dm} \cos (s\omega_o t - \varphi_d)$$

The instantaneous direct axis power is given by:-

$$w_d = v_d . i_d = W_m \cos s\omega_o t \cos(s\omega_o t - \varphi_d)$$

$$= \frac{W_m}{2} (\cos 2s\omega_o t + \cos \varphi_d)$$

where $W_m = V_m . I_{dm}$

Now,

$$\cos \varphi_d = \frac{W_m}{2} \cos \varphi_d / \frac{W_m}{2}$$

$$= \frac{\frac{a + b}{2} - b}{\frac{a + b}{2}}$$

from Fig.87

$$= \frac{a - b}{a + b} \qquad (13.1)$$

Thus the measurement of phase angle from the record of instantaneous axis power requires no pre-calibration, but only an accurate zero reference line.

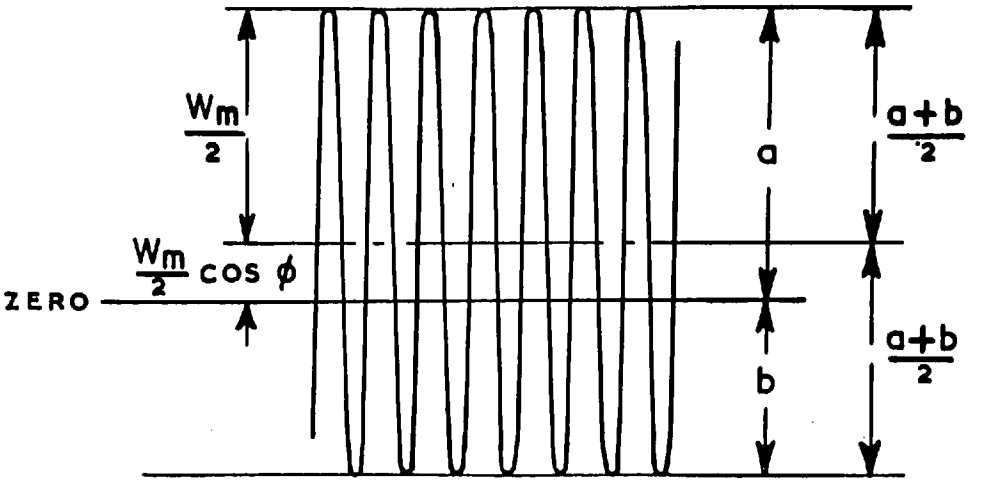

Fig. 87 Instantaneous axis power

APPENDIX II

The Relation between Electromagnetic Torque and Shaft Torque for a Two Inertia System

Consider a two mass system connected by a shaft of single stiffness K shown in Fig.88. Let the two masses have inertias of magnitude J_1, J_2, and assume that the electromagnetic torque is applied to the inertia J_1.

With the angles and conventions as defined in Fig. 88 the equations of motion at the ends are:-

$$T(t) = J_1 \frac{d^2\alpha}{dt^2} + C_1 \frac{d\alpha}{dt} + K(\alpha-\beta) \qquad (13.2)$$

$$0 = J_2 \frac{d^2\beta}{dt^2} + C_2 \frac{d\beta}{dt} + K(\beta-\alpha) \qquad (13.3)$$

Dividing eqn. (13.2) by J_1, and eqn. (13.3) by J_2 and subtracting:-

$$\frac{d^2\alpha}{dt^2} - \frac{d^2\beta}{dt^2} + \frac{C_1}{J_1} \cdot \frac{d\alpha}{dt} - \frac{C_2}{J_2} \cdot \frac{d\beta}{dt} + \left(\frac{K}{J_1} + \frac{K}{J_2}\right)(\alpha-\beta) = \frac{T(t)}{J_1}$$

transforming, with convenient initial conditions:-

$$p^2(\alpha-\beta) + \frac{C_1}{J_1} p\alpha - \frac{C_2}{J_2} p\beta + \frac{K(J_1+J_2)}{J_1J_2} .(\alpha-\beta) = T(p)/J_1 \qquad \ldots \quad (13.4)$$

the damping coefficients C_1, C_2, for this system are very small compared with the other coefficients and, thus, it is a reasonable approximation to allow $\frac{C_1}{J_1}$, $\frac{C_2}{J_2}$ to be equal.

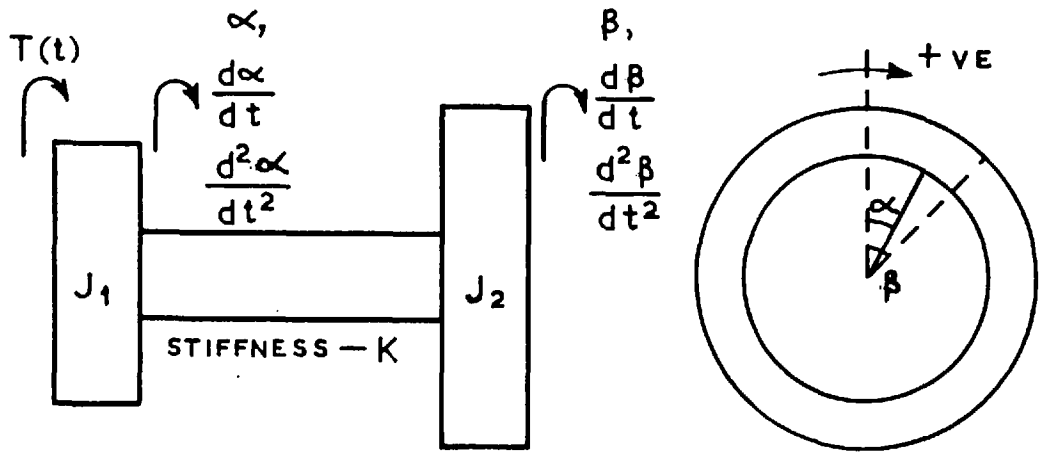

Fig. 88 The two inertia system

Replacing $(\alpha-\beta)$ by γ eqn. (13.4) becomes:-

$$p^2\gamma + \frac{C_1}{J_1} p\gamma + \frac{K(J_1+J_2)}{J_1J_2} = T(p)/J_1 \qquad (13.5)$$

thus:-

$$\gamma(p) = \frac{1/J_1}{p^2 + \frac{C_1}{J_1} p + \frac{K(J_1+J_2)}{J_1J_2}} \; T(p) \qquad (13.6)$$

If T(t) were an impulse function, then T(p) would be unity and the solution for γ would be:-

$$\gamma(t) = A\, e^{-\frac{C_1 t}{2J_1}} \cos\left[\sqrt{\frac{K(J_1+J_2)}{J_1J_2} - \frac{C_1^2}{4J_1^2}} .t + \varphi\right] \qquad (13.7)$$

Let

$$\omega_{nd} = \sqrt{\frac{K(J_1+J_2)}{J_1J_2} - \frac{C_1^2}{4J_1^2}} \qquad (13.8)$$

– the damped natural frequency

and

$$\tau = \frac{2J_1}{C_1} \text{ , the decay time constant}$$

then:-

$$\omega_{nd}^2 = \omega_n^2 - \frac{1}{\tau^2}$$

where ω_n, is the natural frequency, if there were no damping, i.e. $C_1 = 0$ in equation (13.8).

For this system, τ is large compared with ω_n, and

$$\omega_{nd} \approx \omega_n$$

Thus in eqn. (13.6)

$$\gamma(p) = \frac{1/J_1}{p^2 + 2p/\tau + \omega_n^2} T(p) \qquad (13.9)$$

The frequency response of the angle of shaft twist to electromagnetic torque oscillating sinusoidally at frequency ω:-

$$\frac{\gamma(j\omega)}{T(j\omega)} = \frac{J_n\omega_n^2}{K(J_1+J_2)(\omega_n^2 - \omega^2 + j\frac{2\omega}{\tau})}$$

and

$$\gamma(t) = \frac{J_2\omega_n^2 \; T \cos(\omega t+\varphi)}{K(J_1+J_2)\sqrt{(\omega_n^2-\omega^2)^2 + 4\omega^2/\tau^2}}$$

Thus the magnitude of oscillating electromagnetic torque is modified before appearing mechanically in the shaft by:-

$$\frac{K\gamma}{T} = \frac{J_2}{J_1+J_2} \cdot \frac{\omega_n^2}{\sqrt{(\omega_n^2-\omega^2)^2 + 4\omega^2/\tau^2}} \qquad (13.10)$$

APPENDIX III

Calculation of the Direct Axis Pole Tip Flux

Because of the distribution of flux entering the pole shoe, and because of the taper of the pole tip, the calculation is made at a point mid-way along the tip, - at a point A in Fig.89. At point A three quarters of the total flux per pole is assumed to have entered the pole.

Furthermore, since the flux is pulsating at slip frequency, there is always some point of the cycle when the flux is small enough to pass through the tip. The calculation is made, therefore, at an instant in the cycle when the flux is half its maximum value.

Referring to Fig.89, it can be assumed, as an approximation, that the maximum flux in the tip at A is:-

$\frac{3}{4}$ $(\overline{\Phi}_{f\ell} + \overline{\Phi}_{b2})$ in the top half

and $\overline{\Phi}_{b2}$ in the bottom half.

At the instant in the cycle when the flux is half its maximum value, the fluxes in the two halves are half their maximum values. The total flux in the pole tip, at this instant is:-

$$\frac{1}{2} \cdot \frac{3}{4} (\overline{\Phi}_{f\ell} + \overline{\Phi}_{b2}) + \frac{1}{2} \overline{\Phi}_{b2}$$

$$= .375 \ \overline{\Phi}_{f\ell} + .875 \ \overline{\Phi}_{b2}.$$

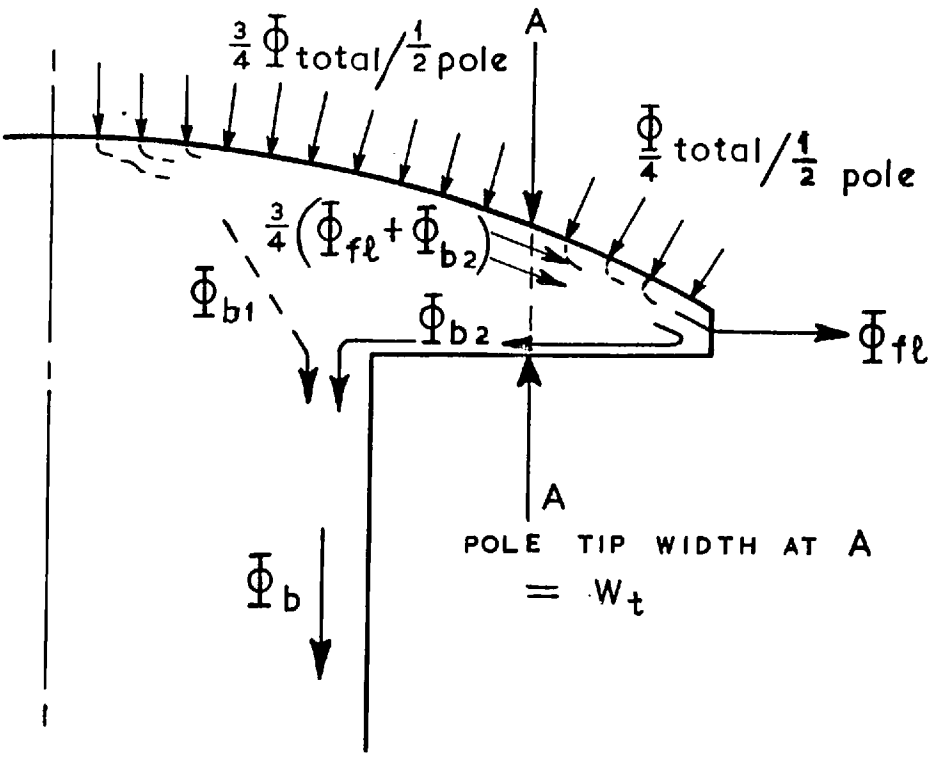

Fig. 89 Calculation of direct axis flux in the pole tip.

The depth of iron required to allow this flux to pass through is:-

$$= \frac{.375\ \overline{V}_{FL}}{4.44\ B_s\ W\ f_o\ T\ k_{w2}} + \frac{.875\ \overline{V}_{B2}}{4.44\ B_s\ W\ f_o\ T\ k_{w2}}$$

from eqn. 2.14

$$= \frac{1}{4.44\ B_s\ W\ f_o\ T\ k_{w2}} [.375\ V_{FL}(\cos \varphi_{FL} + j \sin \varphi_{FL}) + .875\ V_{B2}(\cos \varphi_B + j \sin \varphi_B)]$$

The pole tip is considered completely saturated at point A for more than half of the slip cycle when:-

$$\frac{1}{4.44\ B_s\ W\ f_o\ T\ k_{w2}} \sqrt{[(.375\ V_{FL}\cos \varphi_{FL} + .875\ V_{B2}\cos \varphi_B)^2 + (.375\ V_{FL}\sin \varphi_{FL} + .875\ V_{B2}\sin \varphi_B)^2]} = W_t \qquad (13.11)$$

Equation 13.11 is quadratic in V_{B2}. The useful solution for V_{B2} is:-

$$V_{B2} = -.855\ V_{FL} \cos (\varphi_{FL}-\varphi_B) + \sqrt{[.855\ V_{FL} \cos (\varphi_{FL}-\varphi_B)]^2 - (.735\ V_{FL}^2 - 106\ B_s^2\ W^2\ W_t^2\ T^2\ f_o^2\ k_{k2}^2)} \qquad \ldots (13.12)$$

If the value of V_{B2} calculated from equation 13.12 is less than the voltage V_B obtained in the equivalent circuit calculation, the penetration down from the top of the tip does not reach the penetration up from the bottom, i.e. the tip is not completely saturated and the direct axis equivalent circuit requires no modification.

If V_{B2} is greater than V_B then the pole tip is completely saturated and a flux proportional to $(\overline{V}_B - \overline{V}_{B2}) = V_{B1}$ cannot link the pole tip but penetrates directly to the pole body. The direct axis equivalent circuit is then modified accordng to the manner explained in Chapter 10.1.2.2.

APPENDIX IV

Determination of the Equivalent Pole Shoe Impedance Representing Flux Distribution in the Solid Iron, from a Pair of Curves

The effect of flux distribution in the solid iron pole shoe of a solid pole synchronous motor is accounted for by the determination of an equivalent pole shoe impedance (Chapter 10.3.2.2.). The equivalent impedance, Z'_s, is determined by an iterative calculation of a 100 complex branch ladder network, (Fig.55a). The output of the direct axis computer programme (Fig.64) shows that the ladder network is solved approximately fifty times (the product of the external iteration cycles in the main equivalent circuit and the internal iteration cycles in the subroutine, for the equivalent pole shoe impedance itself) for each slip and voltage. It is clear that if the 100 complex branch network can be replaced by something considerably simpler an overall reduction in computer time, and hence programme running cost, can be obtained.

It was found, in fact, that the iterative calculation of the equivalent pole shoe impedance could easily be replaced by a pair of curves. One curve gives the magnitude of the equivalent impedance (Fig. 90) and the other the angle of the equivalent impedance (Fig.91). It was intuitively realised, and then confirmed by calculation, that for a particular ratio of magnitude of simple pole shoe impedance, Z_s, (eqn. 10.34) to magnetising reactance, X_{md}, or X_{mq}, whichever appropriate, the magnitude and angle of the equi-

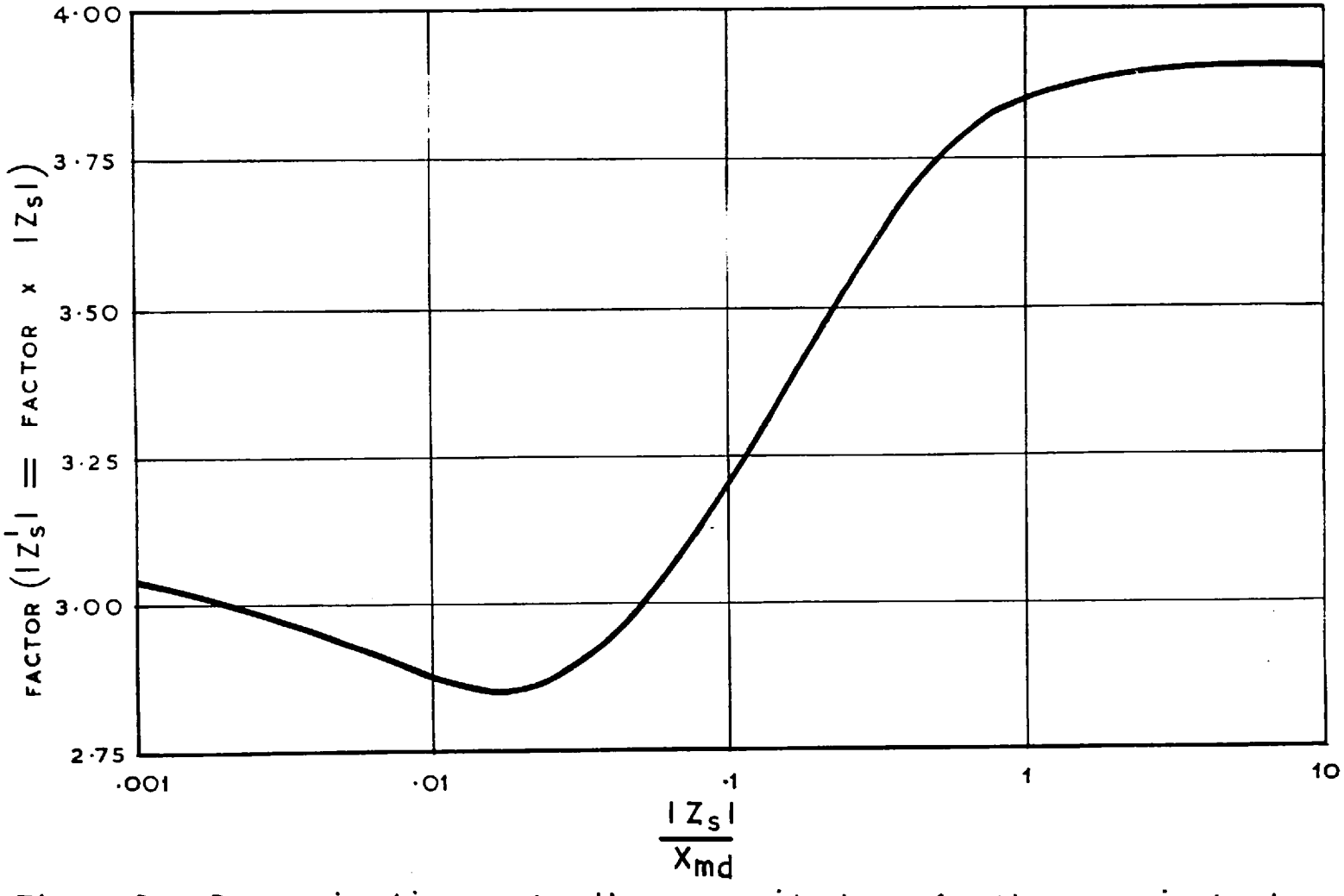

Fig. 90 Determination of the magnitude of the equivalent pole shoe impedance from the ratio $|Z_s| / X_{md}$

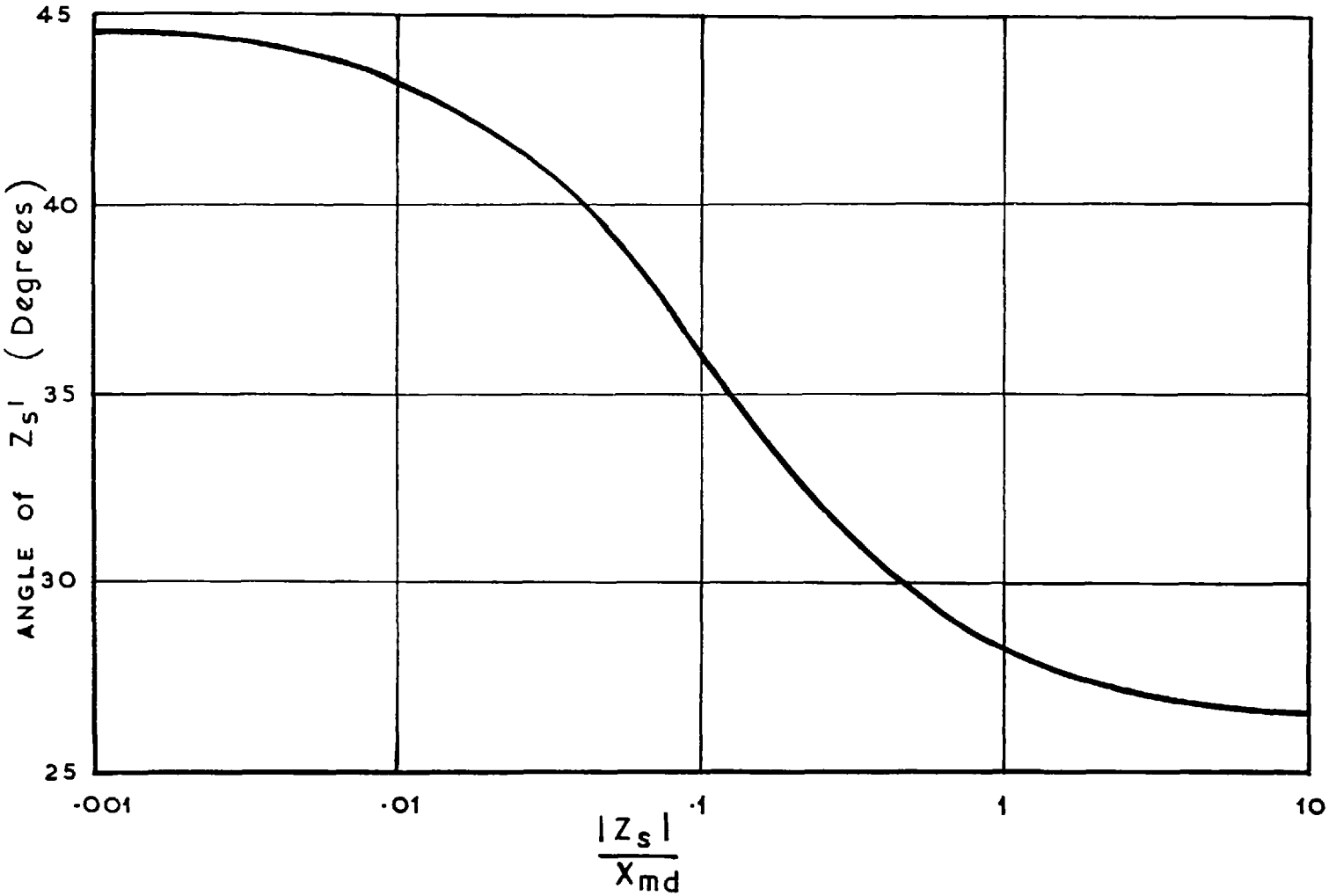

Fig. 91 Determination of the angle of the equivalent pole shoe impedance from the ratio $|Z_s| / X_{md}$

valent pole shoe impedance, representing flux distribution in the solid iron, was always exactly the same.

The subroutine SHUFLX (Fig.63) is now replaced by the alternative subroutine where the equivalent pole shoe impedance is found from the two curves. The curves are divided into twenty sections, each section represented, in the new subroutine, by a simple linear equation. The results obtained using the "curve subroutine" are within .5% of those obtained by the long iterative calculation, and the programme running time is reduced by approximately fifteen times. The final complete programme, in this more economic form, is now in commercial use.